DIMUON PRODUCTION AT THE CERN $P\bar{P}$ COLLIDER

Von der Mathematisch – Naturwissenschaftlichen Fakultät
der Rheinisch – Westfälischen Technischen Hochschule Aachen
zur Erlangung des akademischen Grades eines
Doktors der Naturwissenschaften
genehmigte Dissertation

Vorgelegt von

Diplom – Physiker

Hans – Günther Moser

aus Mannheim

Referent: Professor Dr. K. Eggert
Korreferent: Professor Dr. H. Faissner
Tag der mündlichen Prüfung: 13. 7. 1987

CONTENTS

TABLES

FIGURES

1. INTRODUCTION AND OUTLINE

This work was carried out within the UA1 collaboration which consists of more than 200 scientists from 20 institutions. They operate a huge detector at the CERN SPS−collider. This accelerator produces proton−antiproton collisions at a centre of mass energy of 630 GeV, until 1986 the highest available energy. Although the UA1 detector was originally designed to detect the intermediate vector bosons $W^{\pm}$ and Z^0 predicted by the Glashow−Salam−Weinberg theory [1], it is able to explore a much larger field of physics. Such a field of interest is the physics of heavy quarks: charm, beauty and the not yet discovered top quark. The study of these heavy quarks was the main motivation for this thesis.

We chose events with a pair of muons for our investigations. Such dimuon events lead to the discovery of the Z^0 in 1983. It was soon realized that dimuons offer a clean signature with low background. They should be ideal for the study heavy flavour physics, as muons can cleanly be identified in presence of hadronic activity. The 1983 run delivered 24 dimuon events below the Z^0 mass. Early results from these events have already been published [2], but the small number of events did not allow quantitative statements. In the following runs the detector collected six times the luminosity of 1983, and a more complete picture of the physics leading to dimuons started to emerge [3] [4] [5]. The analysis of these events is the subject of this thesis.

Some of these dimuon events can be interpreted in terms of the Drell−Yan Process and Upsilon decays. However, most of these dimuons have to be explained by the semileptonic decays of heavy quarks, especially beauty quarks. In order to validate this interpretation a detailed comparison of the event properties with theoretical calculations was performed. Generally an excellent agreement is observed. The only major exception is the surprisingly large number of events with muons of equal electrical charge. These like−sign events can be interpreted by $B^0-\overline{B}^0$ oscillations, which are the analogon to the well known $K^0-\overline{K}^0$ oscillations.

The question whether a signal of $t\bar{t}$ production can be found in the dimuons was investigated, too. No signal has been found, but limits on $t\bar{t}$ cross sections depending on an hypothetical mass of the top can be given. From this a model dependent lower limit on the top mass could be deduced.

The thesis is organized as follows: Chapter two starts with a short description of the Standard Model. Then the standard physics sources of dimuons are discussed. This is followed by a brief review of beauty properties and an introduction into the phenomenology of $B^0 - \overline{B}^0$ oscillations. Chapter three describes the SPS collider and the UA1 experiment. The selection of the dimuon data is the subject of chapter four. In chapter five the background to the dimuons is discussed. This is done in detail, as the exact knowledge of the background level is extremely important for the search of $B^0 - \overline{B}^0$ oscillations. In chapters 6 – 11 the events will be interpreted in terms of physics processes. This includes detailed comparisons with Monte Carlo calculations. In chapter 12 the results from the analysis of muons pairs at very low masses are refered. The prospects of future high luminosity runs for the dimuon analysis are discussed in chapter 13. Finally the results are summarized and we finish with a few concluding remarks.

2. THEORETICAL OVERVIEW

2.1 The Standard Model

Our present knowledge of the fundamental laws of nature can be summarized in a theoretical framework generally known as "Standard Model" [6]. The fundamental particles are spin 1/2 fermions, six leptons and six quarks, which can be grouped in doublets of three families:

leptons:	ν_e	ν_μ	ν_τ	$Q = 0$
	e	μ	τ	$Q = -1$
quarks:	u	c	(t)	$Q = +2/3$
	d	s	b	$Q = -1/3$

The top quark ("t") has not been discovered yet.

There exist three fundamental interactions[1], which are mediated by the exchange of spin 1 gauge bosons:

- the electromagnetic interaction, mediated by the massless photon (γ), which couples to electric charge.
- the strong interaction mediated by eight massless gluons, which couple to a quantity called "colour".
- the weak interaction, mediated by the massive bosons W^+, W^- and Z^0, which couple to the "weak isospin".

The electromagnetic interaction has been well known since a long time. It is described in a gauge theory called Quantum Electrodynamics (QED).

In the 70's Quantum Chromodynamics (QCD) was developed in analogy to QED. Rather than to charge the force couples to "colour" existing in "blue", "green" and "red" and to the corresponding anti−colours. As only quarks and gluons carry colour, leptons do not feel strong interactions. Only

[1] In addition there exists gravity, which is not included in the Standard Model.

colourless states (colour singlets) have been observed in nature. The quarks are grouped either in mesons, which consist of a quark carrying colour and an antiquark carrying anti−colour, or in baryons which, consist of three quarks, a "blue" a "green" and a "red" one. Both results in a colourless ("white") state.

The weak interaction, together with the electromagnetic interaction, is described in the Glashow−Salam−Weinberg Theory [1]. The charged Bosons W^+ and W^- induce transitions within a doublet of the "weak isospin"[2] e.g. an electron transforms into an ν_e emitting a W^-. The weak interaction of quarks is slightly more complicated. The physical states d, s, and b are a mixture of the weak eigenstates d′, s′ and b′. Weak interactions of quarks can therefore occur between different families, a charm quark can decay into a strange quark or (less likely) into a down quark. The mixing is described by the Kobayashi−Maskawa matrix ("K−M") [7]:

$$\begin{bmatrix} d' \\ s' \\ b' \end{bmatrix} = \begin{bmatrix} V_{ud} & V_{us} & V_{ub} \\ V_{cd} & V_{cs} & V_{cb} \\ V_{td} & V_{ts} & V_{tb} \end{bmatrix} \begin{bmatrix} d \\ s \\ b \end{bmatrix}$$

The Z^0 induces neutral currents e.g.: $Z^0 \rightarrow e^+ e^-$. Neutral currents between members of different quark families are forbidden by the GIM mechanism. The Z^0 and the γ are a mixture of eigenstates of weak interaction (W^0) and an interaction coupling to "weak hypercharge" (B^0). The mixing is described by the Weinberg angle Θ_W.

The theory requires at least one physical scalar particle called Higgs. The Higgs field is necessary to make the W and Z bosons massive by spontaneous symmetry breaking. The Higgs particle has not yet been discovered. The Standard Model makes no prediction for the Higgs mass[3]. The only theoretical bound on the Higgs mass is an unitarity limit. The Higgs particle should be lighter than about one TeV, otherwise perturbation theory would break down.

---

[2] Only left−handed fermions are in doublets. Right−handed fermions are grouped in singlets (no evidence for right−handed ν's has been found so far) and cannot interact via W exchange.

[3] This is also true for all fermion masses, they are parameters of the theory and have to be determined by experiments.

Although the Standard Model describes Nature very well, it is generally not believed to be the ultimate theory. It needs many parameters which have to be determined experimentally: 6 quark masses, 3 lepton masses (if neutrinos are massless), 3 Kobayashi – Maskawa angles, one phase of the Kobayashi – Maskawa matrix, the electromagnetic coupling, the Weinberg angle, the vacuum expectation value of the Higgs field, the mass of the Higgs particle, and the QCD scale Λ. These are 18 parameters. A more fundamental theory should predict them. The Glashow – Salam – Weinberg model does not tell why there are three families of quarks and leptons. The Higgs mechanism is not really understood and involves theoretical problems ("fine tuning") . Finally it does not include gravity.

2.2 Physics at the $p\bar{p}$ Collider

In proton – antiproton collisions at high energy all the fundamental interactions discussed in the previous section contribute:

- *Weak Interaction:* Production of Z^0 and $W^{\pm}$
- *Electromagnetic Interaction:* Drell Yan Process
- *Strong Interaction:* Production of jets and heavy quarks

An quark and an antiquark can annihilate into a Z^0 or a $W^{\pm}$. This process lead to the discovery of these vectorbosons. Their masses, production cross sections and decay properties are in very good agreement with the predictions of the Glashow – Salam – Weinberg theory.

Quarks and antiquarks can also annihilate into a virtual photon by electromagnetic interaction. The photon can then decay into a lepton pair ("Drell Yan process").

Most frequently the quarks, antiquarks and gluons interact via strong interaction. These processes will generally give pairs of hadron jets, which are most of the time due to light quarks or gluons. QCD processes can also produce heavy quarks, like charm, beauty and possibly top. These heavy quarks give jets, too. However, the heavy quarks decay by weak interaction and a fraction of them decays into muons. Hence muons (in jets) indicate the presence of heavy quarks. In principle heavy quarks decay

in electons as well, but electons can hardly be identified if they are in jets. On the contrary, muons are able to penetrate a large amount of material absorbing all the hadrons, so that they can cleanly be identified after the absorber. Therefore muons are an unique tool to study heavy quark physics.

The weak interaction of heavy quarks is not only responsible for their decay, but it can also lead to flavour oscillations: The Kobayashi – Maskawa mixing allows transitions of neutral heavy mesons (bound states of an heavy quark and a light antiquark) into their antimesons and vice versa, thus transforming a heavy quark into its antiquark. The detection of such oscillations requires to tag the favour of both heavy quarks. This is possible if both quarks decay into muons giving a dimuon event. The sign of the muon reflects the sign (and therefore the flavour) of the heavy quark. A $b\bar{b}$ event normally gives a $\mu^+\mu^-$ pair, but if for example the b transforms into a $\bar{b}$ a $\mu^+\mu^+$ pair can be created.

Thus heavy flavour physics can ideally be studied with dimuon events. An additional advantage of dimuon events is their low background[4] contamination ($\approx$ 26%).

The standard sources of dimuons are discussed in more detail in the following sections. This includes also the Drell Yan process and the decays of J/ψ and Υ. The latter are bound states of a heavy quark and its antiquark and therefore due to heavy flavour production as well. They can decay into a muon pair, but the properties of these events are completely different from dimuons from open heavy flavour production. They are therefore discussed separately.

In principle non – standard sources of dimuons ought to be considered as well. A search for such processes was made in reference [9]. Preliminary results of this analysis do not show any evidence for such processes.

2.3 Drell – Yan Production

The Drell – Yan process is the annihilation of a quark and an antiquark into a virtual photon which decays into a lepton pair [see figure 1 a)]. Lowest order calculations predict a cross – section:

---

[4] Muons can also come from the decay of light quarks, mainly pion and kaon decays. These mesons have a long lifetime and the decay happens after some way of flight. The muons are therefore most of the time not coming directly from the interaction vertex (= not "prompt"). Being not very interesting these decay muons are considered as background.

$$d\sigma/dm = (8\pi\alpha^2/3)\, F(\tau)\, 1/m^3 \qquad \{1\}$$

α is the fine structure constant. m is the invariant dilepton mass. The factor $1/m^3$ expresses the matrix element times phase space factors. The scaling function[5] $F(\tau = m^2/s)$ describes the probability to find in a $p\bar{p}$ collision at centre of mass energy $\sqrt{s}$ a quark – antiquark pair of invariant mass m.

The signature of such events are lepton pairs of opposite sign, which are generally not accompanied by any nearby hadrons (perhaps by fragments from the remaining constituents of the primary proton and antiproton). Hence, the muon pair should be isolated. This simple picture has to be modified taking into account higher order QCD processes as shown in figure 1 b) and c).

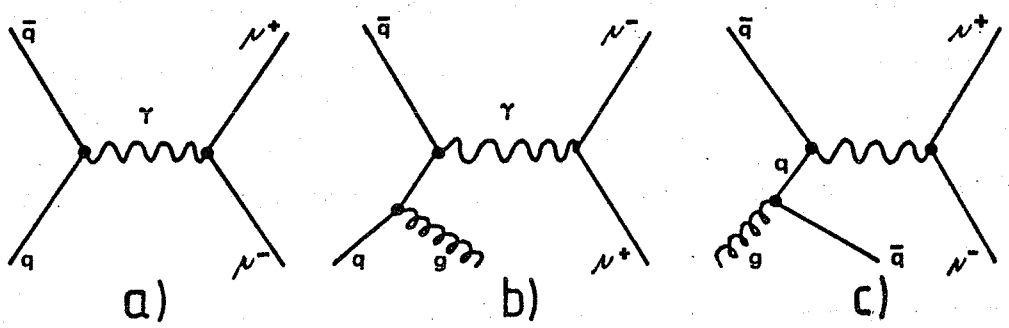

Figure 1: Drell – Yan Process: First and second order.

These processes increase the total cross – section and are responsible for the so – called 'K – factor'. They also cause a different topology of the events. The radiated quarks and gluons show up as hadron jets. These jets are normally far away from the muons, so the muons are still isolated. The muon pair will have a relatively high transverse momentum[6] in order to balance the jet(s), while muon pairs from the lowest order process are at rest in the transverse plane (except for some p_t in order of 1 GeV/c from the Fermi motion of the quarks inside the proton).

The quark – antiquark annihilation can also happen via a Z^0, which also decays directly into lepton pairs. On a single event base this process is indistinguishable from the annihilation into a photon, but it leads to a resonance enhancement of the cross – section at the Z^0 mass.

---

[5] If there are scaling violations (and there are) this has to be modified into $F(\tau,Q^2)$, in our case: $Q^2 = m^2$

[6] As usual in $p\bar{p}$ physics transverse momentum ("p_t") is defined with respect to the beam axis.

2.4 J/ψ and Upsilon Decays

Resonance production of dimuons is also expected through the ϒ and J/ψ states. Such a vector meson, consisting of a bound $b\bar{b}$ (ϒ) or $c\bar{c}$ state (J/ψ), can in principle be produced by the Drell−Yan process, if the virtual photon converts into the bound quark antiquark state. It can also be produced by strong interaction, and this is expected to be one of the main sources at the collider. Another important source of high p_t J/ψ's could be the decay of beauty mesons. A branching ratio B → J/ψ X of about 1 % has been measured [11] [12].

As the strong decays of these mesons are suppressed by the Zweig rule, a sizable fraction of them decays electromagnetically into lepton pairs. As for dimuons from the ordinary Drell−Yan process these muon pairs are unlike−sign and isolated. In the dimuon mass distribution they appear as resonances above the Drell−Yan continuum.

The following table (1) gives an overview of the different quarkonia states[7] [75].

State	Mass/ GeV/c^2	Branching ratio into $\mu^+\mu^-$
J/ψ (1S)	3.1	6.9 ± 0.9 %
J/ψ (2S)	3.7	0.9 ± 0.2 %
ϒ (1S)	9.5	2.8 ± 0.2 %
ϒ (2S)	10.0	1.7 ± 1.6 %
ϒ (3S)	10.4	4.5 ± 0.8 %

Table 1: J/ψ and ϒ states

[7] In principle there should be bound $t\bar{t}$ states as well, but cross−section and branching rations are expected to be so low that this object is at the moment invisible [13].

2.5 Production and Decay of Heavy Quarks

According to theoretical expectations the most important source of prompt muons and dimuons is the associate production of a heavy quark and its antiquark (charm, beauty and possibly top) by strong interaction with subsequent semileptonic decay. The muonic decay branching ratio of heavy quarks is about 10%, hence about 1 % of the heavy quark pairs will lead to dimuon events. Considering that the production cross – section of beauty and charm quarks via the strong interaction is about 10^3 to 10^4 times larger than the cross – section of the electromagnetic Drell – Yan process, it becomes likely that this might be the dominant source. A sizable fraction of the heavy flavour production at the collider occurs at rather large momentum transfer. Therefore cross – sections and kinematic properties should be calculable by perturbative QCD. The reliability of QCD calculations can be seen in figure 2, which shows $d\sigma/dp_t$ for jets measured by UA1 [14]. The measured cross – section is correctly described by QCD over six orders of magnitude !

Heavy quark pairs are mainly produced by gluon – gluon fusion, the relevant diagrams are shown in figure 3 . Quark – antiquark annihilation is less important. The theoretical cross – section expectations for heavy quark production ($c\bar{c}$, $b\bar{b}$ and $t\bar{t}$) is plotted as a function of the centre of mass energy in figure 4 . The cross – sections for $c\bar{c}$ and $b\bar{b}$ should be large at the collider.

The quarks are coloured objects and have to form colourless mesons or baryons. In this step, the so – called fragmentation, some fraction of the initial quark momentum is used to create (light) quark – antiquark pairs, which recombine with the heavy quark to a colourless particle. The remaining light quarks build additional light hadrons. Hence the heavy hadron is contained in a jet of hadrons. The heavy hadron keeps a fraction of the original momentum of the heavy quark. This is expressed by the fragmentation variable z:

$$z = (E + p_{||})_{hadron} / (E + p)_{quark} \qquad \{2\}$$

where $p_{||}$ is the component of the hadron's momentum parallel to the quark direction. The distribution of the fragmentation variable z can be described by the Peterson fragmentation function [19]:

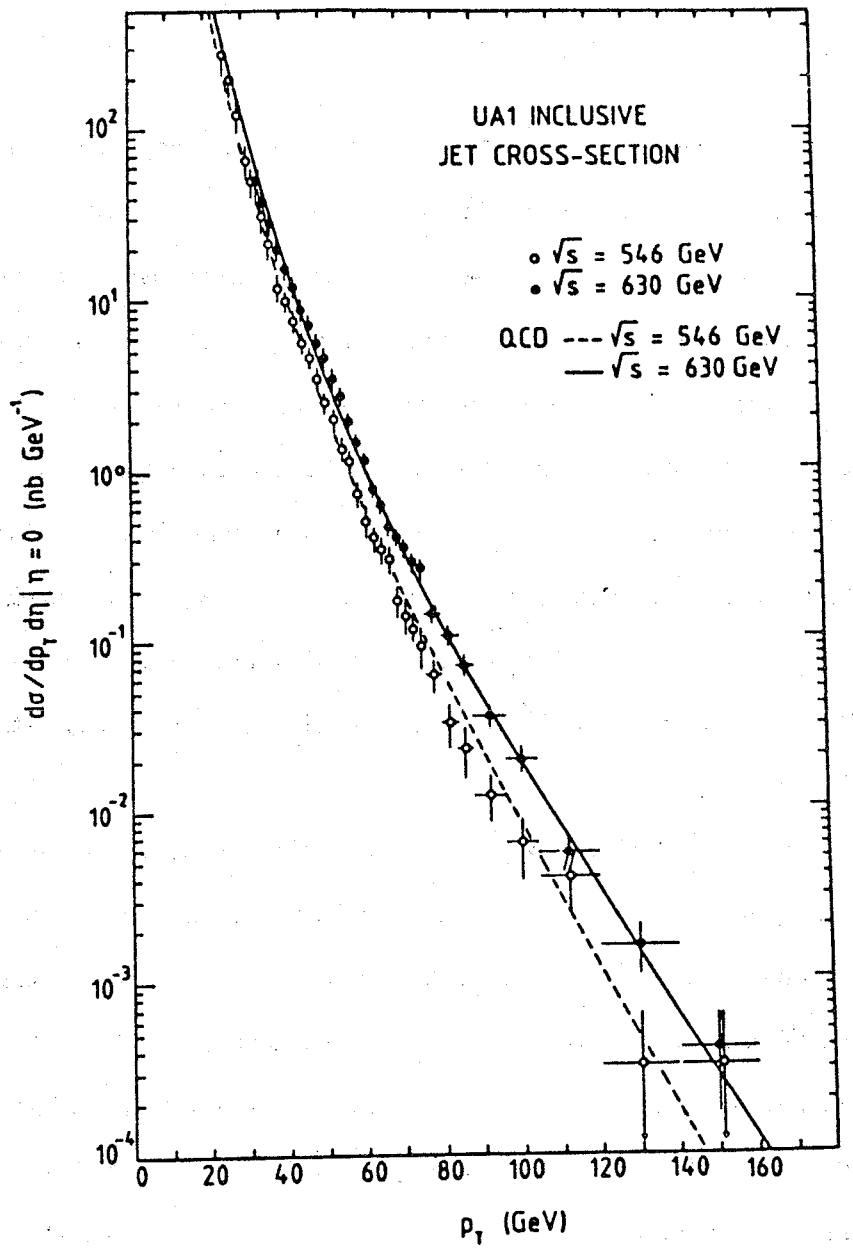

Figure 2: $d\sigma/dp_t$ for jets at $\sqrt{s}$ = 630 (546) GeV (UA1 data)

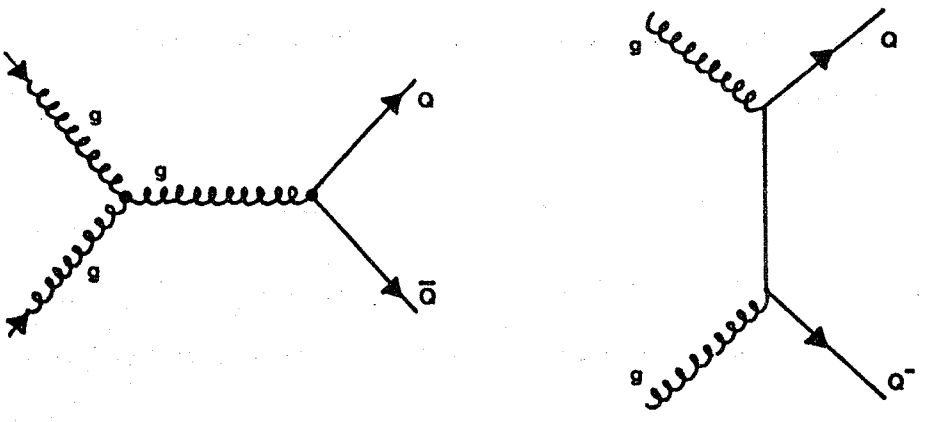

Figure 3: Heavy quark production in $p\bar{p}$ collisions

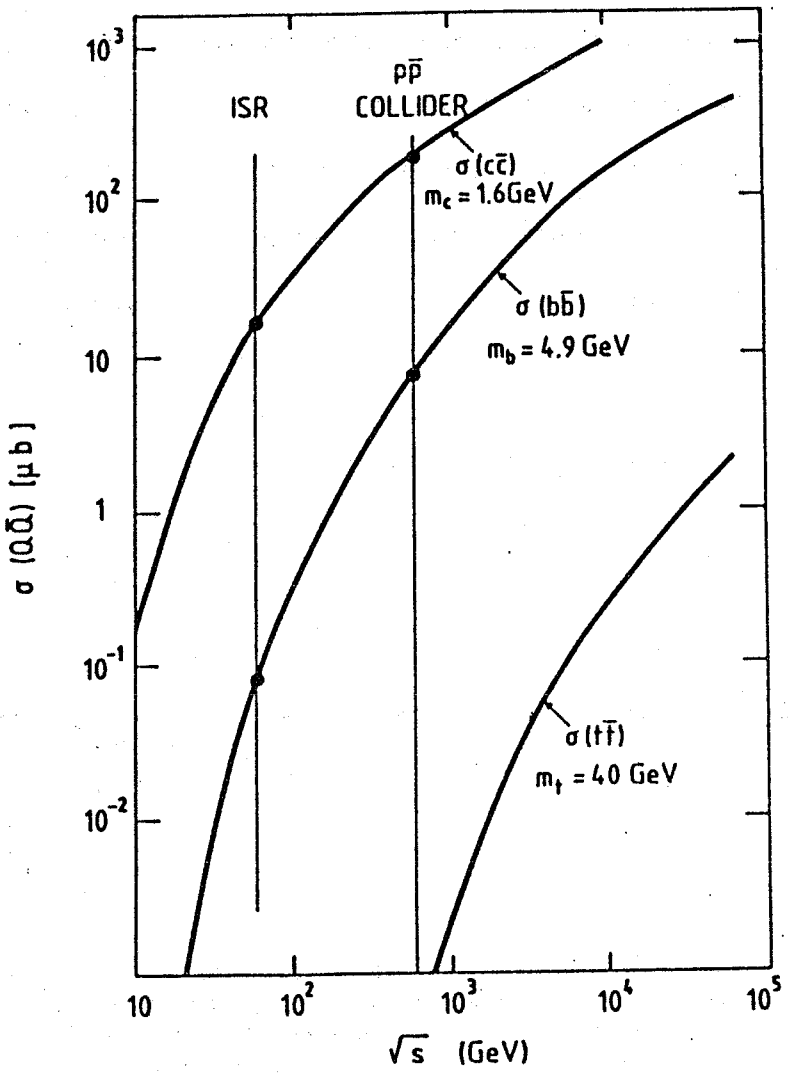

Figure 4: Cross−sections for heavy flavour production at $p\bar{p}$ collisions as a function of $\sqrt{s}$. Isajet calculation using lowest order contributions only. The top mass was chosen at 40 GeV/c^2.

$$D(z) = n / \{z [1 - 1/z - \varepsilon / (1 - z)]^2\} \qquad \{3\}$$

which depends on a single parameter ε.

The semileptonic decay of the heavy quark is mediated by a $W^{\pm}$, e.g. :

$$c \rightarrow s\, W^+(\text{virtual}) \rightarrow \mu^+ \nu\, s$$

$$b \rightarrow c\, W^-(\text{virtual}) \rightarrow \mu^- \bar{\nu}\, c$$

In the case of $b\bar{b}$ production muons can also come from the decay of the secondary charm quark. If for example the b quark decays directly into a μ^- and the $\bar{b}$ decays into a $\bar{c}$ which subsequently decays into a μ^-, an event with a like−sign muon pair is created. If a cut on the muon transverse momentum is applied, the secondary decays are heavily suppressed, as some fraction of the momentum has already been used up in the first decay step. In the case of top quarks there are three possible decay steps:

$$t \to b\,\mu^+\,\nu \text{ then } b \to c\,\mu^-\,\bar{\nu} \text{ and } c \to s\,\mu^+\,\nu$$

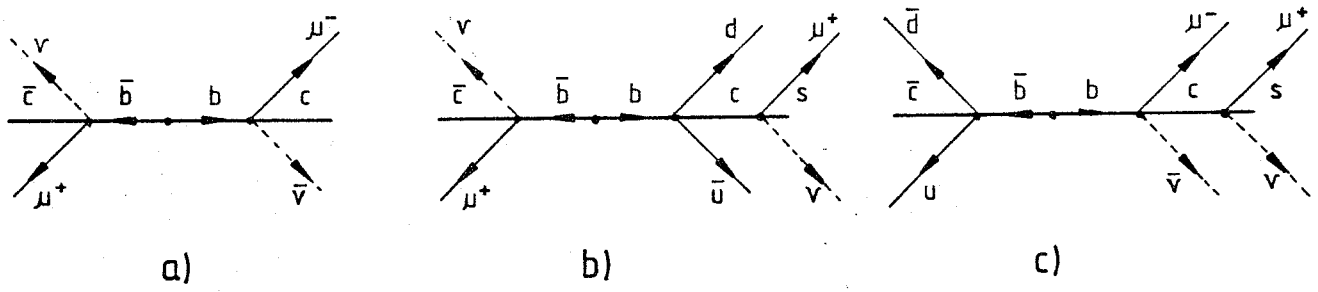

Figure 5: Dimuons from $b\bar{b}$ production
a) Unlike−sign event with both μ's from first generation decays.
b) Like−sign event with one μ from a second generation decay.
c) Unlike−sign event from a cascade decay of one b.
Both muons are in the same jet, $m_{\mu\mu} < m_b$

In heavy flavour production higher order QCD processes have to be taken into account. They contribute to the cross−section and give rise to additional jets, which tend to be far away from the muons and the fragments of the heavy quarks. The heavy quark system acquires a large transverse momentum, which forces the muons not to be back−to−back (some higher order processes are discussed in the appendix).

Another source for heavy quarks is the decay of W and Z:

$$Z \to c\,\bar{c} \text{ or } \to b\,\bar{b} \text{ or } \to t\,\bar{t}$$

$$W^+ \to t\,\bar{b} \text{ and } W^- \to \bar{t}\,b$$

Of course the decays into top are not possible, if the top is too heavy. The $W \rightarrow t\bar{b}$ decay might be especially interesting, as it will produce like−sign dimuons from first generation. On the other hand these processes are very rare as compared to the direct QCD production.

In table 2 a compilation of the number of events expected at this experiment is given. This is based on an Isajet Monte Carlo calculation (see appendix) for an integrated luminosity of 659 nb^{-1} including efficiencies of selection cuts and the detector acceptance[8].

process:	events expected:	comment
Drell−Yan	30	
$gg, gq, q\bar{q} \rightarrow b\bar{b}$	392	
$gg, gq, q\bar{q} \rightarrow c\bar{c}$	44	
$gg, gq, q\bar{q} \rightarrow t\bar{t}$	34	$m(t) = 25$ GeV/c^2
$gg, gq, qq \rightarrow t\bar{t}$	4	$m(t) = 40$ GeV/c^2
$Z^0 \rightarrow b\bar{b}$	0.6	
$Z^0 \rightarrow c\bar{c}$	0.1	
$Z^0 \rightarrow \tau\tau$	0.2	
$Z^0 \rightarrow t\bar{t}$	0.5	$m(t) = 25$ GeV/c^2
$Z^0 \rightarrow t\bar{t}$	0.2	$m(t) = 40$ GeV/c^2
$W^{\pm} \rightarrow t\bar{b}\,(\bar{t}b)$	3	$m(t) = 25$ GeV/c^2
$W^{\pm} \rightarrow t\bar{b}\,(\bar{t}b)$	3	$m(t) = 40$ GeV/c^2

Dimuons from Drell−Yan and heavy flavour production (after cuts at an integrated luminosity of 659 nb^{-1}). $p_t > 3$ GeV/c for each muon and $m^{\mu\mu} > 6$ GeV/c^2

Table 2: Expected number of dimuon events

It can be seen that $b\bar{b}$ production is expected to be the dominant source of dimuons. Ignoring threshold effects the production cross−section for $c\bar{c}$ is the same as for $b\bar{b}$, and they are produced with an identical p_t spectrum. However, the beauty quark has a harder fragmentation than the charm [90]. This means that, on average, the B−mesons keep a larger fraction of the momentum of the original

[8] As described later we demand the p_t of each muon to be larger than 3 GeV/c and the invariant dimuon mass to be larger than 6 GeV/c^2.

quarks. This results in a harder p_t spectrum of muons from beauty quarks than from charm quarks, and once a p_t cut is applied $b\bar{b}$ events are favoured compared to the $c\bar{c}$. In addition, there is a small effect from the V−A coupling in the semileptonic decays of the mesons, which also favours muons from beauty. A QCD calculation of the p_t spectra of beauty quarks, B−mesons and muons from B−meson decays is plotted in figure 6, together with the corresponding spectra for charm.

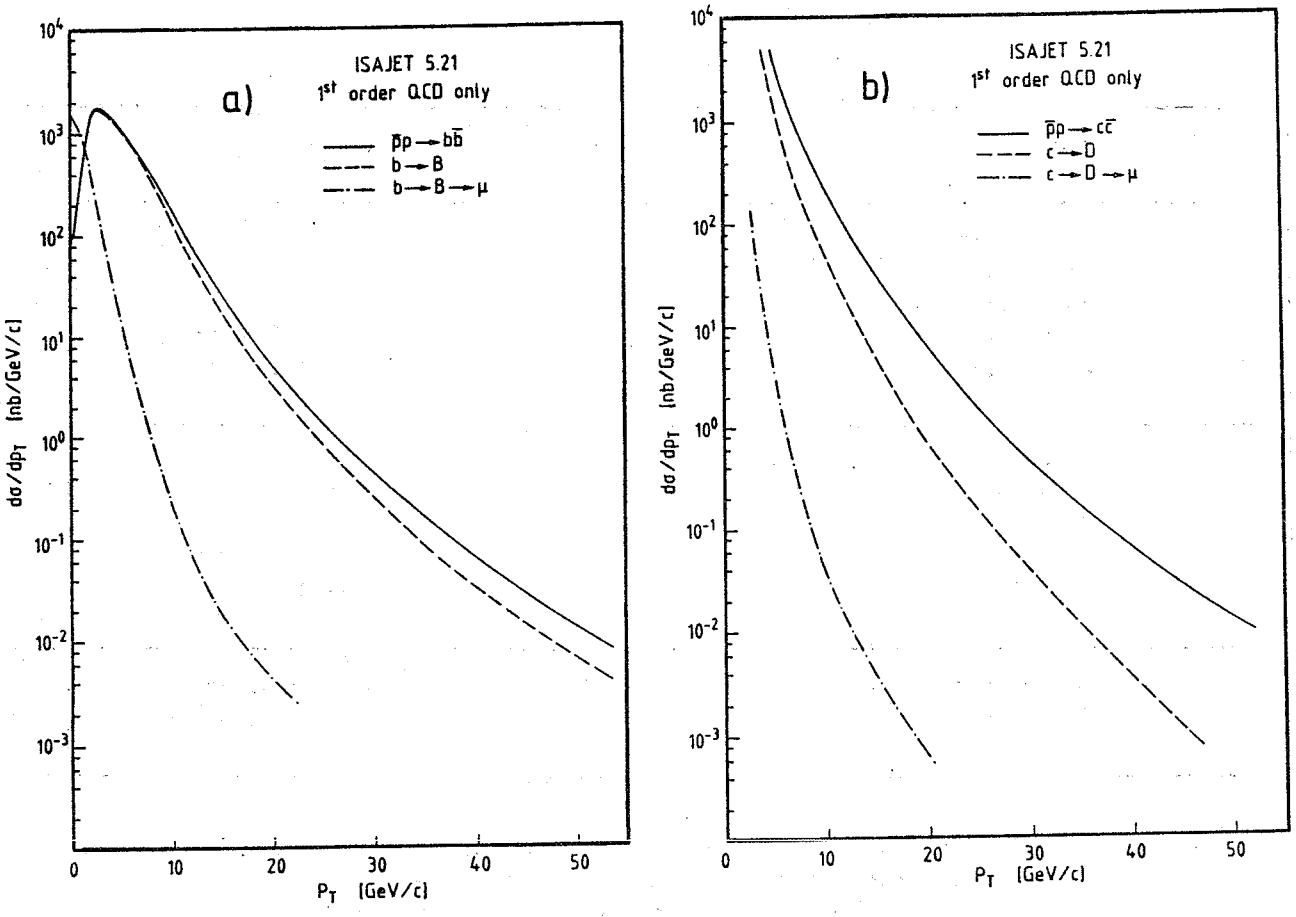

Figure 6: p_t spectra of quarks, mesons and muons.
a) from $b\bar{b}$ production.
b) from $c\bar{c}$ production.
(Isajet calculation, lowest order only)

Of course the numbers in table 2 have to be regarded as an hypothesis. It is the analysis of the data which has to show their validity.

In summary, ignoring top decays, the events from heavy quarks should have the following properties:

- The muons are accompanied by hadrons from the heavy quark fragmentation and from its semileptonic decay. They are therefore not isolated.
- They have predominantly opposite signs, but some like−sign events from second generation decays are expected.
- The muons are generally back−to− back[9] in the transverse plane. Higher order contributions can lead to a fraction of events with smaller azimuthal angles between the muons. These events have additional jets far away from the muons.

Table 2 shows that some contribution from $t\bar{t}$ production is possible, if the top mass is not too heavy. Because of its high mass the total $t\bar{t}$ cross−section at the collider is very small compared to the $b\bar{b}$ cross−section. A top quark of 25 GeV/c^2 should have a production cross−section of about 10 nb, whilst the $b\bar{b}$ cross−section should be in the order of several μb. On the other hand it is much more likely to get a dimuon event from $t\bar{t}$ than from $b\bar{b}$:

- The fragmentation of the top quark is even harder than the b−fragmentation.
- Because of the large mass, muons from top decays have very high momenta and can easily satisfy our p_t cut, even if the top is produced near threshold.
- Muons from second and even third generation decays are less suppressed than second generation muons from beauty quarks.

As the $t\bar{t}$ cross−section depends strongly on the top mass, the expected dimuon rate falls rapidly with increasing top mass. Dimuons from $t\bar{t}$ production are practically absent, if the top is heavier than 50 GeV/c^2. In this case there still exists the possibility to observe a few events from $W \rightarrow t\bar{b}$. This contribution depends only slightly on the top mass, as long as it is light enough to be produced by a $W^{\pm}$ decay.

[9] There are also dimuons from the cascade decay of one b, which will be close together. In our analysis these events are cut away by demanding a dimuon invariant mass larger than 6 GeV/c^2.

2.6 Review of Beauty Physics

As discussed in the previous chapter, $b\bar{b}$ production is expected to be the dominant source of dimuons at the collider. Hidden beauty was found in 1977 with the discovery of the Υ, a $b\bar{b}$ bound state [16]. Open beauty, that is a meson containing a beauty quark and a light antiquark, has only been studied at e^+e^- storage rings, especially at "b−factories" like CESR and DORIS. These experiments use the $\Upsilon(4s)$ resonance, which decays predominantly into pairs of B−mesons. So a lot of experimental information about the beauty quark is already available. This information is used to make more detailed predictions about $b\bar{b}$ physics at the collider. Therefore a short review about known b−properties shall be given.

$B^{\pm}$ ($b\bar{u}$, $\bar{b}u$) and $B_d{}^0$ ($\bar{b}d$)[10] are copiously produced in the decay of the Υ (4s) and most of the data refers to these mesons. The $B_s{}^0$ is too heavy to be produced in (4s) decays. Probably the $\Upsilon(5s)$ will not decay in $B^0{}_s$ either [17]. It is certainly produced in continuum production, but has not been identified yet. A search for the spin one B^* mesons was made by CUSB [17] looking for gamma lines in $\Upsilon(5s)$ data, and a 50 MeV signal from the $B^* \rightarrow B\,\gamma$ transition was found. An overview of the B−mesons and their masses is given in table 3 [18].

Meson	quark assignment	spin	mass
B^-	$b\bar{u}$	0	5271 ± 3 MeV
B^0	$\bar{b}d$	0	5275 ± 3 MeV
B^*	$b\bar{u}$, $\bar{b}d$ (not separated)	1	≃ 5320 MeV
$B_s{}^0$	$\bar{b}s$	0	> 5430 MeV (?)

Table 3: Masses of B−mesons

[10] In this thesis I will chose the convention that a meson containing an anti−b quark is called a B−meson and vice versa (as recommended by the particle data group).

Fragmentation and semileptonic decay link the p_t of the beauty quark, which is calculable by QCD, to the p_t of the muon, which is measured by our experiment. Therefore Monte Carlo calculations of muon properties depend on the exact knowledge of fragmentation and decay.

The beauty fragmentation has been measured in e^+e^- continuum production. The B−mesons were tagged by leptons with large momenta transverse to the jet axis. In this way they are separated from charm decays. The distribution of the lepton momentum parallel to the jet axis was fitted varying the parameter ε. The average z value for the b was found to be 79 ± 3 %, which corresponds to an ε of about 0.015[11] [15] [90].

After the fragmentation the B hadrons decay by weak interaction. As there is no experimental data on B−baryons, the following refers only to B−mesons. First a few things about the theoretical framework of B−decays:

The B−meson decay should be determined by the decay vertex of the beauty quark:

$$b \rightarrow W^- c \ (V_{cb} \approx 0.04) \text{ or } b \rightarrow W^- u \ (V_{ub} < 0.008) \qquad \{4\}$$

In the spectator model, the light ("spectator") quark in the meson is not involved in the weak decay, it recombines in a later step with the beauty decay products. Some spectator diagrams are shown in figure 7 .

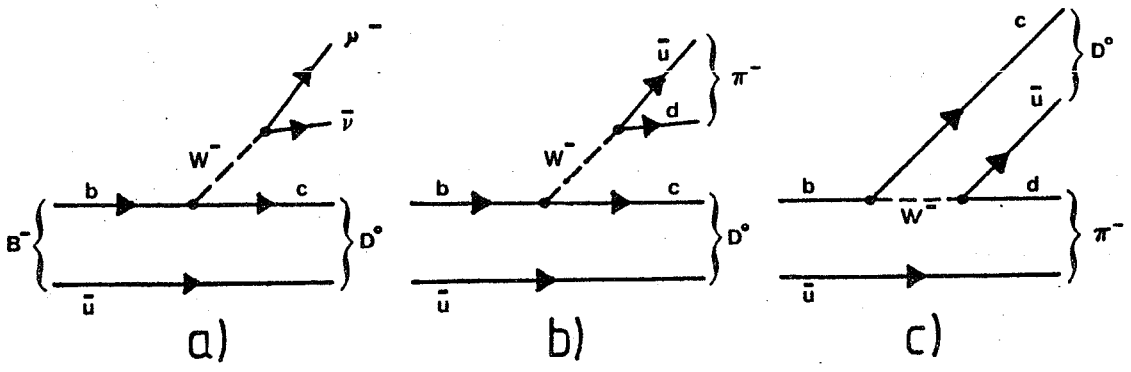

Figure 7: B−meson decay in the spectator model

[11] This ε depends somewhat on the exact fragmentation scheme use in the model (see Appendix)

From simple counting of the possible decay products of the W, an estimate of the leptonic decay branching ratio can be derived (The quark decays have to be multiplied by three as the quarks exist in three colour states):

$$W \rightarrow 3\ u\bar{d},\ 3\ c\bar{s},\ e\nu,\ \mu\nu,\ \tau\nu \qquad \{5\}$$

which gives a muonic branching ratio of 1/9 = 11%. In more detail the partial decay widths can be expressed by:

$$\Gamma = [G_f^2\ m_b^5\ /\ (192\ \pi^3)] \times (|V_{ib}|^2 \times C \times ph \qquad \{6\}$$

G_f is the Fermi coupling constant. V_{id} is the respective Kobayashi – Maskawa matrix element (V_{cb} or V_{ub}). C is a colour factor, which is one for decays into leptons and three for decays into quarks. ph is a phase space correction for decays into massive particles (c and τ).

The spectator model predicts equal branching ratios and lifetimes for all B – mesons ($B^{\pm}$, B^0_d and B^0_s). It is known that this prediction is incorrect in case of the D – mesons. Lifetimes and leptonic branching ratios of $D^{\pm}$, D^0 and F are different. Mechanisms which can lead to such differences are QCD corrections and non – spectator decays.

QCD corrections (fig. 8) generally enhance the hadronic decay modes.

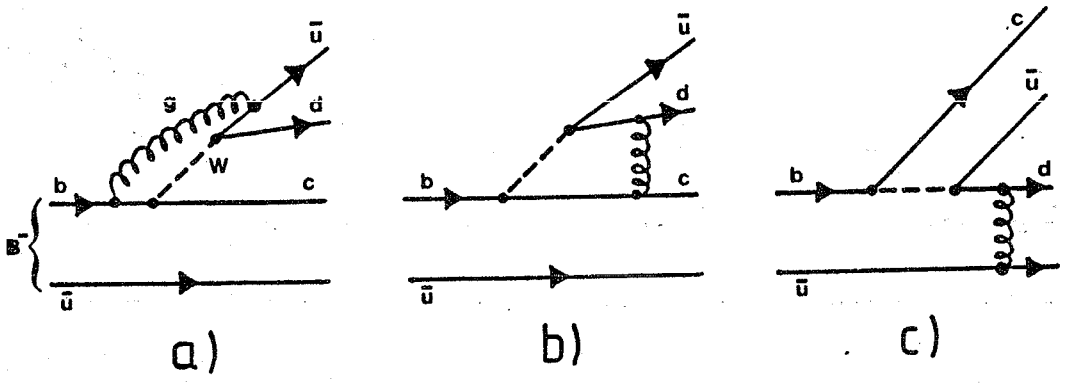

Figure 8: QCD corrections to the spectator model

The gluon exchange between the quark lines changes the colour flow in the diagram. The effect can be demonstrated with the diagrams 7 c) and 8 c): The decay in 7 c) is called colour suppressed as there is

only a 1/3 chance that the recombining quarks are in correct colour states. However, with QCD corrections [8 c)] the colour charges can be rearranged reducing the colour suppression. These corrections can be calculated in leading log approximation. Thus the hadronic widths should be proportional to 3.7 instead of 3 without QCD corrections. Differences between different mesons could be due to interference of final states ("colour clustering") [20].

In addition to the spectator diagrams there exist non−spectator diagrams of the B−decay (fig. 9).

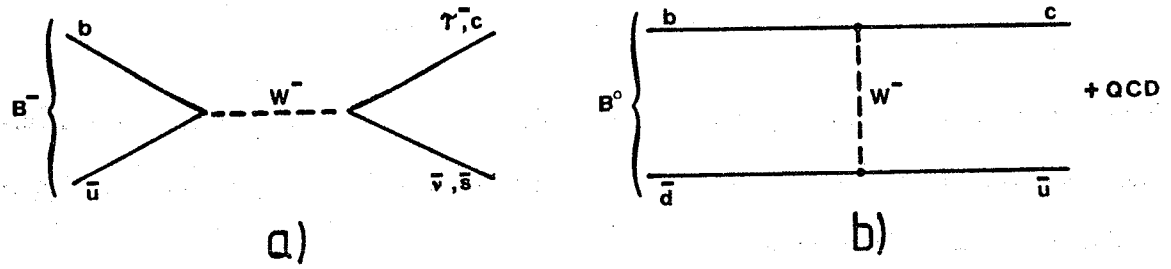

Figure 9: Non−spectator diagrams for B−meson decay

In principle they should give only minor contributions to the B−decays. Diagram 9 a) is heavily suppressed by the small V_{ub} matrix element of the Kobayashi−Maskawa matrix. Both decay modes 9 a) and b) are *helicity suppressed,* as the decaying mesons are in a pseudoscalar (0^-) state and couple to the V−A structure of the weak interaction. However, QCD correction can reduce the helicity suppression. If the up quark radiates a gluon, the $b\bar{u}$ system is not longer in a 0^- state and helicity suppression breaks down. The decays of the neutral B−mesons are especially affected by that, as their non−spectator decays are less K−M suppressed. Such effects could lead to differences in semileptonic branching ratios and lifetimes between neutral and charged B−mesons, as is observed for the D^+ and D^0.

Because of the large mass of the b−quark, QCD corrections and non−spectator decays should be less important for beauty mesons than they are for charmed mesons. Estimates for lifetimes of B−mesons predict $\tau(B^0) > 0.77\ \tau(B^+)$ [20] [21], which would be a smaller difference than that measured for charm mesons: $\tau(D^0) \approx 0.5\ \tau(D^+)$. In this thesis it is assumed that these differences can be neglected.

It shall be mentioned that the decay $B^+ \rightarrow \tau^+\nu$ is of special interest [fig. 9 a)]. Because it is purely leptonic it can be calculated exactly:

$$\Gamma(B^+ \rightarrow \tau\nu) = [G_f^2\, m_b^5/(192\,\pi^3)]\, |V_{ub}|^2\, 24\pi^2\, f_B^2\, (m_\tau^2 / m_B^4)\, (1-m_\tau^2/m_B^2)^2 \qquad \{7\}$$

f_B is the B−decay constant or pseudoscalar coupling constant (similar to f_π and f_K) which is given in a nonrelativistic model by:

$$f_B^2 = 12\, |\psi(0)|^2 / m_B \simeq 100-200\ \text{MeV} \qquad \{8\}$$

$\psi(0)$ is the B wavefunction at origin. f_B measures the probability that the $\bar{b}$ and the u coincide spatially and annihilate. We will need this factor later in the calculation of $B^0-\bar{B}^0$ oscillations. If V_{ub} is known, this decay would allow to measure f_B .

Having described the theoretical aspects of B−meson decays, we now review some experimental results. From the experimental point of view following properties are of interest:

- The B−meson lifetimes
- Semileptonic branching ratios
- The lepton momentum spectrum
- The momentum spectrum of the D−mesons from the B−decay
- The hadronic decay modes.

Branching ratios and lifetimes have been measured, but only for an unknown mixture of neutral and charged B's. The world average for the lifetime is 1.12 ± 0.2 ps [15]. As expected for a Kobayashi−Maskawa suppressed decay, this lifetime is rather long. The muonic branching ratio[12] was measured to be 11.7 ± 0.9 % [15]. This branching ratio comes very close to the one expected in the naive spectator model, so QCD corrections and non−spectator contributions may not be very important. There exists also a measurement of the colour suppressed decay $B \rightarrow J/\psi\ X$ which has a branching ratio of 1.4 ± 0.6 % [11]. This decay mode can be an important source for high p_t J/ψ at the collider.

[12] This was measured with B's from the Υ (4s). Measurements at continuum production give a value of 12.3 ± 0.9 %. The measurements agree within the errors, but they do not need to be the same as the B−meson mixture is different in resonance and continuum production.

The spectrum of leptons and D−mesons from B−decays is compared with ISAJET calculations in figure 10 [22]. For our purpose it is important that the Monte Carlo programs used to calculate $b\bar{b}$ physics correctly reproduce these spectra. For completeness it shall be mentioned that the lepton spectrum can be used to measure the b → u transition. As the up quark is lighter than the charm, the momentum spectrum of leptons from a b → u decay has a higher endpoint than from the b → c decay. From this a limit for b → u of < 8 % was derived [15].

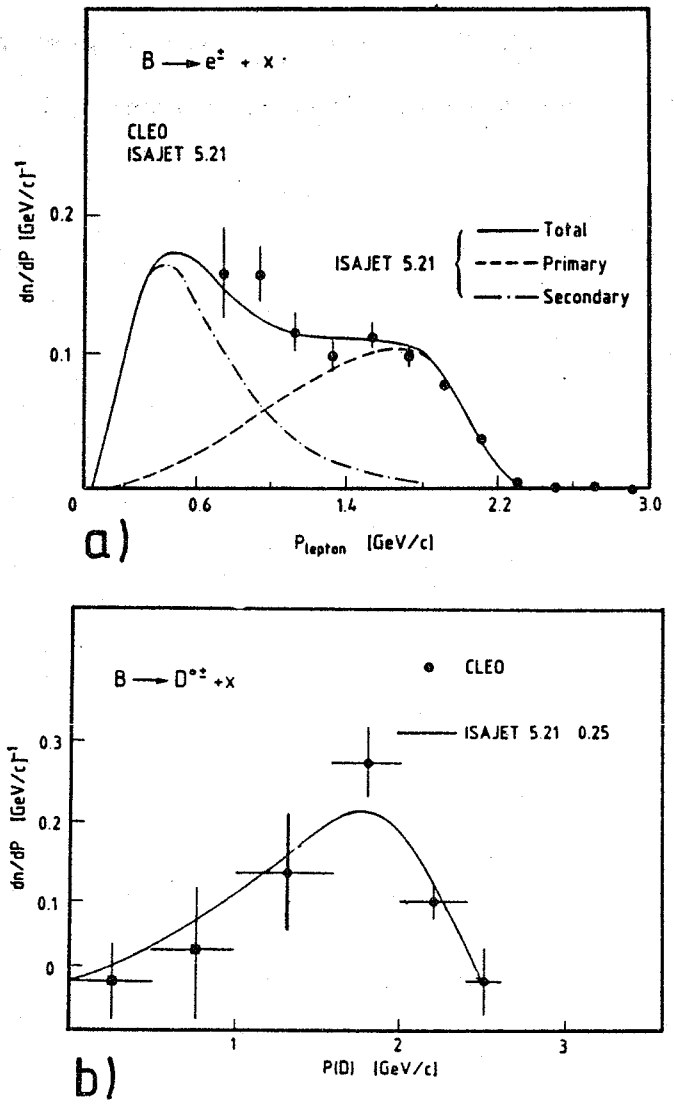

Figure 10: Kinematic properties of B−decays:
(a) lepton momentum spectrum (b) D momentum spectrum
The solid line represents the Isajet simulation of the B−decay.

The properties of hadronic decay modes are important as D−mesons from B−decays can give secondary leptons. Of special interest are two−body decays, e.g.:

$$B \rightarrow D\,\pi, \text{ or } \rightarrow D\,\rho$$

These two−body decays can give a larger momentum to the D's, as compared to three and more body decays, and secondary muons with high momenta become more likely [23]. Although some of these decay modes have been seen with low branching ratios [24], the overall fraction is still unknown.

In conclusion it can be said that the properties of B−mesons are basically understood. Nevertheless more information is needed, especially about lifetime and branching ratios separatly for the different B−mesons, about the role of two body decays, and about the properties of B−baryons.

2.7 Phenomenology of Flavour Mixing

As already mentioned, the quark states participating in the weak interaction are not mass eigenstates, but a mixture described by the Kobayashi – Maskawa matrix V_{ij} . The matrix elements V_{ij} can be parametrized as:

$$\begin{bmatrix} V_{ud} & V_{us} & V_{ub} \\ V_{cd} & V_{cs} & V_{cb} \\ V_{td} & V_{ts} & V_{tb} \end{bmatrix} \qquad \begin{bmatrix} c_1 & c_3 s_1 & s_1 s_3 \\ -s_1 c_2 & c_1 c_2 c_3 - s_2 s_3 e^{i\delta} & c_1 c_2 s_3 + c_3 s_2 e^{i\delta} \\ s_1 s_2 & -c_1 c_3 s_2 - c_2 s_3 e^{i\delta} & -c_1 s_2 s_3 + c_2 c_3 e^{i\delta} \end{bmatrix}$$

with $c_i = \cos(\Theta_i)$ and $s_i = \sin(\Theta_i)$. Θ_1, Θ_2 and Θ_3 are three mixing angles, and δ, a phase which may be responsible for CP violation.

Some of the matrix elements have been measured, the remaining elements can be calculated (90% confidence level of $|V_{ij}|$ [37]):

$$\begin{bmatrix} 0.9743 - 0.9757 & 0.219 - 0.225 & 0.000 - 0.008 \\ 0.219 - 0.225 & 0.9733 - 0.9748 & 0.039 - 0.050 \\ 0.002 - 0.017 & 0.037 - 0.048 & 0.9987 - 0.9993 \end{bmatrix}$$

The matrix is almost diagonal. This leads to Wolfenstein's parametrization [25], which expresses the matrix in terms of λ, with $\lambda = \sin(\Theta_c) = 0.23$ (Θ_c is the Cabibbo angle):

$$\begin{bmatrix} 1 - \lambda^2/2 & \lambda & A\lambda^3(\rho - i\eta) \\ -\lambda & 1 - \lambda^2/2 & A\lambda^2 \\ A\lambda^3(1-\rho-i\eta) & -A\lambda^2 & 1 \end{bmatrix} + O(\lambda^3)$$

$$A = 1.0 \pm 0.2 \qquad \rho^2 + \eta^2 < 0.65$$

This Kobayashi Maskawa mixing of the quarks allows transitions between neutral mesons and their antimesons via second order weak interaction, which change their flavour quantum number F by ± 2 (F being "strangeness","charmness","beautyness", etc.), like $K^0 \rightarrow \bar{K}^0$, $D^0 \rightarrow \bar{D}^0$, $B^0 \rightarrow \bar{B}^0$, $T^0 \rightarrow \bar{T}^0$ and vice versa. The relevant "Box" diagrams for such transitions are shown in figure 11 .

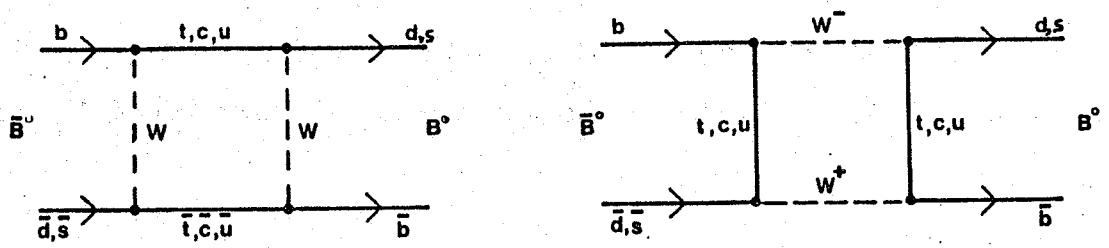

Figure 11: Box diagrams for $\Delta B = 2$ *weak transitions*

The phenomenology of these transitions can be derived as follows: The flavour states M^0 and $\overline{M}^0$ (M represents K,D,B and T) are not eigenstates of the weak interaction, but a linear combination ("mixing") of weak eigenstates M_1 and M_2 (assuming no CP−violation):

$$M^0 = (M_1 + M_2)/\sqrt{2} \quad \overline{M}^0 = (M_1 - M_2)/\sqrt{2} \qquad \{9\}$$

These states may have slightly different masses and decay widths m_1, Γ_1 and m_2, Γ_2 respectively, and their time evolution will be[13] (in the particle's rest frame):

$$a_i(t) = a_i(0)\exp(-im_it - \Gamma_it/2) \quad (i = 1,2) \qquad \{10\}$$

If at $t=0$ a pure M^0 state is produced, then:

$$a_1(0) = a_2(0) = 1/\sqrt{2} \qquad \{11\}$$

The probablity of observing an M^0 state will develop according to:

$$1/2\,|a_1(t)+a_2(t)|^2 = 1/2\exp(-\Gamma t)\,[\,1 + \cos(\Delta mt)] \qquad \{12\}$$

and that for an $\overline{M}^0$ state:

$$1/2\,|a_1(t)-a_2(t)|^2 = 1/2\exp(-\Gamma t)\,[\,1 - \cos(\Delta mt)] \qquad \{13\}$$

[13] I use units with $\hbar = c = 1$

with $\Delta m = |m_1 - m_2|$ and $\Gamma = \Gamma_1 = \Gamma_2$ (for simplicity assuming that the decay widths of both states are equal, which should be a good approximation for the D^0 and B^0, but is wrong for the K^0). Thus the system *oscillates* with the frequency Δm between the meson and the antimeson state, damped by the lifetime $\tau = 1/\Gamma$. If the oscillation frequency Δm is very high, only time integrated quantities can be measured by experiments. Therefore we integrate {13} from $t = 0$ to infinity. Normalizing by the total decay rate Γ we obtain the probability to observe a $\overline{M}^0$ meson instead of the original M^0:

$$\chi = (1/2)\,(\Delta m/\Gamma)^2 \,/\, [1 + (\Delta m/\Gamma)^2] \qquad \{14\}$$

Thus the transition probability depends on the ratio of mass difference to decay width. This is easy to understand, as the mass difference is proportional to the oscillation frequency and the decay width is the inverse of the lifetime. If the lifetime is very short, the system decays faster than it changes state, so χ is close to zero. If the lifetime is much longer than the oscillation time, many transitions occur before the meson decays. The system is in a $\overline{M}^0$ state for about half its lifetime, and χ is close to 0.5.

The strength of these oscillations is often described by the Pais and Treiman parameter r, which is related to χ by:

$$r = \chi / (1 - \chi) = (\Delta m / \Gamma)^2 \,/\, [\, 2 + (\Delta m / \Gamma)^2 \,] \qquad \{15\}$$

If there is a difference in the widths Γ_1 and Γ_2, the exact formula becomes:

$$r = [(\Delta m / \Gamma)^2 + (\Delta\Gamma / 2\Gamma)^2] \,/\, [2 + (\Delta m / \Gamma)^2 - (\Delta\Gamma / \Gamma)^2] \qquad \{16\}$$

$\Delta\Gamma$ is the difference of the decay widths.

These oscillations are well known in the $K^0 - \overline{K}^0$ system, and a review of these physics can be found in [26]. It is very interesting to know, whether these transitions occur with other neutral mesons like the D^0 and the B^0 [29]. Experimental searches for $D^0 - \overline{D}^0$ oscillations have not shown any observable effect [30]. Qualitatively, this can be understood as follows: The decay of a charm quark into a strange quark is within one quark family and therefore K − M allowed ($V_{cs} = 1 - 1/2\,\lambda^2$). This re-

sults in a lifetime which is short compared to the oscillation time, hence no observable oscillations occur. The same argument holds for oscillations in the T^0 system, as the top will decay into a beauty quark very quickly. This is different for the B−system. The beauty quark decays into a charm quark, which belongs to a different family. Hence such a decay is Kobayashi−Maskawa suppressed ($V_{cb} = \lambda^2$). Therefore the B lifetime might be long enough to allow significant oscillations. In fact the B−lifetime has been measured to be 1.2 ps compared to the lifetime of the D^0 of 0.4 ps.

Of course the strength of such oscillations depends also on the mass difference Δm. This Δm can be evaluated from the box diagrams (fig. 11). We have to distinguish between the two different B^0 mesons: the B_d^0 and the B_s^0 . Before we discuss the exact formulae for Δm, we can give a rough estimate of the relative magnitude of Δm for these two mesons:

The contribution of each diagram is proportional to the product of the Kobayashi−Maskawa couplings at the vertices. The different Kobayashi−Maskawa couplings of d− and s−quarks lead therefore to differences in Δm for $B^0{}_d$ and $B^0{}_s$. This is demonstrated in table 4 .

system	via	involved V_{ij}'s	Δm
$b\bar{d}$	c	$(V_{cb}^* V_{cd})^2 = [A\lambda^2 \lambda]^2$	$\propto \lambda^6$
$b\bar{d}$	t	$(V_{tb}^* V_{td})^2 = [1\ A\lambda^3(1-\rho-i\eta)]^2$	$\propto \lambda^6$
$b\bar{s}$	c	$(V_{cb}^* V_{cs})^2 = [A\lambda^2\ (1-1/2\lambda^2)]^2$	$\propto \lambda^4$
$b\bar{s}$	t	$(V_{tb}^* V_{ts})^2 = (\ 1\ A\lambda^2\ )^2$	$\propto \lambda^4$

Table 4: Kobayashi−Maskawa couplings for B_d^0 and B_s^0

We realize that Δm in the B_d^0 system is about a factor $\lambda^2 \simeq 0.05$ less than in the B_s^0 system[14]. Hence it is in the B_s^0 channel that significant oscillations may be expected, in the B_d^0 channel the effect should be smaller. These very simple arguments are confirmed by quantitative calculations [33].

If the box−diagrams for B^0 are evaluated the expression for Δm becomes:

[14] A more detailed calculation gives $\Delta m(B^0{}_d)/\Delta m(B^0{}_s) < 0.21$.

$$\Delta m = |(G_f^2/6\pi^2)\, B\, f_B^2\, m_b\, m_w^2\, F(m_c,m_t,\lambda)| \qquad \{17\}$$

Apart from well known factors like the Fermi coupling constant G_f, following terms appear:

- *$F(m_c,m_t,\lambda)$:* This expresses the dependence on the charm mass, the top mass and the Kobayashi – Maskawa matrix elements (represented by λ). It turns out that the diagram with the double top exchange is dominant over the charm (and in principle the u) exchange, as the heaviest possible intermediate state is preferred. The reason for this is the GIM mechanism, which suppresses flavour changing neutral reactions if the involved quarks have similar masses [35]. Therefore Δm depends strongly on the top mass, approximately like m_{top}^2. The heavier the top the stronger the $B^0 - \bar{B}^0$ oscillations. A good approximation[15] of this factor is (for B^0_s):

$$F \approx \eta_{cc}\,(V_{bc}^*\, V_{sc})^2\, m_c^2/m_W^2 + \eta_{tt}\,(V_{bt}^*\, V_{st})^2\, m_t^2/m_W^2 + 2\,\eta_{ct}\,(V_{bc}^* V_{sc} V_{bt}^* V_{st})\, m_c m_t/m_W^2 \qquad \{18\}$$

  η_{cc}, η_{tt} and η_{ct} are QCD correction factors. η_{tt}, which appears in the dominant term, should be in the range 0.78 – 0.85 for values of Λ_{QCD} of 500 – 100 MeV [33]. For B^0_d only the respective Kobayashi – Maskawa matrix elements have to be replaced in {18} .

- *f_B:* The pseudoscalar coupling constant, or B – decay constant, which was already introduced in the previous chapter (see formulae {7} and {8}). f_B tells the probability that the b – quark and the d – or s – quark coincide spatially. Its numerical value is estimated to be 100 – 200 MeV. Of course f_B need not be the same for B^0_d and B^0_s, but they should be similar. Calculations using QCD sum rules suggest $f_{Bd} \simeq 110$ MeV, $f_{Bs} \simeq 150$ MeV [34].

- *The bag parameter B:* This factor comes from the normalization of the B – meson wavefunction. The estimated value is close to one, with an error of a factor of two. Both factors, f_B and B, are related by following formula (analogous for B^0_d):

---

[15] This formula agrees very well with the exact calculation for top masses below 40 GeV/c². At 60 GeV/c² the deviation is about – 10%. The m_t^2 dependence approaches asymptotically $m_t^2/4$ if the top mass increases. [36].

$$4/3\ B\ f_{Bs}^{\ 2}\ m_b = \langle B_s^0 |\ [b\ \gamma_\mu(1-\gamma_5)\ s]^2\ |\bar{B}_s^0\rangle \qquad \{19\}$$

Many of the parameters introduced above have large uncertainties, and a precise prediction of the strength of $B_s^0 - \bar{B}_s^0$ oscillations is at the moment not possible. Theoretical estimates of χ are in a range of 0.10 to 0.48 for B^0_s, which means that substantial oscillations are expected. In the case of B^0_d an additional uncertainty arises from the K−M matrix element V_{td}, which is determined less precise than V_{ts} . Even for a fixed value of m_{top} χ_d can vary within orders of magnitude[16]. The expected χ values for B_d^0 and B_s^0 depending on the mass of the top quark are shown in figure 12 .

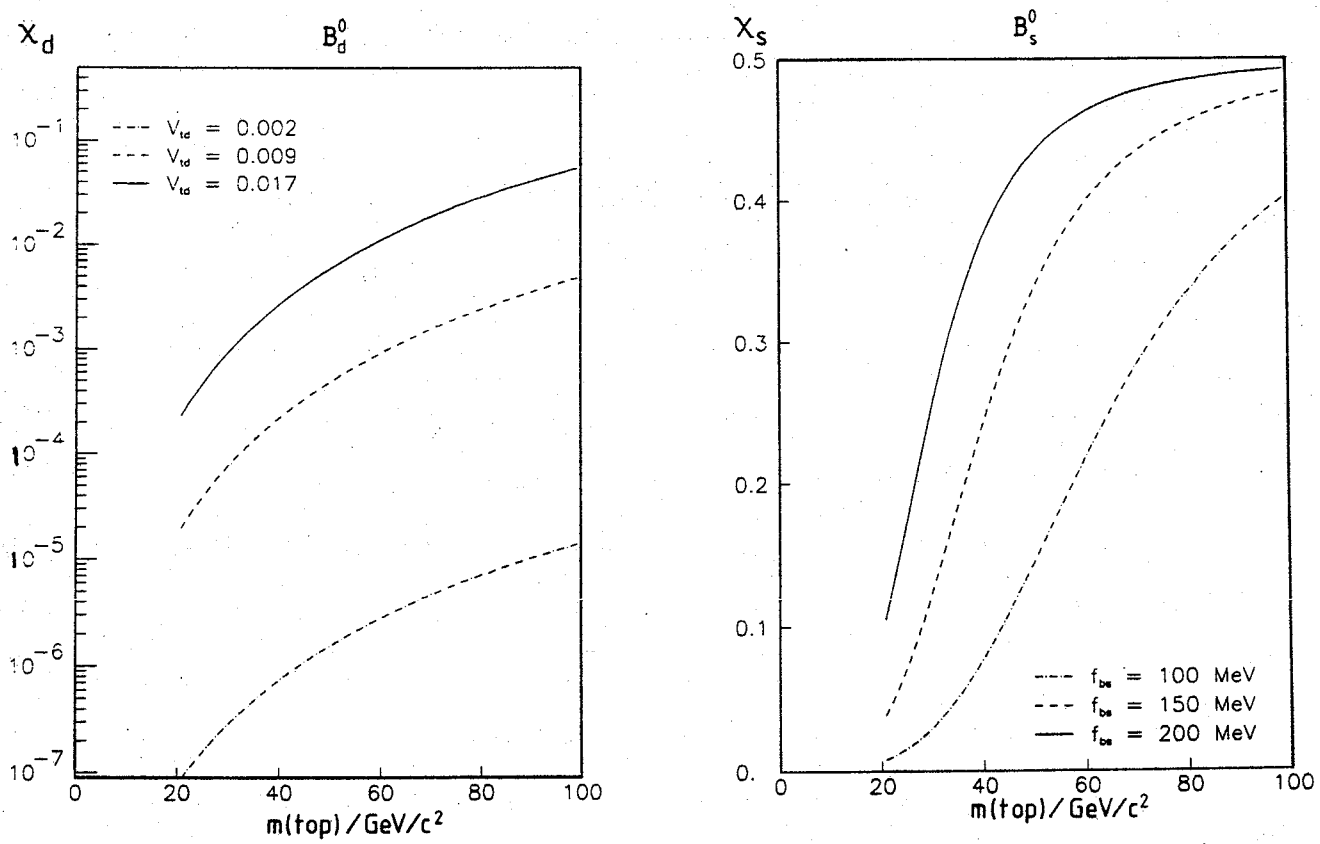

Figure 12: χ − values for B_d^0 and B_s^0 oscillations versus the mass of the top quark. If not noted otherwise, following values were used:
$B = 1, f_B = 100\ MeV, V_{ts} = 0.04, \eta_{tt} = 0.85$
(note the different scales)

[16] If there exist only the three known families of quarks and leptons, the limits on V_{td} are: 0.002 − 0.017 [37].

The experimental signature of such $B^0 - \overline{B}^0$ oscillations would be a high rate of *like−sign* dimuons. In normal $b\overline{b}$ production most of the dimuons will be unlike−sign, as the b decays into a μ^- and the $\overline{b}$ into a μ^+. However, if for example the $\overline{b}$ would hadronize into a B_s^0, which then oscillates, a fraction of these B_s^0 would become a $\overline{B}^0$, which decays into a μ^- and gives a like−sign dimuon event. The fraction of like−sign events is equal to χ (analoguos for B^0_d):

$$N(B^0_s \rightarrow \overline{B}^0_s \rightarrow \mu^-)/N(B^0_s \rightarrow \mu^{\pm}) = \chi$$

The ratio of like−sign to unlike−sign events is given by r:

$$N(B_s^0 \rightarrow \overline{B}_s \rightarrow \mu^-)/N(B_s^0 \rightarrow \mu^+) = r$$

For full mixing ($\chi = 0.5$; $r = 1$), and if only B_s^0 mesons would be produced, there would be as many like as unlike−sign dimuons. In reality things are not so simple:

- Only a fraction of the b−quarks hadronizes into B_s^0 mesons, most of them give B_d^0 mesons, which mix little, $B^{\pm}$ mesons and B−baryons, which do not mix. The probability to pick up a strange quark in order to form a B_s^0−meson (f_s) is only 12 % to 20 % [38]
- Like−sign dimuons can also come from the second generation decay of one of the beauty quarks. Although muons from second generation decays are heavily suppressed by cuts on the muon p_t, this background has to be taken into account.
- Dimuons from charm decays will only give unlike−sign events, and cannot fake $B^0 - \overline{B}^0$ oscillations. However, a high fraction of dimuons coming from charm production will dilute the effect of oscillations and it can be difficult to extract a significant signal. Also the contribution from Drell−Yan production and Υ decays has to be considered. Here an isolation requirement helps to remove such events.

All these effects have to be studied in order to predict a possible effect of $B^0 - \overline{B}^0$ oscillations and its significance. A variable which is sensitive to $B^0 - \overline{B}^0$ oscillations and which can be measured easily is:

$$R = (N^{++} + N^{--}) / (N^{+-}) \qquad \{20\}$$

N^{++},N^{--} and N^{+-} are the numbers of like− and unlike−sign dimuons from heavy flavour decays.

Searches for $B^0 - \overline{B}^0$ oscillations have been made by several experiments: The CLEO collaboration published an upper limit for χ_d of 0.19 at 90% confidence level [27]. Recently the ARGUS collaboration reported a positive signal for $B^0{}_d$ oscillations. They claim a mixing parameter $\chi = 0.19 \pm 0.07$ [69]. Although this value seems to be surprisingly large, it is still compatible with the Standard Model. However, it requires large values of V_{td}, $(B_{Bd} \times f_{Bd}{}^2)$ and a large mass of the top−quark (see formula {17} and figure 12). ARGUS derives a lower limit of 50 GeV/c^2 for m_{top} from their result (see also reference [71]). Both experiments, CLEO and ARGUS, use B−mesons from the Υ(4s) resonance, which does not decay into $B^0{}_s$. They are therefore not sensitive to $B^0{}_s$ oscillations. The MARK II and the JADE experiment use e^+e^- continuum data above the $B^0{}_s$ threshold. The two experiments quote upper limits on $B^0 - \overline{B}^0$ oscillations [31] [32]. These limits apply to a mixture of $B^0{}_d$ and $B^0{}_s$.

3. EXPERIMENTAL SETUP

3.1 The $p\bar{p}$ Collider

At the Aachen Neutrino Conference in 1976, C. Rubbia, P. McIntyre and D. Cline proposed to convert an existing proton synchrotron into a proton – antiproton collider [41]. Such a machine should achieve sufficient energy to produce the $W^{\pm}$ and Z^0 predicted by the Glashow – Salam – Weinberg theory. In fixed target machines of beam energy E, the available centre of mass energy is:

$$\sqrt{s} \approx \sqrt{2ME} \quad \text{M being the target mass (1 GeV/c}^2\text{)} \qquad \{21\}$$

For a beam energy of 300 GeV the available centre of mass energy is only $\sqrt{s}$ = 25 GeV, which is far too low to create the $W^{\pm}$ and Z^0. In a colliding beam machine the centre of mass energy is twice the beam energy. Thus about 600 GeV could be reached, enough to create the W and Z. The main problem of such a proton – antiproton collider was to construct an antiproton source capable to deliver sufficient antiprotons. Otherwise the luminosity which determines the interaction rate[17] would be too low. It was S. van der Meer's invention of the stochastic cooling technique [42] which made such a source possible. After successful tests the $p\bar{p}$ project was approved at CERN in 1978. In 1981 the first $p\bar{p}$ collisions were recorded and in early 1982 the $W^{\pm}$ was discovered [43], followed by the discovery of the Z^0 in 1983 [44] [45].

The CERN accelerator complex is shown in figure 13 . Protons are accelerated in the Proton Synchrotron (PS) to 26 GeV/c. From there they can either be injected into the Super Proton Synchrotron (SPS), or they can be used for antiproton production, in which case they are directed onto a copper target. This antiproton production is very inefficient, only 6×10^6 $\bar{p}$ are collected for 10^{13} protons on the target. These antiprotons have a large momentum spread around the production maximum of 3.5 GeV/c. Before they can be used in the collider, they have to be collected over a long time, and their momentum spread has to be reduced (= cooled). This is achieved in a small storage ring, the Antiproton Accumulator (AA). The idea of stochastic cooling is to measure the average position and

[17] The interaction rate is luminosity times cross – section. The cross – section of the $W \rightarrow \mu \nu$ is 0.6 nb, with a luminosity of 10^{29} $cm^{-2}s^{-1}$ the production rate is 150 W's per month of continuous running

momentum of the antiprotons in the beam, and to correct them later on. Doing this in each revolution of the beam over a long time a large improvement of the beam quality is achieved. In 24 hours of collecting and cooling the AA develops a stack of about 10^{11} antiprotons. They are then extracted and sent back to the PS, where they are accelerated to 26 GeV/c. From there they are injected in the SPS now rotating in a direction opposite to that of the protons. Then protons and antiprotons are accelerated synchronously to the desired energy and kept there for several hours. In 1983 the beam energy was 273 GeV, in 1984 and 1985 this was increased to 315 GeV. Typically there are three bunches, each containing 10^{11} protons, colliding against three bunches with 10^{10} antiprotons each. The bunch crossing time in this mode is 8 μsec. The luminosity was 1.6×10^{29} cm^{-2}s^{-1} in 1983 and was improved up to 5×10^{29} cm^{-2}s^{-1} in 1984 and 85. Beam lifetimes of the order of 24 hours were achieved.

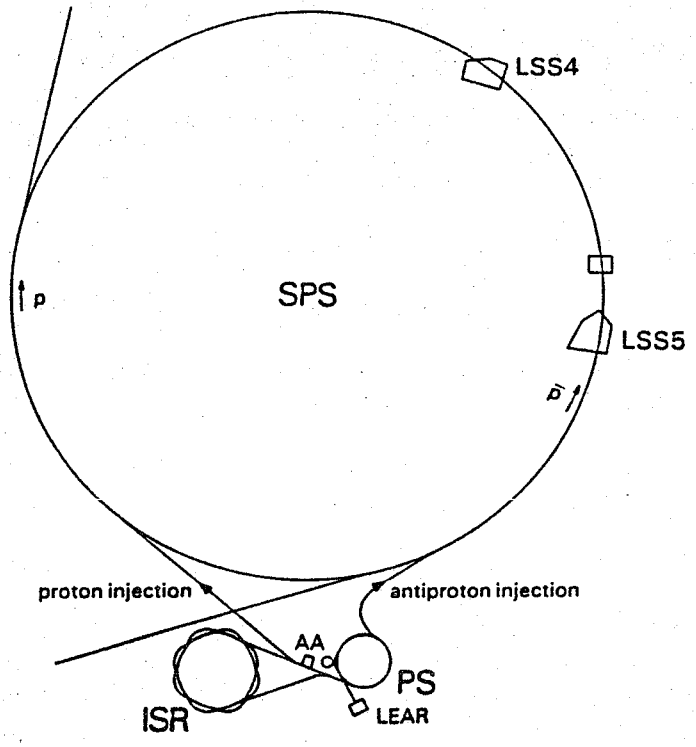

Figure 13: The CERN accelerator complex.
The UA1 detector is located in the "LSS5" experimental area.

3.2 The UA1 Detector

For the $p\bar{p}$ project two major detectors were initially approved: UA1 and UA2. UA1 is a hermetic detector, covering almost the full solid angle around the interaction region. It is able to identify and measure leptons, like electrons and muons, and hadronic jets. A special feature of the UA1 detector is its ability to identify neutrinos by the missing energy technique.

The detector consists of several components, each specialized for a certain purpose. A view of the UA1 detector and of its main components is shown in figures 14 and 15 .

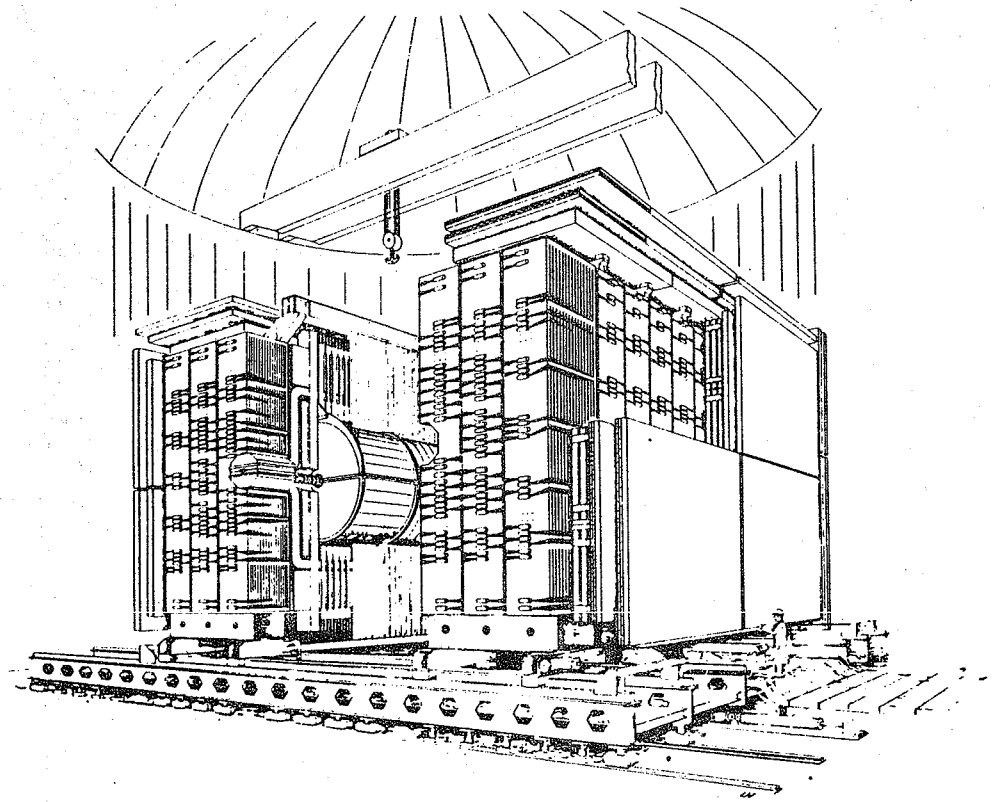

Figure 14: Artist's view of the UA1 detector. It's two halves are separated so the innermost parts can be seen.

- The innermost part is the Central Detector ("CD"), a large cylindrical drift chamber. It measures the tracks of charged particles. The CD operates in a magnetic dipole field of 0.7 T. The momenta of charged particles can be determined from the curvature of their tracks.

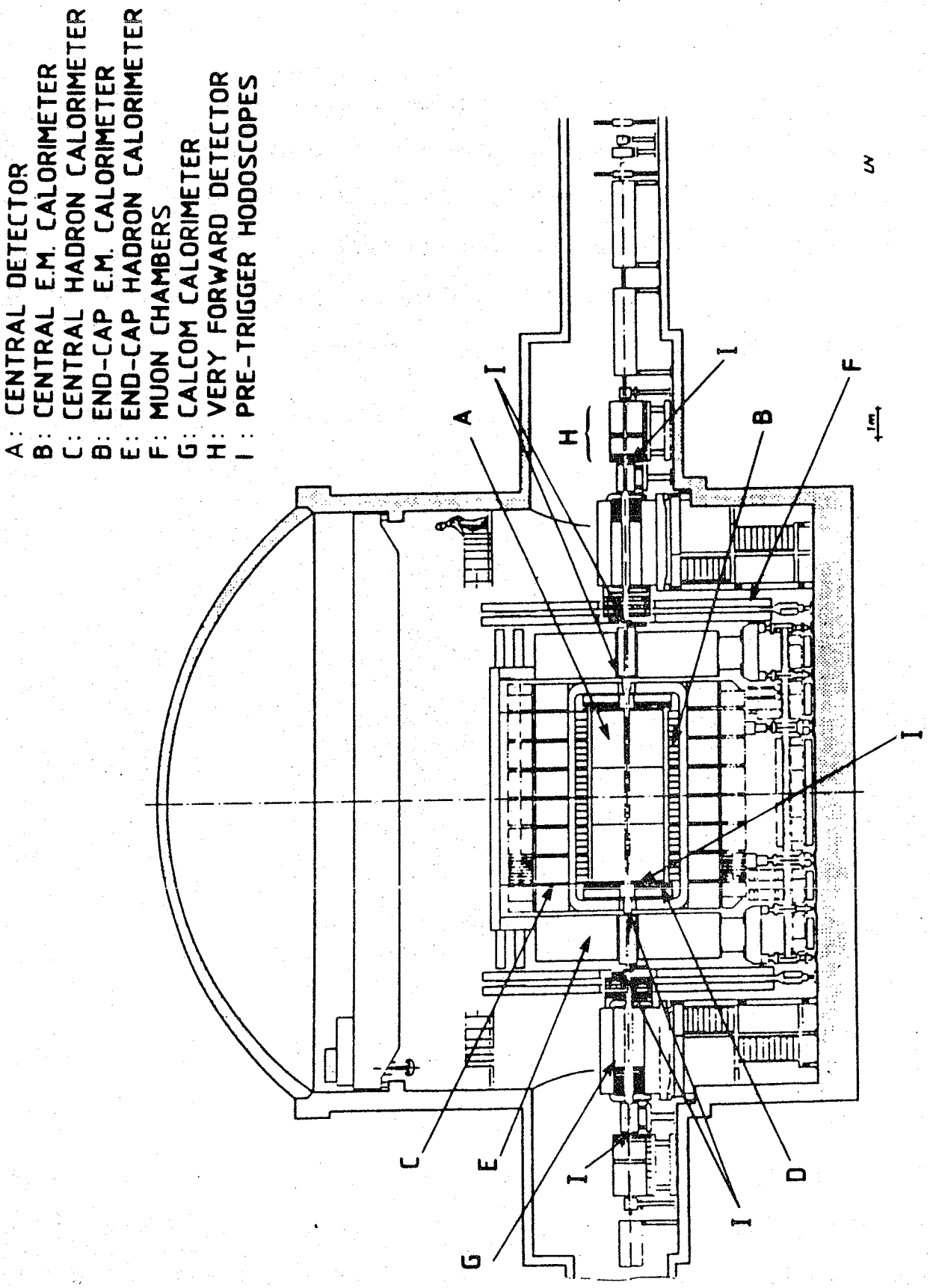

Figure 15: Cross – section through the UA1 detector

- The CD is surrounded by calorimeters. The electromagnetic ("EM") part are the "gondolas" in the central (barrel) region and the "bouchons" in the forward region. They are of the lead scintillator sandwich type and are designed to identify electromagnetic showers from electrons and gammas, and to measure their energy. Hadrons in general deposit only a small fraction of their energy in the EM calorimeters. The remaining energy is then measured in the hadronic calorimeters, the C's and I's, which which surround the gondolas and bouchons. The hadron calorimeters are made out of iron and scintillator plates. The magnetic coil is placed between the gondolas and the C's. The iron of the C's also serves as the return yoke for the magnetic flux. In addition, there are forward and very forward calorimeters along the beampipe (both of the electromagnetic and of the hadronic type). Altogether the calorimeters cover the complete interaction region down to an angle of 0.2 degree to the beam. This allows the transverse energy of a neutrino to be measured. A neutrino escapes the detector without depositing any energy in the calorimeters. Because of momentum conservation the energy distribution in the calorimeters shows an imbalance. This can be used to determine the neutrino's transverse momentum.
- Almost the whole UA1 detector is covered with drift chambers for muon detection ("muon chambers"). Muons are able to pass all the material of the calorimeters and additional iron, which absorb essentially all the hadrons. The muon tracks are then recorded in the muon chambers. In addition to the muon chambers, there are plastic streamer tubes (Iarocci chambers) placed between the calorimeters and the muon chambers. They deliver additional points to the muon tracks measured in the muon chambers and can be used to improve the muon identification . In the sidewalls there are three planes of Iarocci chambers imbedded in magnetized iron. They can be used for a second momentum measurement of the muon track independent from the CD.

In the following chapters the detector components are described in more detail. Additional information on the UA1 detector can be found in [46].

3.2.1 Central Detector

The UA1 central detector is shown in figure 16 . It is a cylindrical array of drift chambers of 2.2 m diameter and of 6 m length. It is segmented into 8 modules, which are divided into drift volumes by wire planes. The separation of these planes is 18 cm. There are two types of wire planes, arranged alternately: One consists of a single layer of field wires, normally kept at − 27 kV. They generate the electric field which causes the electrons to drift to the sense wires. The sense wires are in the other type of wire plane: It has three layers of wires, the outer layers have, alternately, field shaping wires (at − 3 kV) and sense wires. The inner layer has field shaping wires at − 2 kV.

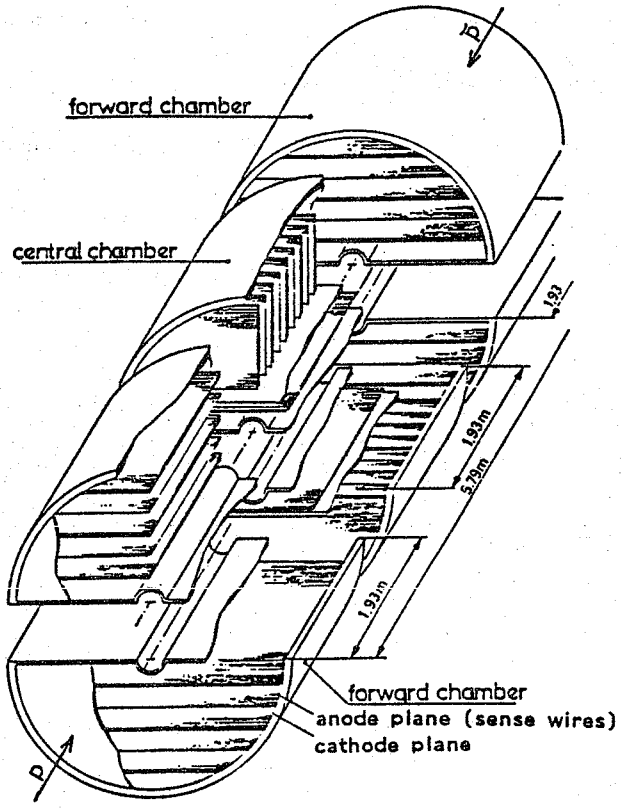

Figure 16: The UA1 central drift chamber

The sense wires collect the electrons from their respective sides of the drift volume. Altogether there are about 6000 sense wires and 17000 field wires.

The chambers are filled with an argon−ethane mixture (60% ethane, 40% argon). The electrons, which are produced by ionizing particles, drift along the homogeneous electric field towards the sense wires. Because of the magnetic field the drift direction is rotated by 23 ° with respect to the direction of the electric field. Close to the sense wires the field becomes larger and gas amplification occurs. The charge is collected and measured at both ends of the sense wires. From the drift time the position can be measured with a precision of typically 290 μm. The coordinate along the wire is measured by charge division with an accuracy of 1.7% of the wire length (which corresponds to 1.7 to 3.7 cm). For this purpose both the charge and the time information is recorded by the readout electronics. This readout electronics has a capability to detect multiple hits, even if the pulses overlap. This improves the resolution for nearby tracks.

3.2.2 Calorimeters

The central electromagnetic calorimeters, the "gondolas", cover an angular range of 25^0 to 155^0 in θ corresponding to ± 1.5 in pseudorapidity: $\eta = -\ln[\tan(\theta/2)]$. There are 48 gondolas, 24 to each side of the CD. The gondolas are semi−circular with an inner radius of 130 cm. Thus they fit around the CD. A pair of gondolas is shown in figure 17 .

They are constructed from a sandwich of 1.2 mm lead sheets and 1.5 mm scintillator sheets. The gondolas are organized into four samplings of 3.3, 6.6, 9.9 and 6.6 radiation lengths, which are read out individually. This gives a total of 29 radiation lengths (at normal incidence), which contain practically all electromagnetic showers completely. The division into four samplings allows the measurement of the shower profile in depth, which is different for electromagnetic showers and showers from interacting hadrons. This helps to improve the identification of electrons and gammas. Each sampling is read out at both sides via wavelength shifter bars (BBQ) followed by light guides. The BBQ bars are read out by one phototube at each end. Altogether four phototubes measure the light, one from each corner of a gondola sampling separately. The relative differences of the light intensities measured by these four tubes are used to determine the position of the shower within the gondola. This is especially important for the azimuthal angle ϕ, as one gondola covers 180^0 in azimuth. The resolution in ϕ is

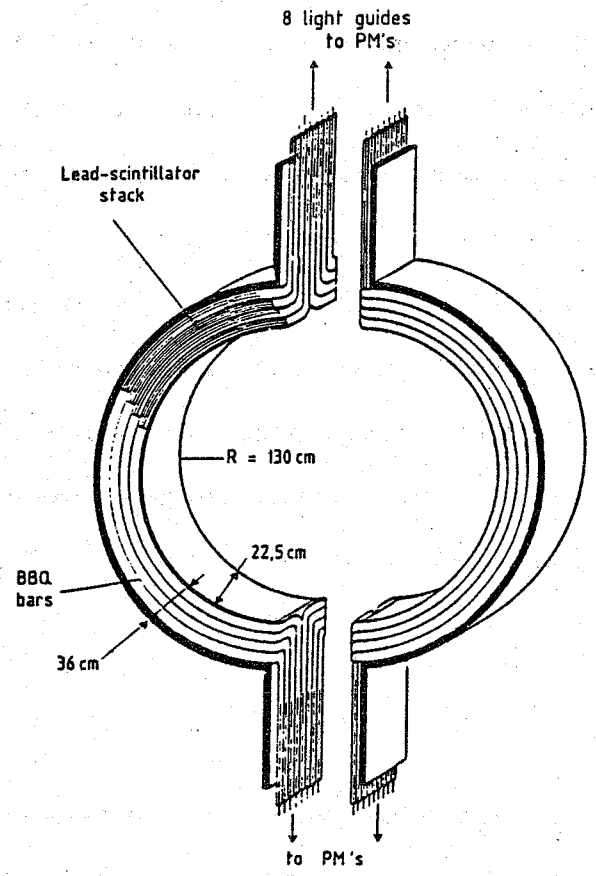

Figure 17: Gondola elements

measured to be $0.24/\sqrt{E}$ (in radians, E in GeV). Although the longitudinal position is given by the 22.5 cm width of one Gondola, it can be improved with a resolution of 6.3 cm/$\sqrt{E}$ (E in GeV). This method works only, if the gondola element is hit by one particle. If two (or more) particles hit one element, an average position is measured, which may not correspond to either particle. E.g., if a gondola is hit at both ends, the hit is reconstructed in the middle of the cell. The energy resolution of the gondolas is $\Delta E / E = 15\% / \sqrt{E}$ (E in GeV).

The endcaps of the electromagnetic calorimeters, the "bouchons", cover the angular range from 5^0 to 25^0 and from 155^0 to 185^0 in θ. This extends the pseudorapidity range to ± 3. The bouchons are circular with an inner radius of 30 cm and an outer radius of 180 cm. They are subdivided into 32 "petals" (fig. 18). Like the Gondolas they are constructed out of lead and scintillator sheets (4 mm lead and 6 mm scintillator) and divided into four independent samplings of 4,7,9 and 7 radiation lengths.

Table 5: The UA1 calorimeters

Calorimeter		Angular coverage θ (°)	Thickness		Cell size		Sampling step	Segmentation in depth	Resolution
			No. rad. lengths	No. abs. lengths	Δθ (°)	Δφ (°)			
Barrel	e.m.: gondolas	25-155	26/sin θ	1.1/sin θ	5	180	1.2 mm Pb 1.5 mm scint.	3.3/6.6/9.9/6.6 X_0	$0.15/\sqrt{E}$
	hadr.: c's		-	5.0/sin θ	15	18	50 mm Fe 10 mm scint.	2.5/2.5 λ	$0.8/\sqrt{E}$
End-caps	e.m.: bouchons	5-25	27/cos θ	1.1/cos θ	20	11	4 mm Pb 6 mm scint.	4/7/9/7 X_0	$0.12/\sqrt{E_T}$
	hadr.: I's	155-175	-	7.1/cos θ	5	10	50 mm Fe 10 mm scint.	3.5/3.5 λ	$0.8/\sqrt{E}$
Calcom	e.m.	0.7-5	30	1.2	4	45	3 mm Pb 3 mm scint.	4 × 7.5 X_0	$0.15/\sqrt{E}$
	hadr.	175-179.3	-	10.2	-	-	40 mm Fe 8 mm scint.	6 × 1.7 λ	$0.8/\sqrt{E}$
Very forward	e.m.	0.2-0.7	24.5	1.0	0.5	90	3 mm Pb 6 mm scint.	5.7/5.3/5.8/7.7 X_0	$0.15/\sqrt{E}$
	hadr.	179.3-179.8	-	5.7	0.5	90	40 mm Fe 10 mm scint.	5 × 1.25 λ	$0.8/\sqrt{E}$

Each sampling is read out by one phototube at the outer edge of the petal. The attenuation length of the scintillator was chosen such that the light intensity measured at the phototube is approximately proportional to $E_t = E \sin\theta$. The position of the shower is measured by two orthogonal planes of proportional tubes, which are placed between the second and third samplings. Thus the shower centre can be measured with a precision of ± 2 mm. Knowing the attenuation length of the scintillator and the position of the shower, its energy can be calculated. The transverse energy resolution of the bouchons is $\Delta E_t / E_t = 12\% / \sqrt{E_t}$ (E_t in GeV).

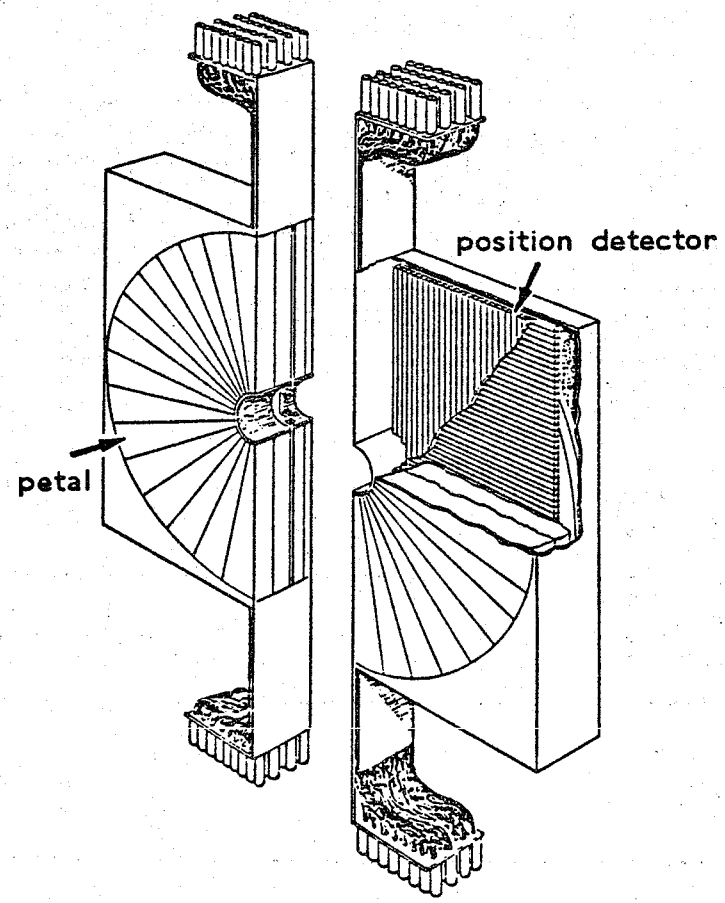

Figure 18: Bouchon, including position detectors

The hadronic calorimeters surround the electromagnetic calorimeters. In the central region the iron return yoke of the magnet is instrumented and serves as a hadronic calorimeter (the "C's"). A module of the C's is shown in figure 19 . There are 16 modules in total, eight at each side of the beam. They are azimuthally segmented into 12 sections, each divided into two samplings in depth of 2.5

interaction lengths. They consist of 5 cm iron plates with 1 cm scintillator plates inbetween. The light is collected by two phototubes per sampling, again via BBQ wavelength shifters and light guides. The energy resolution of the C's was measured as: $\Delta E / E = 80\% / \sqrt{E}$ (E in GeV).

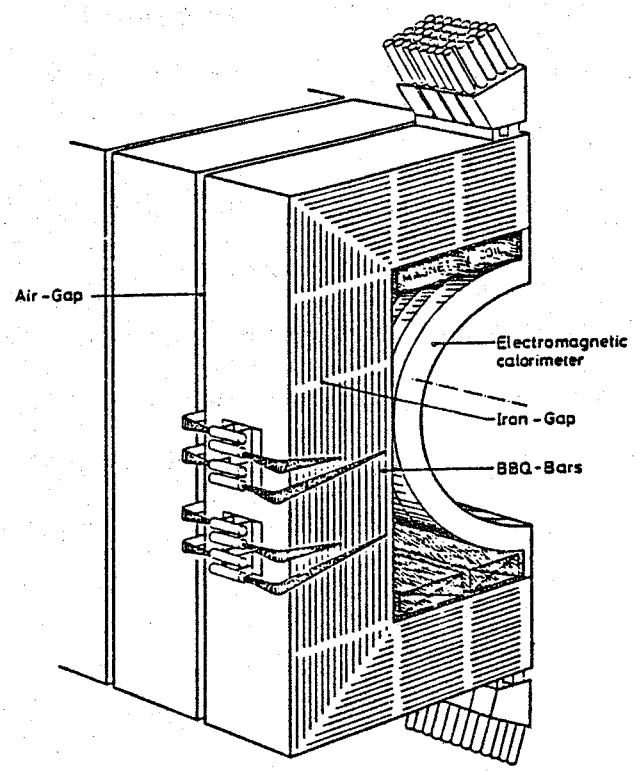

Figure 19: Central Hadronic Calorimeter ("C's")

The endcap hadron calorimeters (the I's), are similar to the C's. They consist of 6 vertical modules at each end of the detector, which are vertically divided into 6 blocks. The 16 blocks which are nearest to the beam are subdivided into 4 smaller blocks. Readout and performance of the I's is similar to the C's.

In the forward direction there are additional calorimeters, both electromagnetic and hadronic. With exception of the missing energy measurement they are not used for the standard muon analysis (e.g. for jet reconstruction) and are not described here. However, their properties are mentioned in table 5 .

3.2.3 Muon Chambers

The outermost element of the UA1 detector is a system of drift chambers for muon detection. There are more than nine interaction lengths of material (calorimeters and iron shielding) between the muon chambers and the interaction region. This ensures that muons are practically the only charged particles able to reach this outer detector system.

The chambers are 4 m × 6 m in size. A few chambers are smaller in order to fit into gaps between the large chambers or between the support structure below the detector. Each chamber consists of two double layers of drift tubes. The two double layers are orthogonal, giving independent measurements of both coordinates of a track. The drift tubes in each double layer are staggered to resolve left − right ambiguities and to minimize dead space. With the exception of the bottom chambers[18] the muon chambers are arranged in modules: two chambers are mounted together, with a gap of 60 cm between them. Because of this lever arm the direction of a track can be measured with high precision. A picture of such a module is shown in figure 20 .

Including the bottom chambers the muon detection system has 34 modules. These modules cover about 70 % of the ϕ angle in the central region of the UA1 detector (± 1.0 in pseudorapidity). In the forward region (up to $\pm$ 2.3 in pseudorapidity) the ϕ coverage rises to 90 %. The geometrical acceptance of the chambers is plotted in figure 21 .

The cross − section of one drift tube is shown in figure 22 . The tubes are made of aluminum; the width of such a tube is 15 cm and the length is up to 6 m. These tubes are filled with the same argon − ethane mixture as the central detector. At both sides of a tube are cathode strips. The outer ones are operated at − 7 kV, the others at − 5 kV. These cathode strips set up a homogeneous drift field. In the centre of the tube is the anode wire which is operated at + 2.8 kV. The anode wire is partially shielded by the aluminum support. Thus electrons on outer trajectories, which have a longer drift time and therefore deteriorate the resolution, cannot reach the wire. The anode wires are connected to charge sensitive preamplifiers. The signals of the preamplifiers are split; one branch is used for the pre-

[18] In the bottom region the drift tubes of the four layers are parallel. The drift tubes are read out at both ends and the coordinate along the wires is measured by the time difference between both ends. Because of lack of space one bottom module consists only of one chamber.

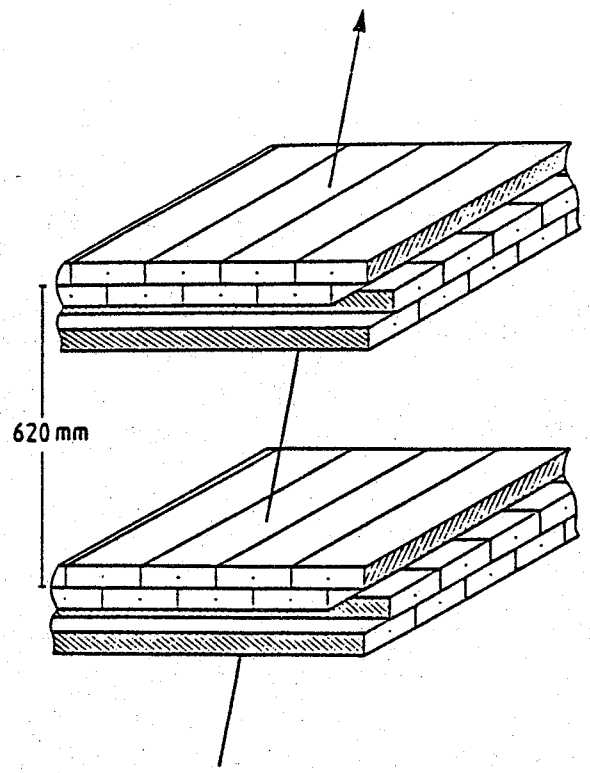

Figure 20: Muon Chambers

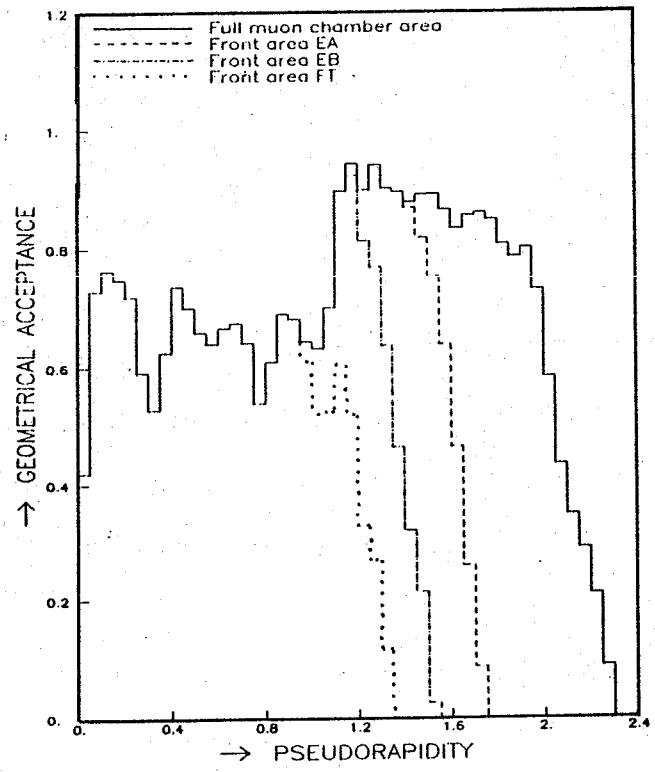

Figure 21: Geometrical acceptance of the muon chambers. The single muon trigger usually used "FT" or "EA", whereas the dimuon trigger used "EA" in 1984 and the full chamber area in 1985.

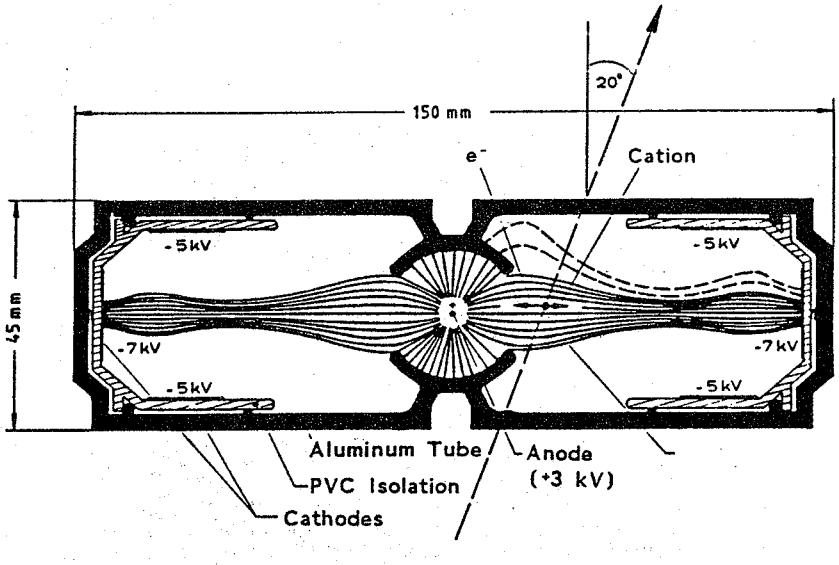

Figure 22: Cross-section of a muon-chamber drift tube

cise measurement of the drift time, the other branch is used by the first level muon trigger.

The resolution of one tube is about 300 μm, the best resolution being obtained close to the centre of a tube. Ideally a muon track will have four hits in each projection. Because of dead space between the tubes and inefficiencies only three hits per projection are required by the track reconstruction program. This results in an efficiency of 92% to reconstruct both projections of a track. The angular resolution which is obtained by the track fit is about 1 mrad.

3.2.4 Trigger Systems

At a typical luminosity of 10^{29} $cm^{-2}s^{-1}$ the total $p\bar{p}$ interaction rate is very high: about 6 kHz. Only a very small fraction of these events are "interesting", most of them are soft collisions. This interaction rate is far too high to be written on tape, as the tape writing speed is limited to about 3 Hz. Therefore a trigger system is needed, which quickly decides if an event is interesting and should be written on tape.

In order to introduce no dead time this decision has to be made before the next bunch crossing, that is within 8 μsec[19]. For this purpose the UA1 detector has three trigger systems:

---

[19] If the collider is operated in 3 bunch mode, which was the case in all runs. A 6 bunch mode is possible and foreseen for the future. Then the bunch crossing will be every 4 μsec.

3.2.4.1 Pretrigger:

This trigger consists of a system of scintillator hodoscopes at both ends of the detector. A sharply timed coincidence of hodoscopes from the proton and antiproton arms and the beam crossing is required for triggering.

This trigger fires with high efficiency for inelastic, non−diffractive $p\bar{p}$ collision, therefore the pretrigger rate is still too high (about 3.5 kHz at 10^{29} $cm^{-2}s^{-1}$) and additional constraints have to be used. However, it reduces background from beam−gas collisions and cosmic rays. Therefore a coincidence with the pretrigger is required for all other triggers[20].

3.2.4.2 Calorimeter Trigger:

This trigger uses calorimeter information. It is possible to trigger on the total transverse energy above a certain threshold, on jets (i.e. clusters in the calorimeters), electrons (i.e. clusters in the gondolas or bouchons), or on missing energy (i.e. left−right imbalance of the calorimeters).

In general, the calorimeter trigger is very important for this experiment. It delivers about 50% of the triggers. However, it is not relevant for the dimuon analysis and we omit a more detailed description of this trigger processor [48].

3.2.4.3 Muon Trigger:

The first level muon trigger has to perform fast track recognition in the muon chambers [49]. It must trigger only on stiff tracks pointing to the interaction vertex. Tracks which are not pointing have to be rejected. These are mainly cosmic ray muons and low p_t muons (most of them are from pion or kaon decays). The latter are bent by a large angle in the magnetic field and by multiple scattering.

As there is not enough time before the next beam crossing to perform a track fit using the drift time information, a rather crude but fast pattern recognition is made, based only on the yes/no information of hits in the drift tubes. To achieve this, 10 neighbouring drift tubes along an expected track

[20] In addition to this standard pretrigger, there exist also pretrigger for special purposes, e.g. a diffractive pretrigger: this trigger requires only one arm of the hodoscope to be fired in time with the beam crossing. These triggers were not used for this analysis.

path are grouped together. One such group is dedicated to each drift tube of the plane closest to the vertex, which is called the "reference tube" (fig. 23). The signals of these 10 tubes are routed to the 10 addresslines of a 1 Kbit RAM memory chip. Thus each possible hit pattern in these 10 tubes addresses a particular bit of the memory. This bit stores the yes/no decision whether or not this pattern is compatible with a track coming from the vertex. The standard requirement is a minimum of three hits per projection and a maximum deviation from the straight line to the vertex of 250 mrad. The resolution which can be obtained by the fast trigger is about 100 mrad, determined by the lever arm of 60 cm between two chambers of a module and half the width of a drift tube (= 7 cm).

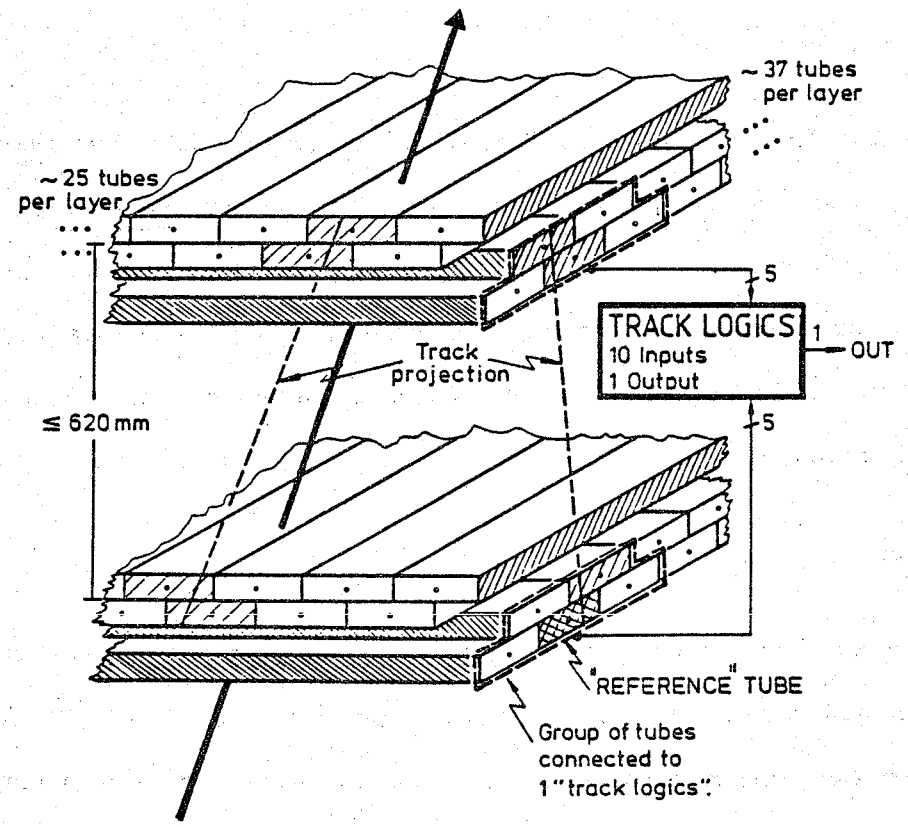

Figure 23: Muon Fast Trigger:
grouping of 10 tubes around a reference tube for both projections of a module

The allowed deviation takes into account:

- The uncertainty of the position of the interaction vertex, because of the finite bunch size.
- Bending of the tracks by the magnetic field.
- Multiple scattering in the material of the calorimeters and the iron shielding.

Bending by the magnetic field and multiple scattering especially affect low p_t muons. So the cut at 250 mrad results in an effective p_t cut. The trigger is fully efficient for muons above 3 GeV/c p_t . After valid tracks have been found in either projection, the track position in the module plane can be reconstructed. Then it is checked whether the hadron calorimeter blocks passed by this possible muon candidate have recorded at least the energy deposition of a minimum ionizing particle. This coincidence makes use of the timing properties of the calorimeter scintillators. Their small time window (100 ns compared to 1.5 μs of the muon chambers) rejects most of the cosmic ray muons, which are generally not exactly in time with the interaction. It is also possible to veto certain regions within a module completely. In the 1984 and 1985 runs this $X-Y$ coincidence was made in up to four parallel processors. They permitted the definition of different trigger regions for special purposes:

- The rate of the inclusive muon trigger is very high and would saturate the data acquisition system. In order to reduce the rate, a large part of the forward region was taken out of the sensitive area. The remaining area is indicated as "FT" in figure 21 . If the luminosity of the SPS was low, a larger region "EA" could be used.
- The rate of the single muon trigger could be reduced by demanding a coincidence with a calorimeter trigger (e.g. μ and jet, μ and electron). For these combined triggers a larger area was used ("EA"). Nevertheless it was not possible to use the complete area of the muon chambers.
- A special dimuon trigger demanded two muon triggers in different modules. Because of the very low dimuon rate (0.05 Hz at 5 x 10^{29} $cm^{-2}s^{-1}$), almost the full area of the muon chambers could be used.

The muon trigger decision is made within 1.0 μsec, to which 1.5 μsec must be added corresponding to the maximal drift time in the muon chambers. Since this is less than 4 μsec in total, it induces no dead time. The trigger rate of all muon triggers, dominated by the rate of the inclusive trigger, was about 10 Hz, which was still too high to be written on tape. For further reduction a second level trigger was necessary, using drift time and sometimes central detector information. This second level triggering was done in 168E emulators, which are part of the data acquisition system.

3.2.5 Data Acquisition

Once an event has been accepted by the trigger processors, the complete information of the detector has to be read out and written on tape. This is done by the data acquisition system, which has to perform the following tasks [50]:

- Digitizing of the analog data.
- All data words have to be collected, ordered and sent to the host computer. In this step a large reduction of the amount of data can be obtained by suppressing zero measurements.
- After all information is available higher level trigger programs are run to reject "uninteresting" events.
- The data has to be written on tape. UA1 uses two output streams: every event which passes the higher level trigger is written to "normal tape", highly selected events (e.g. W, Z candidates) are written also to "special tape" for immediate processing.
- The data acquisition also monitors the detector performance. This helps to detect malfunctions.

The UA1 readout is based on CAMAC and CERN Romulus/Remus electronics. In 1985 a part of the readout chain was replaced by a microprocessor controlled VME system. Tape writing was done by a NORD computer. For online data reduction a series of 168E emulators were used. In these computers more sophisticated algorithms achieve higher rejection factors than the crude but fast first level hardware processors. For the muon part three algorithms are important:

- "MUTUBE": This processor repeats the track reconstruction of the first level hardware trigger. Thus dimuon events with one muon missing the hardware trigger can be recovered.
- "MUTIME": This processor reconstructs tracks in the muon chambers using drift time information. The angular difference of the measured muon track to the direction to the vertex is calculated. If the difference is larger than a certain allowed value, the muon candidate is rejected. This way a reduction factor of 0.33 is achieved. The algorithm is fully efficient for muons with a p_t above 9 GeV/c. The MUTIME algorithm was also used to recover dimuon events with one muon missing the hardware trigger ("software dimuons"). For this purpose looser requirements on the angular difference were used in order to be efficient for low p_t muons. In general the angular cut is made at $25-150$ mrad for single muons, and $50-300$ mrad for dimuons, depending on amount of material, which has to be traversed by the muon [52].
- "VENI": The VENI algorithm reconstructs tracks in the central detector, measures their momentum and matches them with tracks in the muon chambers. It allows to cut directly on the measured p_t of a muon candidate. In order to gain speed the track reconstruction is performed along a road in the CD, defined by the direction towards the track in the muon chamber. The muon chamber track had to be reconstructed by MUTUBE.

The overall reduction rate in the 168E was adjusted to get the 10 Hz input rate down to the maximum possible tape writing rate of 3 Hz. This reduction concerns almost only single muon candidates. As the rate of dimuon triggers was low anyway, a less restrictive selection was applied to them. All dimuon hardware triggers were written on tape, also single muon triggers, with one additional track found by MUTIME. An overview of the various dimuon conditions is given in table 6 .

Run	2μ hardware	MUTUBE	MUTIME	VENI
1983	-- all single μ trigger written on tape --			
1984	all	external point for VENI	software dimuon	p_t > 2 GeV/c for single muons
1985	all		software dimuon single muons	not used

Table 6: 168E conditions for single muon and dimuon events.

(for normal tape selection)

4. ANALYSIS OF THE DIMUON EVENTS

4.1 Event Processing

For each event the UA1 detector delivers about 100 Kbyte of raw data. The reconstruction software has to convert this raw data (e.g. drift times in the CD and the muon chambers) into physical quantities like four vectors of identified particles or jets. The reconstruction of a muon event can be divided into four steps:

- Reconstruction of tracks in the Central Detector.
- Reconstruction of tracks in the muon chambers.
- Matching of CD tracks to tracks in the muon chambers.
- Reconstruction of the rest of the event, e.g. jet finding, missing energy.

The reconstruction is a very complicated process done by sophisticated software. It is impossible to describe it here in full detail, so only an overview is given, concentrating on features which are important for the later analysis.

4.1.1 Reconstruction in the CD

A picture of an event in the CD is shown in figure 24 with all its digitizings. Tracks of the particles can already be identified by eye. The track reconstruction software is described in full detail in reference [51]. Here we give only a brief description: The track reconstruction program identifies tracks by "chaining" nearby points. These chains are then used to build the tracks by joining them together, if they fit to a helix. After the final tracks are found and fitted, a subset defined by certain quality cuts are used to fit the x−coordinate of the interaction vertex[21]. Tracks which are well associated to the vertex are then refitted using the vertex position as an additional point. The fit computes the momentum vector of the track. The momentum resolution which can be obtained is

[21] The y and z coordinates are determined by the beam position. Only the x coordinate (along the beam) is unknown because of the bunch size and has to be determined for each event. The event to event variation is about ± 30 cm.

$$\Delta p/p = 0.005\, p \quad (p \text{ in GeV/c}) \qquad \{22\}$$

for a track of one metre length in the bending plane (x−y plane). The resolutions gets worse, if the track is shorter, or if it has a small angle to the magnetic field (z−direction). The quality of the fit is measured by its χ^2: This measures not only the reliability of the fit in terms of errors on momentum etc., but also tests the hypothesis that the track corresponds to a single particle traversing the CD. The fit tends to have a bad χ^2, if wrong points are used, which can come from another particle crossing at a small angle, or if a particle decays in flight (e.g. $K^+ \rightarrow \mu^+\nu$) causing a kink and a change of the curvature of the track at the decay point. This is important for rejecting some muon background. Instead of χ^2 we use the variable:

$$x_S = \sqrt{2\chi^2} - \sqrt{(2N - 1)} \qquad \{23\}$$

where N is the number of points used in the fit. This variable has the advantage that, for large N, it gives a normal distribution centred at zero with unit variance. In reality this is only approximately true (fig. 25). The deviations are due to systematic errors.

Another variable, called χ^2_Z, measures the goodness of the z−fit. This is the coordinate parallel to the magnetic field and is measured by charge division. The selection cut was made on χ^2_Z per degree of freedom ("χ^2_Z/ndf").

4.1.2 Muon Reconstruction

The identification of a muon starts with the track reconstruction in the muon chambers. A muon will give maximally four hits per projection, which lie on a straight line. Therefore the track finding is much simpler than in the CD. Nevertheless there can be difficulties because of left−right ambiguities, which sometimes cannot be resolved. This can happen, if there are additional hits in the drift tubes coming from delta rays, reflections of the pulse at the end of the wire, or if there are two muon tracks close together. In this case several possible track candidates are fitted. Only tracks with at least three points per projection are considered.

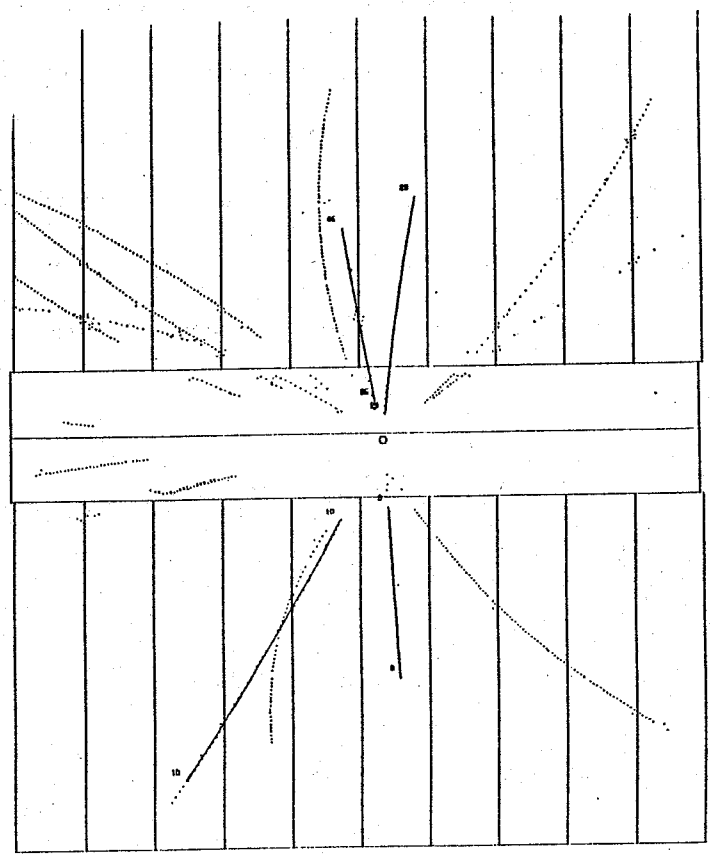

Figure 24: Example of an event in the Central Detector. Projection of the digitizings in the CD onto the bending plane ($x-y$ plane, the UA1 coordinate system is explained in the appendix). It shows all digitizings in the central modules of the CD, for tracks with $p_t > 1$ GeV/c the result of the track fit is shown, too.

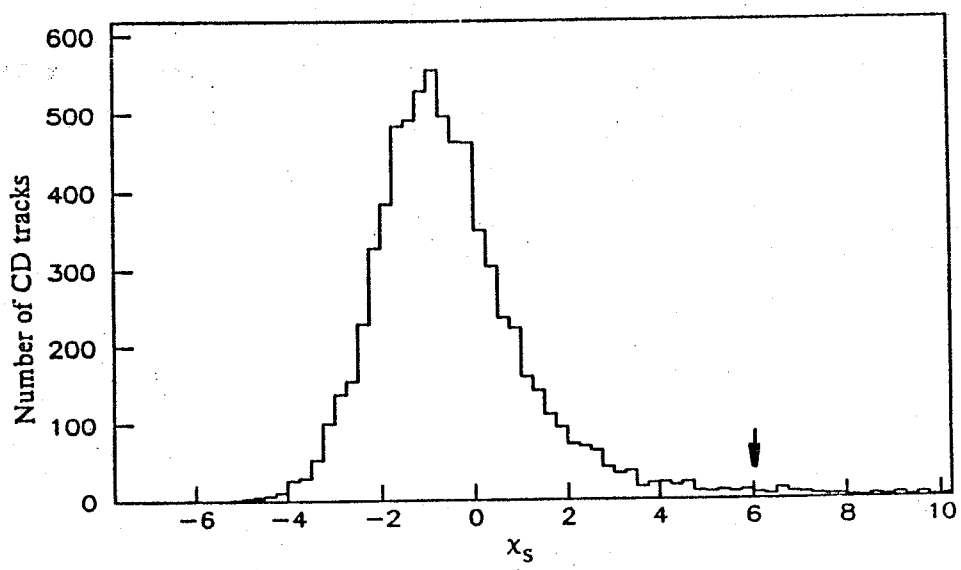

Figure 25: x_S distribution of muon tracks (Cosmic ray muons). The arrow indicates the cut which was used to define the dimuon sample (see text for explanation).

Then the CD tracks are extrapolated to the muon chambers. The extrapolation takes into account the bending of the tracks in the magnetic field in the hadron calorimeters and in the magnetized side walls. The average momentum loss of the muons by ionization is computed and the extrapolation is stopped if the momentum falls below 100 MeV. The possible deviation from the calculated trajectory by multiple scattering is calculated and included in the error of the extrapolation. Then the extrapolated tracks are matched to the tracks in the muon chambers. The goodness of the matching is estimated by calculating the following χ^2:

$$\chi^2(x_i) = \Delta x_i^2 / [\sigma^2(x_i) + \sigma^2(fl_i)] \qquad \{24\}$$

where

Δx_i is the difference between measured track and extrapolation,

$\sigma(x_i)$ the error on Δx_i (including multiple scattering),

$\sigma(fl_i)$ are the systematic errors, reflecting uncertainties of the alignment between muon chambers and central detector,

i stands for the coordinates of the tracks in the chamber plane, x_1 and x_2, and the angles of the track direction, λ and ϕ.

The four χ^2's of position and angle matching are then combined to give χ^2(position) and χ^2(angle). The variable which is used for cuts is the average matching χ^2:

$$\chi^2(\text{av.}) = 1/2\,[\chi^2(\text{position}) + \chi^2(\text{angle})] \qquad \{25\}$$

Typical matching χ^2 distributions are shown in figure 26 .

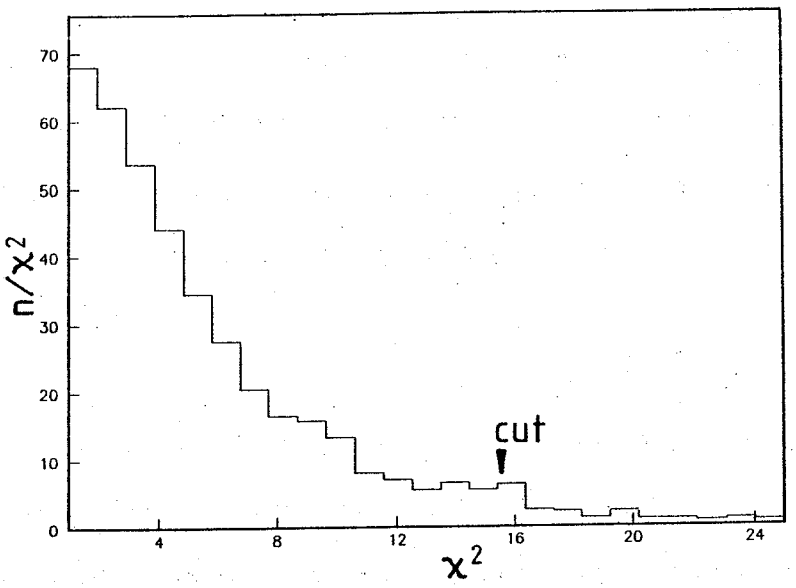

Figure 26: χ^2 distributions for muon − CD matching (Cosmic ray muons). Average matching χ^2

4.1.3 Calorimeter Reconstruction

In the dimuon analysis the calorimeters are used to obtain additional information on the characteristics of the events as

- Isolation of the muons
- Jet activity
- Presence of neutrinos

The definition of the isolation will be discussed later (see 6.1). Here follow some details on the reconstruction of jets and neutrinos.

First the energy deposited in all calorimeter cells has to be reconstructed correctly. This includes the determination of ϕ in the Gondolas and the reconstruction in the Bouchons using the position detectors. Corrections for the ageing of the scintillators and light guides have to be applied, and effects from dead or noisy phototubes have to be eliminated, etc. In muon events an additional correction has to be applied: The muon itself deposits some energy in the calorimeters. At normal incidence a muon looses on average 700 MeV in the Gondolas, and about 2 GeV in the hadronic calorimeters, albeit with large (Landau) fluctuations. As the energy deposited by the muon disturbs the analysis, it should

be subtracted. It is a priori not known how much of the energy in a cell traversed by the muon is due to the muon or to other particles. Therefore only the *most probable* value for the energy loss by ionization is subtracted from the cell (avoiding negative values). One has to face the fact that, because of Landau fluctuations, this value can be wrong by a large factor for an individual event.

4.1.3.1 The UA1 Jet Algorithm

A jet is a collimated bundle of particles from the fragmentation of a quark or a gluon. Such a jet should therefore lead to a local energy cluster in the calorimeters. An algorithm was developed which searches for such clusters and reconstructs the properties of the parton causing this jet. Random fluctuations from the underlying event may fake jets and have to be suppressed. The underlying event is the interaction of the partons which do not participate in the hard process.

The UA1 jet algorithm firstly associates an energy vector to each calorimeter cell:

$$\vec{E}_i = E_i \vec{u}_i \qquad \{26\}$$

E_i is the energy in the cell i, and $\vec{u}_i$ the unit vector from the vertex to the position of the energy reconstructed in this cell. Energy vectors with a transverse energy above 1.5 GeV are called "initiators". The algorithm starts with the highest E_t initiator and adds the energy vectors of all initiators in a cone of $\Delta R < 1$. ΔR is defined as:

$$\Delta R = \sqrt{(\Delta\phi^2 + \Delta\eta^2)} \qquad \{27\}$$

$\Delta\phi$ and $\Delta\eta$ are the separations in azimuth and pseudorapidity[22] of the energy vectors. Then the algorithm tries to built the next jet around the highest initiator outside the cone. It continues until all initiators have been used up. Finally low E_t cells (above 100 MeV) are added to the jets, if they are in $\Delta R < 1$. This algorithm has been studied extensively, especially in order to optimize important parameters like initiator threshold and ΔR requirement.

---

[22] The jets may have a large Lorenz boost along the beam direction. Therefore rapidity is used since differences in rapidity are Lorenz invariant. The pseudorapidity defined as $\eta = -\ln[\tan(\theta/2)]$ is a good approximation to the rapidity (and exact if the particle is massless).

However, studies of Monte Carlo generated jets showed that the jets defined by this algorithm are not a true representation of the parton, but want corrections due to following effects:

- Different response of calorimeters to hadronic and electromagnetic showers.
- Particles of the jet may escape the ΔR cone.
- Particles which do not come from the jet but from the underlying event can fall into the cone.
- Some particles of a jet may escape through gaps in the apparatus.

On average the jet energy is underestimated. The jet correction factors, which are derived from Monte Carlo studies, are typically 1.1 to 1.2, and vary as a function of E_t, η and ϕ. Although the jet algorithm has been designed for high E_t jets ($>$ 20 GeV), it can be shown that it still yields useful results at jet energies of 5 GeV [53]. However, in this regime the efficiency of the algorithm is low and there is a considerable background from faked jets by random clusters of the underlying event. In the dimuon analysis a threshold of 7 GeV on the *uncorrected* jet E_t was chosen. In order to calculate physical quantities only *corrected* four vectors of these jets are used. Only jets within a pseudorapidity range of $-$ 2.5 to 2.5 were considered in the analysis.

A similar algorithm is used to define "CD−jets": Instead of calorimeter cells the tracks measured in the CD are used. The algorithm itself and the relevant cuts are identical with those of the calorimeter jet algorithm.

4.1.3.2 Missing Transverse Energy

A neutrino (or any hypothetical non interacting particle) escapes the detector without interaction. This leads to a momentum imbalance of the rest of the event. In the transverse plane this imbalance can be measured, and the neutrino's transverse momentum can be determined. It is not possible to measure the longitudinal momentum of the neutrino, because many particles from the $p\bar{p}$ interaction can escape unmeasured through the beam pipe. As these particles have very small p_t , they do not disturb the measurement of the transverse energy of the neutrino, but they do carry away a large amount of longitudinal momentum.

In UA1 the sum of the neutrino's transverse momenta is measured by adding all energy vectors of the calorimeters (e.g. {26}). The negative of the transverse component of this sum, called "missing transverse energy" ("E_t^{miss}"), corresponds then to the neutrino transverse momentum sum. In muon events the momenta of the muons have to be included in this sum.

The uncertainty of the E_t^{miss} measurement is rather large, the error from the calorimetry can be parametrized by the following formula:

$$\sigma(E_t^{miss}) = 0.7\sqrt{\Sigma E_t} \qquad \{28\}$$

ΣE_t is the scalar sum of the transverse energy of all calorimeter cells. In principle the error on the muon p_t has to be included, as well as the uncertainty in subtracting the muon's energy deposition, but for low p_t muons these contributions are negligible.

If more than one neutrino is in the event, E_t^{miss} measures the sum of the p_t vectors of all neutrinos. This is the case in dimuon events from heavy flavour production. If both muons come from decays of heavy quarks, at least two neutrinos are contained in the event. As we cut on the muon p_t, we favour asymmetric decays, which give most of their p_t to the muons and produce low p_t neutrinos. In addition the neutrinos tend, like the muons, to be back−to−back, thereby tending to have their transverse momenta cancelled. Therefore no significant missing E_t is expected in dimuon events. Nevertheless the missing E_t spectrum is worth while looking at, since unconventional sources of dimuons (SUSY particles etc.) might produce substantial amounts of missing E_t .

4.2 Event Selection

In the 1983, 1984 and 1985 runs UA1 collected about 11.2 million events (for an integrated luminosity of 659 nb^{-1}). Approximately half of them were triggered by muons. As the full reconstruction of an event is a rather time consuming operation (about 20 sec on an IBM 370/168 computer), it is not possible to process the whole sample completely. Instead, the events were passed through a filter program, which quickly selects muon events by reconstructing only a part of each event:

- The trigger hodoscopes are used to reject a large fraction of beam−gas and cosmic ray events.

- The tracks in the muon chambers were reconstructed and a track pointing to the vertex within 150 mrad was required.
- A "road" was defined in the CD between the vertex and the muon track. Then only this part of the CD was reconstructed.
- The event was accepted if a CD track with $p_t > 3$ GeV/c was found with very loose matching requirements to the muon−track.

Thus events with at least one muon candidate were selected. From this sample different selections were made such as inclusive muons, muons with jets, and dimuons. In these selections the events were completely reconstructed.

The dimuon selection demanded following criteria:

two muons with $p_t > 3$ GeV/c

with the following technical cuts on the CD tracks:

$$\chi_s < 6$$

$$\chi^2_z/\text{ndf} < 9$$

more than 20 points

track lengths in the x−y plane (bending plane) > 40 cm

good association to the vertex

average matching muon − CD : χ^2(av.) < 15

This yielded 1945 events.

This dimuon sample was then divided in :

- *"high mass" sample:* Dimuon mass $m^{\mu\mu} > 6$ GeV/c^2 : 834 events
- *"low mass" sample:* Dimuon mass $m^{\mu\mu} < 6$ GeV/c^2 : 1211 events

The mass cut of 6 GeV/c^2 for the high mass sample should reject events from cascade decays of one beauty quark. Both samples were scanned by physicists on a high resolution interactive graphics facili-

ty. This scan should ensure that the correct decision had always been made by the reconstruction program. Thus the sample was cleaned up by rejecting some sources of background:

Kinks — Kaon decays which have a visible kink in the track. An example of such a track is shown in figure 27 . Sometimes this kink is so distinct that the track reconstruction program splits the track into two, which is easily recognized by the scanner. These events are rejected as well.

Cosmics — Cosmic ray muons can easily be recognized and rejected. In 1985 this was very efficiently done by software. This explains the low number of "scanned" cosmics in the 1985 sample, as compared to 1984.

Leakage — Events were rejected if either muon candidate pointed to a gap in the detector where a particle easily can punch through. The scan decision was verified by software which calculated the amount of material traversed by the particle.

Matching — In the case of matching ambiguities, that is if more than one CD track is an acceptable muon candidate, we tried to resolve the ambiguity. Often the Iarocci chambers added useful information. The event was rejected if the correct track failed the selection criteria.

Dbl. Int. — Double interactions were rejected if the muons came from separated vertices.

This scan left 517 events. 5 events have a dimuon mass compatible with the Z^0 mass and are regarded as Z^0 candidates. As the Z^0's are the subject of a different analysis [72], they were removed from the sample leaving 512 events.

The scan breakdown of the high mass sample is listed in table 7 . The number of validated events from the 1983 run (50) is different from the published number (24) [2]. This is because different cuts have been used in the paper ($p_t > 3$ GeV/c for each muon *and* $(p_{t1} + p_{t2}) > 10$ GeV/c, no mass cut). The low mass events have been treated by [74].

Run :	1983	1984	1985	total
Luminosity	108 nb^{-1}	254 nb^{-1}	297 nb^{-1}	659 nb^{-1}
Triggers	2.5 M	2.2 M	6.5 M	11.2 M
Filter	72 K	210 K	200 K	482 K
Dimuon				
−selection	122	747	1076	1945
M > 6 GeV/c^2	69	295	370	734
Scan:				
Z^0	2	2	1	5
Kink	4	14	28	46
Cosmic	4	79	4	87
Leakage	7	30	17	54
Matching	2	9	16	27
Dbl. Int.			3	3
validated	50	161	301	512

Table 7: *Event selection and scan for dimuons $m_{\mu\mu} > 6$ GeV/c^2*

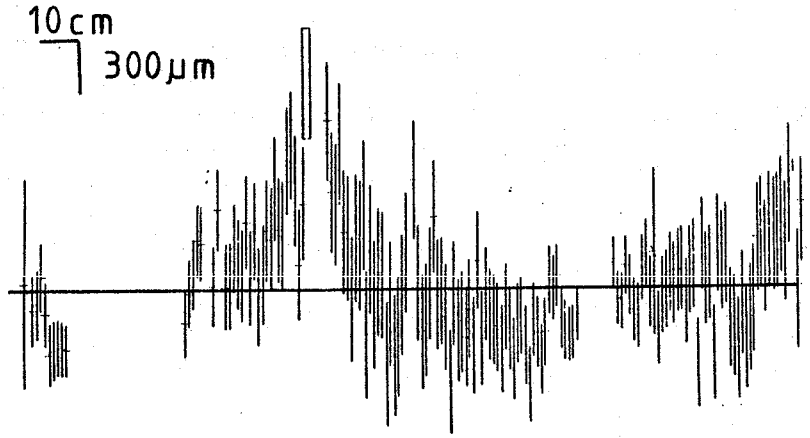

Figure 27: Example of a track identified as "Kink" (Kaon decay). This figure shows the deviation from the fitted track for each point measured in the CD ("residuals"). The curvature of the track is unfolded so that it appears as straight line.

5. DETERMINATION OF THE BACKGROUND

The 512 events which were selected as dimuons are certainly not all due to prompt muons from the physics sources discussed in chapter 2. The sample is contaminated by some technical background from misidentified hadrons and from muons from trivial physics sources. In this chapter possible background sources are discussed and an estimate of their respective contribution to the sample is given. Sources which have to be investigated are:

- Cosmic ray muons.
- Leakage through gaps in the detector.
- Misidentification.
- Decays of kaons and pions.
- Punch through (i.e. non−interacting hadrons).
- Leakage of hadronic showers.

In principle one would like to remove the background entirely, e.g. by clever design of the detector, by identification of background events, by applying strict technical cuts or, if the kinematics of background and signal are different, by physics cuts. In the case of cosmic ray muons it is in fact possible to identify (almost) each background event by software and by scanning. The same is true for leakage through gaps of the detector. The remaining background from these sources is therefore negligible. For the other background sources complete rejection is not possible. This does not matter as long as one is able to calculate the background contribution, and to take it into account in the analysis. If it turns out that the background level is too high for a meaningful analysis, it may still be possible to reduce the background by stricter cuts. More restrictive cuts will also reduce the acceptance. It is therefore a question of optimizing signal to background versus the total number of events. This of course demands a detailed knowledge of the properties of signal and background.

It was already mentioned that after scanning the background from cosmic rays and leakage through gaps is negligible. The remaining background sources will be treated in the following sections.

5.1 Misassociation

If two or more tracks in the CD are reasonable candidates to match to a single muon chamber track, the software might select the wrong one. Such events are considered as background if:

- The correct track fails the selection criteria.
- The correct track has a different sign than the selected one.

In the latter case the event is still a good dimuon candidate, but as the determination of the sign plays an important role in the dimuon analysis, such events are nevertheless considered as background. On the other hand, if the alternative track has the same sign and fulfills the selection criteria, this event is regarded as "good". Such a misassociation would cause only a small mismeasurement of the muon momentum, but all other event properties are likely to stay the same. Most of the misassociated muons were already recognized by scanning of the events (see table 7). These events were either rejected or the assignment was corrected by hand. The latter happened to six events. There remained events with unresolvable ambiguities. Another type of misassociation background can come from muons of low p_t, which reach the muon chambers because of a downwards fluctuation of the muon's energy loss. The extrapolation software stops such tracks in the absorber, and the track in the muon chambers might be matched to another CD−track nearby.

In order to study this misassociation background more systematically all events which have a second track fulfilling very loose matching requirements were selected for a dedicated scan. In this selection the ionization loss, dE/dx, used by the track extrapolation was scaled down by a factor of 0.9. In this way the effect of low p_t muons could be studied, too. 25 events remained after the scan with an unresolvable ambiguity. Using the other track would change only the momentum in 5 events. Of the remaining events, 10 of them are like−sign and 10 are unlike−sign, 8 unlike−sign and 6 like−sign events would fail the selection criteria if the alternative track was correct. Two unlike−sign events would become like−sign and four like−sign events unlike−sign. In the worst case these 10 like−sign and 10 unlike−sign events are background. As it is very unlikely that the software always preferred the

wrong track[23], an estimate of 5 ± 5 in each sample (like and unlike−sign) is more realistic.

5.2 Pion and Kaon Decay

The most important background source is the decay of pions and kaons in flight. The probability that a pion decays in flight in the central detector is 2.3% / p_t and 11% / p_t for a kaon (p_t in GeV/c). Assuming that 58% of the hadrons in an event are pions and 21 % kaons [56] one can calculate an average decay probability of 4% / p_t per hadron. In addition pions and kaons can decay in the 10 cm air gap between the CD and the Gondolas and in the calorimeters before they interact.

The contribution from this background can be calculated using *experimental* data. One starts with an inclusive muon sample with one muon $p_t > 3$ GeV/c. The muon has to pass the same technical selection cuts as applied in the dimuon sample. The probability for each additional track in the CD to decay into a muon which is detected in the muon chambers is calculated. The same cuts are applied on this simulated dimuon as in the dimuon selection. Adding up these probabilities one gets the expected background.

In calculating the probability that a kaon or pion fakes a muon, the following effects have to be considered:

- A kaon decay can cause a distinct kink in the track. This leads to a mismeasurement of the track momentum. In this way a low p_t kaon can fake a high p_t muon. On the other hand this kink results in a bad χ_s of the track fit, and the event may fail the selection cuts. In addition there is a chance that the kink will be detected by scanning.
- Muons from decays have lower momenta than their parents. Hence these decay muons tend to have a larger deviation from the track extrapolation due to multiple scattering and bending in the magnetized iron compared to prompt muons of the parent's momentum. The larger deviation from the expected track path is reflected in a bad matching χ^2 and these tracks are more likely to fail the selection cuts. A mismeasurement of the track because of the decay kink en-

[23] As it is always the track with the better matching χ^2 which is chosen, on a statistical basis the correct tracks should be prefered, so a guess of 50% probability for the correct choice is conservative.

hances this effect. In an extreme case the decay muon has such a low momentum that it is stopped in the absorber and does not contribute to the background at all.

In order to study these effects Monte Carlo generated pions and kaons were made to decay in the CD. Then a simulation of the complete detector response including the fit of the distorted track was performed. From this study probability densities $P(p_t^h, p_t^\mu)$ for the probability that a hadron of p_t^h fakes a muon of the (different) p_t^μ were generated. This was done separately for pions and kaons. Examples of such probability functions are shown in figure 28 for fixed p_t^h .

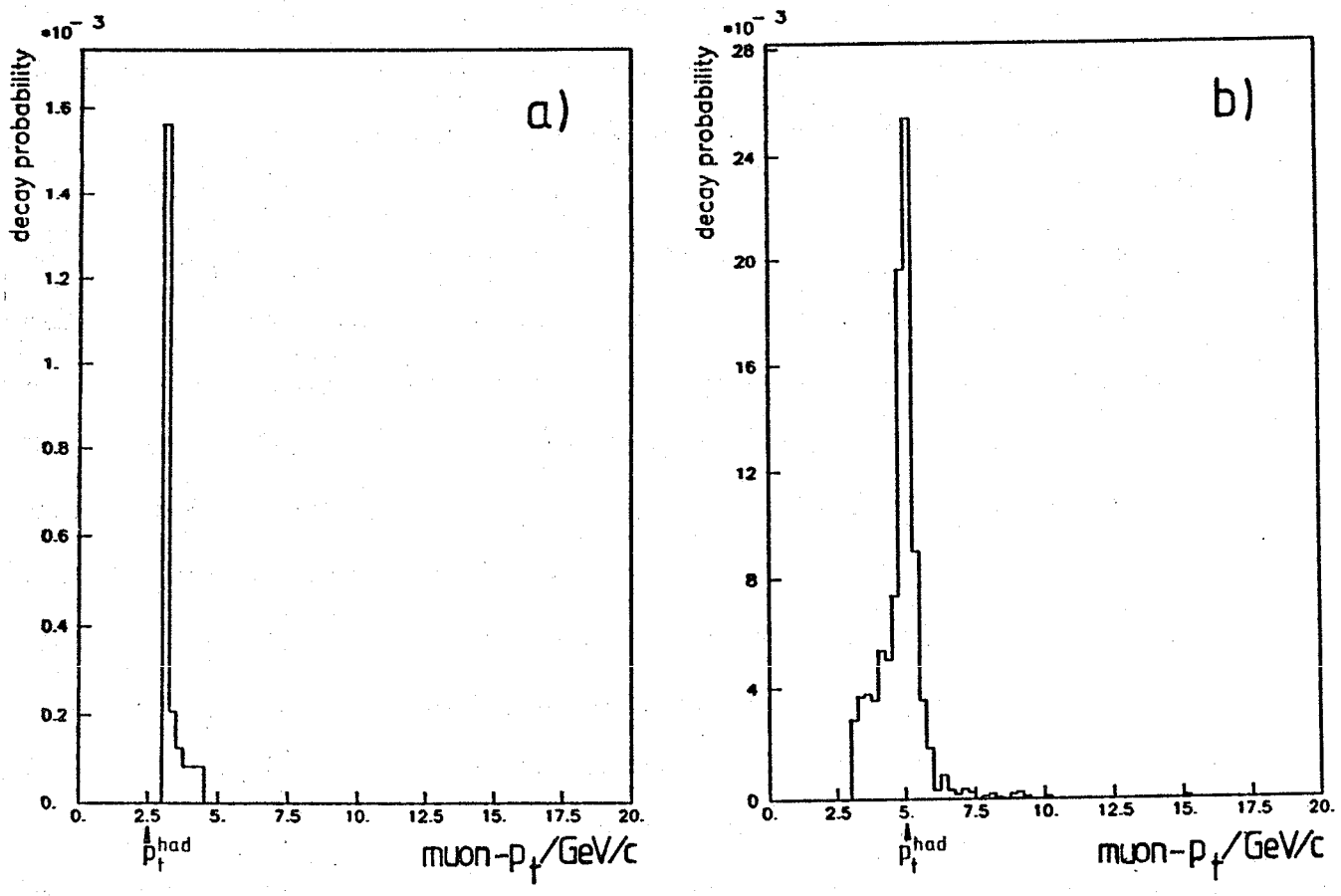

Figure 28: Probability for a hadron to fake a muon of p_t^μ .
a) for hadrons of p_t = 2.5 GeV/c,
b) for hadrons of p_t = 5.0 GeV/c
A cut of p_t > 3 GeV/c was applied on the reconstructed muon track.

These distributions were used to calculate the decay probabilities of the tracks found in the single muon events. As a hadron can cause a complete spectrum of decay muons, each track was allowed to decay several times and appropriate weights were applied. The background estimated by this method has then to be corrected by several factors:

- The trigger efficiency is different for single muons and for dimuons. This correction factor was calculated using a Monte Carlo method which takes into account the different trigger conditions of the various runs.
- If the muon in the single muon event is a decay muon itself, the contribution of this event has to be weighted by a factor of 1/2. If α is the average probability to fake a muon, a dipion (or dikaon or mixed event) contributes to α^2 dimuon background events, and to

$$\alpha(1-\alpha) + \alpha(1-\alpha) = 2\alpha(1-\alpha)$$

single muon events. Letting the second track decay, we get $2\alpha^2(1-\alpha)$ background dimuons, which is just twice the real background if α is small. If the simulated decay muon hits an area of the muon chambers which was not active in the single muon trigger the weight of 1/2 was not applied. The reason is that the "reversed" event, with the decayed hadron being the "real" muon and the "real" muon being the hadron would not have triggered, but delivers the same contribution to the background. This factor must not be applied if the single muon is a prompt muon. Using Isajet Monte Carlo calculations[24] the fraction of prompt muons in the single muon sample, which was used for the background calculation, was estimated to be 20 ± 5 %. The weights of the simulated decays were accordingly corrected. Averaged over all single muon events these corrections reduce the estimate by 0.575 .
- A sample of these single muon events and of the simulated decays were scanned in order to estimate the scan rejection:

[24] We assumed that prompt single muons mainly come from heavy flavour decays. Thus single muon events with $p_t > 3$ GeV/c were generated with Isajet, and the calculated muon inclusive cross-section was compared with the actually measured one. The Isajet $b\bar{b}$ cross-section itself was fixed to the value measured with the dimuons (see chapter 8). As this measurement itself depends on the background subtraction some iterations were necessary.

Reduction factor:	
single muons:	0.80
Monte Carlo pion decays:	0.90
Monte Carlo kaon decays:	0.72

Kaon decays tend to have a more distinct kink in the track than pion decays, therefore kaon decays are more easily rejected by scanning. The average of the reduction factors from the Monte Carlo tracks is consistent with the reduction obtained with the single muon sample.

Altogether the calculation results in an estimate of 116 events from pion or kaon decays. 58 background events are −like sign, 58 unlike−sign. This reflects that there is no long range correlation between two decaying hadrons. This method of calculating the background not only yields an absolute number, but as the decays are simulated in real events, the background events can be analyzed in exactly the same way as the data. Therefore all kinematical distributions of the dimuon system and of the rest of the event (jets, neutrino, etc.) can be calculated as well.

Unfortunately this estimate suffers from some systematic errors due to uncertainties of the basic assumptions. The estimate is based on about 4000 single muon events. Therefore the statistical error from the limited number of single muon events can be neglected. The major uncertainty arises from the incomplete knowledge of the pion and kaon content in the events. The values used were obtained with the aid of measurements of the K/π ratio from UA2 and UA5 [55]. Unfortunately the measurements for pions and kaons were made at low p_t (< 2 GeV/c) and have to be extrapolated to the p_t range of 3 GeV/c. For that we used inclusive pion and hadron spectra from UA2 and UA1 [55]. The p_t spectra of pions and hadrons were parametrized. The π/h and p/π ratios resulting from these parametrizations are shown in figure 30 . We assumed that K/π is constant as a function of $m_t = \sqrt{(m^2 + p_t^2)}$, where m is the particle mass (fig. 29) . Hence one finds at $p_t = 3$ GeV/c as best values 21% kaons and 58% pions. The errors of this extrapolation are rather large, ± 17% for K/π and ± 50% for p/π, corresponding to the extreme values of 29% kaons and 61% pions or 17% kaons and 55% pions. These errors transform into a ± 17% error of the background estimate. Including other systematic er-

rors like uncertainties in the trigger efficiency, and in the detector simulation, yields a total error of ± 25% [56].

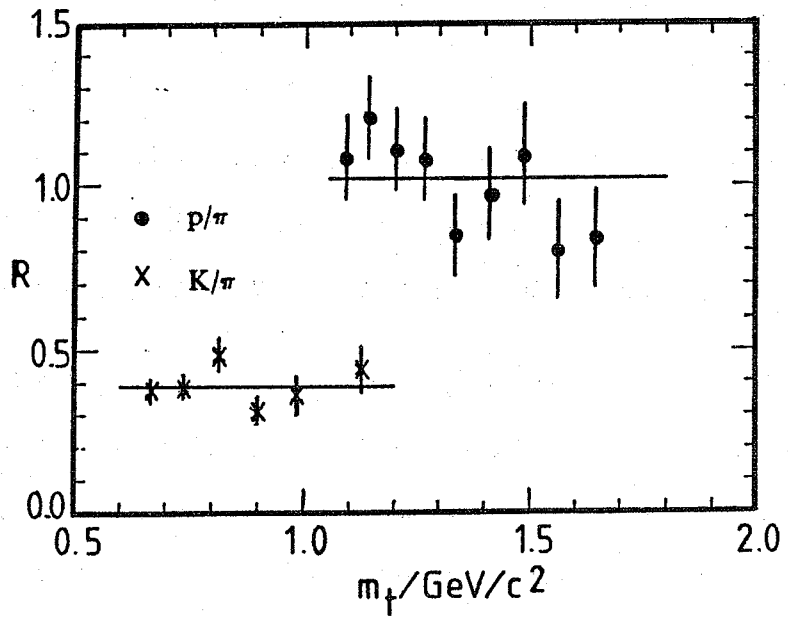

Figure 29: K/π ratio as a function of $m_t = \sqrt{(m^2 + p_t^2)}$ [55]

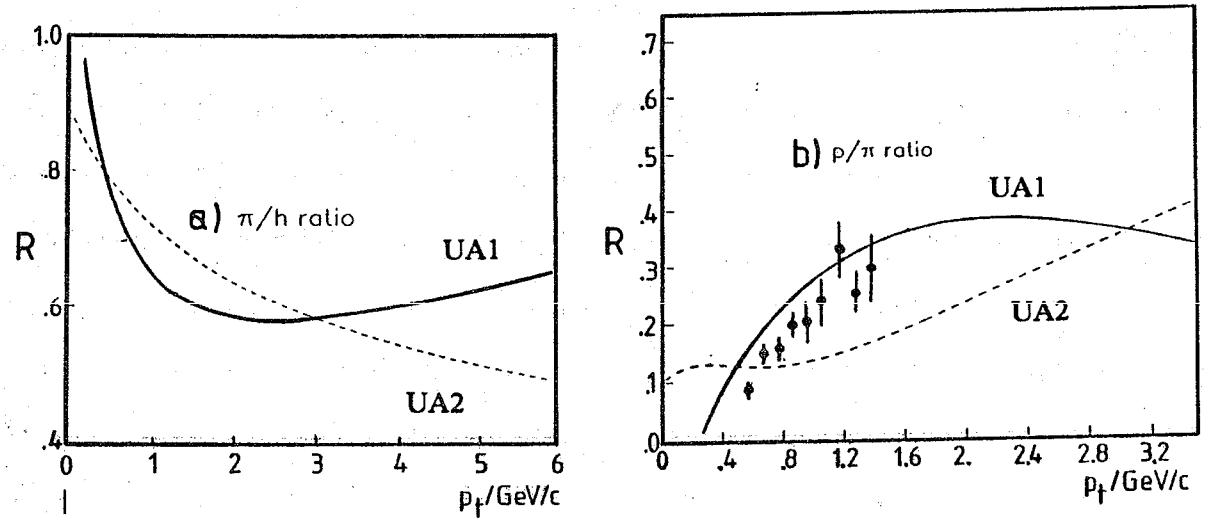

Figure 30: Extrapolation of the π/h (a) and the p/π (b) ratios. The two curves are from different parametrizations of the p_t spectra and reflect the uncertainty of this extrapolation.

A good cross check of this estimate can be made by calculating the background for the inclusive muon sample by a similar method (see appendix D). The outcome of this calculation is:

- At low transverse momentum the p_t distribution of the inclusive muons is consistent with background alone, suggesting that the single muons at low p_t are indeed dominated by background (see appendix).
- As the estimate slightly exceeds the number of measured events at low p_t one possibly tends to *overestimate* the background.

5.3 Punchthrough

Punchthrough means that a hadron traverses all the material to the muon chambers without interaction (except for ionization loss). By definition, such a particle is indistinguishable from a muon. As there are more than nine hadronic interaction lengths of calorimeter and iron absorber in front of the muon chambers (at normal incidence) the probability for such a process is very low, namely $e^{-9} < 10^{-4}$ per incident hadron. This is further reduced by elastic and quasi−elastic scattering.

The total contribution can be calculated in the same way as the decay background. One has to replace the decay probability of a hadron by its probability to punch through. For this calculation different values were used for the interaction lengths of pions, kaons and protons [47]. Again it was assumed that 58% of the tracks are pions, 21% kaons and the remainder protons[25]. The calculation resulted in a background from punchthrough of 1.5 events.

5.4 Leakage

Hadronic showers which are not completely contained in the calorimeters can produce tracks in the muon chambers, which may then be matched with the incident hadron track in the CD. The same is true for muons which are produced as decay products of secondary particles in the shower.

As the nine interaction lengths of absorber normally contain a hadronic shower completely, this background is already small. It is further reduced, once the matching criteria are applied. From test beam measurements the probability of faking a muon by shower leakage was measured to be less than

[25] For the punchthrough background the exact numbers are irrelevant.

10^{-4} per incident hadron [54]. This contribution is even smaller than the already small contribution from punchthrough and can be neglected.

5.5 Alternative Estimate of the Background

Although the background calculation described above uses real events, the whole method is based on Monte Carlo calculations of decay probabilities. These calculations depend strongly on how well the response of the detector is simulated. Therefore one would like to confirm this calculation by a more direct measurement of the decay background.

A parameter which is sensitive to background muons is the χ^2 of the matching of a muon chamber track to the extrapolation of the CD−track. A decay muon tends to have a lower momentum than is measured in the CD. Consequently the CD track is wrongly extrapolated to the muon chambers, and the error of this extrapolation is underestimated. Both lead to a worse matching χ^2 than for real muons. This effect can clearly be seen comparing matching distributions of J/ψ candidates, which are essentially background free, with low p_t single muon data, which are dominated by background (fig.s 31 and 32). The single muon events have a significantly smaller fraction of events with small χ^2 ($<$ 0.5) and a larger fraction of events with a very bad χ^2 ($>$ 5). The respective χ^2 distributions of the dimuon data [fig. 31 and 32 c] are between the two extremes. One can now try to determine the background in the dimuon data by fitting a linear superposition of the χ^2 distributions from J/ψ events (i.e. good muons) and from single muon events (i.e. background muons) to the data. Before doing this one has to verify that all samples are indeed comparable, and not systematically biased by the selection procedure.

- The J/ψ candidates were selected from the "low mass" sample with p_t > 3 GeV/c for each muon. Unlike−sign dimuons with a dimuon mass between 2.5 and 3.5 GeV/c^2 were used for this purpose (fig. 33). As these events were selected the same way as the "high mass" events, no selection bias is expected.

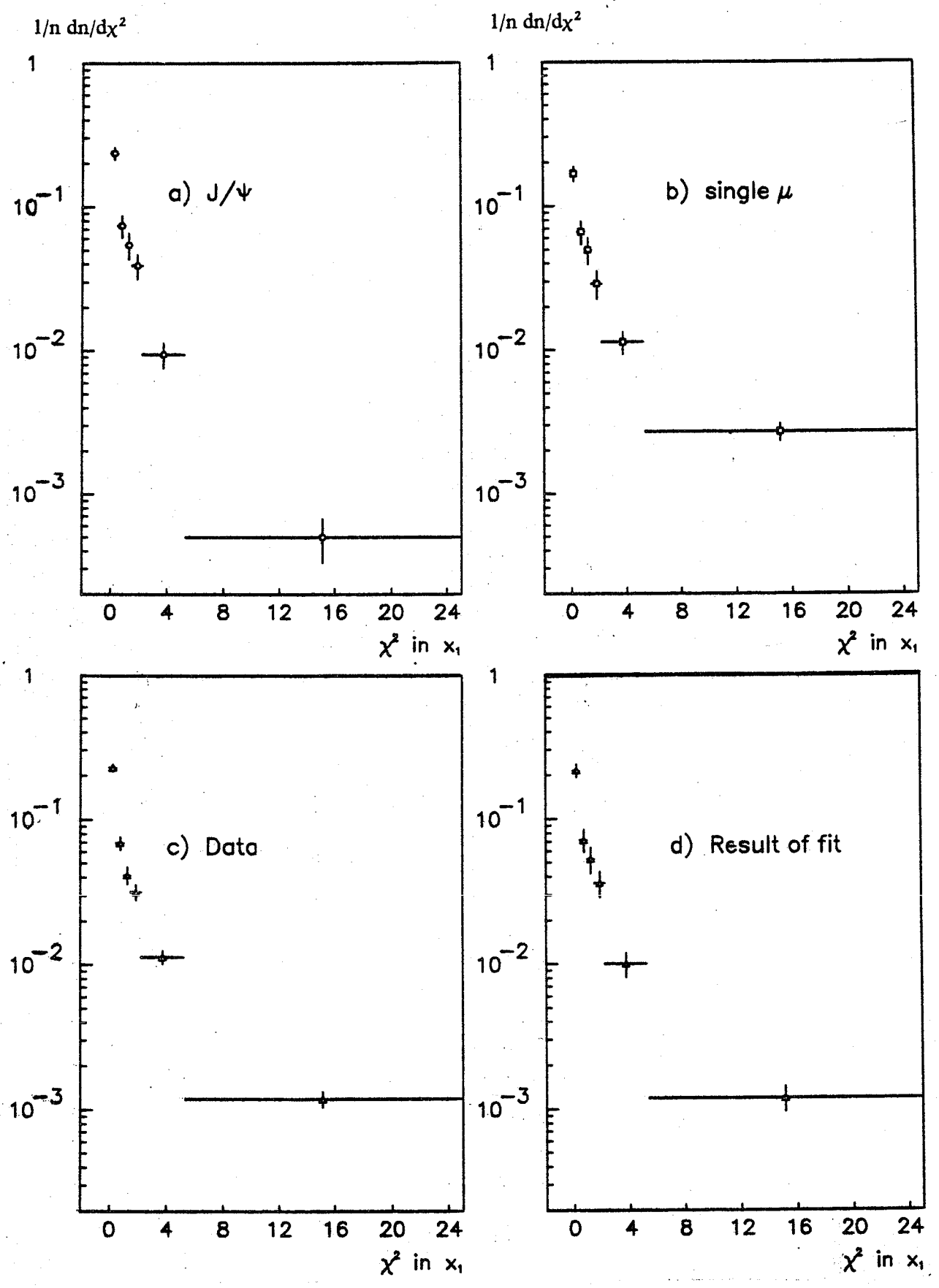

Figure 31: χ^2 of matching CD − muon chambers (in position)

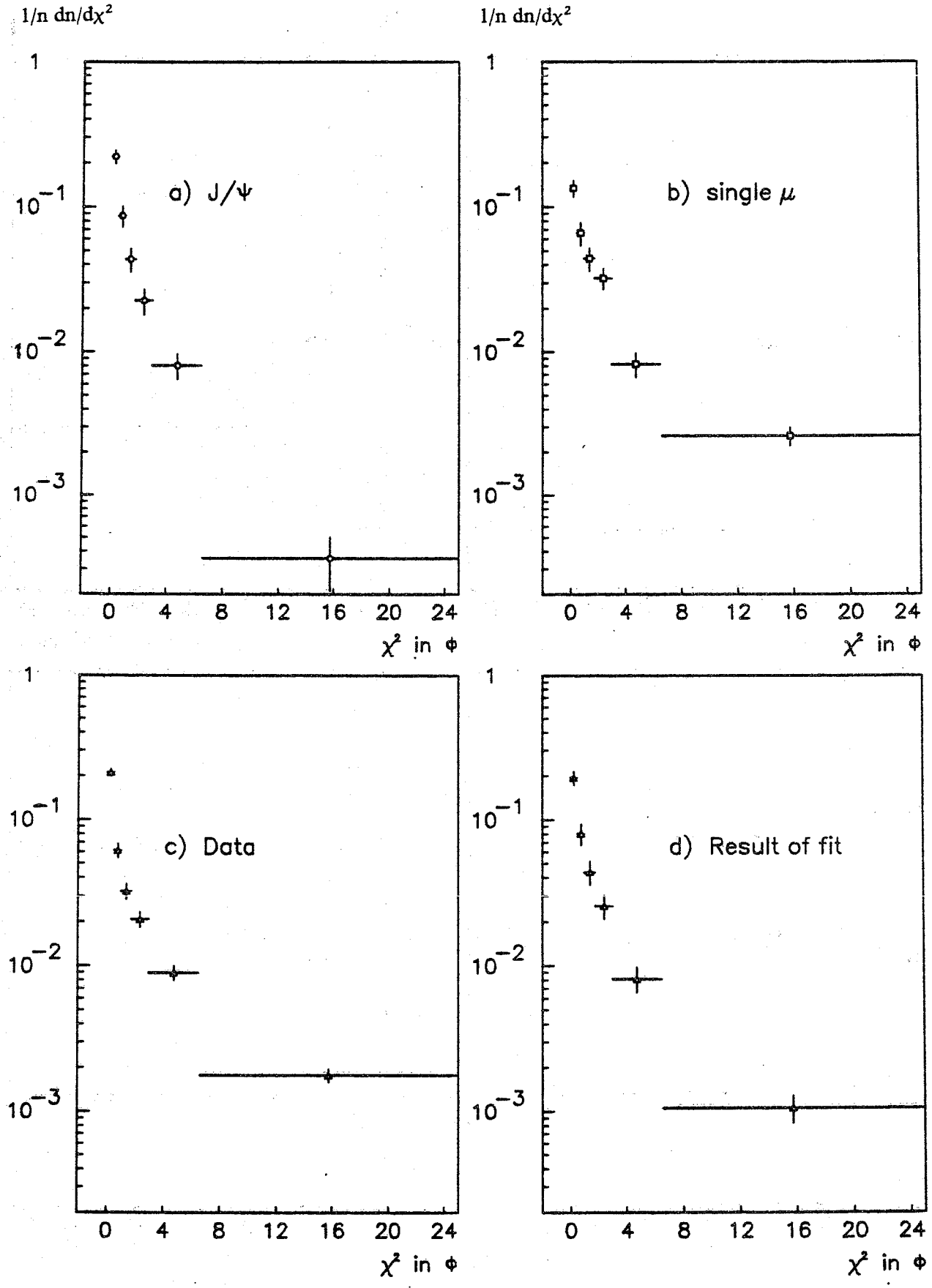

Figure 32: χ^2 of matching CD − muon chambers (in angle)

- The single muon events came from special runs without second level trigger (= 168E) rejection. This was necessary, since the standard 168E selection criteria are more restrictive for single muons than for dimuons and tend to clean up the sample. Single muons were selected if they had $p_t > 3$ GeV/c and satisfied the same technical cuts as applied to the dimuons. This sample was scanned in order to remove recognizable background. This left 242 out of 267 events.

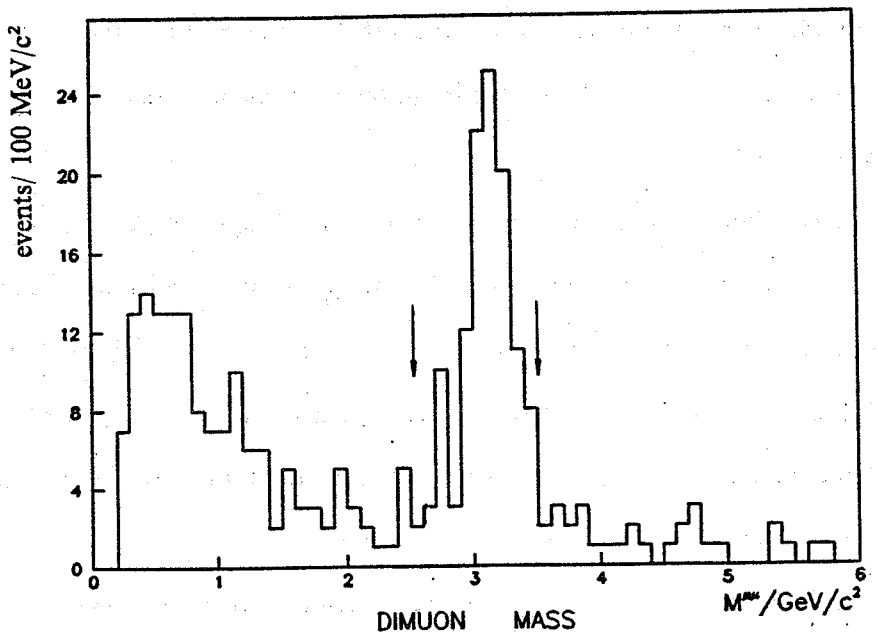

Figure 33: Dimuon mass distribution of the $M < 6$ GeV/c^2 sample (unlike−sign events). The cuts used to define the J/ψ candidates for the reference sample of good muons are indicated.

In all samples the matching χ^2 was recalculated using cosmic ray corrections. The alignment of the muon chambers with the CD was measured with a high statistics sample of cosmic ray muons. From these data corrections to the position of muon tracks in the muon chambers and improved error floors were deduced. These corrections (few cm) are small compared to the deviations due to multiple scattering for low p_t muons. Therefore they are not necessary for the selection of the dimuon sample, but they should be applied for the fit. As these corrections were only available for 1984 and 1985 data, the 1983 events were not used in the fit. After rebinning in order to obtain reasonable statistics in each bin (> 16 events), a least squares fit was performed. The distributions from the like and unlike−sign

events were fitted separately, constraining the background to be equally like and unlike−sign. This constraint is justified as there is no charge correlation in background events, provided both (decay) muons are not closely together. The fit results in a 244 ± 50 background muons in a sample of 886 muons. The χ^2 per degree of freedom of the fit is 1.2. The resulting matching χ^2 distributions of the fit are shown in figure 31 d) and 32 d). The result has to be corrected because:

- The single muons contain a fraction of prompt muons which is estimated to be 20 ± 5 % (see 5.2). This leads to an overestimate of the background. We verified that the result of the fit depends linearly on the fraction of good muons in the background sample. Hence the result has to be reduced by 0.8.
- A possible contribution of background to the J/ψ sample leads to an underestimate of the background. The decay background under the J/ψ peak can be estimated extrapolating the sidebands in the $M^{\mu\mu}$ distribution. This gives a continuum of 10 events, 30 % of them might be decay background. A similar estimate can be made using the like−sign events under the J/ψ peak (6 events, about half of them might be background). In both cases a background of 3 ± 3 % is found, which adds 2 % to the total background.
- As inclusive distributions are used (both muons of dimuon events enter independently), the fit results in a number of background muons. This has to be converted into a number of background events. If all background events would consist out of two faked muons, this conversion factor would be just 0.5. However, as explained in section 5.2, there exists a small fraction of background events with one prompt and one decay muon. Taking this into account the conversion factor is 0.575 instead of 0.5 .

Applying all these correction factors the background to the dimuons is measured to be 27 ± 7 % or 138 ± 36 events . This includes now the 1983 events. For that the estimate, which was obtained for 1984 and 1985 alone, was scaled by the ratio of the respective event numbers. This estimates the total background from all sources: decays, leakage and misassociation.

The error is dominated by the statistical error from the finite number of muons in the data (886 muons), the J/ψ sample (220 muons) and the single muon sample (242 muons). As this estimate is based on real data only, most of the systematic errors should cancel. The remaining systematic uncertainty[26] is in the order of 2 %. The advantage of this estimate is that it does not depend on the pion and kaon content, neither on the precision with which the detector can be simulated.

The background calculation from the previous sections predicts a total background of 25 $\pm$ 6 % or 127 $\pm$ 32 events, which is in excellent agreement with the result of the fit. As both methods for estimating the background are independent, they can be combined reducing the error. Thus we find a background contribution to the total dimuon sample of:

$$26 \pm 5\ \%\ \text{ or } 132 \pm 21 \text{ events}$$

Both methods can be used to estimate the background in subsamples of the selected events, or in different samples such as the low mass dimuons. In all these samples both methods agree very well confirming the validity of our background calculations (see table 8).

[26] Mainly due to a possible disturbance of the track measurement due to nearby tracks. This effects the data more than the J/ψ, as these events are better isolated.

sample used (84 and 85)	# of events	background calculation	background fit
$M > 6$ GeV/c^2 non − isolated	362	101 ± 25	112 ± 25
$M > 6$ GeV/c^2, unlike − sign non − isolated	233	51 ± 12	55 ± 17
$M > 6$ GeV/c^2, like − sign non − isolated	129	51 ± 12	61 ± 13
$M > 6$ isolated	81	13 ± 3	14 ± 8
$M < 6$ GeV/c^2, unlike − sign	295	33 ± 8 *)	49 ± 17
$M < 6$ GeV/c^2, like − sign	40	16 ± 4 *)	21 ± 10

*) *only decay background*

The isolation definition is explained in chapter 6.

Table 8: Comparison of background estimates.

6. EVENT CLASSIFICATION

In the previous chapters the two main classification parameters have already been discussed:

1. The *sign* of the muon pair. All events from the Drell−Yan process, Υ decays and first generation decays of heavy quarks have muons with opposite electric charge. Muon pairs with equal sign muons are expected from second generation decays of b−quarks. Possibly they could come from $B^0 - \overline{B}^0$ oscillations, and from more exotic sources such as $W^+ \rightarrow t\overline{b}$.

2. The *isolation* of the muons. This can be used to distinguish events heavy flavour decays from the Drell−Yan process and from Υ decays. The former are expected to have hadronic energy from the quark fragmentation and the decay debris around them, whereas the latter should generally not be accompanied by any hadrons.

Criterion 1) is experimentally straightforward, once it is ensured that the sign of the muons is correctly measured. Actually, this is only a problem for very high momentum tracks. The muons of the dimuon sample are at rather low momentum and the sign of the tracks is well measured (more than 3 σ in the worst case). Some uncertainty can arise from misassociation, as already discussed in chapter 5.1 .

For the isolation a well adapted criterion has to be developed. Naively one would expect that muons from heavy flavour decays are in, or at least close to, jets. However, the energy of these jets is often so low that they will not be reconstructed by the UA1 jet algorithm. Therefore it is necessary to have a criterion which is more efficient and does not depend on complicated algorithms. The simplest procedure is to add up all the transverse energy deposited in the calorimeter cells in a cone around the muon track. The problem one has to overcome is, that even a genuine isolated muon may have some hadronic energy around it, coming from the "underlying event". The underlying event is caused by the interactions of the partons not contributing to the hard process. It creates hadronic noise, about 3.6 GeV per unit of rapidity (in $\phi = 0 - 360^0$) [57], with large fluctuations. Therefore the cone size has to be chosen small enough not to pick up too much of this underlying event. When cutting on the

energy inside the cone one has to consider this contribution. On the other hand, the cone has to be large enough to collect a good fraction of the hadronic debris of heavy flavour decays. Also limitations from the finite granularity of the calorimeters have to be taken into account. We chose a cone size of 0.7 units in ΔR, with $\Delta R = \sqrt{(\Delta\phi^2 + \Delta\eta^2)}$, $\Delta\phi$ is the difference in the azimuth angle and $\Delta\eta$ the difference in pseudorapidity. The scatter plot with the sum of the transverse energy in this cone ("ΣE_t") around each muon is shown in figure 34 , separately for unlike−sign (a) and like−sign (b) events.

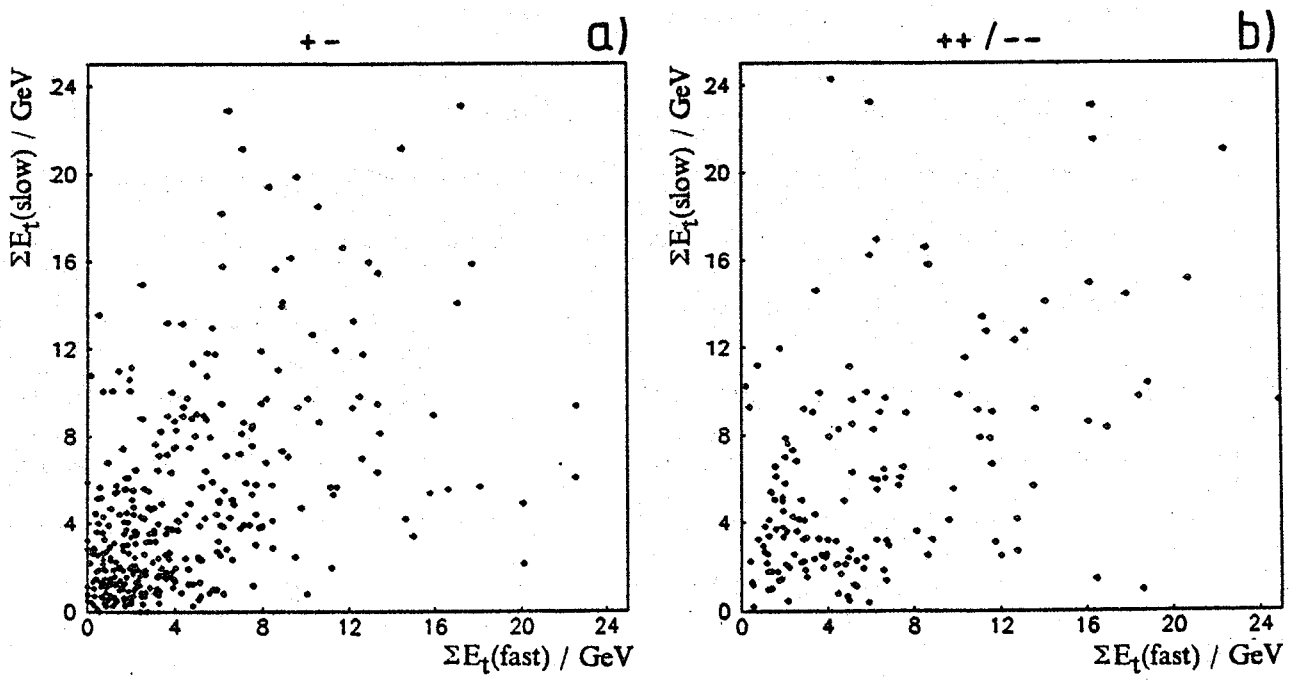

Figure 34: ΣE_t of the faster muon versus ΣE_t of the slower muon.
ΣE_t is the sum of E_t in a cone of $\Delta R = 0.7$ around the muon.
a) unlike−sign events, b) like−sign events.

As expected the unlike−sign events show a cluster at low ΣE_t for both muons, whereas this region is sparsely populated in the plot of the like−sign events. This becomes more evident if the variable S is plotted:

$$S = [\Sigma E_t(1)]^2 + [\Sigma E_t(2)]^2 \qquad \{29\}$$

[27] The choice of using the squared radius has the advantage that the distribution of S would be flat for uniform density in the two dimensional plot.

S is the radius squared[27] of each entry in the scatter plot, figure 34 . Whilst the distributions for like−sign and unlike−sign events are similar at $S > 9$ (GeV)^2, the unlike−sign events show a clear excess of events at $S < 9$ (GeV)^2. (fig. 35).

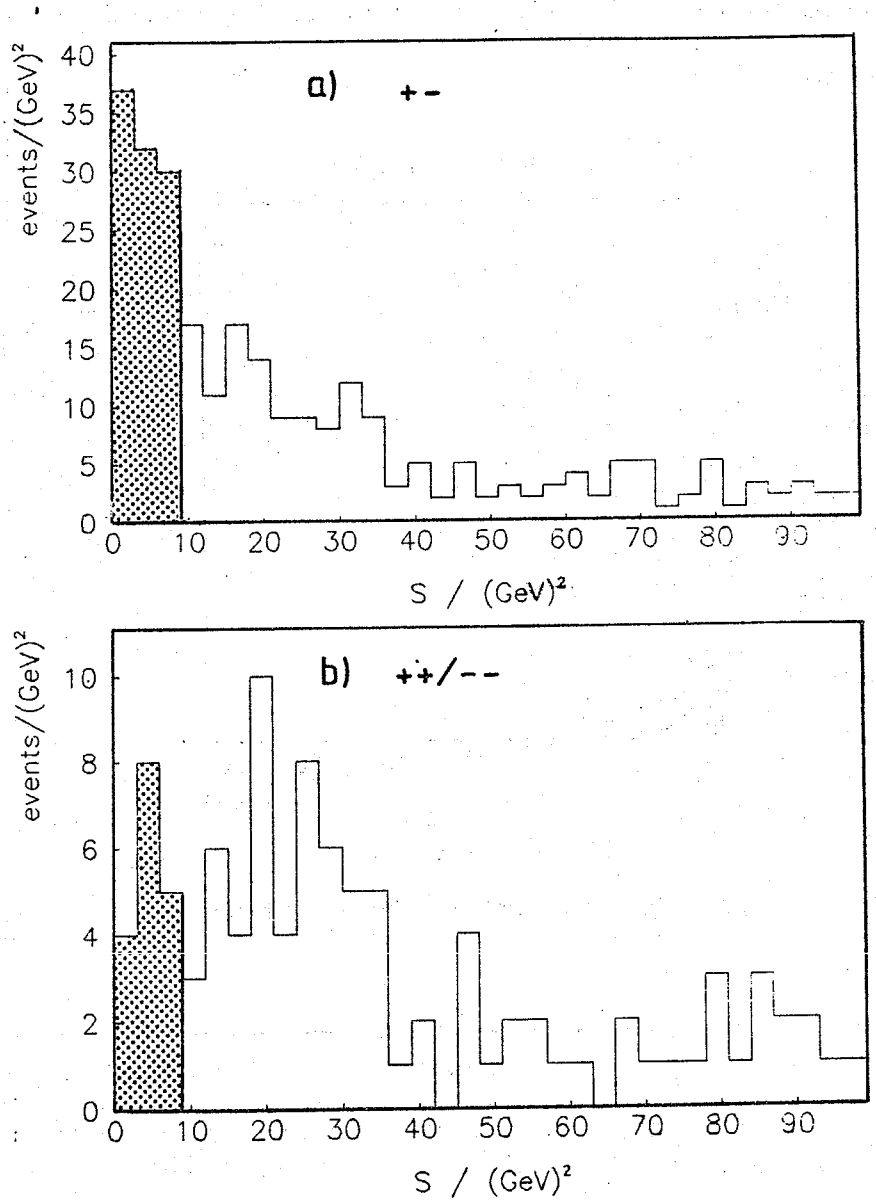

Figure 35: Distribution of the isolation variable S.
a) unlike−sign events, b) like−sign events
$S = [\Sigma E_t(1)]^2 + [\Sigma E_t(2)]^2$
The dotted regions indicates the isolated events with $S < 9$ (GeV)^2.

This excess of the unlike−sign events can be interpreted as the contribution from Drell−Yan and Upsilon, which is of course absent in the like−sign events. Consequently we define an event as isolat-

ed *if S is less than 9 (GeV)*^{2} . The efficiency of this cut for genuine isolated events was estimated using muons from $W^{\pm} \rightarrow \mu\nu$ decays, which should be isolated. Muons from two randomly chosen events were mixed and the S value was plotted (figure 36). 82 ± 7 % of these mixed events satisfy the isolation criterion. This agrees with the value of 85 ± 3 % calculated using Isajet Drell−Yan events and full detector simulation.

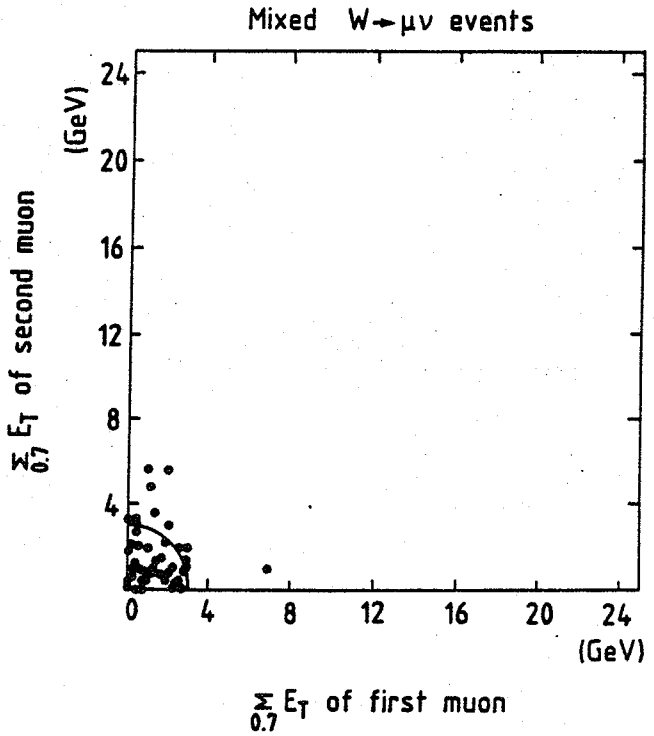

Figure 36: Isolation of mixed W → μ ν events.

	unlike−sign	like−sign
isolated	99	17
non−isolated	256	140

Table 9: Classification in terms of isolation and sign of the muons

The events can now be divided into four classes according to the sign of the muons and the isolation (see table 9, and for the background table 10). The isolated unlike−sign events are the Drell−

	calculation	fit	combined
isolated	15 ± 4	16 ± 8	15 ± 4
non−isolated	112 ± 28	122 ± 31	117 ± 21

(half of the background events are like−sign, half are unlike−sign)

Table 10: Classification of the background according to isolation

Yan and Upsilon candidates; the non−isolated events are referred as heavy flavour candidates. As already mentioned the separation is not 100%, since a small fraction of events from Drell−Yan and Upsilon contaminates the sample of non−isolated unlike−sign events. On the other hand, the existence of a few isolated like−sign events shows that some events from heavy flavour decays can pass the isolation cut. Therefore a small fraction of the events in the isolated unlike−sign sample may come from heavy flavour decays. This reflects the hard fragmentation of the b−quark. Sometimes most of the b's energy is shared by the muons and the invisible neutrinos. Then the hadrons around the muons are so soft that the event is indistinguishable from a genuine isolated event. This is especially true for unlike−sign events with both muons coming from first generation decays. Second generation decays which lead to like−sign events should be less isolated.

Nevertheless the isolation cut creates two almost separated samples either with Drell−Yan and Υ events or with events from heavy flavour decays.

Once the isolation criterion has been developed, it is a nice exercise to plot the dimuon mass distribution for all isolated unlike−sign dimuons. This should reveal all the vector particles which can decay into muon pairs. The mass cut of 6 GeV/c^2 is removed and the Z^0 candidates are added to the sample[28]. For the low mass events the isolation cut has to be modified. If the two muons are so close together that the respective cones overlap, a 3 GeV cut on the transverse energy in a single cone (also $\Delta R = 0.7$) around the common dimuon axis is applied instead. Altogether this results in 255 events. Because of the large mass range from 1 to 200 GeV/c^2, a logarithmic mass scale is used. This also

[28] These Z^0 candidates have looser selection requirements than the rest of the dimuons.

matches the deterioration of the mass resolution at large masses. The plot (fig. 37) clearly shows three peaks: the J/ψ, the ϒ and the Z^0, all well above a continuum, which should mainly be due to the Drell – Yan process.

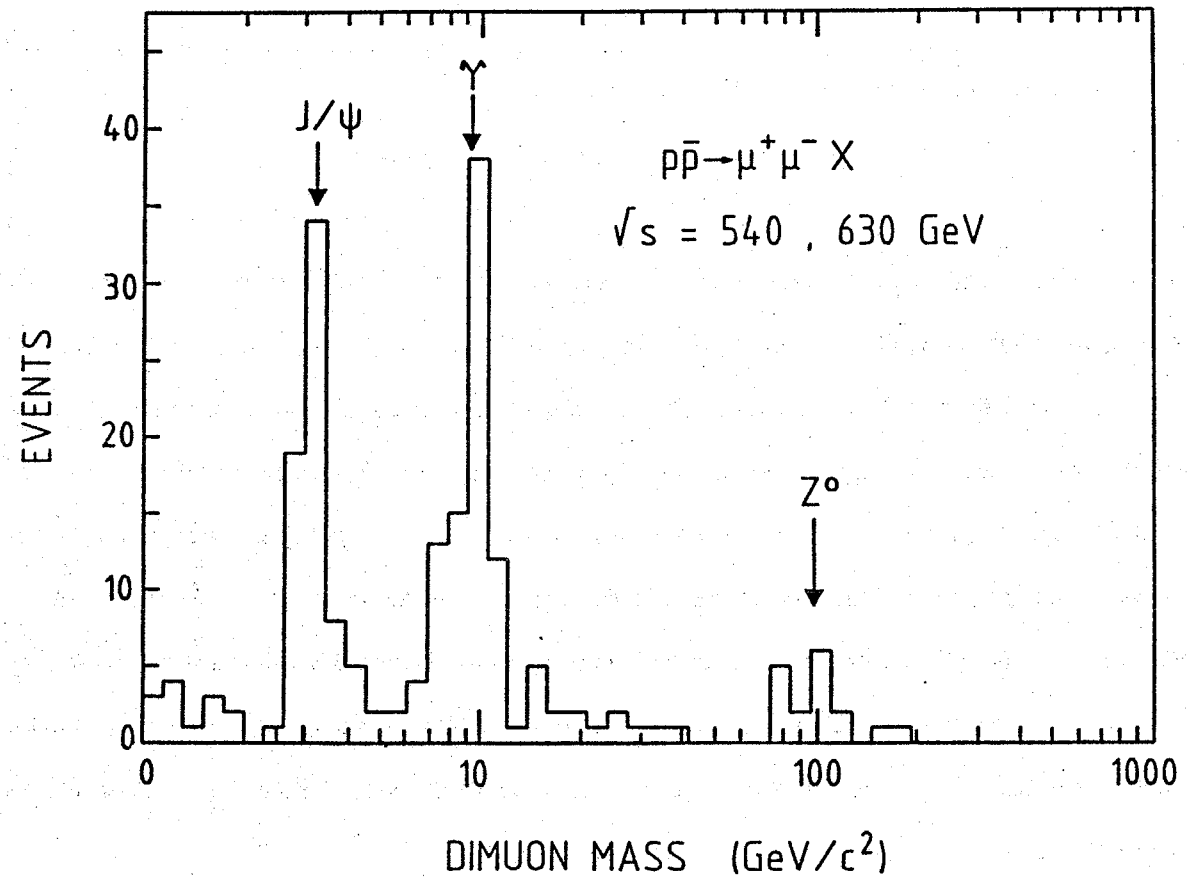

Figure 37: Dimuon mass distribution for unlike – sign, isolated events, p_t > 3 GeV/c for both muons. (Background not subtracted, not corrected for acceptance)

In the following chapters we will restrict ourselves again to the intermediate mass events between 6 GeV/c^2 and 50 GeV/c^2. Events with a higher dimuon mass are regarded as Z^0 candidates and are subject to a separate analysis [72]. A short overview on the low mass events will be given in chapter 12; a complete discussion can be found in [74].

7. DRELL – YAN PROCESS AND UPSILON DECAYS

The 99 isolated, unlike – sign events with $m^{\mu\mu}$ between 6 GeV/c^2 and 50 GeV/c^2 should be mainly caused by the Drell – Yan process and by Upsilon decays. In addition, there should be some contamination from heavy flavour decays. Another possible source for isolated unlike – sign events might be the decay $Z^0 \rightarrow \tau^+\tau^-$ with both τ's decaying into muons. The rate of this process is estimated to 0.2 events and can be neglected. The background from pion and kaon decays was calculated by applying the isolation cut to simulated background events resulting in 7.5 ± 1.5 background events. This was confirmed by the background fit giving 9 ± 4 events. We use the weighted mean of 8.0 ± 1.5 events.

In order to separate the contributions from Drell – Yan, Upsilon decays and heavy flavour, we made use of differences in the dimuon mass distributions. The Upsilon will of course appear as peak around 10 GeV/c^2. The theoretical dimuon mass distribution for Drell – Yan events is approximately proportional to $1/m^3$ (see {1}) Because of physics cuts and the acceptance of the apparatus this distribution is distorted. We studied this effect with the Isajet Monte Carlo. Drell – Yan events were generated according to the theoretical distributions. The detector response was simulated, and the events were analysed like real data. The same was done with simulated events from heavy quark production. The dimuon mass distributions obtained by these simulations are shown in figure 38 .

Compared to events from the Drell – Yan process, events from heavy flavour decays are more concentrated at low dimuon masses. This effect becomes even stronger once the isolation cut is applied. This can be understood as follows: In events with a high dimuon mass the quarks have to be produced at high Q^2. As on average a certain fraction of the quark momentum ends in hadronic fragmentation products, these muons are accompanied by more hadronic energy. Hence, dimuons from heavy flavour decays with high invariant dimuon mass are more strongly suppressed by the isolation cut.

The contributions from the different processes can be obtained by fitting the shape of their respective mass distribution to the data:

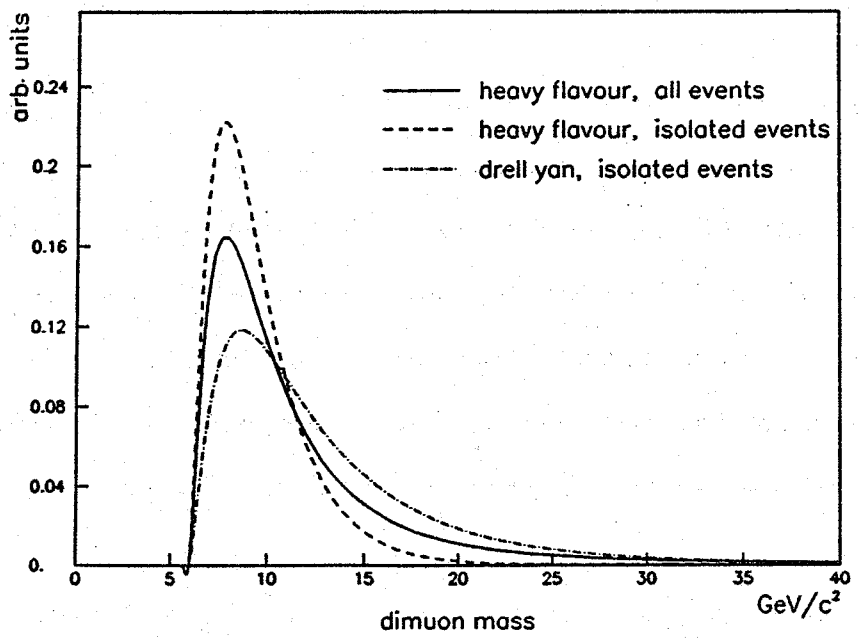

Figure 38: Dimuon mass distributions from Isajet. a) Drell−Yan Events (dashed−dotted line) b) Heavy flavour decays (solid line) c) Heavy flavour events, with isolation cut applied (dashed line)

- For Drell−Yan and isolated heavy flavour events the parametrized distributions from Isajet were used.
- The distribution for background from pion and kaon decays was calculated from single muon data with a second simulated decay muon. The distribution was parametrized and the contribution was fixed to 8 events. A gaussian error of ± 1.5 events on the background was incorporated in the fit.
- For the Upsilon we used a superposition of three gaussian distributions around m(ϒ), m(ϒ′) and m(ϒ″) with 0.5 GeV widths, reflecting the known experimental resolution in this mass region. The ratios of N(ϒ) : N(ϒ′) : N(ϒ″) were fixed at 1 : 0.30 : 0.15 [58]. The result of the fit is not very sensitive to the choice of these values.

A maximum likelihood method on an event by event basis was used to obtain the best fit. The result is shown in figure 39 .

The fit results in 40 ± 7 events from Upsilon decays, 29 ± 9 events from the Drell−Yan process and 22 ± 9 events from heavy flavour decays. The tail at high masses is consistent with the expecta-

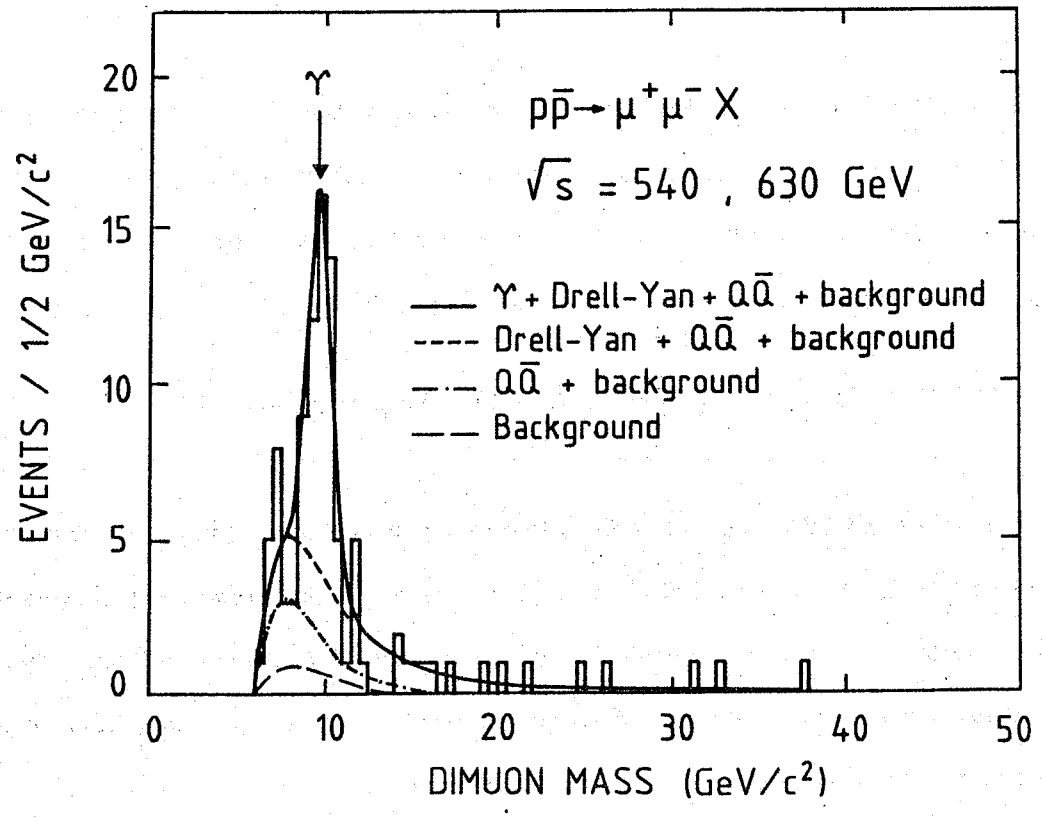

Figure 39: Mass spectrum of the isolated unlike−sign events. The fitted contribution from the Drell−Yan, Upsilon, Heavy flavour and background (fixed to 8 events) are shown too.

tions: Isajet estimates 0.8 ± 0.5 Drell−Yan events with a dimuon mass above 30 GeV/c² while we observe 3 events. Nevertheless there would be room for $Z \rightarrow \tau^+\tau^-$ decays. On the other hand, a dimuon event from $Z^0 \rightarrow \tau^+\tau^-$ could have substantial missing transverse energy. None of the isolated dimuons with $m^{\mu\mu} > 30$ GeV/c² has E_t^{miss} in excess of 1 σ (as defined in {28}).

Knowing the acceptance of our cuts and the efficiency of the apparatus from Isajet simulations, we can calculate a cross−section for the Drell−Yan process:

$$\sigma(\mathrm{DY}, m^{\mu\mu} > 11\ \mathrm{GeV/c^2}) = 0.26 \pm 0.08_{stat} \pm 0.05_{sys}\ \mathrm{nb}$$

for dimuon masses above 11 GeV/c²

(the systematic error includes errors of acceptance calculations, background subtraction and luminosity measurements)

A theoretical calculation of the Drell−Yan cross−section at collider energies was made by Altarelli et al. [59]. It predicts a cross−section for masses above 11 GeV of 0.27 nb, which is in very good agreement with the measured value. If we use the theoretical rapidity distribution of the Drell−Yan pair from Altarelli [59] (i.e. $\partial\sigma/\partial y(y=0) = 0.2\,\sigma$), we obtain a differential cross−section of:

$$\partial^2\sigma \,/\, \partial m \partial y \;(y=0,\, m^{\mu\mu} = 10\ \mathrm{GeV/c^2}) = 15 \pm 5_{stat} \pm 3_{sys}\ \mathrm{pb/GeV/c^2}$$

Our result is compared with earlier data from low energy pp collisions (figure 40), and good agreement is observed. The plot demonstrates that simple scaling predictions from pp experiments still hold at the very small τ ($= m^2/s$) of the collider. This is particularly interesting, as it shows that at small τ the contribution from the annihilation of sea quarks (which is the only possible channel at pp) dominates over valence quark annihilation (which can occur in $p\bar{p}$).

As the generation of Upsilons was not implemented in Isajet, one could not perform accurate acceptance calculations for this process. We used the acceptance for Drell−Yan events at 10 GeV/c² instead. This need not be the same, as the acceptance depends on the rapidity and p_t distribution of the events. Drell−Yan events are produced by quark antiquark annihilation, whereas Upsilons should be made by a kind of gluon fusion process. In principle, this can cause different kinematic properties. However, such differences should not be too large. As the acceptance does not depend strongly on p_t and rapidity in the Upsilon region, it is believed that the arising error is small. Under this assumption the cross−section times branching ratio of the Upsilon states is:

$$(BR) \times \sigma(p\bar{p} \to \Upsilon,\Upsilon',\Upsilon'') = 1.0 \pm 0.2_{stat} \pm 0.2_{sys}\ \mathrm{nb}$$

The differential cross section $\partial\sigma/\partial y$ compares well with data at lower energies (fig. 41). Again we used the assumption $\partial\sigma/\partial y\ (y=0) = 0.2\,\sigma$ [59]. Our measurement is also in good agreement with a gluon fusion model [61], and shows that there is approximate scaling down to $\sqrt{\tau}$ of 0.016 .

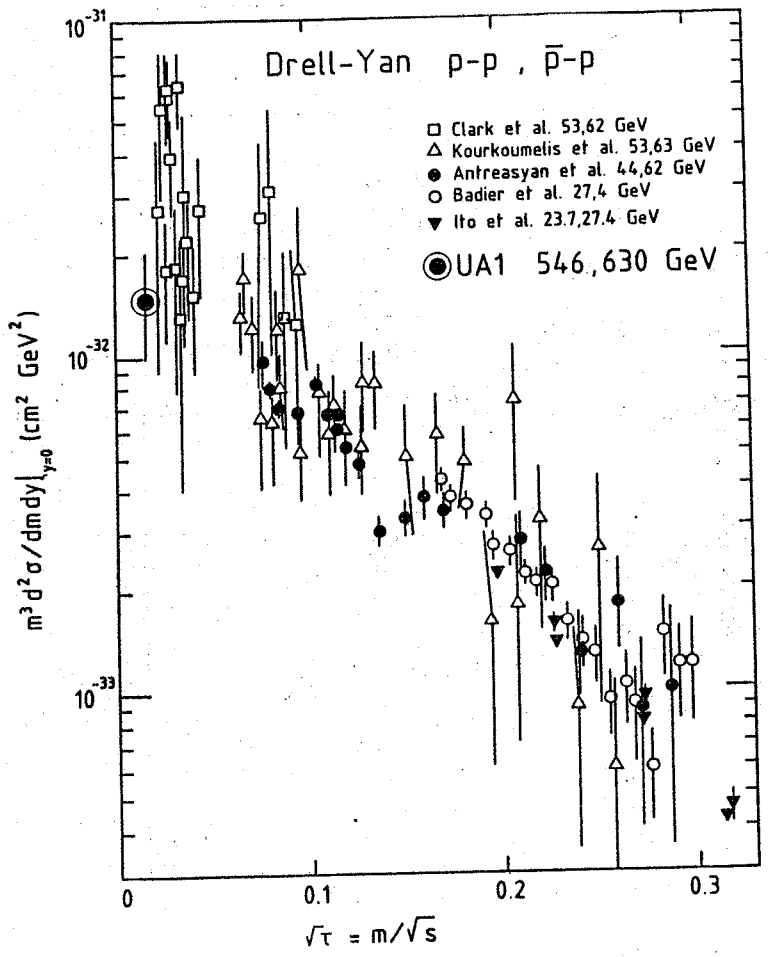

Figure 40: UA1 cross−section for Drell−Yan compared with data at lower energies [60].

It might be interesting to look at the jet activity in Drell−Yan events in order to extract some information on higher order QCD contributions. To get rid of the Upsilons and most of the events from heavy flavour decays we used only events with a dimuon mass larger then 11 GeV/c^2 (23 events). The fraction of events with jets of E_t > 7 GeV/c and $|\eta|$ < 2 is given in table 11 for the data and the Isajet Monte Carlo. The jet activity in the events is higher then predicted by Isajet, but the statistical significance is poor. As the cut on the E_t of the jet is rather low, the Isajet prediction depends strongly on the correct simulation of the underlying event. A cut on higher E_t might help, but with the present statistics it is not possible.

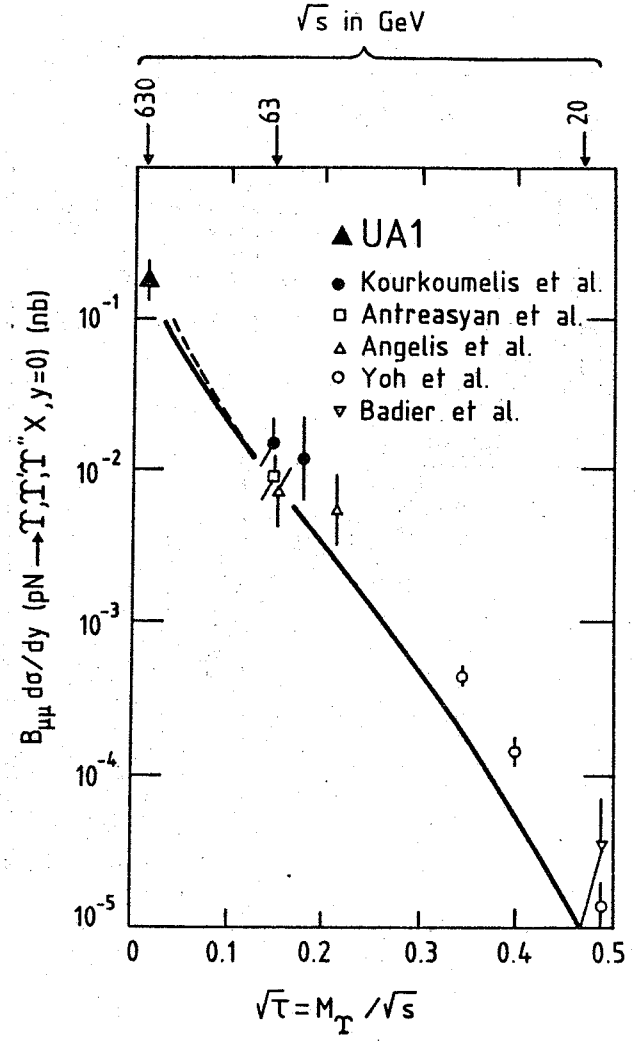

Figure 41: UA1 cross−section for Upsilon compared with data at lower energies [58] *and a theoretical calculation from ref.* [61].

	data	Isajet
one jet	21 ± 9 %	11 ± 4 %
two and more jets	9 ± 6 %	2 ± 2 %

Multiplicity of jets with E_t > 7 GeV and η < 2 in Drell−Yan events above 11 GeV/c^2.

Table 11: Jet activity in Drell−Yan candidates

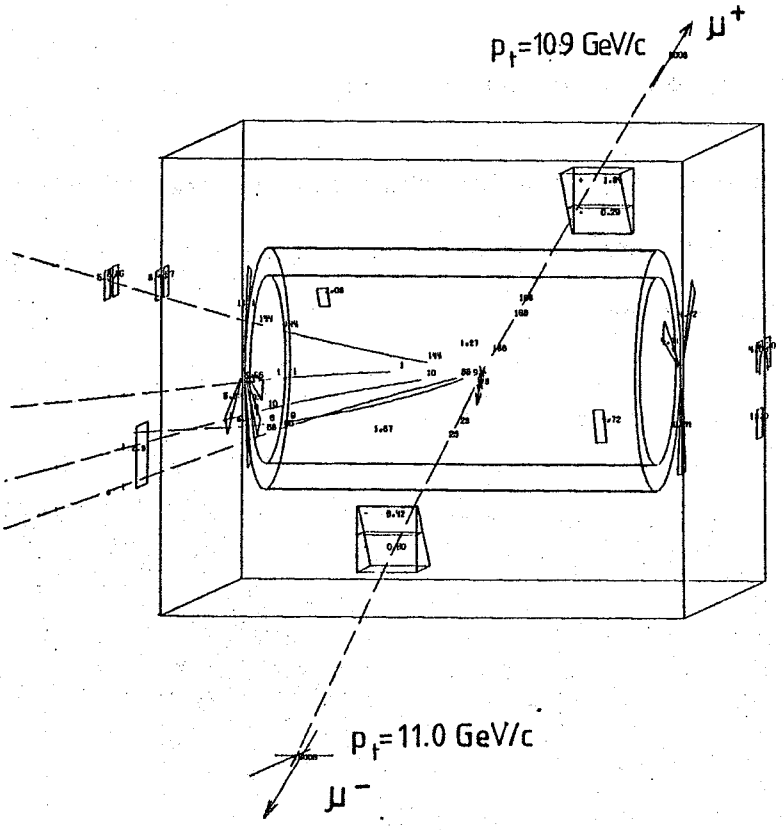

Figure 42: Drell−Yan candidate (event 19010/67) The invariant dimuon mass is 25 ± 3 GeV/c^2, the isolation variable S = 5.0 (GeV)^2 . The dimuons system has a p_t of 0.8 GeV/c .

8. HEAVY FLAVOUR PRODUCTION

8.1 General Properties of the Non − Isolated Events

In this chapter the properties of the non − isolated events are discussed. In these events the muons are imbedded in hadronic activity, a large fraction of them are in well identified hadron jets. An example of such an event is shown in figure 43 .

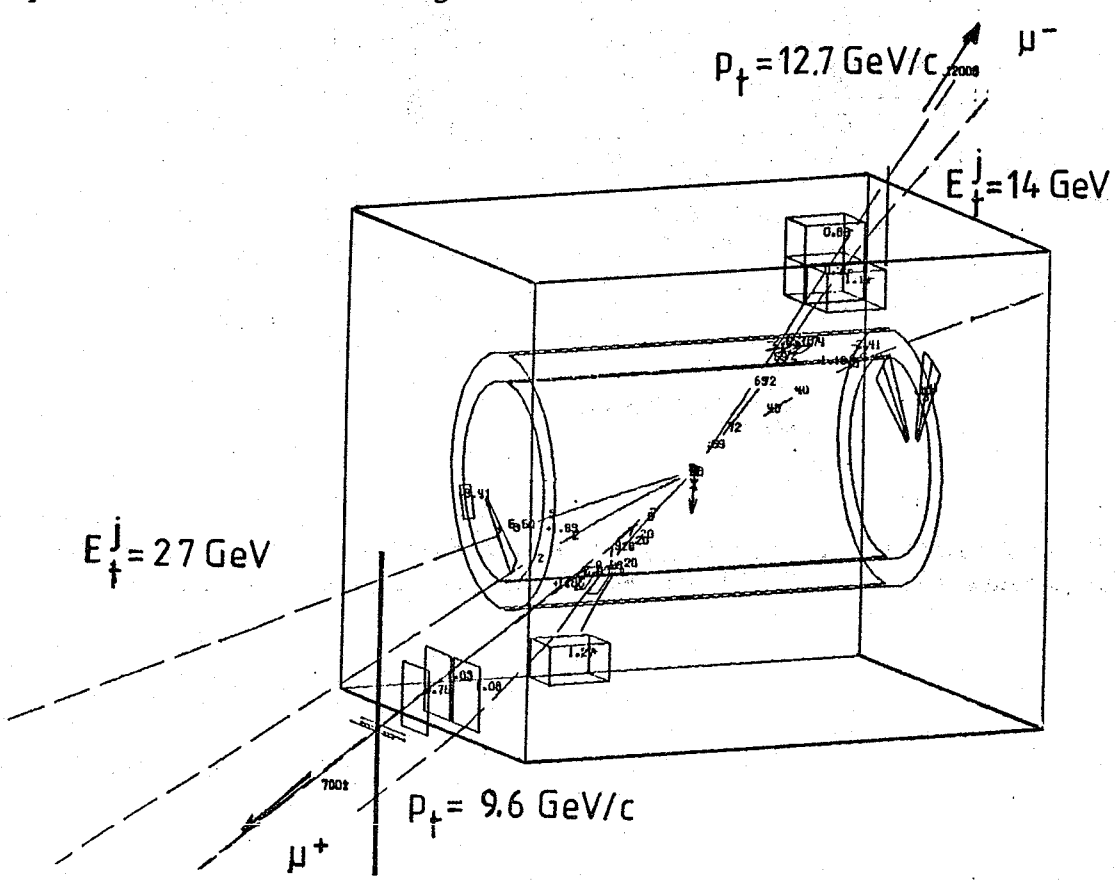

Figure 43: Example of a non − isolated event ("heavy flavour candidate") Both muons are in clearly identified jets, the mass of the muon − muon − jet − jet system is 108 GeV/c² (event 17049/365).

We have a sample of 396 events which are not isolated according to our cut; 256 of them are unlike − sign, 140 are like − sign. The background calculations resulted in a background of 117 events, which are equally like and unlike − sign. The most natural interpretation of the remaining 279 events is the production of heavy quarks and their subsequent semileptonic decays. In order to verify this interpretation a detailed comparison of the data with QCD calculations was done. These calculations were performed with the Isajet Monte Carlo.

In brief, Isajet generates $b\bar{b}$ and $c\bar{c}$ according to lowest order QCD. The heavy quarks are hadronized using Peterson et al. fragmentation functions. The decay chains of the heavy hadrons are simulated up to the level of final state particles (pions, kaons, muons, etc.). This is followed by a simulation of the detector response. Finally the same reconstruction and analysis procedure is applied as for real data. A more detailed description of the Isajet Monte Carlo can be found in the appendix (A 2.1).

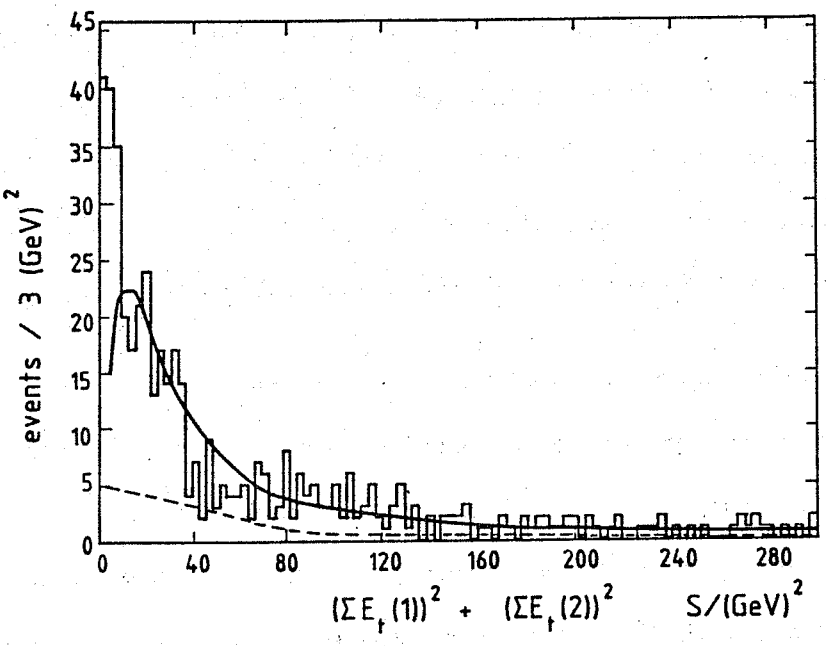

Figure 44: Isolation variable S for all events. The solid line is the Isajet calculation ($b\bar{b}$ and $c\bar{c}$) plus the expected background. The curve is normalized to the number of non−isolated events. The dashed line is the background alone.

The first thing to compare is the isolation of the events, as this was used to define the different samples. The distribution of the isolation variable S is shown in figure 44 together with the calculation of Isajet and the expected background. The Isajet curve was normalized to the non−isolated data [S > 9 $(GeV)^2$], after subtraction of the decay background. As the isolation cut is only 82% efficient for Drell−Yan and Upsilon, we expect 15 ± 8 events from these sources in the non−isolated sample. Therefore we allowed for 15 Drell−Yan and Upsilon events in the normalization of the Isajet curve. The Isajet calculation is in good agreement with the data. Again we realize the excess of isolated events, which are interpreted by Drell−Yan and Upsilon.

We can estimate the number of isolated events from heavy flavour decays by extrapolating the Isajet curve into the $S < 9\ (GeV)^2$ region. This should be consistent with the result obtained by the fit of the dimuon mass distributions (see chapter 7). Using the extrapolation one would expect about 59 isolated events (43 from heavy flavour and 16 background events). The fit found 22 ± 8 unlike−sign isolated events from heavy flavours, to which we have to add 8 ± 2 background events. In addition we observe 17 like−sign isolated events. They cannot come from Drell−Yan and Υ and are interpreted as heavy flavour decays as well. The background from pion and kaon decays in the isolated like−sign sample is expected to be 8 ± 2 events. This results in 47 ± 9 isolated events from heavy flavour and background, which is consistent with the 59 events expected from the extrapolation of the isolation curve. A slight discrepancy of these numbers can be understood, as it is difficult to calculate the exact isolation properties by Monte Carlo, especially if the events are almost isolated:

- Presently there exists no good theoretical model for the underlying event.
- The isolated events from $b\bar{b}$ stem from the hard tail of the fragmentation function. Their exact properties depend strongly on details of the fragmentation mechanism.
- Additional difficulties arise from the poor energy resolution of the calorimeters at low energies, and from the Landau fluctuations of the energy deposition of the muons in the calorimeters.

Small changes there can significantly change the Isajet prediction of isolated events from $b\bar{b}$, but they will have only a minor impact on the *shape* of the mass distribution of isolated events. Hence the number of isolated events from heavy flavour obtained by the mass fit is more reliable. Taking all this into account, Isajet describes the isolation properties fairly well. For further comparison between Isajet and the data the isolation cut will be applied on the Monte Carlo events as well as on the data.

From now on we refer only to the non−isolated events. Important dynamic properties of the events which should be compared with Monte Carlo are:

- p_t distribution of the muons.
- Dimuon mass distribution
- E_t of the muon−jet systems
- Mass of the muon−muon−jet−jet system.

The first two items, based only on muon properties, have the advantage of being directly measured by experiment. The inclusive p_t distribution of the muons and the dimuon mass spectrum are shown in figure 45 . In figure 46 the two dimensional p_t distribution of both muons is plotted. In these plots the Isajet prediction is normalized to the background subtracted data. The agreement between data and Monte Carlo is excellent.

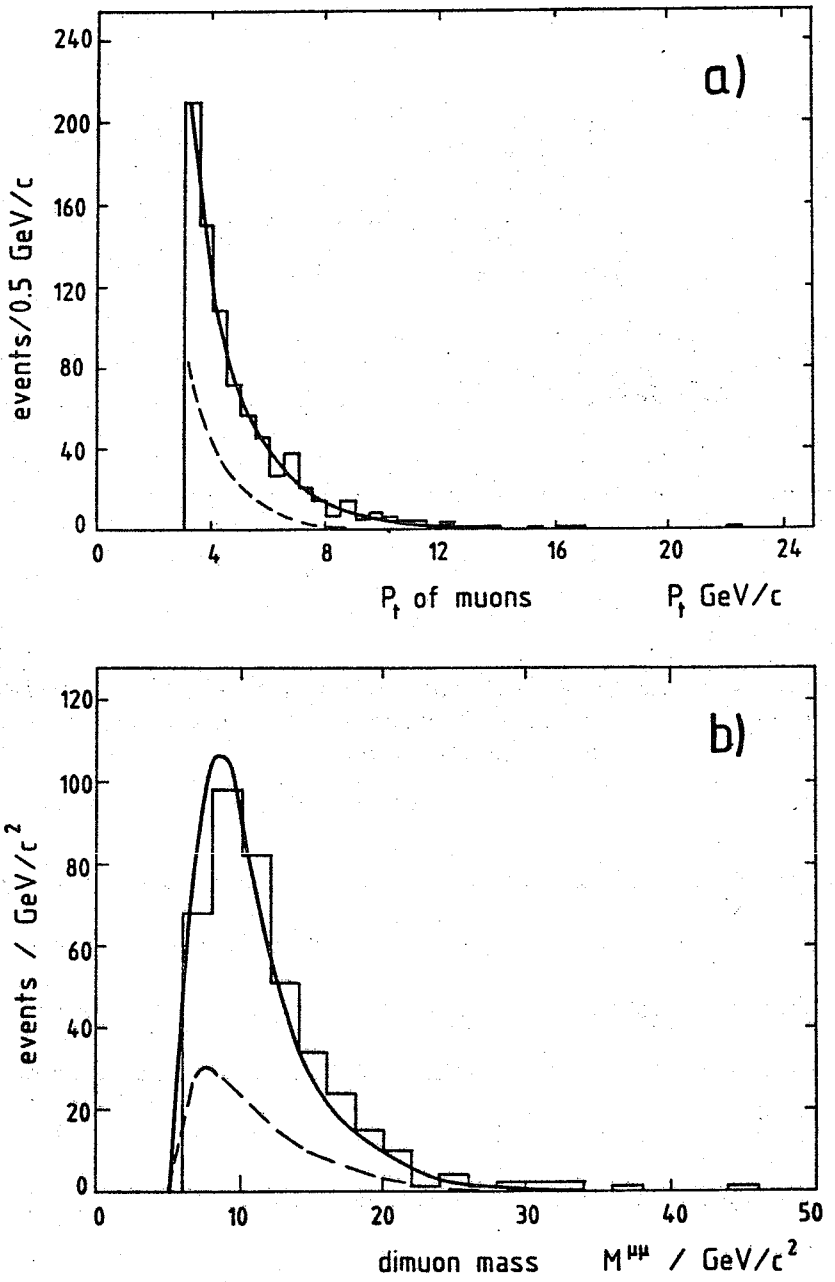

Figure 45: Kinematic properties of the non−isolated events. The sum of the Iajet calculation and of the background is shown as solid line, the background alone as dashed line.
a) inclusive muon p_t b) dimuon mass

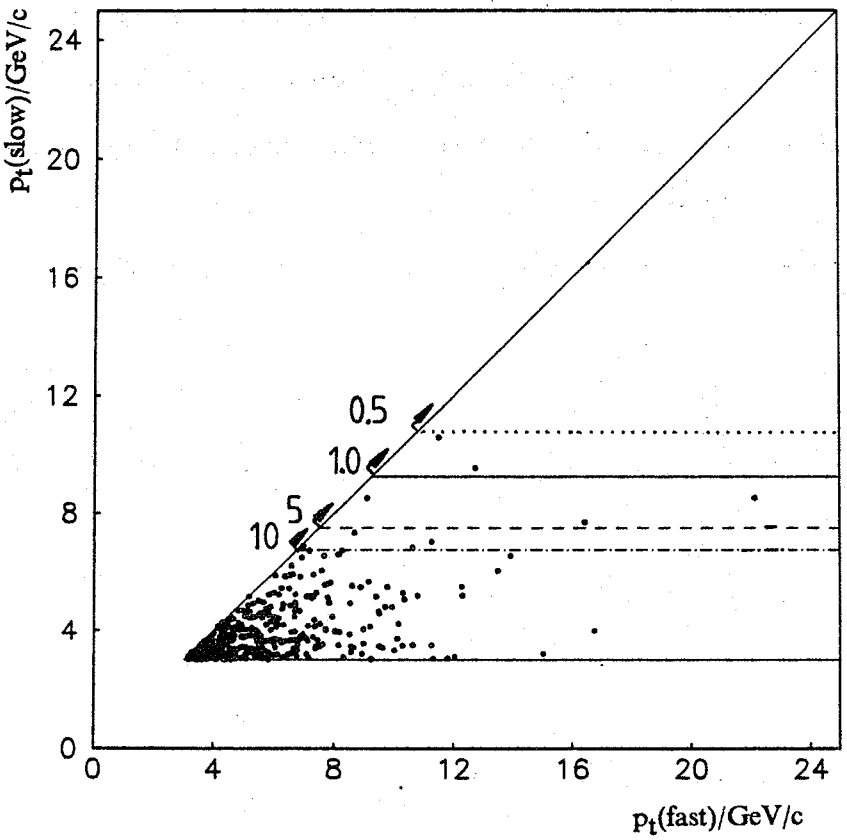

Figure 46: p_t of the fast muon versus p_t of the slow muon for all non−isolated events. Indicated are the regions where 0.5, 1, 5 and 10 events are expected. Isajet was normalized to all non−isolated events after background subtraction.

These distributions reflect the kinematic properties of the b−quarks only indirectly, as fragmentation and decay have to be included. The muon−jet system is more closely related to the original b−quark[29]. We have to find an appropriate way to define the muon−jet system. A very clear definition is offered by the data themselves: In figure 47 we plot the ΔR of *each* jet with an E_t above 7 GeV to the *nearest* muon [$\Delta R = \sqrt{(\Delta\phi^2 + \Delta\eta^2)}$, see {27}].

From this distribution it becomes evident that jets can be separated into two classes:

[29] The muon−jet system should contain all decay products of the b, except the neutrino. As there are always two neutrinos in a dimuon event from heavy flavour decay, it is not possible to use the missing energy technique. The neutrinos tend to be back−to−back and hence their missing energy vectors tend to cancel themselves.

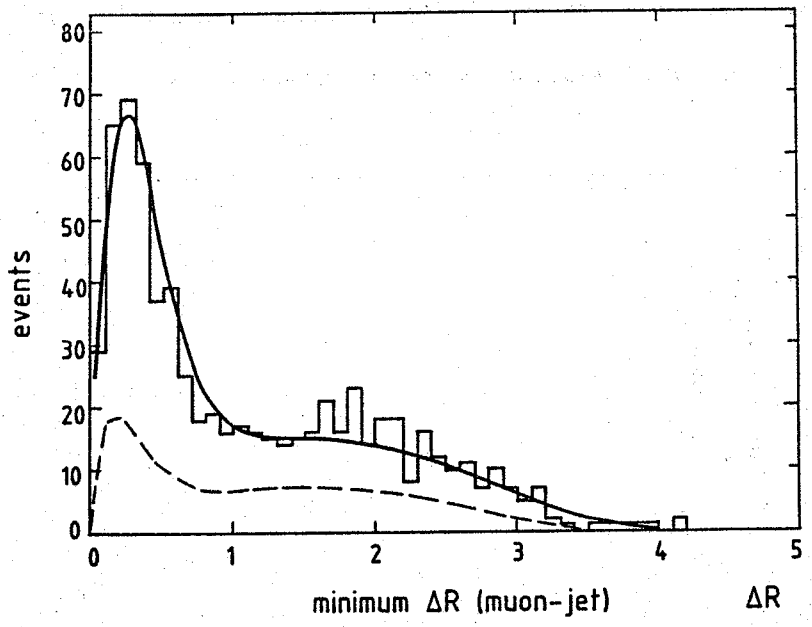

Figure 47: ΔR of each jet to the nearest muon. ΔR is defined in {27} . Only jets above 7 GeV E_t enter. Also shown is the Isajet calculation plus background (solid line) and the background alone (dashed line).

- There is a clear peak from jets clustering at $\Delta R < 1$. These jets should be mainly due to fragmentation and decay products of the heavy quarks, which decay into the muons. We call the jets within $\Delta R < 1$ "associated jets".
- Apart from the peak at small ΔR, there is an almost flat component which extends up to a ΔR of four. These jets should come from all kinds of higher order QCD processes such as initial and final state radiation, gluon splitting into heavy quarks etc.. Jets which have $\Delta R > 1$ are called "non−associated jets".

The muon−jet system is then defined as the muon and its nearest associated jet. It may happen that no jet is found in $\Delta R < 1$, either because it fails the E_t cut at 7 GeV, or because of the low efficiency of the UA1 jet algorithm to reconstruct low E_t jets. In this case the vector sum of all calorimeter cells in $\Delta R < 1$ around the muon is used as "jet". The four vectors of the muon and its associated jet are added to define the muon−jet system. The E_t distribution of this muon−jet system is shown in figure 48 (a), the distribution of the invariant mass of both muons and both associated jets in figure 48 (b).

Again Isajet is normalized to the background subtracted data. Although this method could possibly suffer from systematic effects of reconstructing, correcting and associating jets, Isajet and data are in good agreement.

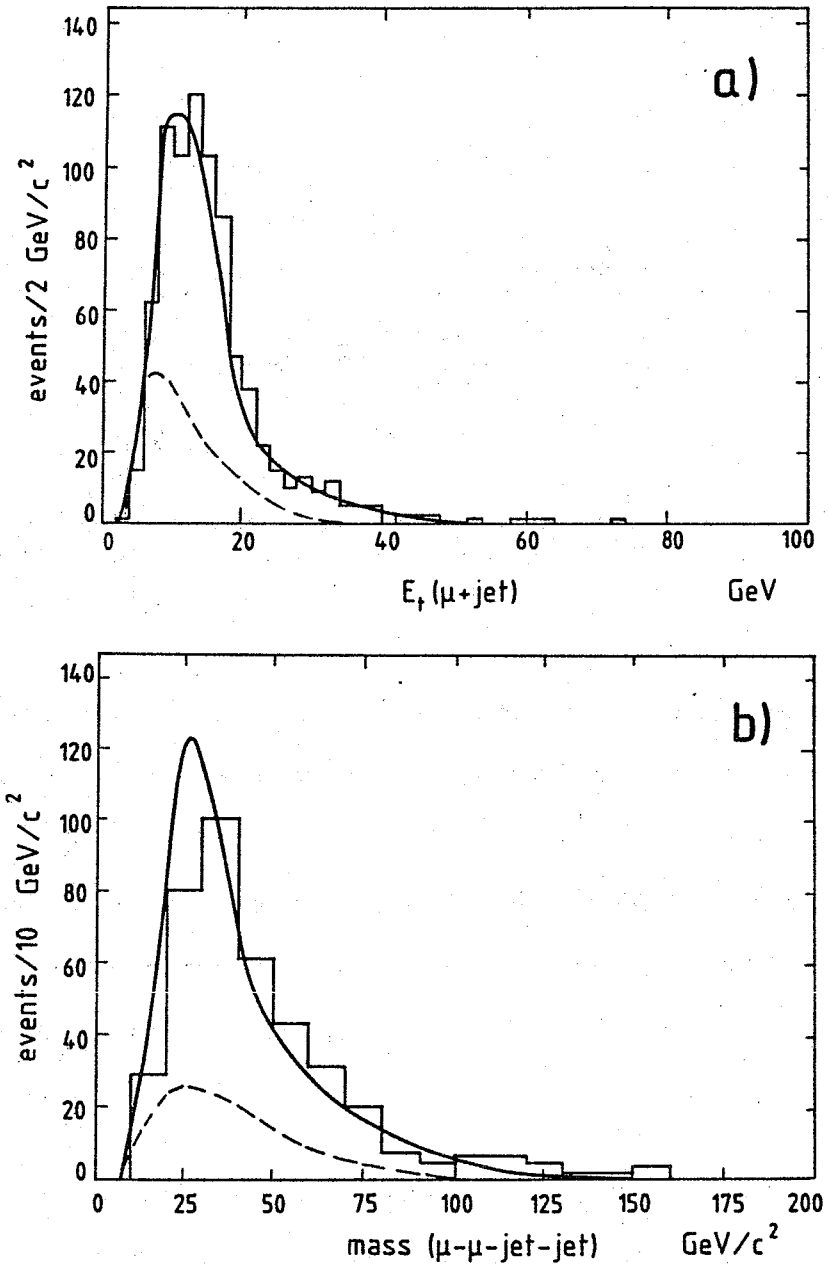

Figure 48: Properties of the muon jet system. The solid line is the sum of the Isajet calculation and background, the dashed line the background alone. Isajet is normalized to the background subtracted data.
a) E_t of muon−jet b) mass of muon−muon−jet−jet

Another property of the events, which could be used for a comparison with the Monte Carlo, is the missing transverse energy. The E_t^{miss} distribution of the data is plotted in fig. 49 together with the Isajet predictions and the expected background. The distribution of E_t^{miss} from Isajet is shown before and after detector simulation. It can be seen that the measured E_t^{miss} is mainly due to the limited resolution of the apparatus. Therefore we cannot extract much information about the real neutrinos. Nevertheless, the good agreement between the data and the Monte Carlo after detector simulation shows that detector effects are understood and well simulated.

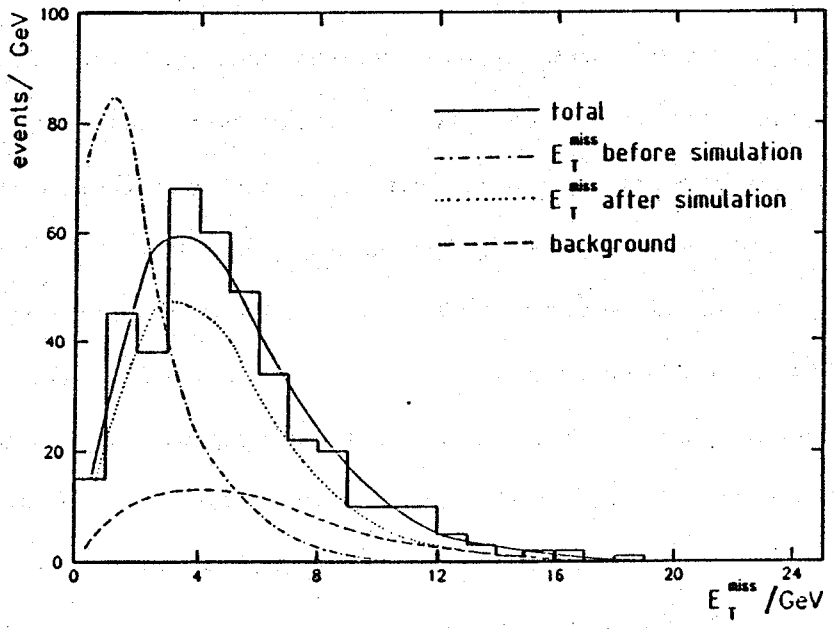

Figure 49: Missing transverse energy in the non−isolated events. Also shown is the expected contribution from decay background (dashed line), from Isajet, before detector simulation (dashed−dotted line), and after detector simulation (dotted line) and the sum of background and MC (solid line)

8.2 Separation of $c\bar{c}$ and $b\bar{b}$

As shown in the previous chapter, the hypothesis of heavy flavour decays describes overall properties of the dimuon data very well. According to Isajet calculations the largest fraction of these events come from $b\bar{b}$ production, only about 10% from $c\bar{c}$. We already have some evidence which supports the hypothesis of a large $b\bar{b}$ production at the collider:

- The Upsilon signal in the isolated events, which shows the production of "hidden" beauty.

- The existence of a large number of *like−sign* non−isolated events. There is no known physics source except $b\bar{b}$ production which can produce such a large number of like−sign dimuons[30]. Background from pion and kaon decay explains only 59 of the like−sign events; the remainder of the 140 events must come from $b\bar{b}$, either form second generation decays or from oscillations.

The relative amount of $b\bar{b}$ and $c\bar{c}$ in the unlike−sign, non−isolated events can be measured using the p_t of the muon with respect to the axis of its accompanying jet ("p_t^{rel}"). Since beauty particles are heavier than charmed particles, they tend to produce muons with larger p_t^{rel} . For this analysis we demand that *both* muons are close to clearly identified CD−jets. It is not possible to use calorimeter jets, as their direction is not measured precisely enough. The CD−jets are reconstructed using the standard UA1 central−detector−jet algorithm. The jet axis has to be within $\Delta R < 1$ around the muon, and the jet must contain at least one track with $p_t > 1$ GeV/c besides the muon track (The muon track is always included in these jets). This leaves a subsample of 113 unlike−sign events and 63 like−sign events. The p_t cut of 1 GeV/c reduces background from tracks picked up from the underlying event. Such "faked" jets would distort the p_t^{rel} distribution. The probability to pick up a high−p_t track in a cone of $\Delta R < 1$ can be checked using random cones in minimum bias events. From this it was calculated that in less than 10% of the events one jet is faked and in less than 1.5 % both. If the cut is lowered to 0.7 GeV/c, this background will double accounting for most of the additional events selected (the sample would then increase by 20%). Raising this cut would mean a severe loss of statistics. The p_t^{rel} of the muon is calculated with respect to the axis of this jet. The Isajet Monte Carlo was used to generate p_t^{rel} distributions for muons from b− and c−quarks respectively. The Monte Carlo should account for following effects which smear the original p_t^{rel} distributions:

- Neutral particles are not used for the reconstruction of the jet axis.
- Charged particles from the underlying event may be picked up by the jet algorithm.

---

[30] There is in principle the possibility of getting like−sign dimuons from higher order $c\bar{c}$ production, e.g., in a gluon−gluon scattering with both gluons splitting into $c\bar{c}$ pairs. According to Isajet this should account for only 0.5 like−sign events.

- Experimental resolution in the CD (which is important in the coordinate which is measured by charge division).
- Effects of the fragmentation of the heavy quark.

According to Isajet, muons from beauty jets have an average p_t^{rel} of 0.90 GeV/c, whilst muons from charm jets have 0.55 GeV/c on average, only 3 % of them have a p_t^{rel} above 1.0 GeV/c. The decay background and its p_t^{rel} distribution was determined by applying the same cuts on simulated decay muons. Thus we expect 25 unlike and 25 like−sign events in this sample with an average p_t^{rel} of 0.74 GeV/c[31]. After subtraction of the background a maximum likelihood fit of the Monte Carlo generated distributions to the data was performed. An allowance of 18 % error on the background was made. The fit results in a charm fraction $N(c\bar{c})$ / [$N(c\bar{c})$ + $N(b\bar{b}]$ of 15 ± 11 % in the subsample of 113 unlike−sign events. The fit was performed with the 63 like−sign events as well. In this case one has to consider a slight complication. Like−sign events from $b\bar{b}$ can come either from second generation decays of one b−quark, or, if it exists, from $B^0 - \bar{B}^0$ oscillations and first generation decays. The p_t^{rel} distribution is slightly different for muons from first and second generation decays. As the contribution from oscillations is a priori not known, only the fast muon, which is predominantly from first generation, is used. The fit results in a $c\bar{c}$ content of 0 % with less than 18 % at 90 % confidence level. This is exactly the expected result, as there is no way to get like−sign events from $c\bar{c}$. The p_t^{rel} distributions for like and unlike−sign events are shown in figure 50 including the fitted curves from $c\bar{c}$, $b\bar{b}$ and background. The results of the fit are summarized in table 12 .

Both results can be combined to obtain the total $c\bar{c}$ contribution in the non−isolated events. Adding like and unlike−sign events we find a $c\bar{c}$ content of 11.0 ± 8.0 %. This value has to be corrected because the efficiency of the CD−jet requirement is different for events from $b\bar{b}$ and $c\bar{c}$. As the charm fragmentation is softer than the beauty fragmentation, muons from charm have generally more hadronic energy around them and are therefore more likely to pass the cut. The selection efficiencies from Isajet are:

---

[31] It might appear astonishing that the p_t^{rel} of the background is larger than that of $c\bar{c}$, but most of the decay muons should come from gluon jets which are rather "fat". For such jets an average p_t^{rel} of 0.8 GeV/c for hard tracks ($z > 0.5$) has been measured in this experiment [62].

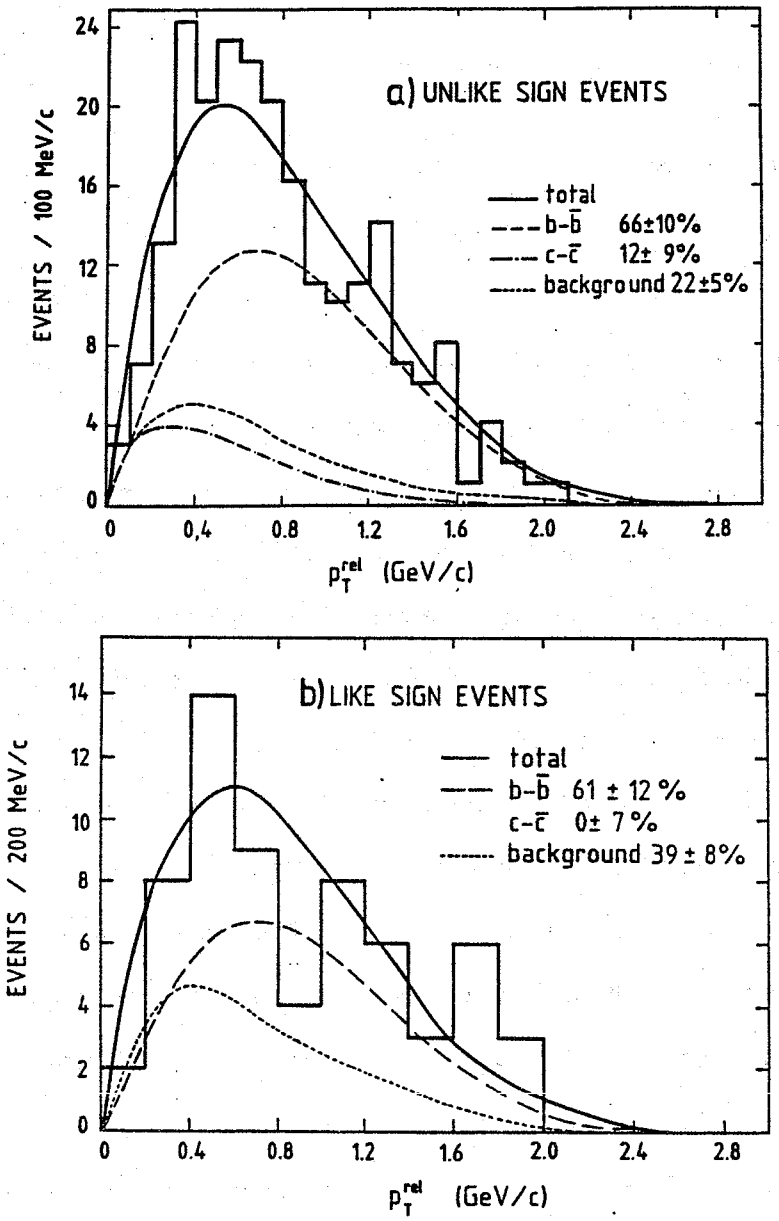

Figure 50: p_t^{rel} of the muon relative to the jet. The curves are results of a fit of Monte Carlo generated p_t^{rel} distributions from $c\bar{c}$ and $b\bar{b}$.
a) unlike−sign events. b) like−sign events.

$$N(\text{selected } b\bar{b}) \,/\, N(b\bar{b}) = 0.40$$

$$N(\text{selected } c\bar{c}) \,/\, N(c\bar{c}) = 0.55 \qquad \{30\}$$

	unlike − sign events	like − sign events
$b\bar{b}$	74.5 ± 11	39 ± 8
$c\bar{c}$	13.5 ± 10	0 ± 4
background (fixed)	25 ± 5	25 ± 5

Table 12: Results of the p_t^{rel} fit (Number of events)

Correcting the result from the fit the total $c\bar{c}$ content becomes:

$$N(c\bar{c}) / [N(c\bar{c}) + N(b\bar{b})] = 8.0 \pm 6.0\ \%$$

This should be compared with the Isajet calculation of 10 %.

The correction factors applied need some comment. Isajet uses a rather soft fragmentation function for the charm quark. This results firstly in a relativly small charm content and secondly in a higher selection efficiency for CD − jets from charm. If the charm fragmentation is harder, the selection efficiency would become closer to that for beauty events. E.g. the Eurojet Monte Carlo (see appendix A 2.2) uses a harder charm fragmentation than Isajet. This Monte Carlo calculates a relative charm content of 23 %. In this case the correction factor for charm would be less than 0.55, and we can use the uncorrected results as upper limit. 11 ± 8 % is certainly not inconsistent with 23 %, but the much better agreement with the Isajet calculation justifies the choice of the correction factors used.

8.3 Jet Activity

In our naive picture of heavy flavour production the muons will be accompanied by jets. We have already made use of the jet activity in the events by defining the muon − jet system and the p_t^{rel} of the muon to the jet axis. A jet was classified as associated if its axis was within a cone of $\Delta R < 1$ around the muon. This was justified by the ΔR(muon − jet) distribution of the data, which clusters at $\Delta R < 1$ (fig. 47) For the analysis of the jet activity additional cuts are necessary in order to clean the sample from mismeasured jets:

- We demand central jets within $|\eta| < 2$. Thus the contributions from the spectator fragments of the proton and antiproton are suppressed. This cut also makes the acceptance for jets more similar to the muon acceptance.
- Veto on double interactions. 34 events are rejected because they are identified as double interactions according to following criteria:

  More than 350 GeV scalar energy in $\eta < 0$ or $\eta > 0$

  or

  A second well identified vertex, cleanly separated from the main vertex and compatible with the beam size.

  It was always ensured by scanning that both muons come from the *same* vertex. Double interactions should not disturb the muon properties very much, but the higher activity in these events might give rise to additional jets.
- The analysis was repeated demanding $E_t(\text{jet}) > 10$ GeV for the uncorrected jet E_t. This reduces the contribution from fluctuations of the underlying event and reconstruction errors.

The multiplicity of jets per event is shown in figure 51 , for all jets and for non−associated jets only. All distributions are after background subtraction. The predictions from Isajet are superposed for:

- *Lowest order processes only:* In a lowest order process only associated jets should appear. As Isajet applies radiative corrections to its lowest order calculations, a fraction of these events has non−associated jets from initial and final state radiation.
- *Including higher order processes:* Processes like gluon splitting into heavy quarks or flavour excitation can be simulated by Isajet to a certain degree, although Isajet does not use correct higher order matrix elements (for details see appendix A 2.1). These processes give rise to non−associated jets.

Fair agreement is observed between the Monte Carlo predictions and the data, although the fraction of high multiplicity events is larger than predicted. This might be a systematic shift due to uncertainties in the jet reconstruction efficiency and the absolute energy calibration of the calorimeters.

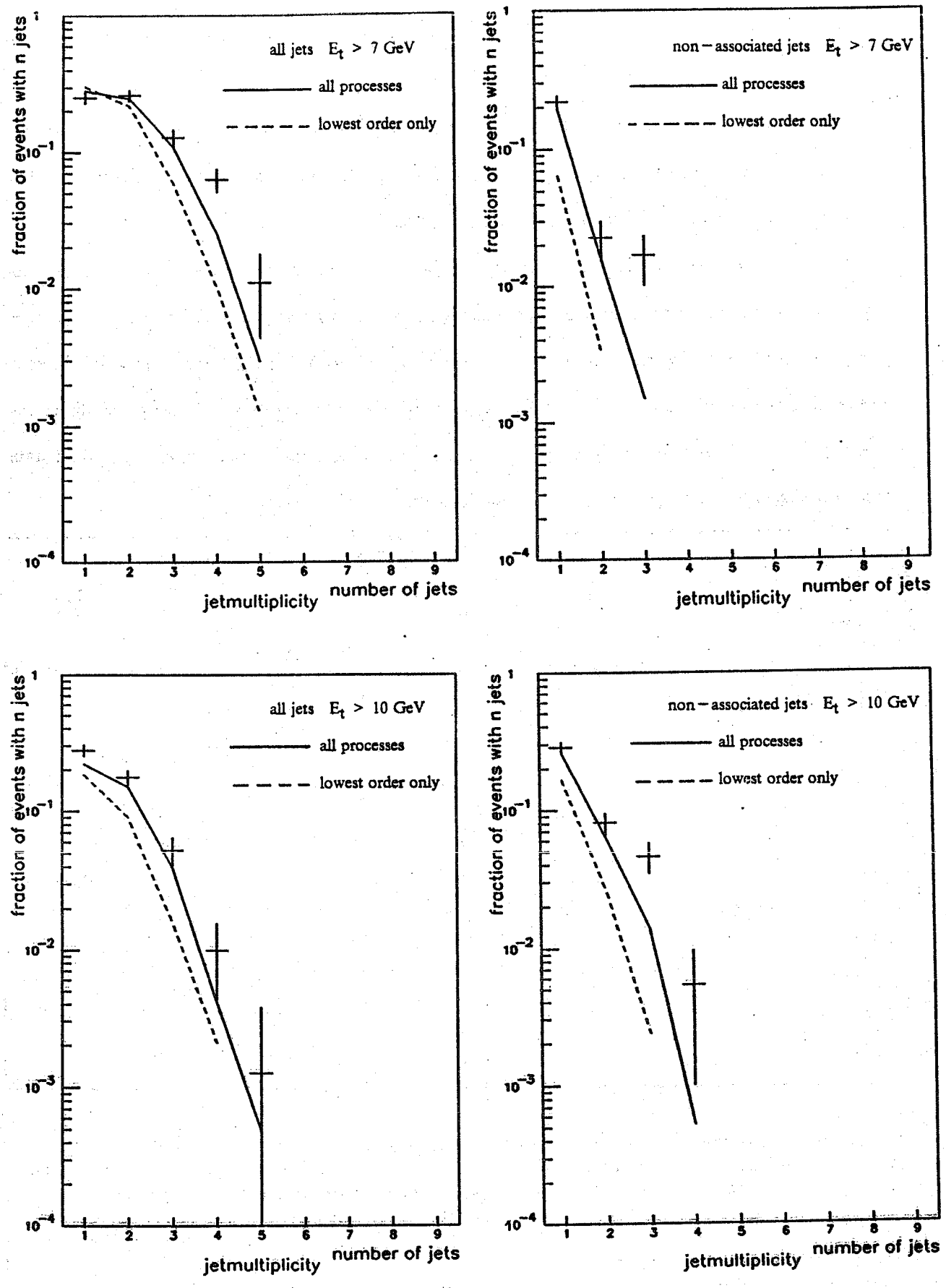

Figure 51: Multiplicity of jets.

Nevertheless, the multiplicity distributions, in particular those of the non−associated jets, can only be explained once higher order processes are taken into account.

The E_t distributions of associated and non−associated jets are shown in figure 52 . Both spectra are well described by Isajet. The loss of efficiency for low E_t jets is due to the cut on the uncorrected jet E_t and the subsequent application of jet correction factors .

Differences between associated and non−associated jets can be seen in the $\cos(\theta^*)$ distributions (fig. 53). θ^* is defined as the angle from the incoming protons in the rest frame of the muon−muon−jet−jet system[32] including all non−associated jets. Whilst the $\cos(\theta^*)$ distribution of associated jets is almost flat, the distribution for non−associated jets is peaked in forward and backward directions [$\cos(\theta^*) = \pm 1$]. This is expected, as most of the non−associated jets should come from initial state radiation. Again the Isajet predictions are in good agreement with the data.

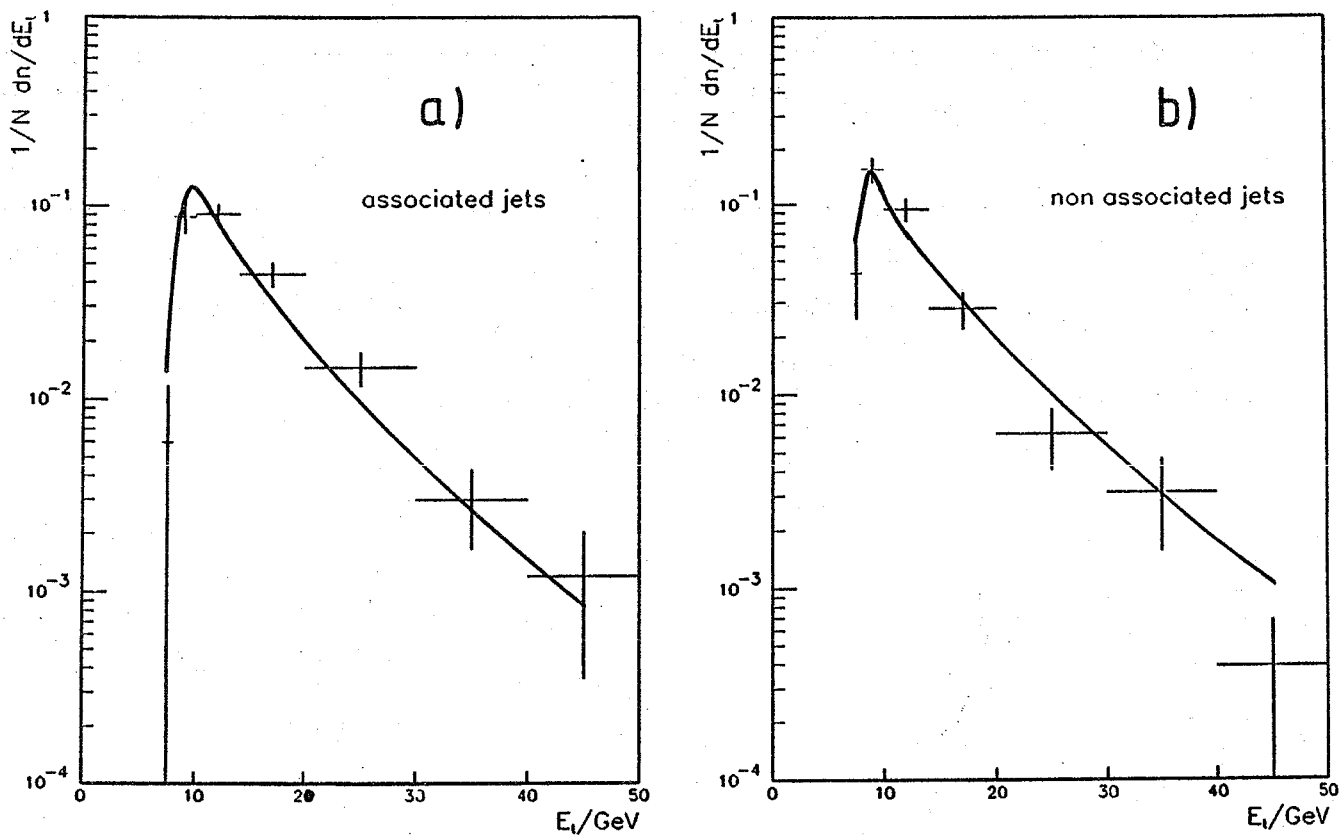

Figure 52: E_t spectrum of jets in dimuon events (background subtracted). A cut of 7 GeV was applied to the uncorrected jet E_t , whilst the corrected one is plotted. The jets have to be in $\eta < 2$. The Isajet calculation (solid line) was normalized to the total number of jets in each histogram. a) associated jets b) non−associated jets.

[32] As defined in chapter 6.3 .

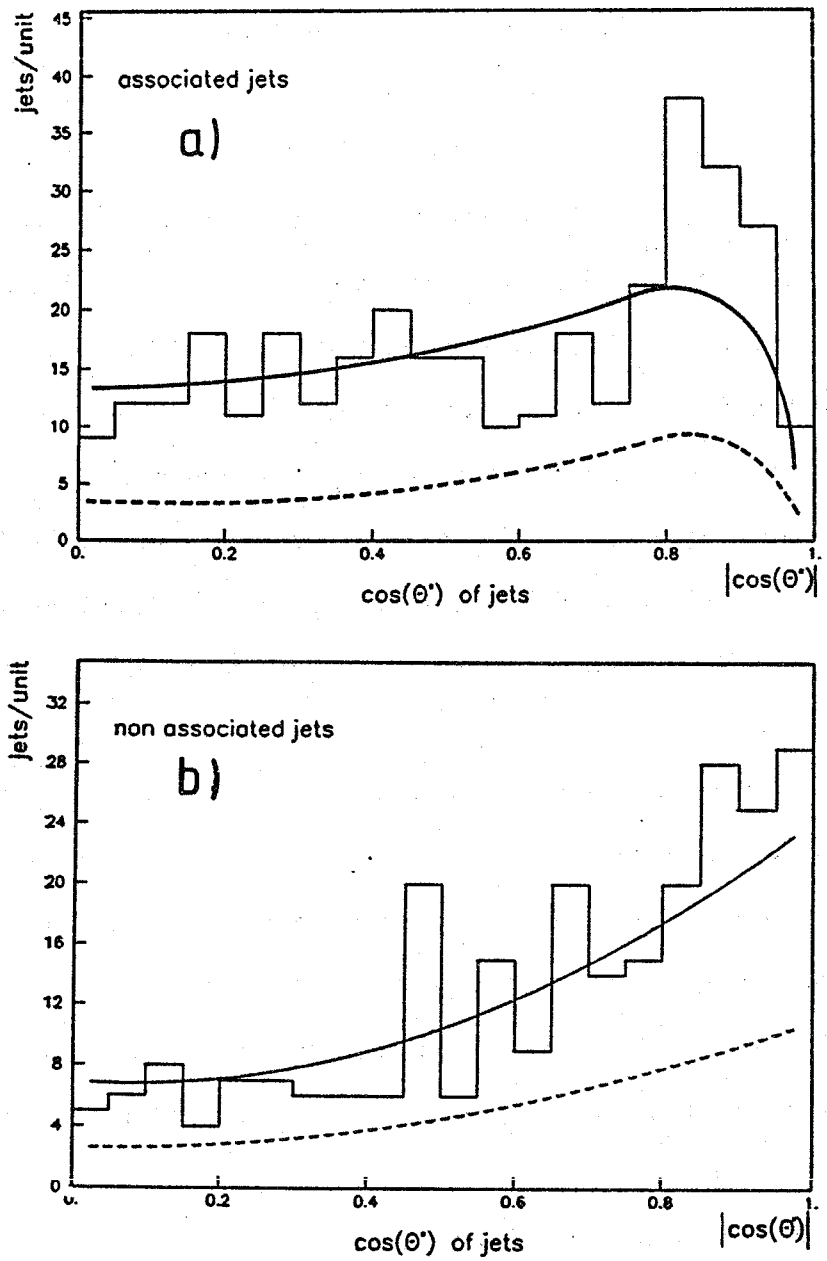

Figure 53: $\cos(\theta^*)$ distribution of jets in dimuon events. See text for the definition of $\cos(\theta^*)$. The solid line is the Isajet calculation plus the background, the dashed line is the background alone. Isajet was normalized to the background subtracted data.
a) associated jets, b) non−associated jets.

8.4 Higher Order Processes

The high activity of non−associated jets already indicates the importance of higher order QCD processes. Unfortunately jet counting is not a very precise method for measuring the amount of higher

order contributions, at least if low E_t jets have to be used. Systematic errors from the jet reconstruction efficiency, the contribution from the underlying event, and the absolute energy calibration are difficult to estimate and can account for large uncertainties. The contribution from higher order QCD is better determined by looking at muon properties only, which are measured very precisely.

Quantities which are sensitive to higher order processes are the azimuthal angle difference between the muons ($\Delta\phi$) and the p_t of the dimuon system. In a lowest order QCD process, e.g. gluon−gluon fusion to a $b\bar{b}$ pair, both final state quarks are back−to−back, and they have only a small p_t of the magnitude of the fermi motion of the proton constituents. This is reflected by the muons, here of course some smearing by fragmentation and semileptonic decay of the quarks occurs. In higher order processes with three or more partons in the final state, the heavy quark system has to balance the p_t of the rest of the final state. Hence the muons are forced to be not back−to−back and the dimuon system can get substantial p_t .

Although Isajet does not use the exact matrix elements for $2 \rightarrow 3$ processes, it is nevertheless able to simulate the effects of such (and even more complicated) processes to a certain degree by giving radiative corrections to the lowest order process. It is possible to simulate lowest and higher order processes separately and to compare their respective properties with the data. The $\Delta\phi$ between the muons is plotted in figure 54 . Superposed are the contributions from Isajet lowest order and higher orders, the background and the sum of all. Both Isajet contributions are normalized to the background subtracted data by a *common* scale factor.

As expected, the lowest order contribution peaks at 180^0 and disappears for $\Delta\phi$ less than 100^0. The $\Delta\phi$ distribution from higher order processes is much flatter, extending from 0^0 to 180^0. Altogether Isajet describes the data very well and the following conclusions can be drawn:

- It is evident that the data at low $\Delta\phi$ can only be described by higher order processes.
- Isajet correctly estimates the relative contribution from higher order processes. We observe after background subtraction 27 ± 5 events[33] at $\Delta\phi < 100^0$. Isajet after correct normalization predicts 24 events from higher order processes and only one event from lowest order in this

[33] The error reflects the uncertainty of the background subtraction (14 ± 5 events background with $\Delta\phi < 100^0$).

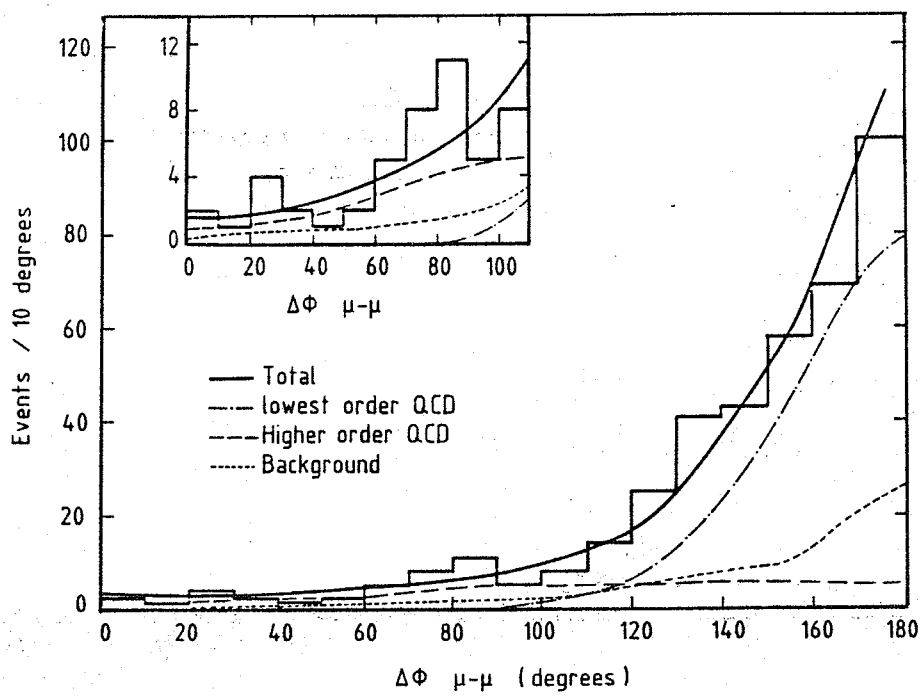

Figure 54: Δφ between both muons (non−isolated events). Superposed are the contributions from Isajet, separately for lowest and higher order contributions and the expected background. Isajet is normalized to the background subtracted data (using the same scale factor for lowest and higher orders).

region.

The quantitative agreement is not trivial, as higher order corrections often show infrared divergences, which have to be controlled by somewhat arbitrary cut−off parameters.

The same conclusion can be drawn from the distribution of the dimuon p_t . The Isajet higher order processes explain well the events with high p_t, again supporting the importance of higher order QCD (figure 55).

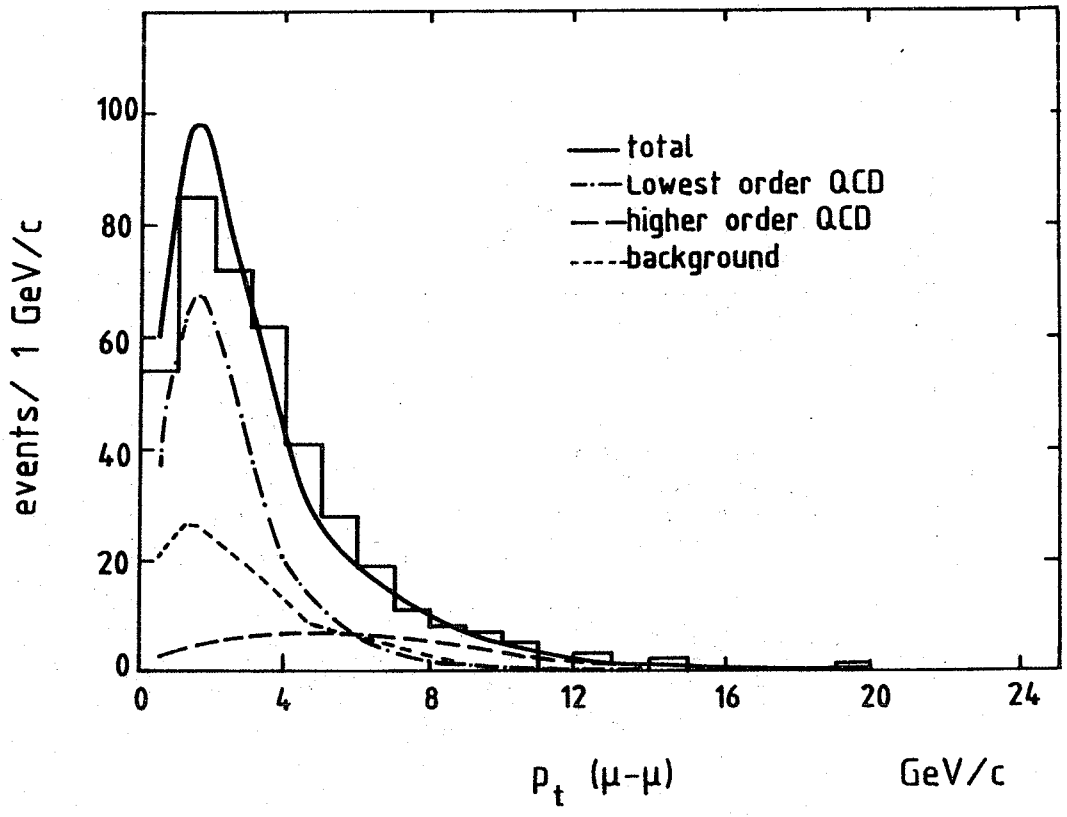

Figure 55: p_t of the dimuon system.
Superposed are the contributions from Isajet, separately for lowest and higher order contributions and the expected background.

8.5 Cross – Section for $b\bar{b}$ Production

In order to calculate a cross – section for $b\bar{b}$ production we have to know the relation between the number of heavy quark pairs originally produced, and the number of dimuons which are finally detected. This depends on:

- p_t and rapidity distributions of the heavy quarks
- Fragmentation and decay of the heavy quarks
- Efficiency of the apparatus
- Acceptance of the physics cuts

All this can only be studied with Monte Carlo calculations. As the agreement of the Isajet Monte Carlo and the data is very good, we can be confident that Isajet performs a reliable simulation of these effects. Starting with $b\bar{b}$ and $c\bar{c}$ production from lowest order QCD and including (to a certain extend) higher order corrections, Isajet predicts absolutely 436 events from heavy flavour production in the di-muon events. 90% of the events are due to $b\bar{b}$, only 10% come from $c\bar{c}$. Dimuons production from top or from $Z^0 \rightarrow b\bar{b}$ is not considered in that calculation. The higher order processes account for 21% of the events from $b\bar{b}$.

We observe a total of 512 events, from which we have to subtract 134 background events and 84 events from Drell−Yan and Upsilon[34] resulting in 294 events. Thus the cross−section calculated by Isajet has to be scaled down by a factor of 0.67. Isajet computes a partial cross−section of 1.66 μb for lowest order $b\bar{b}$ production, with the p_t of both b−quarks above 5 GeV/c, and the rapidity within 2.

If we assume that all Isajet processes need the same scale factor (0.67), this cross section becomes:

$$\sigma(p\bar{p} \rightarrow b\bar{b}) = 1.1 \pm 0.1_{stat} \pm 0.4_{sys}\ \mu b$$

$$p_t > 5\ \text{GeV/c (both b−quarks)}$$

$$|\eta| < 2\ \text{(both b−quarks)}$$

lowest order processes only

The systematic error includes errors of the acceptance, the luminosity and uncertainties of the Monte Carlo (e.g. fragmentation parameter, structure functions). The reasons for limiting the quoted cross−section to the lowest order process and to the restricted kinematic region are:

- Heavy quark production outside this kinematical region (especially forward production) will hardly give dimuons within the acceptance of the detector and physics cuts. Therefore acceptance corrections would be large and would introduce large systematic errors.
- Higher order processes might contribute to a large fraction of the total cross−section, but most of the dimuons from them will not pass the physics cuts. E.g. gluon splitting into heavy quark pairs tends to produce dimuons of low invariant mass, which fail the 6 GeV/c^2 cut.

[34] Corrected for the 82% efficiency of the isolation cut.

Omitting forward production and low mass dimuons, the remaining corrections due to higher order processes are small ($\approx$ 21%). Thus the systematic error from the theoretical uncertainty in calculating these processes is reduced.

In figure 56 our result is compared with a lowest order QCD calculation [63]. The theoretical cross section is in very good agreement with the measured one. Also shown is the prediction for Tevatron energies $\sqrt{s}$ = 2 TeV. There the $b\bar{b}$ cross−section is about five times larger.

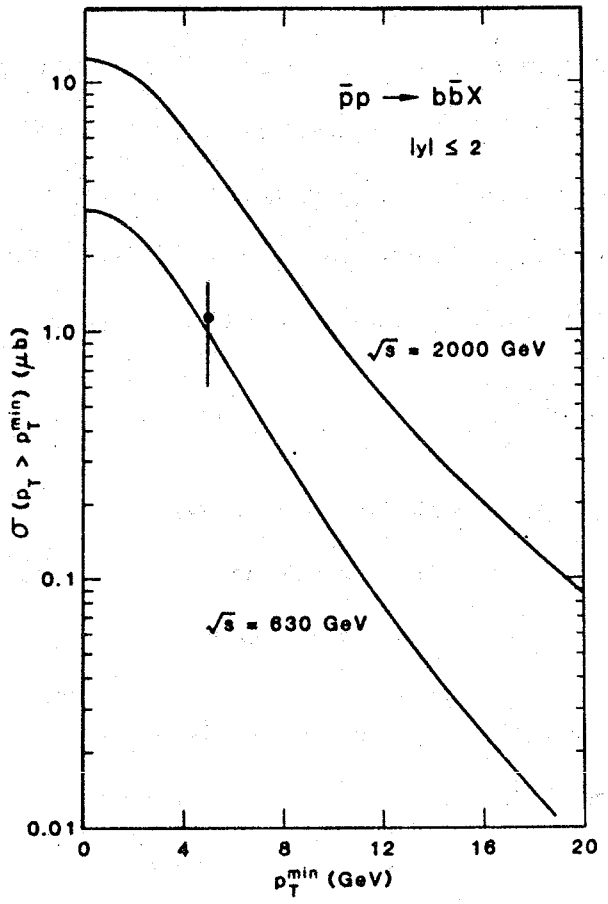

Figure 56: Cross−section for $b\bar{b}$ production in $p\bar{p}$ collisions. The solid line is a lowest order QCD calculation of $\sigma(p\bar{p} \rightarrow b\bar{b})$, as a function of the minimum p_t of both b−quarks [63]. *The UA1 result for $p_t > 5$ GeV/c is shown, too.*

8.6 Single Muon Data

Heavy flavour physics can also be studied using single μ data. As only one quark must decay into a muon, the efficiency of tagging a $b\bar{b}$ event is much larger. On the other hand, the decay background to single muons is higher than to dimuons. It requires a higher p_t cut to reduce this background. The single muon selection demands $p_t > 6$ GeV/c.

As the single muon sample is very large, a scan of the complete sample was not possible. Instead of this tight matching cuts, which reduce the background, were developed. Additional software was used to reduce cosmics, leakage and Kinks [77]. The background was found to be 60% at 6 GeV/c p_t and drops to about 20% at 10 GeV/c p_t . The inclusive muon p_t spectrum after background subtraction[35] is shown in figure 57 .

This spectrum is compared with Isajet calculations using following processes: $b\bar{b}$, $c\bar{c}$ (including higher order processes) and $W \rightarrow \mu\nu$. In the single muons the $c\bar{c}$ contribution is less suppressed than in the dimuons, about 25% of the events should be due to $c\bar{c}$ (instead of 10% in the dimuons). Also higher order processes are much more important for the single muons than for the dimuons. According to Isajet 60% of the single muons events should be due to gluon splitting and flavour excitation, whilst these processes account for only 22% of the dimuon events. The main reason for the larger suppression of higher order processes in dimuon events is the $m^{\mu\mu} > 6$ GeV/c^2 cut. Dimuons from gluon splitting tend to be close together and to have a low invariant dimuon mass.

- The data are in good agreement with the hypothesis of heavy flavour production.
- Higher order processes are much more important for the inclusive muons than for the dimuons. They are necessary to explain the data.
- The high p_t tail is well explained by $W \rightarrow \mu\nu$

The spectrum between 10 and 15 GeV/c was used to normalize the Isajet calculations. This range was chosen as it has a fairly small background and heavy flavour production still dominates over $W \rightarrow \mu\nu$.

[35] The calculation of the single muon background is described in the appendix.

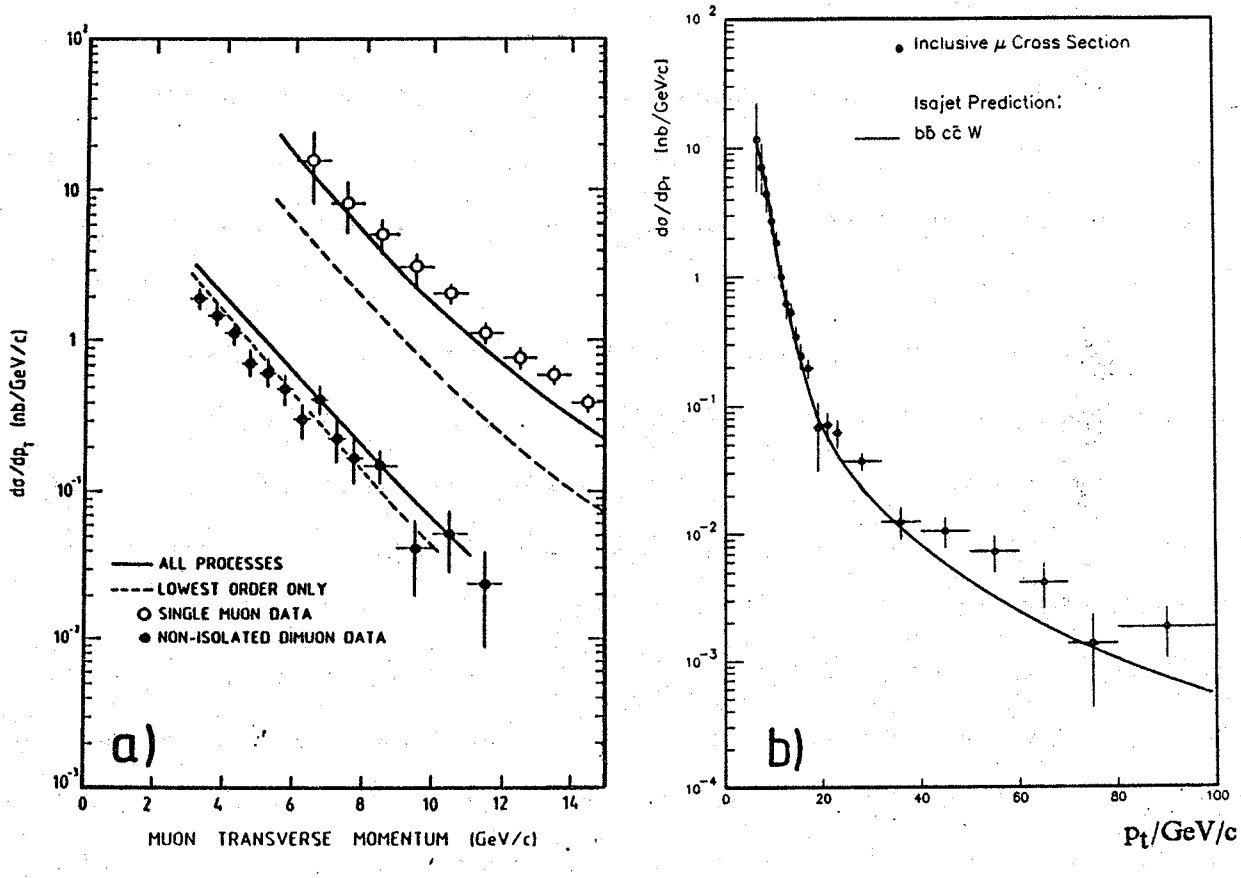

Figure 57: $d\sigma/dp_t$ of inclusive muons
a) Single muons with 6 GeV/c < p_t < 15 GeV/c. For comparison the inclusive p_t distribution of the dimuons with p_t > 3 GeV/c is shown, too. The lowest order Isajet calculations are shown as dashed lines, the calculations including higher order processes as solid lines.
b) Single muons with p_t > 6 GeV/c (full p_t range). The heavy flavour contribution of Isajet was normalized to the data (see text for details). The high p_t tail is dominated by $W \rightarrow \mu\, \nu$

The normalization factor κ is:

$$\kappa = d\sigma/dp_t \text{ (measured)} \,/\, d\sigma/dp_t \text{ (calculated)} = 1.27 + 0.27 - 0.18$$

This normalization factor is larger than that one obtained in the dimuon analysis (i.e. 0.67, see chapter 6.5). This is probably because higher order processes play a more important role in single muon events than they do in dimuon events. As Isajet does not perform correct higher order calculations, this deviation is not astonishing.

Altogether this data are understood and a large heavy flavour production is also seen in the single muons.

9. EVIDENCE FOR $B^0 - \bar{B}^0$ OSCILLATIONS

9.1 Determination of the Mixing Parameter χ

From the previous analysis one can conclude that the events are basically understood. It is evident that most of them are due to $b\bar{b}$ production. This implies that we might be able to decide whether $B^0 - \bar{B}^0$ oscillations can be seen in our data or not.

In chapter 2 we discussed that the ratio of like−sign events over unlike−sign events is sensitive to $B^0 - \bar{B}^0$ oscillations. We observe 140 like−sign and 256 unlike−sign pairs in the non−isolated events. Subtracting 58.5 like−sign and 58.5 unlike−sign background events we calculate a ratio:

$$\mathbf{R = (N^{++} + N^{--})/ N^{+-} = 0.41 \pm 0.07 \pm 0.03}$$

the first error is statistical, the systematic error comes from uncertainties of the background subtraction. In principle we have to subtract 15 unlike−sign events which are expected to be non−isolated Drell−Yan pairs and Upsilon decays. Then R becomes:

$$\mathbf{R = 0.45 \pm 0.08 \pm 0.04}$$

Alternatively we can calculate R using all events subtracting background and the measured number of Upsilon and Drell−Yan events, resulting in:

$$\mathbf{R = 0.44 \pm 0.07 \pm 0.04}$$

consistent with the values above.

Like−sign dimuons can come from second generation decays $b \rightarrow c \rightarrow \mu$ and from $B^0 - \bar{B}^0$ mixing. The estimates of various Monte Carlo calculations (Isajet, Eurojet) for R are in the range of 0.21 − 0.26 for no mixing, and about 0.40 for maximal mixing in the B^0_s channel (see table 13). These numbers look very suggestive, but we have to discuss the Monte−Carlo predictions and their uncertainties in more detail in order to interpret our results.

If both B−hadrons are produced incoherently, the expected value of R can be expressed by the following formula:

$$R = \{2\chi(1-\chi)\, N_f + [(1-\chi)^2 + \chi^2]\, N_s\} / \{[(1-\chi)^2 + \chi^2]\, N_f + 2\chi(1-\chi)\, N_s + N_c\} \quad \{31\}$$

N_f Events with both b and $\bar{b}$ decaying in first generation (and both b and $\bar{b}$ decaying in second generation, but that is negligible). According to Isajet these are 69% of the events.

N_s Events from $b\bar{b}$ with one muon from a first generation and one muon from a second generation decay (Isajet: 21 %).

N_c Events from $c\bar{c}$ (Isajet: 10 %).

χ Mixing parameter: Fraction of B−hadrons decaying into a "wrong" sign muon because of $B^0 - \bar{B}^0$ oscillations

$$\chi = N(B \to \bar{B} \to \mu^-, \bar{B} \to B \to \mu^+) / N(B,\bar{B} \to \mu^\pm) \quad \{32\}$$

The dependence of R on χ is plotted in figure 58 using the standard Isajet assumptions for N_f, N_s and N_c . If we set χ to 0 (no mixing) the Isajet prediction is (with 10% $c\bar{c}$):

$$R = 0.26$$

The measured R of 0.41 preferes $\chi \approx 0.1$, again for 10% $c\bar{c}$. Similar results are obtained by the Eurojet Monte Carlo, and by independent calculations from references [39] [40] (see table 13).

The spread on R comes mainly from uncertainties in the relative contributions from second generation decays and from $c\bar{c}$. The error on R can be estimated as follows: The amount of events from second generation depends on the kinematic properties of the $B \to D\ (D^*) \to \mu$ decay and on the branching ratios $B \to \mu$ and $D \to \mu$. Isajet was tuned to reproduce the lepton and D−meson spectra measured at e^+e^- experiments (fig. 10). The uncertainties of the measured branching ratios were pro-

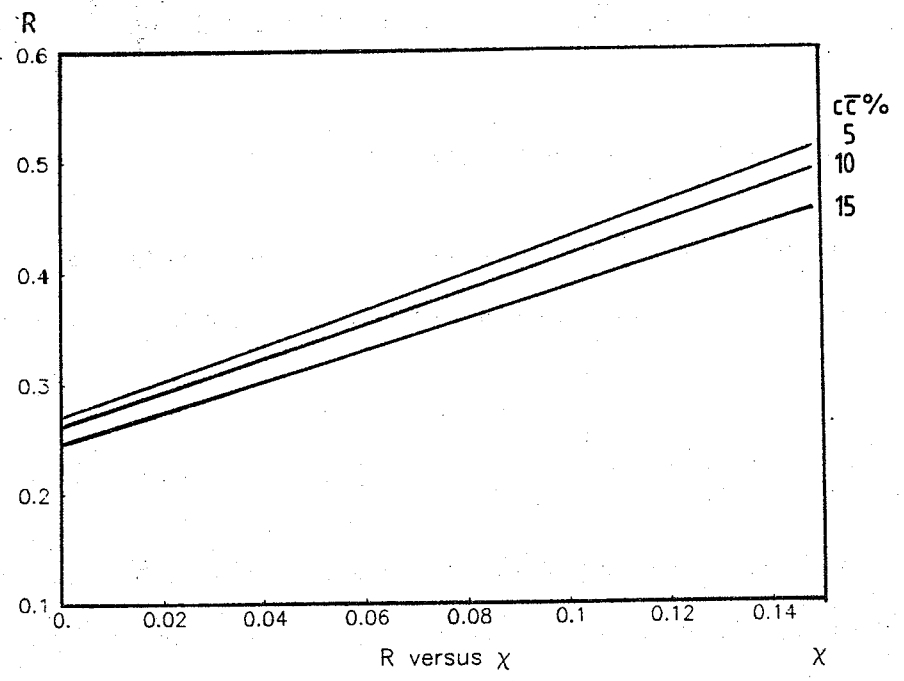

Figure 58: Dependence of R on the mixing parameter χ. The curves are for $c\bar{c}$ contributions of 5, 10 and 15 %. The standard value of Isajet is 10% .

reference	no oscillations	$B^0-\bar{B}^0$ oscillations with χ: 0.05	0.10	0.15	$c\bar{c}$
Isajet	0.26	0.34	0.42	0.50	10 %
Eurojet	0.18	0.28	0.31	0.43	23 %
Barger et al.	0.25	0.31	0.36	0.42	23 %
Halzen et al.	0.25	0.38	0.41	0.48	11 %

Table 13: Predictions for R with and without $b\bar{b}$ oscillations

(R is defined in {20})

pagated and resulted in an error of ± 0.02 on R . The relative $c\bar{c}$ contribution depends on the semi-leptonic branching ratios of charm and beauty and on their fragmentation functions. The Isajet estimate of 10 % is consistent with our measurement of 8 ± 6 % using p_t^{rel} . Varying the $c\bar{c}$ contribution by ± 50 % changes R within 0.02. Altogether we estimate the theoretical error of R for the no mixing

case to be ± 0.03. This is also consistent with the spread of various independent calculations (see table 13).

One might think of additional effects which can influence R:

- Double $b\bar{b}$ and especially double $c\bar{c}$ production. These processes should give an equal amount of like and unlike−sign dimuons. The charm content of gluon jets was measured by UA1 [64]:

$$\rho = (\text{number of } D^*)/(\text{number of jets}) = 0.08 \pm 0.02 \pm 0.04$$

  The result agrees with theoretical calculations using leading log approximation [65]. Isajet also accounts for these processes and is in fair agreement with reference [65] (fig. 59). According to Isajet they give only 0.5 like and 0.5 unlike−sign events and are included in our analysis.
- Events from $t\bar{t}$ and $W \rightarrow t\bar{b}$ can give a high fraction of like−sign events. Assuming a mass of the top of 25 GeV/c^2, we would expect 12 like−sign and 20 unlike−sign events, which would change the ratio by 0.01 . With increasing mass of the top the number of events expected drops rapidly: about 3 like−sign and 3 unlike−sign events for $m_{top} = 40$ GeV/c^2. In fact this contribution can be limited to maximally 5.2 like−sign and 7.5 unlike−sign events, see chapter 10.

Thus the expectation from Isajet is R = 0.26 ± 0.03 for no mixing. The probability that this value fluctuates to the measured 0.41 ± 0.07 ± 0.03 corresponds to 2.1 standard deviations.

The statistical significance of only 2.1 standard deviations can be improved by performing a likelihood fit, which makes use of different kinematic properties of first and second generation beauty decays and of background events. The basic idea is to fit a linear combination of the p_t spectra of first− and second generation beauty decays, charm decays and decay background to the like−sign and unlike−sign events. As the p_t spectrum of muons from second generation b−decays is softer than that of first generation decays, the fit should be able to discriminate between both. This can be demonstrated by plotting the p_t spectra of the *slower* muon for Isajet unlike−sign events [60 a)], and Isajet

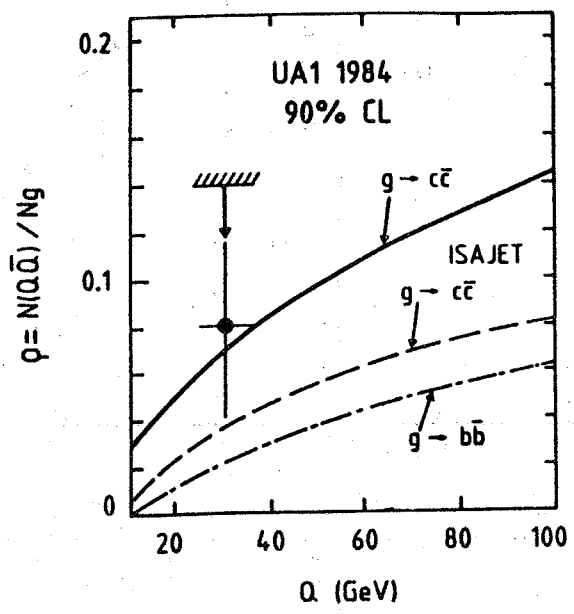

Figure 59: Fraction of gluon jets splitting into a $c\bar{c}$ pair. The fraction is shown as a function of Q, the mass of the virtual gluon. The calculation is from reference [65]: *$g \rightarrow c\bar{c}$ (solid line), $g \rightarrow b\bar{b}$ (dashed dotted line). The Isajet calculation for $g \rightarrow c\bar{c}$ is shown as dashed line. Because of a cutoff this is underestimated. The Isajet calculation of $g \rightarrow b\bar{b}$ (not shown) agrees entirely with* [65]. *The experimental point comes from the measurement of the number of D^* inside jets by UA1* [64]

like−sign events [60 b), no oscillations!]. The latter is slightly but significantly softer. This has to be compared with the background subtracted spectra of unlike−sign [60 d)] and like−sign [60 e)] data. It can be seen that the p_t^{slow} distribution of the like−sign events is a little bit harder than that of pure second generation decays. In these plots the difference does not seem very significant, but the fit itself uses the two dimensional distributions $d\sigma^2/dp_t^{fast}dp_t^{slow}$, which contain the correlations between the p_t 's of both muons. As the p_t spectrum of the decay background is much softer than that of beauty decays, the fit can correct errors of the background normalization. Therefore the fit was allowed to vary the background contribution within its error (± 18%). By the same token the fit can also adjust the Isajet expectations for first and second generation decays and $c\bar{c}$ within the given errors. The best estimate of the mixing parameter χ was determined by a log−likelihood method. The method is explained in more detail in the appendix (E) and in reference [66]. The result of the fit is shown in figure 61, from which we deduce the best estimate for χ:

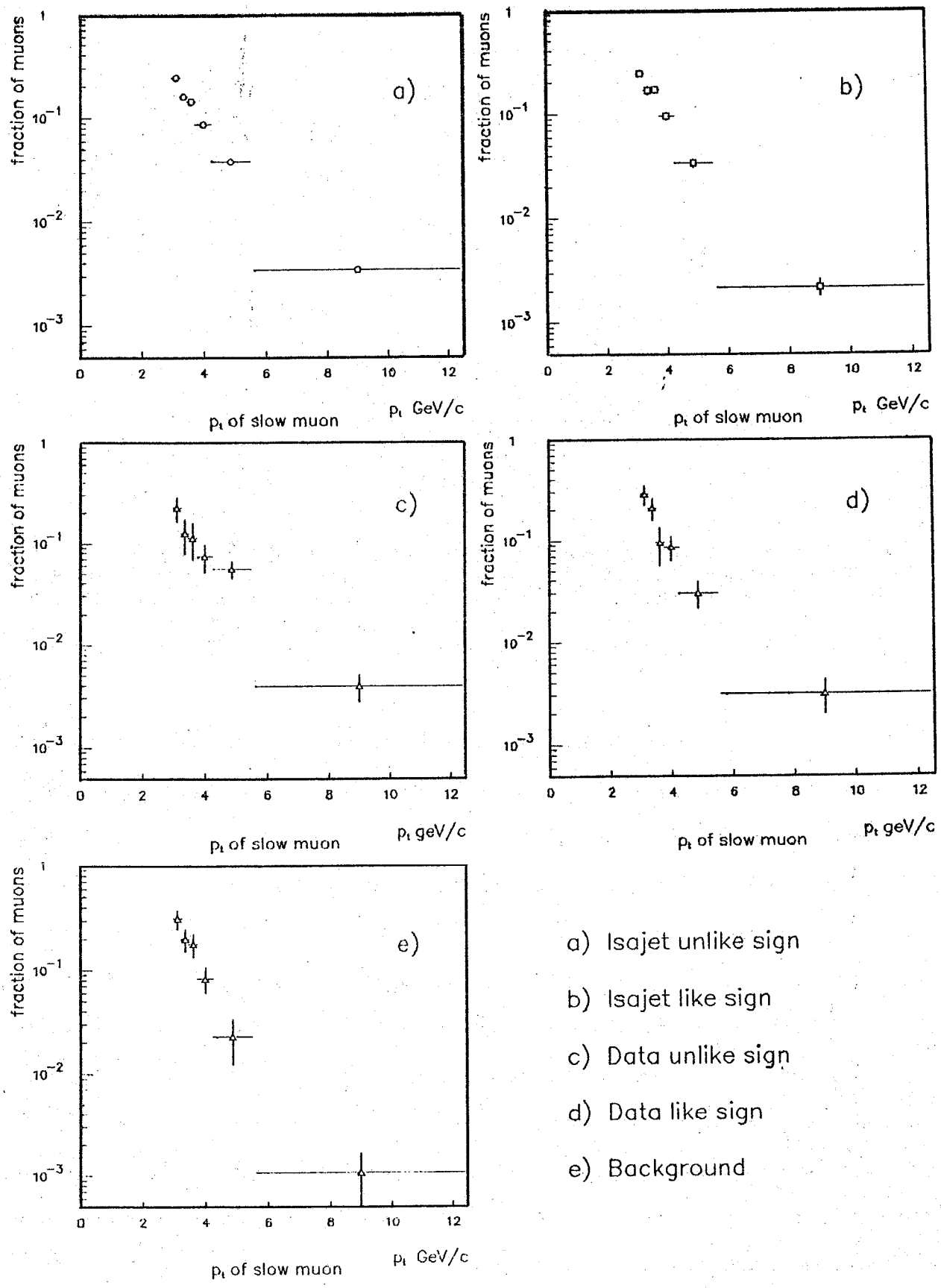

Figure 60: p_t distribution of the slow muon

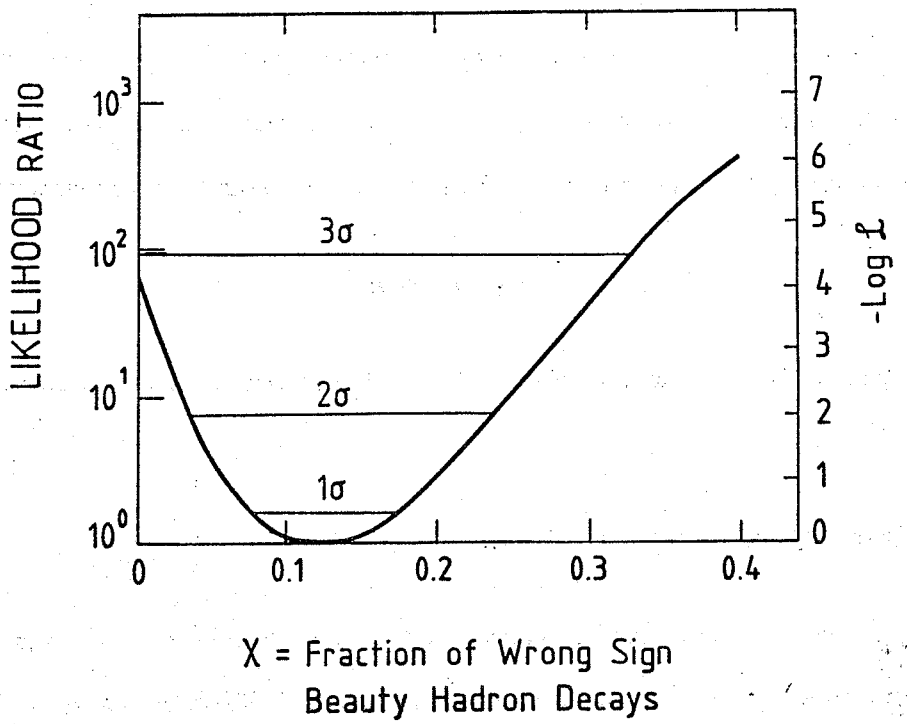

Figure 61: Likelihood function of the mixing parameter χ Plotted is the negative logarithm of the likelihood as a function of the mixing parameter χ.

$$\chi = \mathbf{0.121 \pm 0.047}$$

$$\chi > \mathbf{0.065 \text{ at } 90\ \% \text{ C.L.}}$$

The alternative of $\chi = 0$ (no mixing) is disfavoured by a likelihood ratio of 1:73 or 2.9 standard deviations. This χ value need not agree with that obtained from R and formula {31}, as the fit changes some parameters (N_c, N_f, N_s) within their errors. Using the kinematic properties, the significance improves by 0.8 standard deviations.

If the contribution from Drell−Yan and Upsilon is considered, the fit results in:

$$\chi = \mathbf{0.158 \pm 0.059}$$

$$\chi > \mathbf{0.091 \text{ at } 90\ \% \text{ C.L.}}$$

The no−mixing case is disfavoured by 3.3 standard deviations. In the following we will use the more conservative value of $\chi = 0.121 \pm 0.047$, which is also consistent with our publication [4].

The fit can also be done leaving the background normalization as a free parameter. Because of the different p_t spectra of background and signal, the fit should reproduce the nominal background. In fact, the fit obtains 106 ± 36 background events (instead of 117 ± 21) and a mixing parameter of:

$$\chi = 0.127 \pm 0.06.$$

(without subtraction of Drell Yan and − Upsilon). This confirms nicely the results quoted above.

9.2 Interpretation of the Result

The non − zero value of χ deserves more detailed discussion: In principle both B^0_d and B^0_s can oscillate and contribute to χ ($D^0 - \bar{D}^0$ oscillations can be ignored [30]). Although B^0_d oscillations are expected to be small we cannot exclude them a priori, as we are not able to distinguish experimentally between the two cases. We have to write χ as an average over B^0_d and B^0_s:

$$\chi = [(BR)_d f_d \chi_d + (BR)_s f_s \chi_s] / \langle BR \rangle \qquad \{33\}$$

f_d, f_s The fraction of beauty quarks which hadronize into B^0_d or B^0_s respectively.

χ_d, χ_s Mixing parameter for B^0_d and B^0_s respectively. These parameters are defined in formula {14} .

$\langle BR \rangle$ Average branching ratio for all B hadrons, weighted by their relative occurance:

$$\langle BR \rangle = (BR)_d f_d + (BR)_s f_s + (BR)_u f_u + (BR)_B f_B \qquad \{34\}$$

$(BR)_i$ The muonic branching ratios of B − hadrons.

(i: d = B^0_d ; s = B^0_s ; u = $B^{\pm}$; B = baryons).

Most of these parameters are unknown. For some of them exist limits or reasonable estimates already:

The branching ratios $(BR)_i$ have not been measured individually yet. The differences should be small and are neglected here. We use 12% for all states.

f_s is the fraction of beauty quarks picking up a strange quark to form a B^0_s meson. Values for f_s can be estimated from the K/π ratio measured in e^+e^- experiments. There the measured value suggests an f_s of about 0.13 ± 0.02. It was also found that f_s increases with increasing Q^2 [38]. The PEP data were taken at $\sqrt{s} = 29$ GeV, while the average mass of the muon−muon−jet−jet system for the di-muons is 46 GeV/c^2. As the average Q^2 is higher at the collider than at e^+e^- storage rings, a higher value of f_s can be expected at the collider. Another measurement comes from the pp collider ISR at $\sqrt{s} = 45$ and 63 GeV [67]. This experiment uses leading kaons and pions (fig. 62). K^+ and π^+ should come from scattered quarks from the protons. Therefore the ratio $N(K^+)/N(\pi^-)$ gives an almost direct measurement of f_s/f_d:

$$N(K^+)/N(\pi^+) = 0.456 \pm 0.003 \pm 0.018$$

The true value is slightly larger, as some of the pions come from K^* decays:

$$f_s / f_d = 0.55 \pm 0.05$$

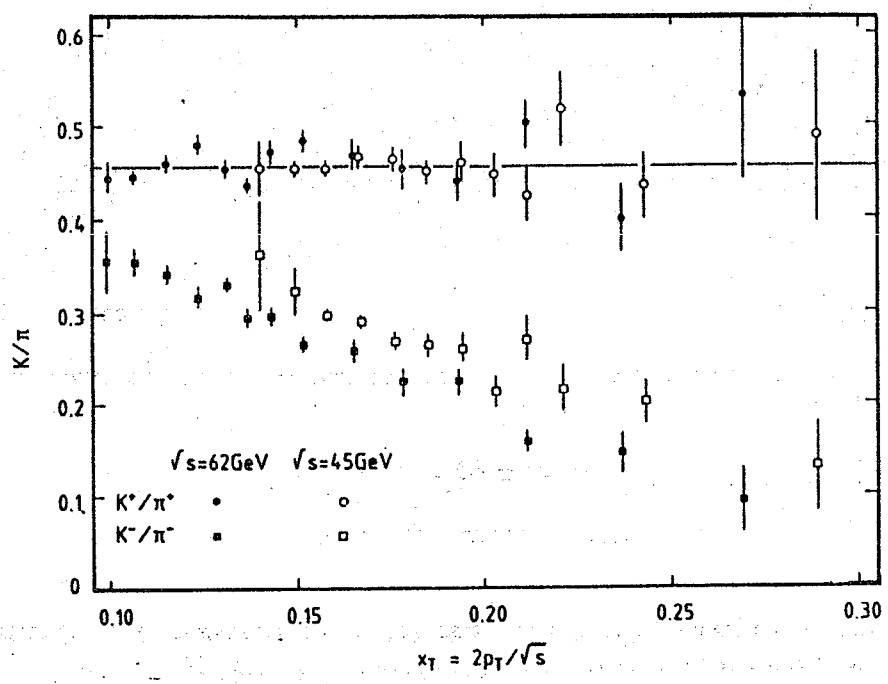

Figure 62: Ratio $N(K^+)/N(\pi^+)$ and $N(K^-)/N(\pi^-)$ from the ISR. K^+ and π^+ should come from scattered quarks from the protons and can be used for an almost direct measurement of f_s [67].

The advantage of this measurement is that, in contrast to the e^+e^- data, f_s was measured for leading particles with an average z of 0.7 − 0.8. As f_s is assumed to depend on the fragmentation z, this should be more comparable with b−quarks, which fragment very hard [68]. The average z of B−mesons in the dimuon sample should be: $<z> = 0.9$ (Isajet). Of course, this value is biased by the cut on the muon p_t Using the ISR result ($f_s/f_d \approx 0.5$) and allowing for 10% of B−baryons, one obtains the following:

$$f_u : f_d : f_s = 0.36 : 0.36 : 0.18 \qquad \{35\}$$

which we will use as standard values. Assuming maximal mixing of B^0_s ($\chi_s = 0.5$) and no mixing in B^0_d ($\chi_d = 0$), these values lead to a χ of 0.09 corresponding to an R value of 0.40 (using formula {31}). Both values are certainly consistent with the measured ones: $\chi = 0.121 \pm 0.047$ and $R = 0.41 \pm 0.08$. The dependence of χ on χ_s (and r_s {15}) and f_s (assuming $\chi_d = 0$) is shown in figure 63 .

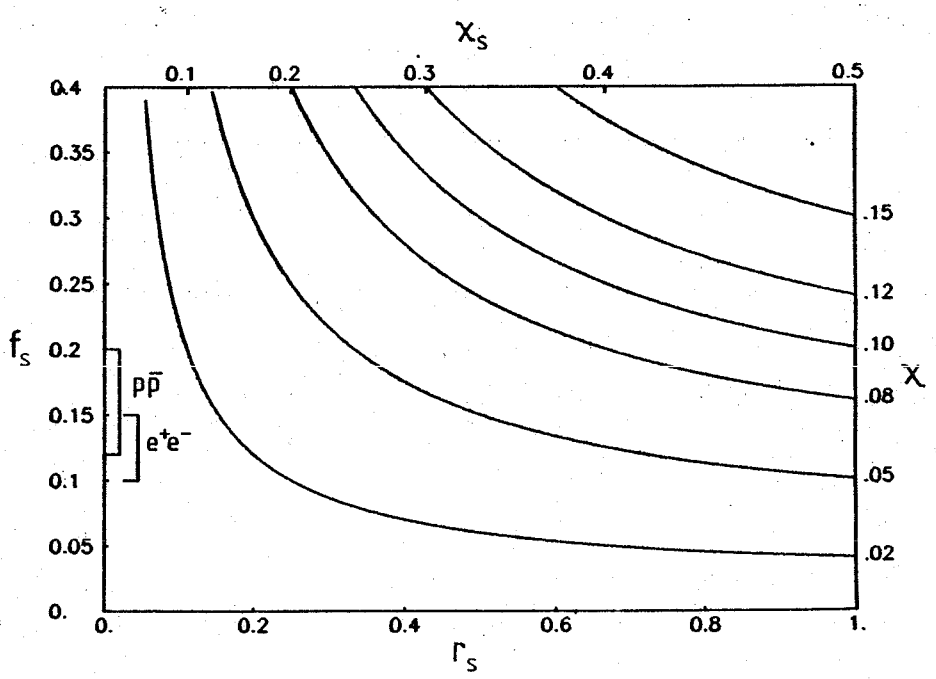

Figure 63: Dependence of χ on r_s, χ_s and f_s . Plotted are lines of constant χ. $\chi_d = 0$ is assumed. Indicated are the expected values of f_s in the PETRA and SPS region

9.3 Comparison with Other Experiments

We can compare our result with measurements from e^+e^- experiments. Searches for $B^0 - \overline{B}^0$ oscillations were made by ARGUS, CLEO, JADE and MARK II. Their results are summarized in table 14 .

	$b\bar{b}$ source	$\sqrt{s}$ in GeV	result	method
CLEO	$\Upsilon(4s) \rightarrow B\bar{B}$	10.6	$\chi_d < 0.19$ 90% C.L.	dileptons
ARGUS	$\Upsilon(4s) \rightarrow B\bar{B}$	10.6	$\chi_d = 0.19 \pm 0.07$	dileptons
MARK II	$e^+e^- \rightarrow b\bar{b}$	29	$\chi < 0.12$ 90% C.L.	dileptons
JADE	$e^+e^- \rightarrow b\bar{b}$	34	$\chi < 0.13$ 90% C.L.	asymmetry

Most experiments use the rate of like − sign dileptons.
The JADE experiment obtained its limit from the lepton charge asymmetry.
See text for references.

Table 14: Results on $B^0 - \overline{B}^0$ oscillations from e^+e^- experiments

The CLEO experiment uses the $\Upsilon(4s)$ resonance, which decays into $B^{\pm}$ and B^0_d . CLEO gives an upper limit of χ_d of 0.19 at 90% C.L. It rules out full mixing for B^0_d , but this experiment is not sensitive to B^0_s mixing.

The MARK II collaboration at PEP uses continuum data above the $\overline{B}^0_s$ threshold and should therefore be sensitive to B^0_d and B^0_s mixing. They give a limit of $\chi < 0.12$ at 90 % C.L. [31]. Their data is at lower Q^2 and f_s might be lower than at the SPS collider. Taking this into account and considering the error on our χ, MARK II is not in conflict with the UA1 result. A similar limit of $\chi < 0.13$ at 90% C.L was obtained by the JADE collaboration at PETRA [32]. The limits form CLEO and MARK II are shown in figure 64 together with the lower limit on χ from UA1. The limits are compatible with all values of χ_s from 0 to 0.5.

A positive signal for B^0_d oscillations was recently reported by the ARGUS collaboration [69]. Their value of the mixing parameter χ_d is 0.19 ± 0.07 . The $\pm$ 1 standard deviation bands of the UA1

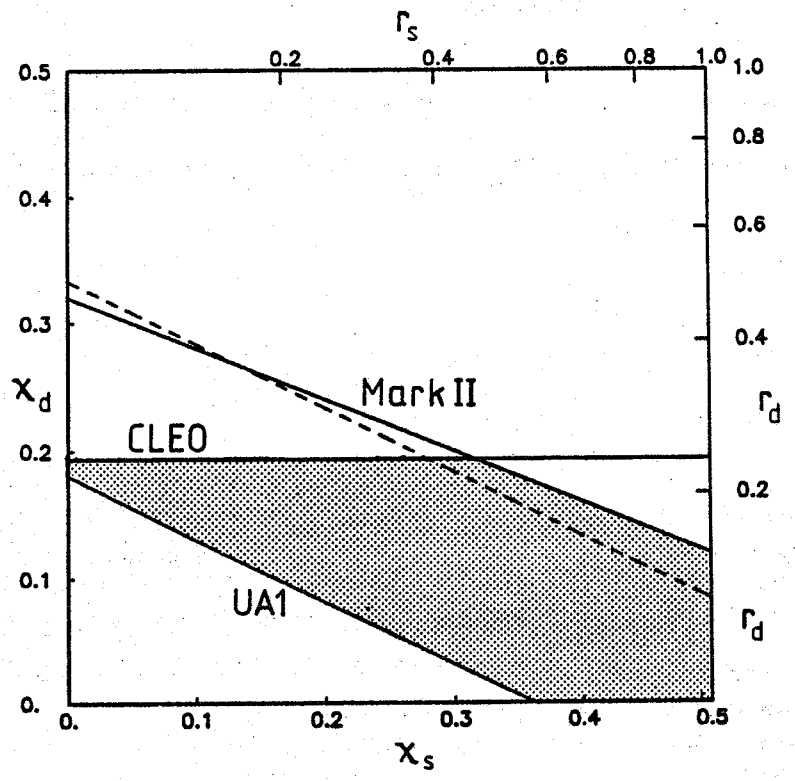

Figure 64: Limits on χ_s and χ_d from MARK II, CLEO and UA1. The solid lines are 90% confidence level limits from UA1, CLEO and MARK II. The dashed line corresponds to the measured value of χ = 0.12. The UA1 data are evaluated assuming f_s = 0.18, whilst f_s = 0.15 was used for MARK II data. This is justified by the lower Q^2 of the e^+e^- data.

and the ARGUS measurements are shown in figure 65 . Both measurements are consistent within a large area in the $\chi_s - \chi_d$ plane.

Further limitations on the allowed region in the $\chi_s - \chi_d$ plane can be obtained by combining the likelihood functions of all measurements. We use following likelihood functions:

- *UA1:* Gaussion distribution: χ = 0.121 ± 0.047
- *CLEO:* Gaussian distribution: χ_d = 0.096 ± 0.096 [27]
- *ARGUS:* Gaussian distribution: χ_d = 0.187 ± 0.069 [69]
- *MARK II:* Gaussian distribution: χ = 0 ± 0.075 [31]

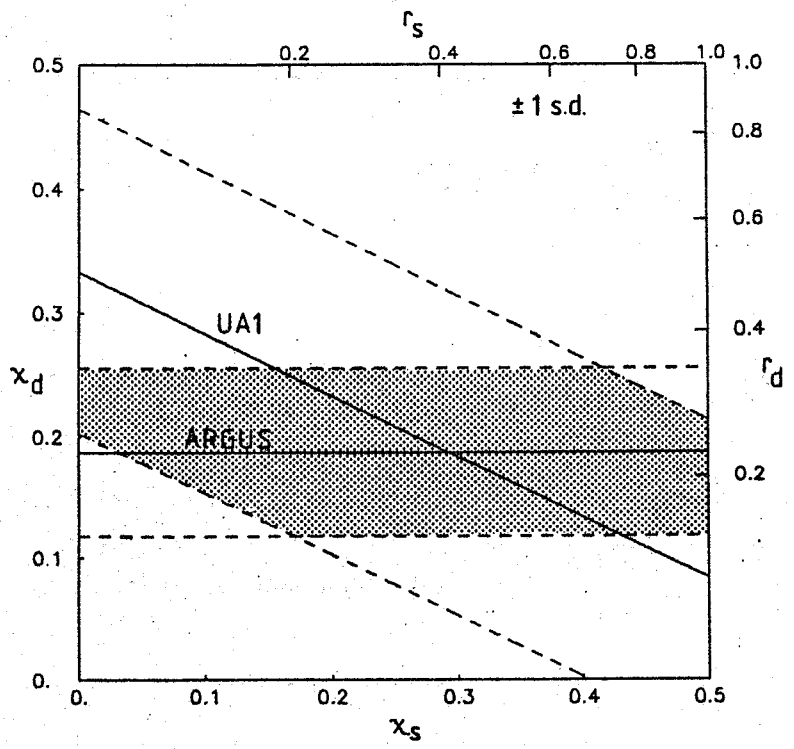

Figure 65: ± 1 standard deviation bands of UA1 and ARGUS (same values for f_s and f_d as in figure 64).

We assumed $f_s = 0.18$ for the UA1 data and $f_s = 0.15$ for the MARK II data. The f_s for MARK II should be lower than that for UA1, because of the lower Q^2 of the MARK II data. However, if we consider a dependence of f_s on the fragmentation, their f_s should be larger than the 0.13 measured at e^+e^- experiments. We believe that 0.15 is a reasonable guess. We always assumed that 10% of the b−quarks hadronize into baryons. The result of the combined fit is shown in figure 66 . All experimental results are consistent and allow a large region in the $\chi_s - \chi_d$ plane. Whilst χ_d is restricted between 0.08 and 0.20, there is no restriction from experimental data on χ_s: all values between 0 and 0.5 are possible.

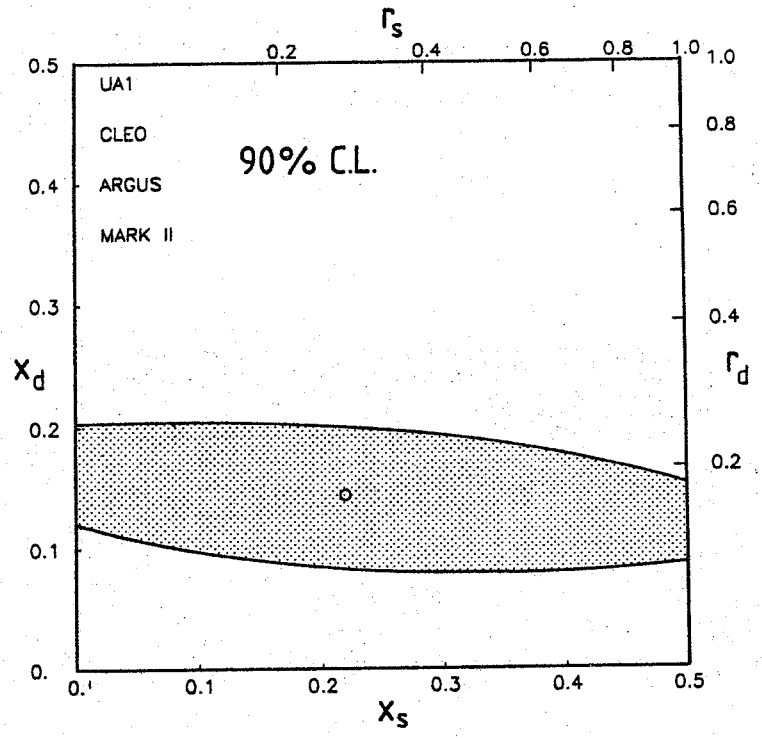

Figure 66: Combined fit of χ_d and χ_s . The limit is from a combined fit using results from UA1, MARK II, ARGUS and CLEO (90% confidence level). The same assumptions on f_s were made as in figure 64 .

9.4 Constraints on χ_d and χ_s from the K−M Matrix

From figure 66 it can be concluded that all experiments are compatible with $\chi_s = 0$. In section 2.7 it was argued that $B^0{}_s$ mixing should be stronger than $B^0{}_d$ mixing. Hence it seems to be very unlikely that χ_d is larger than χ_s . Indeed, it is possible to restrict the allowed region in the $\chi_s - \chi_d$ plane using the theoretical calculations of the box diagrams, and existing limits on Kobayashi−Maskawa matrix elements. This additional information allows to give a lower limit on χ_s

Writing again the expressions for $B^0{}_s$ and $B^0{}_d$ oscillations one finds:

$$\Delta m/\Gamma(B^0{}_s) \approx \text{const.} \times B_{Bs}\, f_{Bs}{}^2\, |V_{tb}|^2\, |V_{ts}|^2\, f(m_t{}^2)\, \tau_{Bs}$$

$$\Delta m/\Gamma(B^0{}_d) \approx \text{const.} \times B_{Bd}\, f_{Bd}{}^2 |V_{tb}|^2\, |V_{td}|^2\, f(m_t{}^2)\, \tau_{Bd} \qquad \{36\}$$

The main difference between $\Delta m/\Gamma(B^0_s)$ and $\Delta m/\Gamma(B^0_d)$ should be due to $|V_{td}|$ and $|V_{ts}|$. The dependence on the top mass, $f(m_t^2)$, is the same for both systems and bag−factor, decay constant and lifetime should be similar. Theoretical prejudices favour $\tau_{Bs} > \tau_{Bd}$ and[36] $B_{Bs} f_{Bs}^2 > B_{Bd} f_{Bd}^2$ [33] [20]. This suppresses $\Delta m/\Gamma$ of B^0_d relative to B^0_s . For simplicity we use:

$$B_{Bs} f_{Bs}^2 \tau_{Bs} = B_{Bd} f_{Bd}^2 \tau_{Bd}$$

In the Standard Model with three families the K−M matrix is a unitary 3 × 3 matrix. Although the matrix elemtents V_{td} and V_{ts} have not been measured yet, they are already constrained by the known matrix elements and by the unitarity of the matrix [37]:

$$0.002 < |V_{td}| < 0.017$$
$$0.037 < |V_{ts}| < 0.048 \qquad \{37\}$$

From these limits it follows that:

$$(\Delta m/\Gamma)_{Bd} / (\Delta m/\Gamma)_{Bs} = |V_{td}|^2/|V_{ts}|^2 < 0.21 \qquad \{38\}$$

Thus we can obtain for each value of χ_s an upper bound for χ_d (with $\beta = |V_{td}|^2 / |V_{ts}|^2$ and formula {14}):

$$\chi_d < \beta^2 \chi_s / [\, 1 - 2\chi_s(1 - \beta^2)] \qquad \{39\}$$

This bound is shown in figure 67, together with the lower limit from UA1 and the 90% C.L. contour of the combined results from UA1, MARK II, ARGUS and CLEO.

Combining the UA1 result and the K−M bound, a lower limit of $\chi_s > 0.3$ at 90% confidence level can be given. This limit depends on the assumed parameters f_s and f_d . Results for different values of f_s and f_d are listed in table 15 .

---

[36] The latter is because f^2 is proportional to $|\psi(0)|^2$. Non relativistic potential models lead to $|\psi(0)| \propto \mu$. $\mu = m_1 m_2/(m_1 + m_2)$ is the reduced mass of the quark−antiquark system, which is $\simeq m_d$ and $\simeq m_s$ respectively. Hence $f_{Bs} > f_{Bd}$. [70]

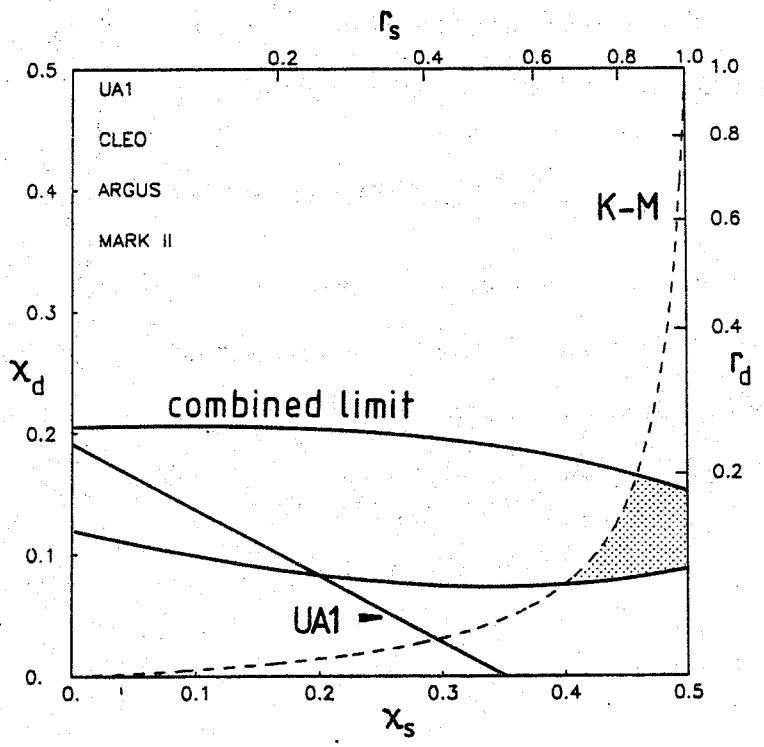

Figure 67: Limits on χ_d and χ_s from the K−M matrix. The lower bound on χ from UA1 and the contour from the combined fit of ARGUS, MARK II, CLEO and UA1 are shown as solid lines (90% C.L.). The limit from the K−M matrix elements V_{ts} and V_{td} is shown as dashed line.

Limit from UA1 and V_{td},V_{ts} :

f_s	f_d	χ_s	r_s	$\Delta m/\Gamma$	Δm ($\tau = 1.12$ ps)
0.18	0.36	0.30	0.42	1.20	7.1×10^{-4} eV
0.15	0.375	0.33	0.49	1.39	8.1×10^{-4} eV
0.13	0.385	0.35	0.54	1.53	8.9×10^{-4} eV

(for various values of f_s and f_d, at 90% C.L.)
the standard values used in this analysis are $f_s = 0.18$ and $f_d = 0.36$,
10% of the b−quarks hadronize into baryons.

Table 15: Lower limits on χ_s , r_s and Δm.

An even more stringent limit can be obtained from the overall fit of all experiments:

χ_s	r_s	$\Delta m/\Gamma$	Δm ($\tau = 1.12$ ps)
0.40	0.67	2.00	1.2×10^{-3} eV

As this limit is dominated by the ARGUS result, the dependence on f_s and f_d can be neglected.

It has to be stressed that these limits are valid only in the case of three quark families. Otherwise V_{td} and V_{ts} are not sufficiently constrained by the unitarity of the K−M matrix.

Finally we can study the consistency between ARGUS, UA1 and the K−M limit. This should answer the question, whether the χ from UA1 is large enough to account for the χ_d, which is measured by ARGUS, and the value of χ_s expected from {39} . Applying formula {39} to the ARGUS result ($\chi_d > 0.099$ at 90% C.L.) a lower limit of $\chi_s = 0.42$ can be derived. Using $\chi_d = 0.19 \pm 0.07$ and $0.42 < \chi_s < 0.50$ the expected range of χ can be calculated with formula {33} as a function of f_s (fig. 68):

$$\chi = 0.09 - 0.18 \quad (\text{for } f_s = 0.10 - 0.18)$$

These values agree very well with our measured value of 0.12 ± 0.047 for a large range of f_s. In contrast to the case of $\chi_d = 0$ (fig. 58), they are closer to our central value without requiring f_s to be relatively large.

Altogether the new ARGUS result is in best agreement with our measurement and confirms our result.

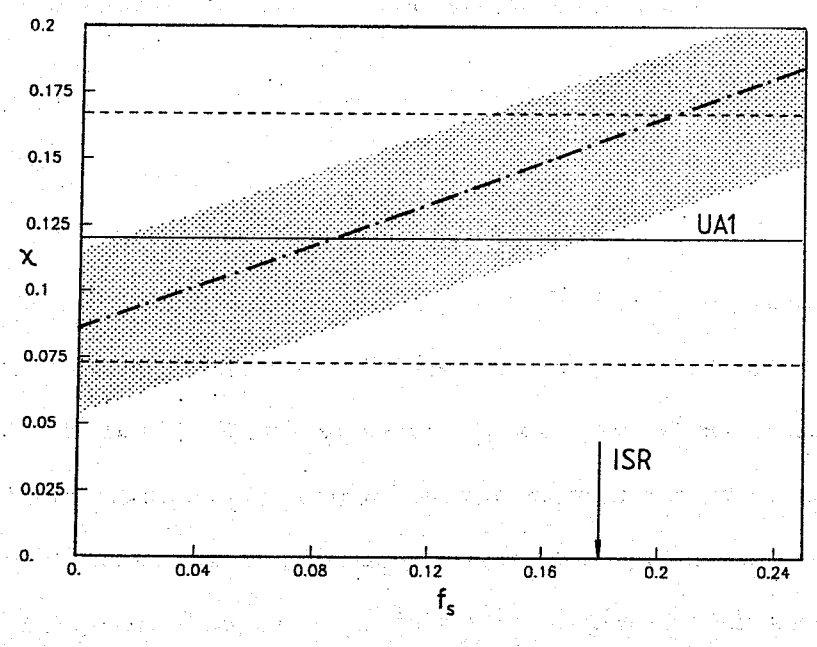

Figure 68: Mixing parameter χ as a function of f_s. The dashed dotted line is obtained using $\chi_d = 0.19$ (ARGUS) and $\chi_s = 0.5$. The dotted region indicates the range of χ, if χ_d is varied within 1 s.d. ($\pm$ 0.07) and χ_s within the limits obtained from the ARGUS result and and formula {39} ($0.42 < \chi_s < 0.50$). The UA1 result is shown as solid line, the $\pm$ 1 s.d. as dashed lines. The arrow indicates the preferred value for f_s from the K^+/π^+ ratio measured at the ISR.

10. LIMITS ON $T\bar{T}$ PRODUCTION

In the previous analysis the heavy flavour contribution to the dimuons was interpreted by $b\bar{b}$ and $c\bar{c}$ alone. In chapter 2 we argued that there can be a sizable number of events from top if the top quark is rather light. The search for an eventual contribution from top production will be described in this chapter.

The main sources for top are the QCD production of $t\bar{t}$ and the decay of a W into $t\bar{b}$. The cross-section for $t\bar{t}$ production falls rapidly with increasing mass of the top. The branching ratio of W into $t\bar{b}$ depends only slightly on the mass of the top, as long as the top is light enough to be produced in a W decay. In order to study the number of events expected and their properties, $t\bar{t}$ and $W \rightarrow t\bar{b}$ events were generated with Isajet for masses of 25, 30, 40 and 50 GeV/c^2. As Isajet does not use exact higher order matrix elements, we scaled the cross-sections calculated by Isajet to the values from Eurojet, which includes higher order calculations (up to α_s^3). Thus the Isajet $t\bar{t}$ cross-section was multiplied by 1.8 . The $W \rightarrow t\bar{b}$ cross section was obtained from the *measured* W cross-section and the well known branching ratio $W \rightarrow t\bar{b}$. Therefore the calculations for $W \rightarrow t\bar{b}$ are more reliable than the corresponding ones for $t\bar{t}$. Cross-sections and number of events from both channels are listed in table 16 .

mass GeV/c^2	$\sigma(t\bar{t})$ in nb	events at 659 nb^{-1}	$\sigma(W \rightarrow t\bar{b})$ in nb	events at 659 nb^{-1}
25	12.8 (8.8)	29	1.63 (1.48)	3.3
30	5.1 (3.5)	13	1.55 (1.40)	3.5
40	1.1 (0.7)	3.2	1.30 (1.18)	3.0
50	0.3 (0.2)	1.3	1.00 (0.90)	2.1

The cross-sections are from Eurojet 2 → 2 and 2 → 3 processes at $\sqrt{s}$ = 630 GeV (540 GeV). The expected numbers of events are for dimuons satisfying the standard cuts and including the complete detector acceptance.

Table 16: Expectations for $t\bar{t}$ and $W \rightarrow t\bar{b}$ production

These numbers suggest that $t\bar{t}$ production should give a detectable signal, if the top mass is lower than 40 GeV/c^2. If no signal is found, it should be possible to establish a lower limit for the top mass. The number of events expected from $W \rightarrow t\bar{b}$ is too small to give a detectable signal or to obtain useful limits. Hence we will concentrate on $t\bar{t}$ production only.

As the top mass is rather large compared to the beauty mass, dimuons from $t\bar{t}$ (and $t\bar{b}$) have different kinematic properties:

- Muons from top decays have a much harder p_t spectrum.
- The muons have a large transverse momentum with respect to the original top quark direction. Therefore muons from top decays are not necessarily back−to−back and have a flatter distribution in $\Delta\phi$.
- By the same token the muons can have large angles to the remaining hadrons of the top fragmentation and decay. Therefore they can be isolated.
- The two neutrinos will have large E_t as well, and need not be back−to−back. So the neutrino vectors do not cancel as in $b\bar{b}$ events, but can both contribute to a large missing E_t .
- Top events have more central jets with a harder E_t spectrum.
- The general activity of top events is high. This can result in a higher charged multiplicity and a higher ΣE_t (scalar sum of the E_t of all energy cells).

A comparison of properties of dimuon events from $t\bar{t}$ production with $b\bar{b}$ is shown in figure 69 . For those plots a top mass of 25 GeV/c^2 was chosen. The differences become even more distinct if the top mass is higher. One has to make use of these differences in order to extract a possible signal from top. The difficulty is that a possible top signal might be hidden in the tails from conventional sources. The way to overcome this problem is to use as much information as possible. One should avoid too many cuts, as they will also reduce the top signal, which might already be tiny. In order to optimize both a likelihood method was used: For each event the hypothesis that it comes from a $t\bar{t}$ event was tested as follows:

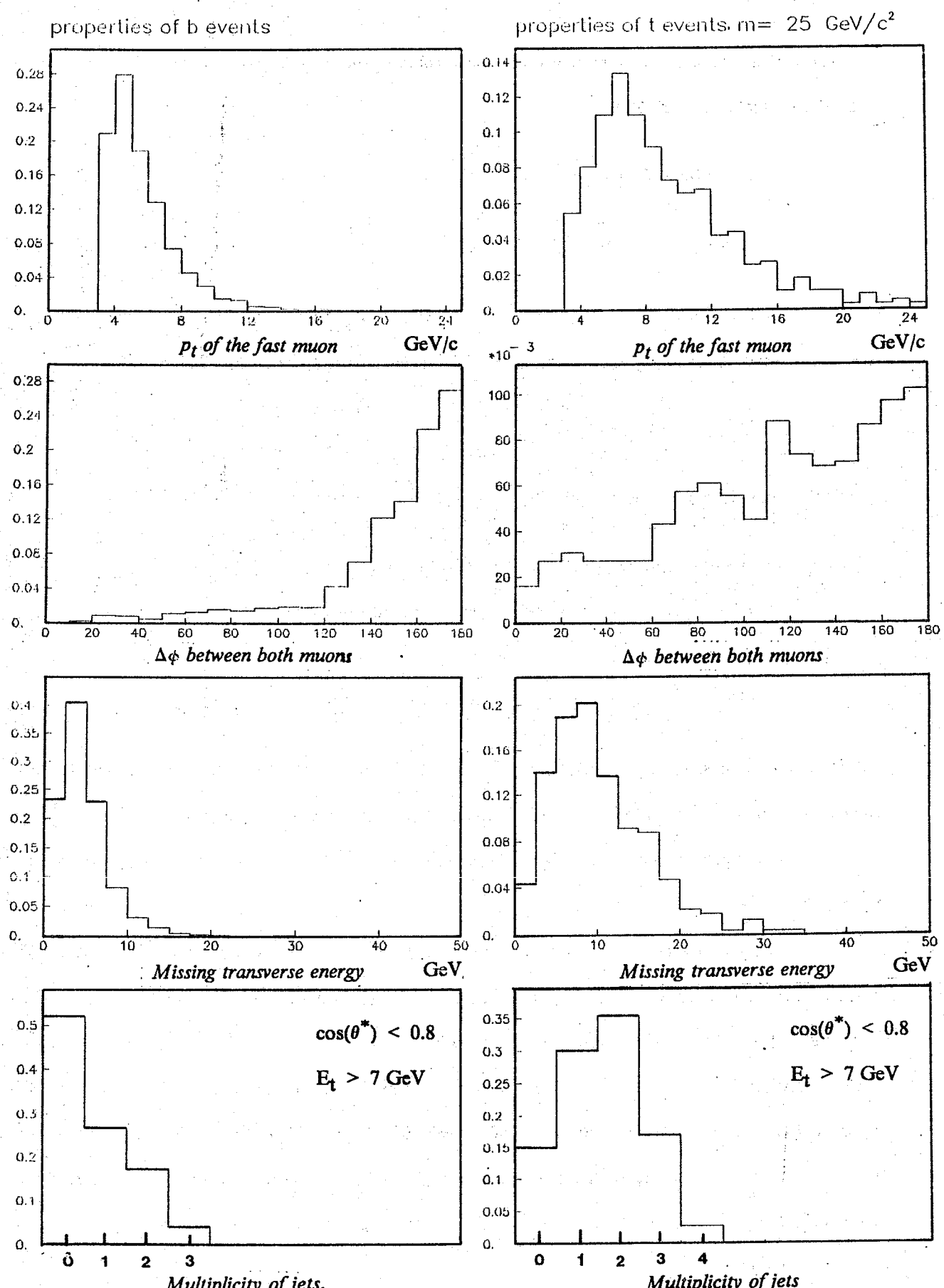

Figure 69: Comparison between $t\bar{t}$ ($m = 25\ GeV/c^2$) and $b\bar{b}$

(arbitrary units)

The probability that a kinematic variable has a value in the range between x_i and $x_i + \Delta x_i$ is given by the normalized distributions:

a) for $b\bar{b}$: $1/N\ (dN/dx_i)_b\ \Delta x_i = P_b(x_i)$

b) for $t\bar{t}$: $1/N\ (dN/dx_i)_t\ \Delta x_i = P_t(x_i)$

We take the ratio of the probability of the top hypothesis and the probability of the $b\bar{b}$ hypothesis. The "top likelihood" of an event is the product of these ratios for different variables:

$$\mathcal{L}_{top} = \Pi\ [P_t(x_i)_i\ /\ P_b(x_i)_i\ ] \qquad \{40\}$$

Following variables enter in the product

two dimensional p_t distribution: $d^2N/dp_{t1}dp_{t2}$

difference of the azimuth angle between the muons ($\Delta\phi$)

missing E_t

number of jets with $\cos(\theta^*) < 0.8$ and $E_t > 7$ GeV

This likelihood should tell how much more likely an event comes from $t\bar{t}$ production than from $b\bar{b}$, provided that both are produced in equal numbers. This interpretation is only valid if the variables, which enter in the product, are uncorrelated. Otherwise it is merely a test function in order to separate top and $b\bar{b}$ events.

In order to obtain a better rejection of events from $b\bar{b}$ a very loose isolation cut was applied: The minimum ΣE_t of both muons has to be less than 9 GeV (ΣE_t is defined in $\Delta R < 0.7$, as usual). The effect of this cut on Monte Carlo events is shown in figure 70 .

It is very efficient for $t\bar{t}$ events, but reduces $b\bar{b}$ events with a high top likelihood. Dimuons from $b\bar{b}$, which are produced at high Q^2, can have high p_t muons in large jets. Additional jets can come from initial state radiation. Because of the additional jets, the muons need not be back−to−back. Such events can get a high value of $\mathcal{L}_{top}$. As the muons are in high E_t jets, these events are removed by the isolation cut.

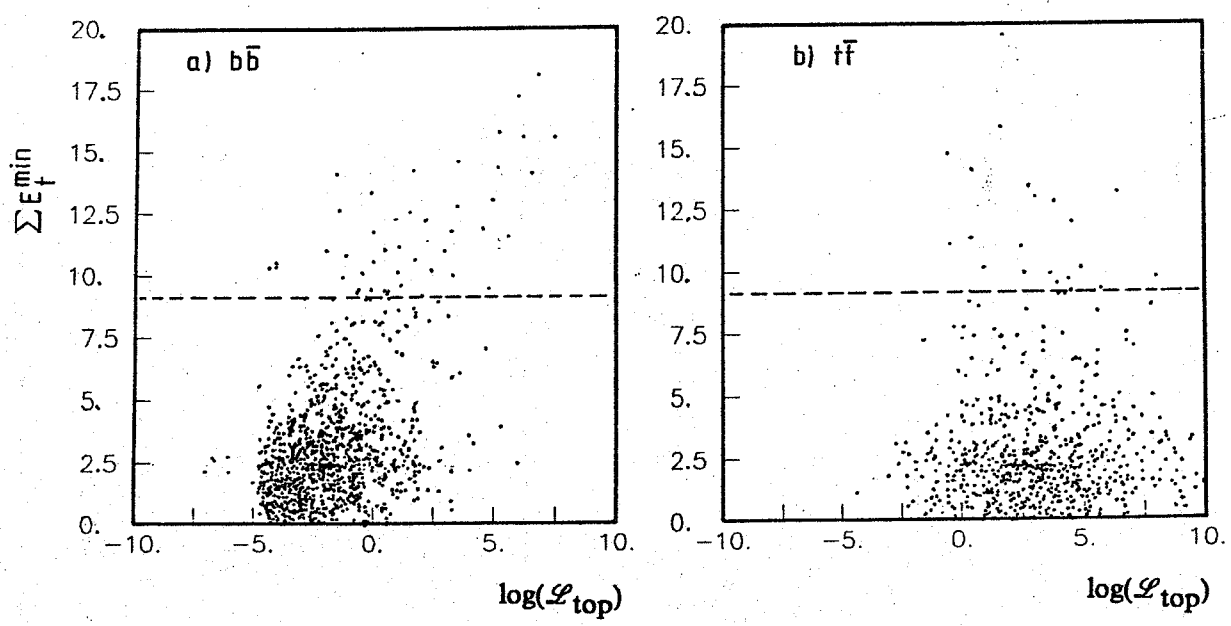

Figure 70: top−likelihood versus isolation. ΣE_t^{min} is ΣE_t around the better isolated muon. a) Isajet $b\bar{b}$ events b) Isajet $t\bar{t}$ events (25 GeV/c²)

The distributions of the top likelihood for Isajet $t\bar{t}$ and $b\bar{b}$ events are shown in figure 71, for top masses of 25 and 30 GeV/c². All distributions are after the isolation cut. Events form $t\bar{t}$ are concentrated at high log($\mathcal{L}_{top}$), whereas $b\bar{b}$ events populate the low values. Unfortunately the separation is not complete, there is still a considerable overlap. The separation becomes better for higher top masses.

In figure 72 the log($\mathcal{L}_{top}$) distribution of the data for the m_{top} = 25 GeV/c² hypothesis is shown. Superposed are the expected distributions from Isajet for a mixture of $b\bar{b}$, $c\bar{c}$, Drell−Yan and background. Also shown is the expected contribution from $t\bar{t}$. The observed distribution is well described by conventional sources. Even the tail towards high log($\mathcal{L}_{top}$), which would contain a large fraction of a possible top signal, is explained by the no top "cocktail". In the region log($\mathcal{L}_{top}$) > 5.2, where no events are observed, $t\bar{t}$ production would contribute with 5.0 events.

This can already be used to give an upper limit on the $t\bar{t}$ cross−section (46% of the nominal value, however without systematic errors). The limit can be improved using the complete region with log($\mathcal{L}_{top}$) > 2. This region was divided into three bins. The poisson probability to observe the actual

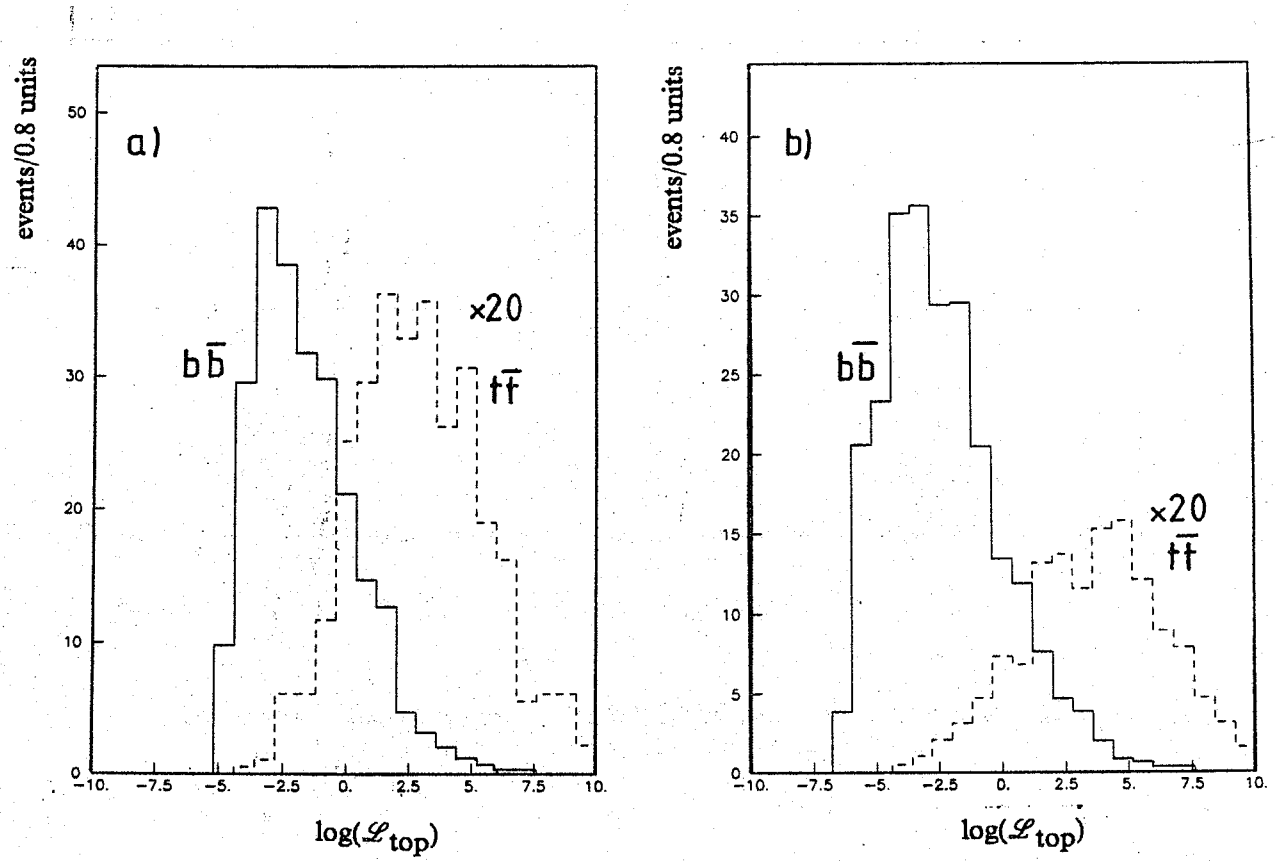

Figure 71: $\log(\mathcal{L}_{top})$ for Isajet $b\bar{b}$ and $t\bar{t}$. $\Sigma E_t^{min} < 9$ GeV. Events at 659 nb^{-1}, ¬ ($t\bar{t}$ × 20) a) hypothesis $m_{top} = 25$ GeV/c^2 b) $m_{top} = 30$ GeV/c^2

number of events in those bins was calculated as a function of the expected top events and the contribution from conventional sources[37]. From that we can exclude more than 6.0 $t\bar{t}$ events with 90 % confidence level. 17.4 events from $t\bar{t}$ are expected in that region. This can be converted into an upper limit on the $t\bar{t}$ cross−section. For that we have to consider the errors of the acceptance and the luminosity. The lower limit on $\sigma(t\bar{t})$ is 4.8 nb at 90% confidence level for a top mass of 25 GeV/c^2.

This analysis was repeated for the hypothesis of m_{top} = 30, 40 and 50 GeV/c^2 (for 30 GeV/c^2 see fig. 73). The results and extracted limits are summarized in tables 17 and 18 . These limits also include uncertainties from the statistics of the Monte Carlo and from errors in acceptance and luminosity.

[37] In calculating the limits the probability distributions were renormalized allowing for the probability to get the observed number of events from no top sources alone. This is especially important if the expected background exceeds the actually observed number of events.

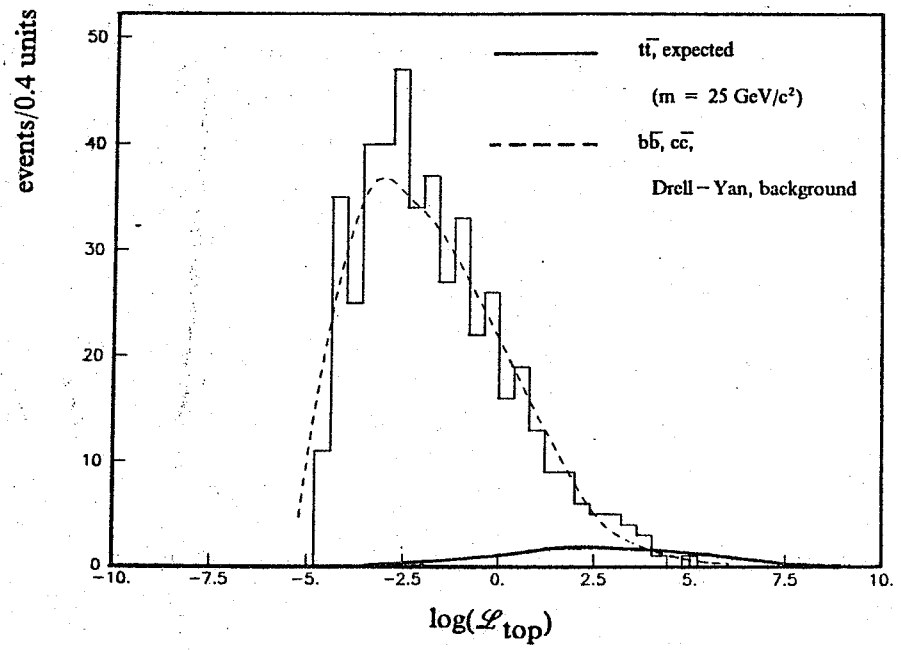

Figure 72: $\log(\mathcal{L}_{top})$ of data (hypothesis: m_{top} = 25 GeV/c²). ΣE_l^{min} < 9 GeV. Superposed are the expected distributions for a mixture of conventional sources ($b\bar{b}$, $c\bar{c}$, Drell − Yan and background, dashed line) and $t\bar{t}$ (solid line).

The limits and the expectations from Erojet are shown in figures 74 and 75 as a function of the top mass. From these plots we can state:

$$\mathbf{m_{top} > 35\ GeV/c^2\ \ (90\ \%\ C.L.)}$$

which improves the existing limits from e^+e^- experiments by more than 10 GeV/c².

Unfortunately this limit depends strongly on the Monte Carlo model, especially on the absolute cross − section calculation of Eurojet. Such calculations can be uncertain within a factor of two. However, as $t\bar{t}$ is produced at rather high Q^2, the calculations should be more accurate than in the case of $b\bar{b}$. The cross − section limits in table 18 are less model dependent, but there might be uncertainties from the fragmentation and the decay kinematics. On the other hand, the top fragmentation should be very hard, and its semileptonic decay should be well described by the spectator model. Uncertainties in fragmentation and decay should not affect the limits very much.

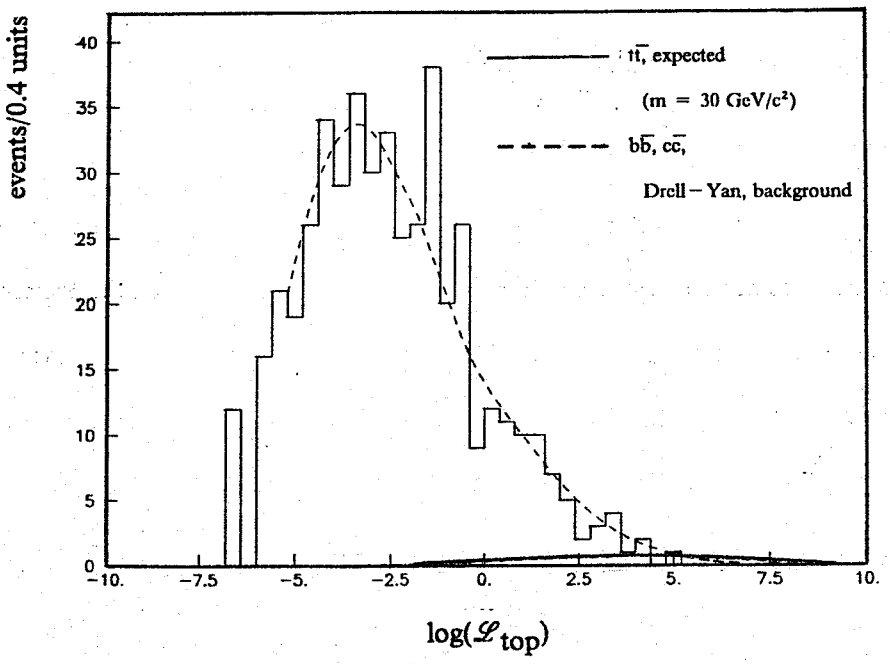

Figure 73: $\log(\mathcal{L}_{top})$ of data (hypothesis: $m_{top} = 30\ GeV/c^2$). $\Sigma E_t^{min} < 9\ GeV$. Superposed are the expected distributions for a mixture of conventional sources ($b\bar{b}$, $c\bar{c}$, Drell − Yan and background, dashed line) and $t\bar{t}$ (solid line).

It should be mentioned that these limits can also be used to exclude an hypothetical b′, a "down" quark (charge = −1/3) of a forth family. If such an object exists and if it is lighter than the top quark, it can only decay into charm. The cross section would be identical with that assumed for $t\bar{t}$ production. The signature of such events would be very similar to $t\bar{t}$. Only muons from third generation decays would be absent, and there might be small differences in the decay kinematics. As third generation decays do not contribute to the events with high $\mathcal{L}$(top), the analysis is valid for $b'\bar{b}'$ production as well:

$$m_{b'} > 35\ GeV/c^2\ (90\ \%\ C.L.)$$

(same assumptions on cross − sections as for $t\bar{t}$)

m_{top}:	25 GeV/c^2	30 GeV/c^2	40 GeV/c^2	50 GeV/c^2
a) log($\mathcal{L}$): 2.0 − 4.0				
data	23	15	15	not used
no−top	20 ± 7.4	20 ± 6.9	19 ± 7.5	−
$t\bar{t}$	8.6 ± 1.4	2.8 ± 0.5	0.53 ± 0.1	0.0
b) log($\mathcal{L}$): 4.0 − 5.2				
data	2	3	4	1
no−top	5.0 ± 2.0	2.7 ± 1.4	4.9 ± 1.5	1.9 ± 1.2
$t\bar{t}$	3.8 ± 0.5	2.3 ± 0.4	0.39 ± 0.1	0.06 ± 0.01
c) log($\mathcal{L}$) > 5.2				
data	0	0	0	0
no−top	1.7 ± 1.5	1.5 ± 1.9	0.8 ± 1.9	0.9 ± 0.5
$t\bar{t}$	5.0 ± 0.7	3.8 ± 0.7	1.48 ± 0.27	0.94 ± 0.30

Table 17: Events seen and expected in different bins of log($\mathcal{L}_{top}$)

m_{top} GeV/c^2	events expected log($\mathcal{L}$) > 2	events excluded 90% C.L.	95% C.L.	$\sigma(t\bar{t})$/nb expected	$\sigma(t\bar{t})$/nb excluded 90% C.L.	95% C.L.
25	17.4	6.0	6.1	12.8	4.8	6.3
30	8.9	4.8	6.2	5.1	3.0	3.9
40	2.4	3.5	4.5	1.1	1.8	2.3
50	1.0	2.3	3.0	0.3	0.8	1.0

Table 18: Cross−section limits for $t\bar{t}$ ($\sqrt{s}$ = 630 GeV).

As a byproduct of these limits we can reduce the possible contribution of top to the like−sign events to maximally 5.2 events (and 7.5 unlike−sign), which can be neglected in the analysis of $B^0 - \bar{B}^0$ oscillations.

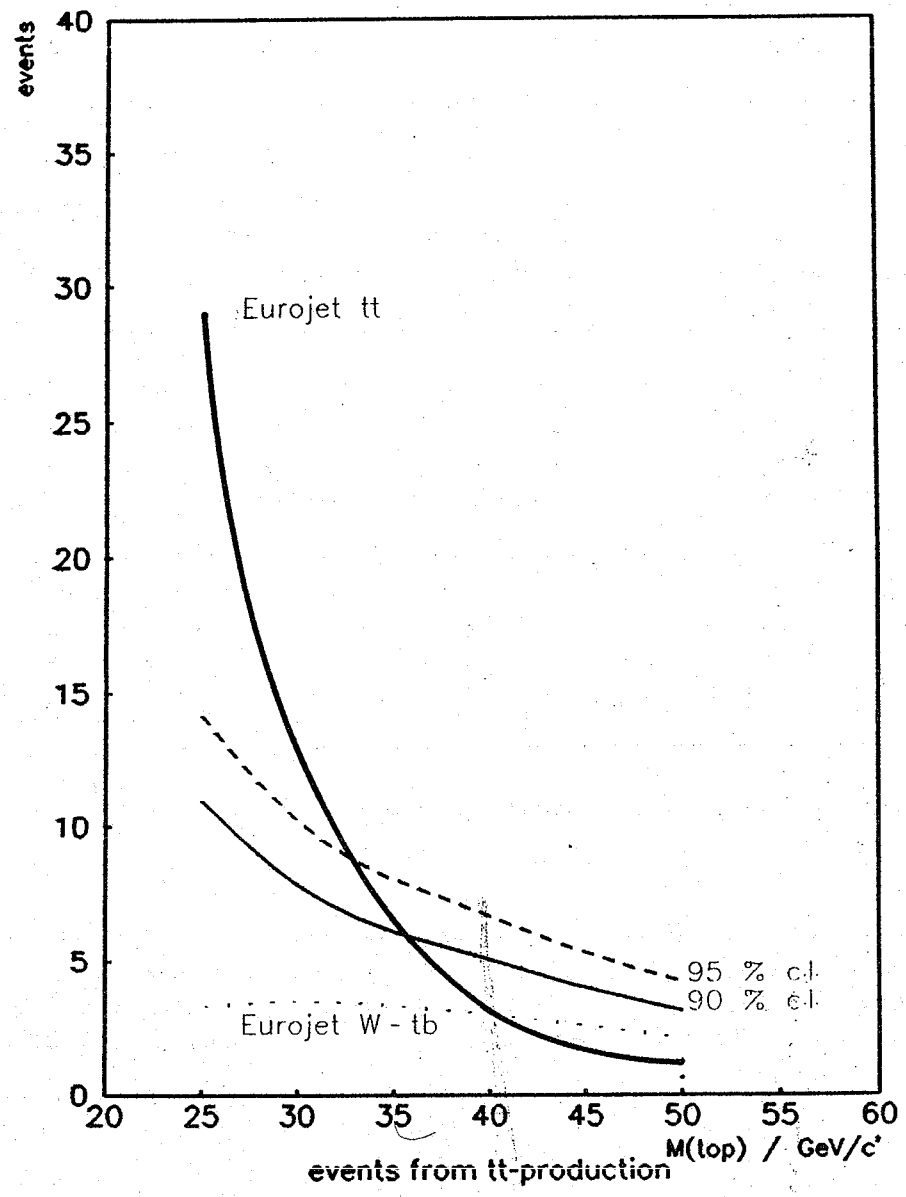

Figure 74: Limits on $t\bar{t}$ production (I).
Number of excluded events (90 % and 95 % confidence level)
Also shown is the number of events expected using the cross sections from Eurojet. The limits are for $t\bar{t}$ production only, $W \rightarrow t\bar{b}$ was not considered.

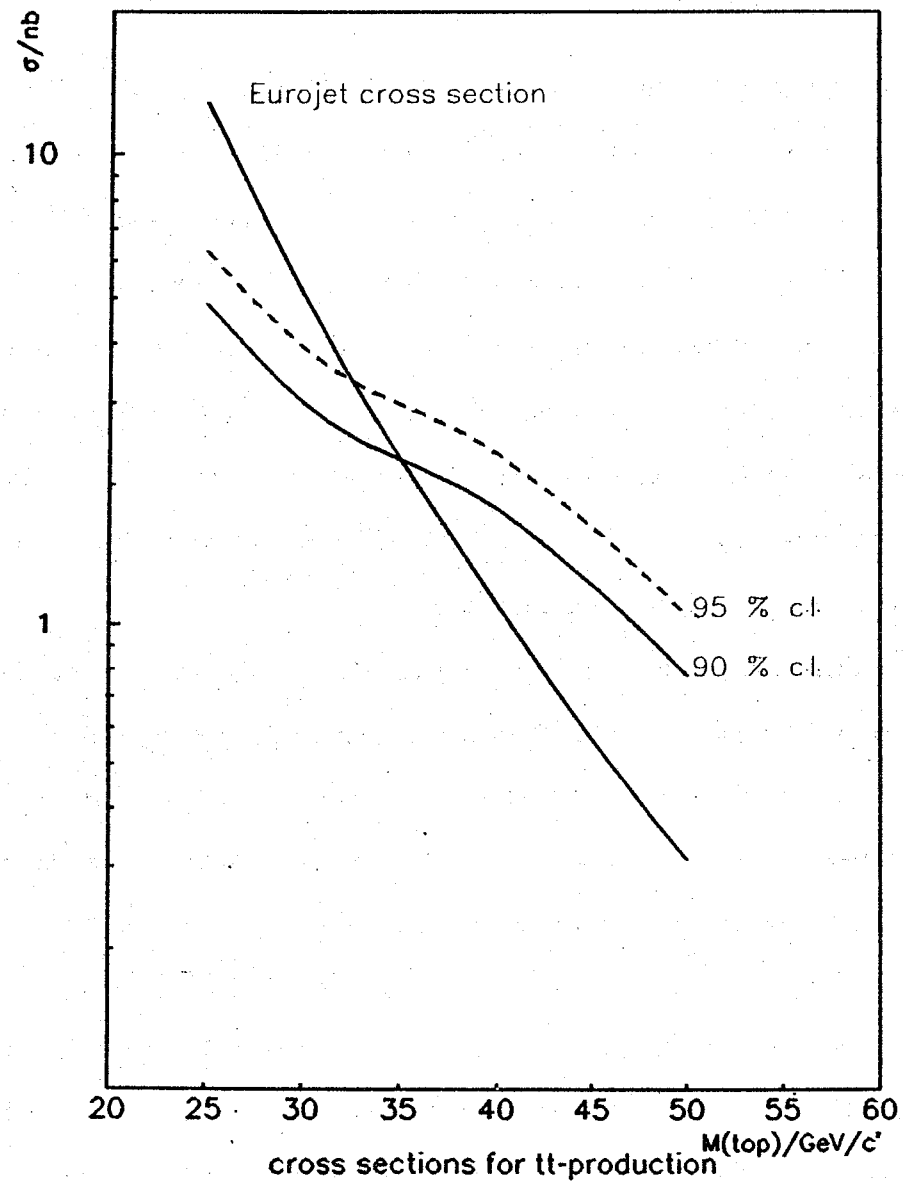

Figure 75: Limits on $t\bar{t}$ production (II). Excluded cross sections for $t\bar{t}$ production (90 % and 95 % confidence level). Also shown is the Eurojet prediction.

11. ISOLATED LIKE−SIGN EVENTS

The overall picture of the dimuon events looks as if everything is explained by the Standard Model. However, in the data of the 1983 run a couple of puzzling like−sign isolated events were found, which at that time could not be interpreted in terms of standard dimuon sources [2]. One event (8038/31 or "Q", fig. 76) is very outstanding, having two μ^+ with $p_t > 10$ GeV/c each, which are almost exactly back−to−back. Besides that, the event is very quiet, no jets have been reconstructed, The only remarkable activity is an Λ which is found 90^0 away from the muons in the transverse plane. In addition an event with a similar configuration (8254/1179 or "S") was found, this time with two μ^- and an $\bar{\Lambda}$, but the muons at lower p_t (7.3 and 5.1 GeV/c respectivly). Nevertheless it looks like a "mirror" partner of event "Q". What happened since that?

Firstly, UA1 collected almost six times the luminosity of 1983. No additional events with isolated like−sign muons above 10 GeV/c (like event "Q") have been found, but some new events with isolated muons at lower p_t, similar to "S", appeared. Secondly, we tightened the isolation requirement used in the early analysis, namely $\Sigma E_t < 4$ GeV for each muon, in order to improve the separation of Drell−Yan from heavy flavour events. Especially events from $b\bar{b}$ production at low Q^2 could easily satisfy the $\Sigma E_t < 4$ GeV cut. Both events "S" and "Q" fail the new isolation cut {29} .

If we now plot p_t of the fast muon versus p_t of the slow muon for the like−sign events satisfying the new isolation cut [$S < 9$ (GeV)^2], everything agrees with $b\bar{b}$ (Isajet) and background (fig. 77). However, if we go back to the old definition, $\Sigma E_t < 4$ GeV, we find the following (fig 78):

In addition to the 17 events already satisfying the $S < 9$ (GeV)^2 cut 23 new events were selected. These 40 events are called "semi−isolated". Most of them cluster at low p_t of both muons. Their distribution is well reproduced by the Monte Carlo. Events with semi−isolated muons in the medium p_t range, like event "S", are in good agreement with QCD, too. Only Event "Q" sticks out in a region where practically no event is expected.

What is the probability of such an event? From the background estimate the probability to have an like−sign event with both muons above 10 GeV/c p_t is 1.5×10^{-4}, even if we do not cut on the isolation. The background simulation found no semi−isolated event of that type, which enables us to

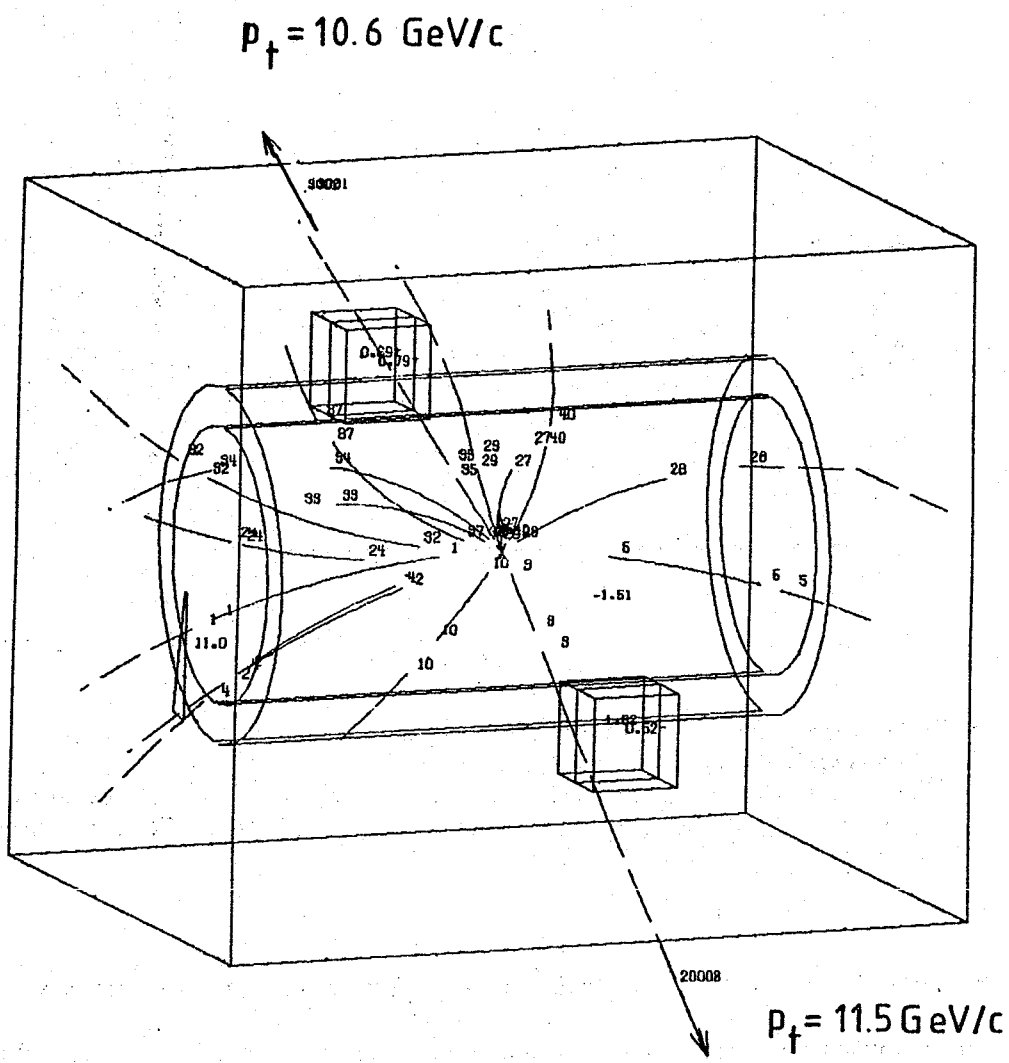

Figure 76: Picture of event 8038/21 "Q"

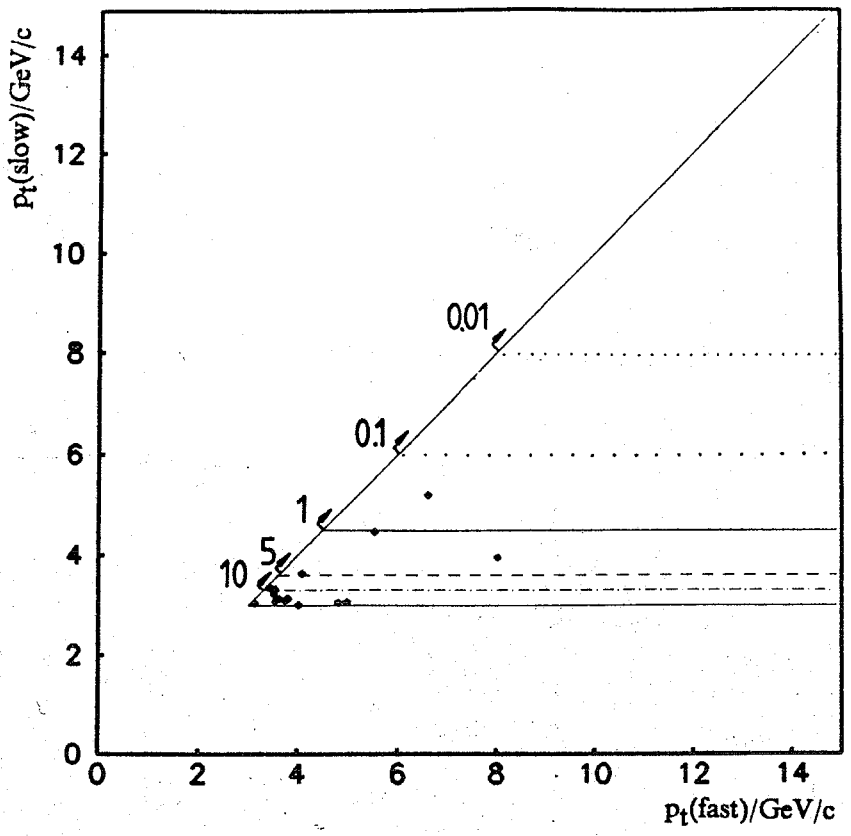

Figure 77: p_t(fast) versus p_t(slow), like−sign isolated events.
Events satisfying $S < 9$ (GeV)^2
The number of events expected from Isajet plus decay background are indicated. A mixing parameter χ of 0.12 is assumed. Isajet was normalized to all (including non−isolated) events.

give an upper limit of $< 10^{-4}$ at 90% confidence level. Both muons are very well measured, and their signs are determined with more than 6 σ significance. Thus the event cannot be a mismeasured Drell−Yan candidate.

Looking for physics sources one can exclude top, this might give isolated like−sign dimuons, but such events have a high jet activity. In order to study the probability to get such an event from $b\bar{b}$ a Monte Carlo production of 10 pb^{-1} was used. This production estimates 0.3 ± 0.1 unlike−sign events with $p_t > 10$ GeV/c, and 0.03 ± 0.03 like−sign events at an integrated luminosity of 659 nb^{-1}. None of them should be semi−isolated. Like−sign semi−isolated events at lower p_t (4 GeV/c) are typically

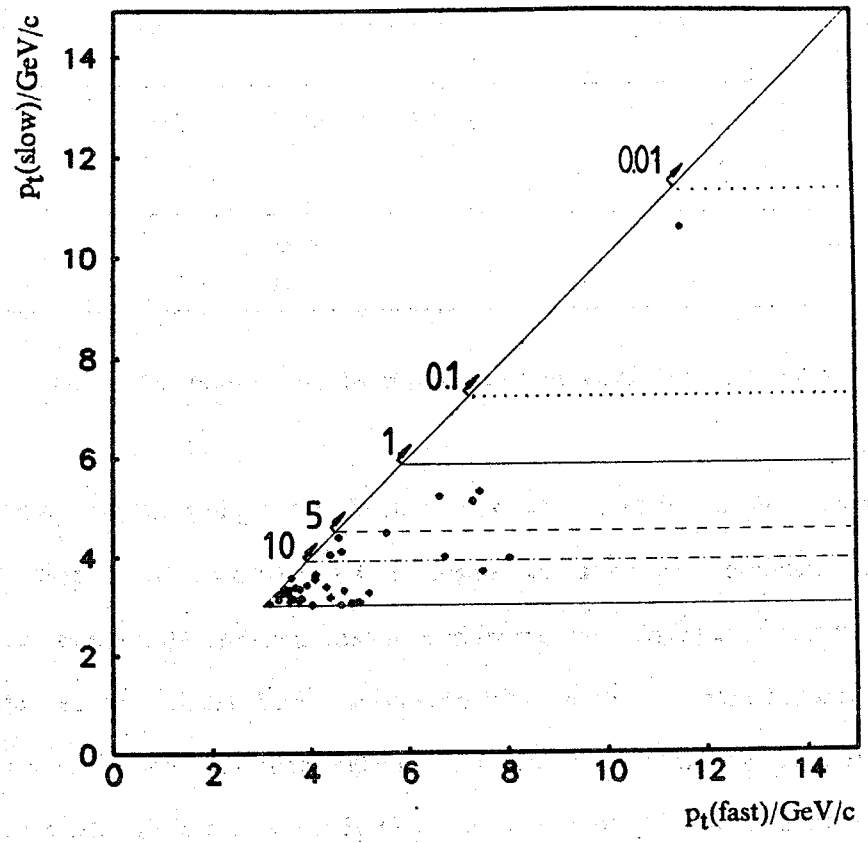

Figure 78: p_t(fast) versus p_t(slow), like−sign semi−isolated events.
ΣE_t < 4 GeV for each muon.
The number of events expected from Isajet plus decay background are indicated. A mixing parameter χ of 0.12 is assumed. Isajet was normalized to all (including non−isolated) events.

suppressed by a factor of 0.15 compared to non−isolated like−sign events. If this factor is still valid at higher p_t, we would expect only 0.005 like−sign semi−isolated events. These numbers are without $B^0-\overline{B}^0$ oscillations. As this production run out of statistics for high p_t muons, a special Isajet production was made concentrating only on high p_t b's (10 pb^{-1}). The results above were confirmed, but this time one MC event was found which comes close to the isolation cut. In table 19 event "Q" and this special Isajet event are compared.

Except of the sign of the muons all other properties are quite similar, both events show no jet activity. This *single* MC event would correspond to 0.08 unlike−sign events. As the Isajet Monte Carlo

event	sign	p_t GeV/c	ΣE_t GeV	$\Delta\phi$ deg	η	$m^{\mu\mu}$ GeV/c^2	ΣE_t GeV
8038 31	+ +	11.5 10.6	3.1 1.5	188	0.05 −0.10	22.1	48
Isajet	− +	11.1 10.8	2.1 4.1	175	0.04 1.54	28.3	54

Table 19: Comparison of event 8029/31 with an Isajet event

has not implemented $B^0 - \bar{B}^0$ oscillations, we can calculate the probability that this event becomes like−sign because of oscillations. Using a mixing parameter of $\chi = 0.12$ we would expect 0.02 like−sign events of that type. The respective number without mixing is 0.005. This shows that it is not completely impossible to get such an event like "Q" from $b\bar{b}$, provided that $B^0 - \bar{B}^0$ oscillations exist. However, the probability is only 1/50 based on one accidentally found MC event, so the event still remains somewhat mysterious. In table 20 an overview on the high p_t events and the MC expectations is given.

	all	unlike – sign	like – sign	unlike – sign semi isol.	like – sign semi isol.
data	5	4	1	4	1
$b\bar{b}$ $\chi = 0$	0.33	0.30	0.03	0.08	0.005
$b\bar{b}$ $\chi = 0.12$	0.33	0.24	0.09	0.06	0.02
Drell – Yan	2.2	2.2	–	2.2	–
Back – ground	3×10^{-4}	1.5×10^{-4}	1.5×10^{-4}	$< 10^{-4}$	$< 10^{-4}$

($\chi = 0$: no mixing, $\chi = 0.12$: mixing)
Because of the low statistics from the $b\bar{b}$ Monte Carlo the values given here are uncertain within a factor of two.

Table 20: *Probability for events with $p_t > 10$ GeV/c for both muons.*

12. LOW MASS DIMUONS

Coming to the end we want to give a short review of the analysis of the $m^{\mu\mu} < 6$ GeV/c^2 data. They are not the subject of this thesis and more detailed descriptions can be found in [73] [74]. Nevertheless they are related to the dimuon analysis and therefore are worth while mentioning.

As described in chapter 4.2, the "low mass" sample is defined by following physics cuts:

$$p_t > 3 \text{ GeV/c (both muons)}$$

$$m^{\mu\mu} < 6 \text{ GeV/c}^2$$

The selection resulted in 1211 events, 335 were validated by scanning. 295 events are unlike−sign, 40 are like−sign. The background in this sample is estimated to 38 ± 9 unlike−sign and 19 ± 5 like−sign events.

A rich variety of physics processes can contribute to this sample:

- Drell−Yan process with QCD corrections
- Cascade decays of $b \rightarrow c\,\mu\,\nu$ and subsequently $c \rightarrow s\,\mu\,\nu$
- Higher order QCD processes such as gluon−gluon scattering with one gluon splitting into a $c\bar{c}$ or $b\bar{b}$ pair. In the case of $b\bar{b}$ this can lead to like−sign events by second generation decays and by oscillations.
- Decays of high p_t J/ψ's
- Decays of light mesons like ρ, ω and ϕ

Many of these processes involve higher order QCD processes, as for example a low mass Drell−Yan pair must recoil against a QCD jet in order to get enough p_t to satisfy the selection cuts. These processes are difficult to calculate. Especially if the dimuon mass becomes very low, the Monte Carlo calculations are biased because of cut−off parameters. E. g. for the gluon splitting process $g \rightarrow c\bar{c}$ Isajet demands the $c\bar{c}$ mass to be larger than 6 GeV/c^2. It is hard to relax this cut without disturbing other properties of the Monte Carlo (e.g. jet evolution).

The production of light mesons involves problems as well. They have very small branching ratios[38] in muon pairs, but they are copiously produced in ordinary QCD−processes. Their contribution depends on fragmentation functions of light quarks and gluons, and reliable calculations are difficult. Unfortunately the mass resolution is poor in the region around one GeV/c^2, so that this contribution cannot be separated easily from the continuum.

This is different for the J/ψ. In figure 33 it can be seen that the J/ψ signal appears as a clear peak in the $m^{\mu\mu}$ distribution. As the J/ψ shows up so clearly, an attempt was made to relax the cuts on the muons in order to get a larger sample. This J/ψ selection demanded only one muon with p_t above 3 GeV/c, but the dimuon mass must be in a window around the J/ψ mass:

one muon $p_t > 3$

a second muon such that:

$2\ \mathrm{GeV/c^2} < m^{\mu\mu} < 4\ \mathrm{GeV/c^2}$

$p_t^{\mu\mu} > 4\ \mathrm{GeV/c}$

identical technical cuts as dimuon selection

This yielded 1803 events, but there is some overlap with the standard dimuon selection. After fiducial cuts and scanning 458 unlike−sign events remained (and 61 like−sign events). The dimuon mass distribution of the unlike−sign events is shown in figure 79 .

The mass spectrum was fitted by two gaussian distributions representing the J/ψ and the ψ' and a constant background (see table 21). The cross−section for J/ψ production was found as:

$$\sigma(J/\Psi,\ p_t > 5\ \mathrm{GeV/c}) = 0.08 \pm 0.03\ \mu\mathrm{b}$$

There exist two possible sources for J/ψ events:

- Decay of B−mesons : B → J/ψ + X

[38] The relevant branching ratios are [75]:
$\rho \to \mu\mu$: 0.0067 ± 0.0012 %, $\omega \to \pi\mu\mu$: 0.010 ± 0.002 %, $\phi \to \mu\mu$: 0.025 ± 0.003 %

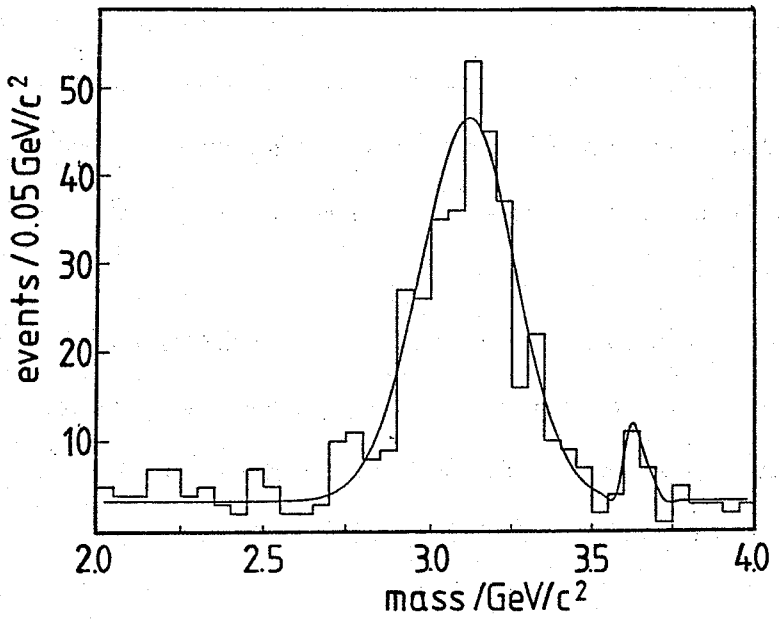

Figure 79: Dimuon mass distribution of J/ψ selection: one muon p_t > 3 GeV/c, 2 GeV/c² < $m^{\mu\mu}$ < 4 GeV/c² , unlike−sign events. The distribution was fitted by two gaussian distributions (J/ψ and ψ′) and a constant background.

state	events	mass/GeV/c²	widths/ GeV/c²	mass (world)
J/ψ	303 ± 18	3.11 ± 0.01	0.14 ± 0.01	3.0969 ± 0.0001
ψ′	14 ± 4	3.64 ± 0.04	0.25 ± 0.01	3.6680 ± 0.0001

The masses and widths found are in excellent agreement with the world average ("world") and the expected experimental resolution.

Table 21: Results of the J/ψ search.

The branching ratio of this decay was measured as 1.4 ± 0.6 % [11]. J/ψ's from B−decays should be non−isolated. (The few ψ′ found can only be explained by B−decays).

- QCD production of χ states and subsequent transition: χ → J/ψ + γ (Because of the Zweig rule J/ψ's cannot be directly produced by gluon fusion). These J/ψ's should be isolated.

A large fraction of the J/ψ's is non−isolated, which again indicates large $b\bar{b}$ production. At the moment Monte Carlo calculations estimate the cross−section of J/ψ from B−decays to 30 nb, which

explains only a part of the signal. Also QCD calculations of χ production have difficulties to explain the amount of isolated J/ψ's, but these calculations are very uncertain and things may change [76].

The remainder of the low mass events (p_t > 3 GeV/c each muon) was found to be consistent with the physics sources listed above (fig. 80 and 81). Like in the analysis of the $m^{\mu\mu}$ > 6 GeV/c^2 data, the events from Drell−Yan could be separated by an isolation requirement:

$$\Sigma E_t(\mu) < 3 \text{ GeV for both muons}$$

and

$$\Sigma E_t(\mu\mu) < 3 \text{ GeV}$$

$\Sigma E_t(\mu\mu)$ is the E_t in a cone around the direction of the dimuon. The isolation cut differs from that used for the $m^{\mu\mu}$ > 6 GeV/c^2 data. This cut takes into account that in the low mass sample the muons are close together.

From the isolated events a cross−section for low mass Drell−Yan pairs with high p_t could be obtained:

$$\sigma_{DY}(p_t{}^{\mu\mu} > 6 \text{ GeV/c}, m^{\mu\mu} < 6 \text{ GeV/c}^2) = 1.3 \pm 0.2_{stat} \pm 0.5_{sys}$$

The non−isolated events are consistent with heavy flavour production. The number of like sign events is consistent with $B^0 - \overline{B}^0$ oscillations. At very low masses there is room for events from decays of light vector mesons.

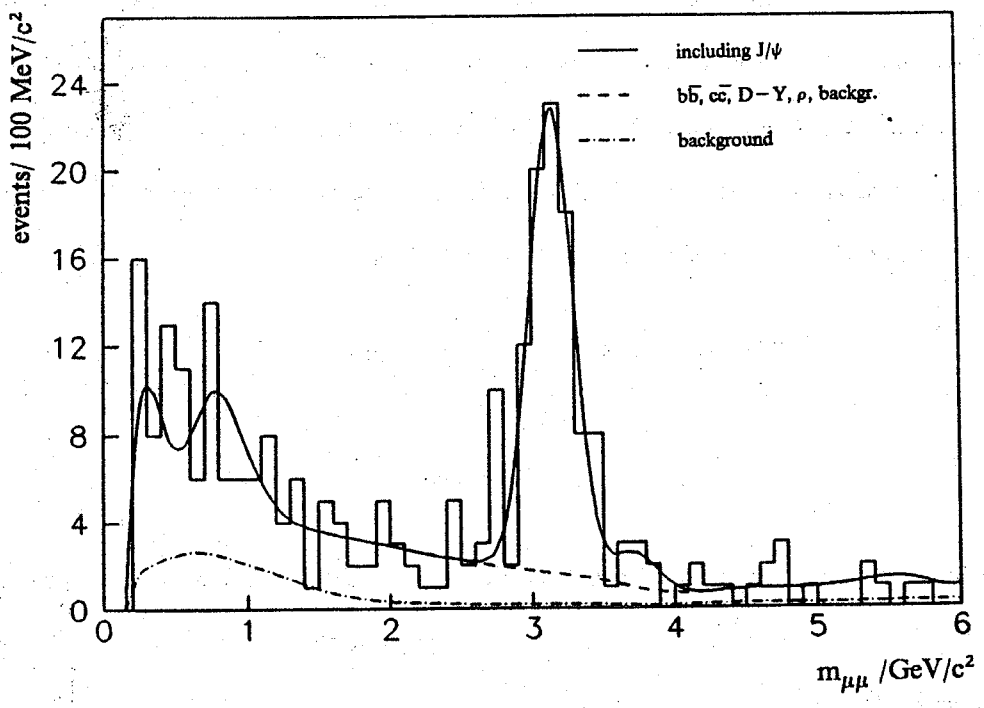

Figure 80: Dimuon mass distribution of unlike−sign events $m^{\mu\mu} < 6\ GeV/c^2$ [74].

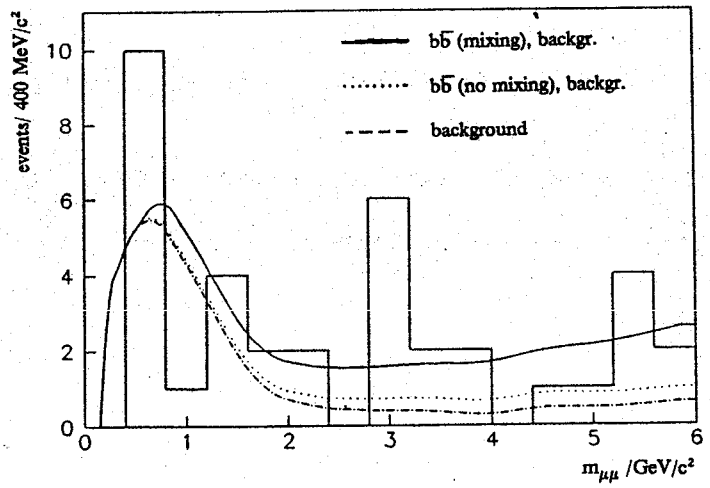

Figure 81: Dimuon mass distribution of like−sign events $m^{\mu\mu} < 6\ GeV/c^2$ [74].

13. THE FUTURE: ACOL

The main limitation of the present $p\bar{p}$ collider is the low luminosity due to the difficult antiproton accumulation. In 1987 the AA will be replaced by an improved facility called ACOL. Then the SPS collider should reach ten times the present luminosity. Together with this improvement the UA1 detector will undergo a major upgrading program. The main improvement will be the replacement of the present electromagnetic calorimeters (Gondolas and Bouchons) by an uranium calorimeter which is read out by a warm liquid (tetramethylpentane or "TMP"). [78]. The advantages of this new technology are:

- *High resolution:* The determination of the energy deposition in a TMP calorimeter is reduced to the measurement of the absolute charge deposited. This can be done much more precise than the measurement of the light intensity of a conventional scintillation calorimeter. Hence the energy resolution is much better.
- *High Granularity:* The new calorimeter will have a tower structure which improves the spatial resolution. This will result in a better electron identification, jet definition and measurement of isolation. A new trigger processor will make use of these advantages.
- *Radiation Hardness:* In contrast to a scintillation calorimeter, TMP readout does not suffer from radiation damage and ageing. This enables a better calibration and long term stability of the apparatus improving the energy resolution.
- *Higher Density:* Because of the high density of uranium a combined electromagnetic *and* hadronic calorimeter can be placed in the same space formerly needed by the electromagnetic calorimeters alone. The present hadronic calorimeter will work as a "leakage" detector.
- *Compensation:* The new calorimeter will have an almost equal response to electrons and hadrons. This improves the energy resolution of jets.

With the high statistics from ACOL and the improved energy resolution it should be possible to measure the $W^{\pm}$ and Z^0 masses with a precision of $100-200$ MeV. This is a factor $10-30$ better than presently quoted.

Together with the cental calorimeters other parts of the UA1 detector will be improved: New forward calorimeters will give a better rejection against double interactions, which are more frequently at high luminosities. The muon detector will be improved in order to stand the higher rates. This includes an enlarged iron shielding in the forward direction and more sophisticated higher level triggers. Under discussion is the installation of a microvertex detector.

Thus the improved $p\bar{p}$ collider and the upgraded UA1 detector will still be an ideal place for probing the Standard Model or looking for new physics beyond it.

Concerning dimuon physics the main program can be:

- The high luminosity will increase the present dimuon sample by more than a factor of ten. This will certainly reduce the statistical errors on all measured quantities e.g.: cross−sections and the ratio like−sign to unlike−sign events. This is especially important for the measurement of R. At present the statistical error is dominant over the systematic error (± 0.07 compared with ± 0.03). Therefore higher statistic is urgently needed to improve the R measurement. The systematic error on R from the uncertainty of the background subtraction can be improved, too. Using the matching of CD track to muon chamber track (chapter 5.5) the error on the background is itself limited by the statistics of the individual reverence samples. The the systematic error can also be reduced by demanding a higher p_t of the muons. This suppresses the contribution from background and second generation decays and their uncertainty becomes less important. With 10^4 dimuon events it should be possible to determine the mixing parameter χ with a precision of $\pm\ 0.008_{stat} \pm 0.010_{sys}$. This should be compared with the present accuracy of $\pm\ 0.038_{stat} \pm 0.020_{sys}$. There is hope that the systematic error of the Monte Carlo (at present ± 0.02) can be reduced, once better data on fragmentation and branching ratios are available.
- Having higher statistics it might also be possible to reconstruct hadronic final states of B−mesons decays. An interesting candidate is the decay $B^0_s \rightarrow \mu\ \nu$ F [79], the F could be identified by the decay chain $F \rightarrow \pi\ \phi$, $\phi \rightarrow K^+K^-$. The reconstruction of a few events of this kind in the like−sign events could give a hint that the oscillations are due to B^0_s .

- The new calorimeters will improve the measurement of the isolation of muons. Separation of Drell−Yan and Upsilon from heavy flavour events will become easier. Also the search for a top signal will become much easier if the isolation is better defined. The improved resolution of jets might enable a search for resonance decays like $W \rightarrow t\bar{b}$ giving two muons and two jets.
- The high luminosity will allow the search for rare processes. Provided the top quark is light enough $W \rightarrow t\bar{b}$ will give in the order of 50 events, a signal which should be found. The advantage of this channel is that the cross−section of $W \rightarrow t\bar{b}$ is well known. The sensitivity for $t\bar{t}$ production will also be extended towards higher masses. In addition, one can look for all kinds of exotic particles such as leptoquarks, SUSY−particles, and whatever else.

Because of the positive signal for $B^0 - \bar{B}^0$ oscillations one can ask the question, if the B^0 system shows, analogous to the K^0, CP violation. Up to now CP violation has been observed in the K^0 system *only* [82] and is yet not competely understood. Although the phase in the K−M matrix offers an explanation within the Standard Model alternative models are not ruled out [26]. In the dimuons CP−violation would show up as a difference in the rates of plus−plus and minus−minus dimuons:

$$\varepsilon = [N^{++} - N^{--}] / [N^{++} + N^{--}] \qquad \{41\}$$

CP violation can be relatively strong in the B^0_d system [81]:

$$\varepsilon(B^0_d) \approx 10^{-2}$$

It was always believed that this system does not show large mixing. Hence it should produce no or only few like−sign dimuons, and CP violation might be invisible. On the other hand, CP−violation is expected to be much smaller in the B_s, which should mix substantially:

$$\varepsilon(B^0_s) \approx 10^{-4}$$

At present we observe 78 (++) events and 79 (−−) events: $\varepsilon = 0.013 \pm 0.080$. However, only 25% of the like−sign events are due to mixing, the remainder comes form second generation decays

and from background. Therefore an eventual CP violation would be reduced by a factor of 1/4. Correcting for that, we obtain:

$$\varepsilon_{CP} < 0.42 \text{ at } 90\% \text{ C.L.}$$

which is not very exciting.

It needs a much higher statistics to reach the precision, which is required by the theoretical expectations. If the CP violation is in the order of 10^{-4} (e.g. if only B^0_s would mix) about 10^9 dimuon events are needed. In a less pessimistic scenario one can assume $B^0_d - \overline{B}^0_d$ mixing ($\chi_d = 0.19$ as measured by ARGUS [69]), and a CP violation of 10^{-2} in the B^0_d channel[39]. This would need a statistic of about 10^6 like−sign dimuons. This is also not possible with ACOL, but can be done with a specialized high luminosity machine ("b−factory").

Nevertheless an attempt should be made to measure this ε parameter as precisely as possible. The small CP violation in the B^0_s system is due to delicate cancellations of different amplitudes [80]. Any non standard contribution to the box diagram can change this dramatically. Such non standard contributions can be SUSY particles, Higgses, right handed W's, leptoquarks, quarks of a fourth family etc., even if their masses are too high to be directly produced at the collider. Thus a precise measurement of ε can probe the Standard Model and open a window to new physics.

Another promising way to look for CP violation in the B system are the hadronic decays of B− mesons. If two amplitudes with different weak and strong phases contribute to the same decay channel, CP violating effects can be large. Candidates for such decays are (fig. 82):

$$B^- \rightarrow F^- D^{0*}$$

$$B^- \rightarrow D^- D^{0*}$$

This of course is not a subject of dimuon physics, but requires single muons (to tag one b and measure its sign) and a micro vertex detector in order to reconstruct the hadronic decay.

---

[39] However, there are arguments that CP violation in B^0_d decreases if mixing increases. Thus $\varepsilon(B^0_d)$ might be much less than 10^{-2} [33].

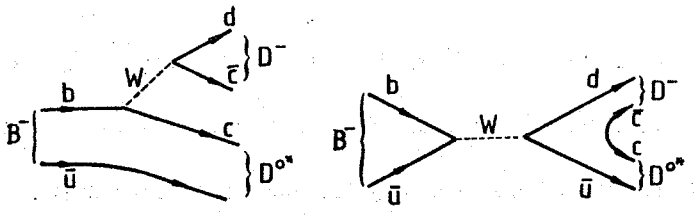

Figure 82: CP violation in hadronic decays of B− mesons. The interference of both diagrams may lead to a CP violating difference of the partial decay widths of $B^+ \to D^+ D^{0*}$ *and* $B^- \to D^- D^{0*}$ *(replacing "d" by "s" gives the decay:* $B^- \to F- D^{0*}$ *)* [83].

14. SUMMARY AND CONCLUSIONS

In $p\bar{p}$ collisions at 630 (540) GeV centre of mass energy heavy quarks are copiously produced, mainly by gluon fusion. About 10% of them decay semileptonically into muons. These muons are normally in jets of hadrons from the fragmentation and the decay of the heavy quarks, they are *non−isolated*. Muons can cleanly be identified in the presence of hadronic energy. Thus non−isolated muons are an ideal tool to tag heavy quarks. The cleanness of the signature can be improved by demanding both quarks to decay into muons, resulting in a dimuon event.

In order to study heavy quark physics at the collider, we selected dimuon event satisfying following cuts:

$$\mathbf{p_t > 3\ GeV/c\ (each\ muon)}$$

$$\mathbf{m^{\mu\mu} > 6\ GeV/c^2}$$

This resulted in **512** events. The background in the sample, mainly from pion and kaon decays, is estimated to 26%.

The events can be classified according to their sign and isolation. Unlike−sign isolated events can be interpreted in terms of the Drell−Yan process and Upsilon decays. We extracted the following cross−sections from these events:

$$\textbf{Drell−Yan production: } \sigma(\ m^{\mu\mu} > 11\ GeV/c^2\ ) = 0.26 \pm 0.08_{stat} \pm 0.05_{sys}\ nb$$

$$\textbf{Upsilon production: } (BR) \times \sigma(\Upsilon,\Upsilon',\Upsilon'') = 1.0 \pm 0.2_{stat} \pm 0.2_{sys}\ nb$$

The non−isolated events are regarded as heavy flavour candidates. They should be dominated by $b\bar{b}$ production. Although $c\bar{c}$ is (at high p_t) produced in equal amounts as $b\bar{b}$, dimuons from $c\bar{c}$ are suppressed because of the softer fragmentation of the charm−quark. The $c\bar{c}$ contribution can be measured using the p_t of the muon relative to the axis of its accompanying jet:

$$N(c\bar{c})/[N(c\bar{c}) + N(b\bar{b})] = 8.0 \pm 6.0\ \%$$

This number is in good agreement with QCD calculations.

Heavy quarks can be produced by lowest order processes like gluon fusion or quark−antiquark annihilation, or by higher order processes such as gluon splitting or flavour excitation. Higher order processes tend to produce muon pairs with high p_t and hence the muons are not back−to−back in the transverse view. From the $\Delta\phi$ and the $p_t^{\mu\mu}$ distribution we can state that higher order processes account for approximately 21% of the dimuons from $b\bar{b}$, in agreement with theoretical models.

The kinematic properties of the events were compared with QCD calculations. These calculations describe the data well, which allows us to give a cross−section for $b\bar{b}$ production:

$$\sigma(p\bar{p} \rightarrow b\bar{b}) = 1.1 \pm 0.1_{stat} \pm 0.4_{sys}\ \mu b$$

$$p_t > 5\ \text{GeV/c (both b−quarks)}$$

$$|\eta| < 2\ \text{(both b−quarks)}$$

lowest order only

In general all properties of the events are in excellent agreement with QCD calculations. Only the large number of like−sign events cannot be explained in terms of second generation beauty decays or background. The most natural explanation of the excess of like−sign dimuons is in terms of $B^0 - \bar{B}^0$ oscillations. Like in the $K^0 - \bar{K}^0$ system a B^0 meson can oscillate into a $\bar{B}^0$ by second order weak interaction. Thus a B^0 meson, which normally decays into a μ^+, can transform into a $\bar{B}^0$, which decays into a μ^-. The probability of this process, described by the mixing parameter χ, is measured as:

$$\chi = N(B \rightarrow \bar{B} \rightarrow \mu^+)/N(B \rightarrow \mu^{\pm}) = 0.121 \pm 0.047$$

It should be stressed that the significance of this result depends strongly on the correct background subtraction. We used two independent methods to calculate the background. Both agree very well. Thus we are confident that the background is understood in detail.

There exist two B^0 mesons which can show oscillations: B^0_d and B^0_s. Experimentally we cannot distinguish between them. However, in the Standard Model with three families the physical allowed

region of the mixing parameters χ_s and χ_d is restricted by the Kobayashi – Maskawa matrix elements V_{td} and V_{ts}. In this model we can give a limit on χ_s:

$$\chi_s = N(B^0_s \to \bar{B}^0_s \to \mu^-)/N(B^0_s \to \mu^\pm) > 0.30$$

(90% C.L.)

We assume that 18% of the b – quarks hadronize into B^0_s mesons. The limit can be improved by combining our result with results from other experiments (CLEO, MARK II, and recently ARGUS):

$$\chi_s > 0.40 \text{ at } 90\% \text{ C.L.}$$

The oscillations in the B^0 system occur via the exchange of virtual top quarks. The top is the charge +2/3 partner of the beauty quark. At present there exists no *direct* evidence for the top quark. The cross – section for $t\bar{t}$ production at the collider falls rapidly with increasing top mass. If the top is light enough, $t\bar{t}$ production should give a sizable number of dimuon events. A search for events from $t\bar{t}$ production did not find any signal. Using the Isajet model with the cross – section from Eurojet calculations a lower limit for the top mass can be given:

$$m_{top} > 35 \text{ GeV}/c^2$$

(90% C.L.)

However, this limit depends on the absolute cross – section for $t\bar{t}$ production calculated by the Monte Carlo.

Apart from the merely numerical results stated above the following conclusions can be drawn: Heavy flavour physics, especially beauty physics, can be done successfully at the collider. Compared with e^+e^- machines the disadvantage of "noisy" events is counterbalanced by the higher cross – section for heavy quark production.

The evidence of $B^0 - \bar{B}^0$ oscillations is certainly the most important result of this analysis. These oscillations are an (indirect) evidence for the existence of the top quark. They also announce interesting prospects for the future. Provided an improved theoretical understanding of the bag parameter and the

B−decay constant, a more precise measurement of the mixing parameter χ will allow stringent constraints on the Kobayashi−Maskawa matrix elements V_{td} and V_{ts} and on the mass of the top quark. In addition these oscillations are one precondition for the search for CP violation in the B−sector.

The next collider runs of UA1 will certainly deliver more precise results and will lead to a deeper understanding of these phenomena. On the other hand the sensitivity, which is necessary for the detection of CP violation, will certainly not be reached. This needs a specialized machine which should provide at least 10^9 $B\overline{B}$ pairs a year.

This analysis made heavy use of Monte Carlo calculations. These calculations are needed to link the properties of quarks to the actually measured parameters such as muon p_t or isolation. Generally the Monte Carlo described the data very well and this agreement allowed important conclusions. However, limitations of the present Monte Carlo programs are already visible. Some of them come from incomplete knowledge of parameters (e.g. branching ratios, fragmentation ε's etc.). There is hope to cure that once more experimental data will be available. Other limitations require more theoretical input, for example the calculations of higher order contributions, or the replacement of phenomenologic models by exact calculations. Also the immense amount of computer time needed for those calculations becomes a problem.

In summary the beauty quark is a very interesting object for future research. Further progress in beauty physic needs certainly:

- Good muon data from high luminosity collider runs
- Precision measurements of branching ratios, lifetimes, fragmentation parameters etc. by e^+e^- experiments
- Better theoretical understanding of the B−decay and the box diagram (f_B and bag parameter)
- Accurate and fast Monte Carlo generators
- In the near future a high luminosity "b−factory"

APPENDIX A

MONTE CARLO CALCULATIONS

A.1 QCD Calculations:

Calculations of QCD processes in proton antiproton collisions make use of a factorization of the complete process into three parts (fig. 83), using the quark parton model.

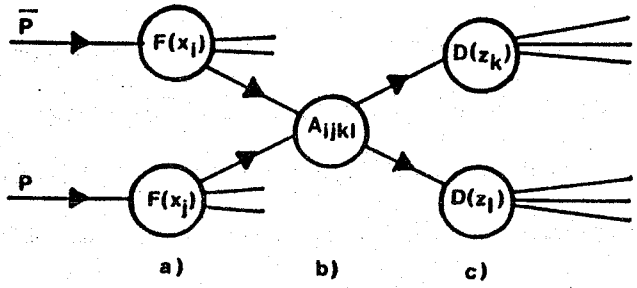

Figure 83: Factorization of a hard process in $p\bar{p}$ collisions

In this model a proton consists of quarks, antiquarks and gluons, normally called partons. The process is then described as the interaction between these pointlike constituents of the proton.

A.1.1 Structure Functions

In the first step [a) in figure 83] one has to describe the probability of finding a certain parton in the proton, carrying a fraction x_i of the proton's longitudinal momentum p. The parton's longitudinal momentum is simply: $p_i = x_i p$. This probability is expressed by the structure function $F_i(x)$. $F_i(x)$ is defined as the density of a parton (i) at the fractional momentum x. The normalization of the structure function has to fulfill:

$$\sum_i \int_0^1 x_i F_i(x_i)\, dx_i = 1 \qquad \{42\}$$

One has to sum over all parton species and to integrate from 0 to 1. Structure functions of quarks were measured in deep inelastic scattering of muons and neutrinos on hadronic targets. The gluon structure function can be deduced using the normalization requirement {42} . It was found that gluons account for roughly 50% of the proton momentum. Parametrizations of these structure functions are available, for example, from Eichten et al. [84] Duke and Owens [85] and Gluck, Hofmann and Reya [86]. These parametrizations also include the Q^2 dependence of the structure functions which leads to scaling violations. Unfortunately different structure functions give different results, which reflects the theoretical uncertainty and some lack of experimental input.

A.1.2 Matrix Elements

The interaction of two incoming partons with momenta p_i and p_j giving two outgoing partons with momenta p_k and p_l is described by the parton cross−section:

$$d\sigma/dt = \alpha_s^2(Q^2/\Lambda^2) \mid A_i \mid^2 / s^2 \qquad \{43\}$$

s and t are the Mandelstam variables:

$$s = (p_i + p_j)^2$$
$$t = (p_i - p_k)^2$$
$$u = (p_j - p_k)^2 \qquad \{44\}$$

α_s is the strong coupling constant which "runs" as a function of Q^2:

$$\alpha_s(Q^2/\Lambda^2) = 12\pi/[(33 - 2\,n_f)\ln(Q^2/\Lambda^2)] \qquad \{45\}$$

n_f is the number of flavours involved in the process and Λ defines the QCD scale, it is normally taken to be 200 MeV.

$|A_i|$ is the matrix element of the process. Lowest order calculations of the matrix elements for various processes were made by Combridge et al. [87] and some of their results are listed in table 22 .

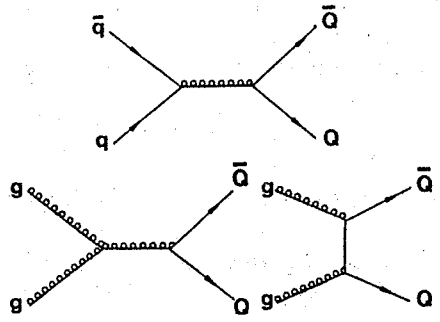

process	$\lvert A_i \rvert^2$
$q_i\,\bar{q}_j \to Q_k\,\bar{Q}_l$	$4/9\,(s^2 + u^2) / t^2$
$g_i\,g_j \to Q_k\,\bar{Q}_l$	$1/6\,(u^2 + t^2)/(ut) - 3/8\,(u^2 + t^2)/s^2$

s,t and u are defined in {44}

Table 22: Lowest order matrix elements for $Q\bar{Q}$ production.

As α_s is rather large compared to the electromagnetic coupling constant α_e ($\alpha_s \approx 0.15$ at $Q^2 = (50\ \text{GeV})^2$ and $\alpha_e = 1/137$ respectively) higher order processes are quite important in QCD. The next order involves processes with three outgoing partons ("$2 \to 3$"), mainly gluons from initial and final state radiation. One can either calculate the correct $2 \to 3$ matrix elements [88], or use an approximation by applying radiative corrections to the partons as suggested by Fox and Wolfram [89].

If the matrix elements and the structure functions are known, the cross-section is given by the expression:

$$E\,d\sigma/d^3p = \Sigma \iint dx_i\,dx_j\,F_i(x_i)\,F_j(x_j)\,(s/\pi)\,d\sigma_{ijkl}/dt \times \delta(s + t + u) \qquad \{46\}$$

The sum has to be done over all relevant parton types. The delta function ensures energy and momentum conservation[40].

[40] If the outgoing partons are massive, the delta function has to be changed into $\delta(s + t + u - 2m^2)$.

A.1.3 Fragmentation

Unfortunately the outgoing quarks and gluons are not directly observable. They fragment into collimated bundles of hadrons, which are seen as jets. The important parameter describing the fragmentation is defined by:

$$z = (E + p||)_{hadron} / (E + p)_{quark} \qquad \{2\}$$

p|| is the hadron's momentum parallel to the quark's momentum. For a very high momentum z is the fraction of the quark momentum which is transfered to the hadron in the fragmentation. For light quarks and gluons the distribution of z was found to be [99]:

$$D(z)_{u,d,s,g} \simeq 1 - a + 3a\,(1-z)^2 \quad (a \simeq 0.89) \qquad \{47\}$$

This results in a rather "soft" fragmentation, that means that the hadrons on average keep only a small fraction of the initial parton momentum. On the contrary, heavy quarks show a much "harder" fragmentation, which can be parametrized according to Peterson et al. [19]:

$$D(z)_{c,b} = n / \{ z[\,1 - (1/z) - \varepsilon / (\,1 - z\,)]^2 \} \qquad \{3\}$$

The parameter ε depends on the quark mass and therefore on the flavour of the heavy quark. The smaller ε, the "harder" is D(z), it peaks at higher z values. Typical values of ε for charm and bottom quarks are listed in table 23 .

flavour	<z>	ε
charm	0.59	0.15
bottom	0.77	0.015

Table 23: Charm and beauty fragmentation parameters

[90]

These values have to be taken with care! In e^+e^- experiments they are often derived from:

$$z' = 2\,E_{hadron} / \sqrt{s}, \qquad (48)$$

with $\sqrt{s}$ being the centre of mass energy of the e^+e^- collision. Those z' values have to be corrected because:

- The centre of mass energy of the actual interaction can be less than $\sqrt{s}$ because of initial state γ radiation.
- The heavy quark can radiate gluons (= final state radiation) before it forms a meson.

The true $z-$distribution is harder than the measured one. On the other hand one, has to take the same effects (especially gluon radiation) into account, if one uses these ε values for calculations. If, for example, the calculation includes radiative corrections to the outgoing partons (final state radiation), a harder fragmentation has to be used in order to reproduce the overall D(z).

In Monte Carlo calculations several methods of simulating fragmentation are used:

- Independent fragmentation as proposed by Feynman and Field [91]. The quarks produced in the interaction fragment independently according to their respective D(z). The quarks and gluons produced in this fragmentation step are again fragmented. The emerging cascade finally stops if all quarks are on shell or have hadronized.
- String fragmentation, according to the Lund model [92]. Here the quarks are connected by colour strings. The strings are associated to the colour field between the quarks. The energy in the string rises with the increasing distance between the quarks ($\simeq$ 1 GeV/fm) . The string breaks if the energy is high enough to create new particles.
- The Webber model [93]. This approach is different from the phenomenologic models above. It calculates QCD cascade processes using leading log approximation and Altarelli Parisi splitting functions. Only at the very end of the cascade, when the partons reach a certain mass cut Q_0, colourless clusters are formed in a phenomenological model. These clusters decay subsequently into hadrons.

Independent fragmentation and string fragmentation models depend on many parameters which have to be put in by hand and tuned to reproduce the data. Such parameters are:

- Fragmentation functions D(z) for each parton type.
- Transverse momentum distribution of hadrons with respect to the initial parton axis.
- Flavour ratio u : d : s .
- Ratio of vector/pseudovector mesons
- Baryon production.
- Production of heavy quarks

The Webber model in principle needs only two parameters, the QCD scale Λ and a cut−off mass Q_0 .

These models have been extensively tested in e^+e^- experiments. The experiments favour the string and the Webber model, as independent fragmentation fails to describe correlations between soft particles in three jet events [90]. Except for such details all models describe the data very well, especially the behavior of leading particles is well reproduced. As the behavior of soft particles in $p\bar{p}$ collisions is anyway obscured by the underlying event, the independent fragmentation model is used in our analysis.

A.2 Monte Carlo

It is impossible to calculate all quantities which are important for the analysis of the data analytically. Monte Carlo simulations have to be used instead:

Events are generated according to the theoretical cross−sections and evolved up to the level of final state particles. In addition, it is possible to include a complete simulation of the detector response in the event simulation: Charged tracks produce digitizings in the CD. Particles which hit the calorimeters give electromagnetic or hadronic showers distributed over several calorimeter cells. The energy deposited in each cell is converted into a number of photoelectrons, which can fluctuate according to poisson statistics. The deviation of muon tracks by multiple scattering is simulated. The detector sim-

ulation delivers "raw data", which can be analysed by the same procedure as real data. This enables the study of effects of physics cuts, resolution of the apparatus, and reconstruction algorithms.

On the other hand a precise Monte Carlo calculation needs high statistics and therefore much computer time. Including detector simulation one minute per event is realistic. For our analysis we made use of two different Monte Carlo programs which are described in the following sections.

A.2.1 Isajet

The Isajet Monte Carlo was written by F. Paige and P. Protopopescu [94]. It generates QCD and Drell−Yan type events in $p\bar{p}$ or pp collisions. The main features of this program are:

- It uses structure functions from Eichten et al. [84]. The user can choose Duke and Owens [85] structure functions alternatively.
- QCD cross−sections of heavy quark production are taken from the *lowest order* calculations of Combridge [87]. Charm quarks are treated as massless, for beauty and top quark the mass is taken into account.
- Radiative corrections are applied to final state partons using the leading log approximation of Fox and William [89]. Corrections to incoming partons are done by backwards evolution as suggested by Gottschalk [95]. A cut−off mass of 6 GeV for these radiative corrections was chosen. Below that mass the partons are hadronized using phenomenologic fragmentation models.
- Quarks and gluons are fragmented assuming independent fragmentation. For heavy quarks the Peterson et al. fragmentation function is used, with the following ε values:

$$\varepsilon(\text{charm}) = 0.3$$

$$\varepsilon(\text{beauty}) = 0.02$$

$$\varepsilon(\text{top}) = 0.02\ m(\text{beauty})^2/m(\text{top})^2$$

The probability to pick up an up, down or strange quark is set to:

$$u : d : s = 0.43 : 0.43 : 0.14$$

The ratio of vector mesons to pseudoscalar is 3:1. Baryons are produced by generation of di-quarks with a relative rate of 10 %. The fragmentation products are generated with an average p_t^{rel} of 0.35 GeV/c . The fragmentation parameters were carefully tuned to describe e^+e^- data correctly (fig. 85).

- Beam jets (= "underlying event") are generated according to a model originally proposed by Abramorskii, Kanchelli and Gribov [96], which is based on multi pomeron exchange. The basic parameters of this model have been tuned to reproduce UA1 data (e.g. $W^{\pm}$ or two−jet data).
- The B−mesons decay model of Eurojet [98] was implemented in Isajet. It reproduces the measured lepton and D−meson spectra from e^+e^- experiments (fig. 10). The branching ratios used for the muonic decay of B−mesons are listed in table 24 (together with those for D−decays, the muonic branching ratio for top is 11%).

meson	rate	BR	meson	rate	BR
B^+	38.7 %	12 %	D^+	38.7 %	17.0 %
B^0	38.7 %	12 %	D^0	38.7 %	7.5 %
B^0_s	12.6 %	12 %	F	12.6 %	6.5 %
B−baryon	10.0 %	12 %	C−baryon	10.0 %	7.5 %

Table 24: Beauty and charm hadrons in Isajet.

Production rate and muonic branching ratios

Because of the radiative corrections heavy quarks are produced in two ways:

- In the hard process described by the matrix element [most of the time gluon fusion, see fig 84 a)]. Although such events can have additional partons from initial and final state radiation they are called "lowest order".
- In gluon − gluon scattering one gluon can split into a heavy quark pair [fig. 84 b)]. A similar process can happen to an incoming gluon which splits into a heavy quark pair. One of these

quarks takes part in a hard scattering process with another gluon or light quark ("Flavour excitation"). The probability for this process is determined by the heavy quark content of the structure functions. Gluon splitting and flavour excitation are called "higher order processes".

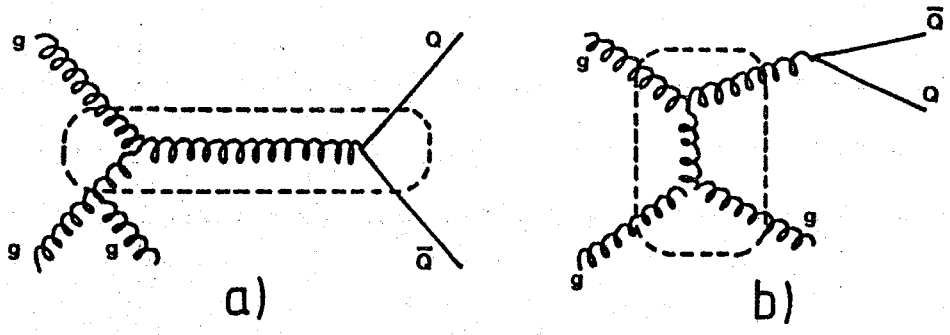

Figure 84: Heavy quark production in Isajet.
a) Fusion Process ("lowest order") plus initial state radiation
b) Splitting of an outgoing gluon
The dashed box indicates the process which is calculated using the 2 → 2 matrix element.

It has to be mentioned that this naming of "lowest order" and "higher order" is not correct in terms of perturbation theory. E.g. Processes (a) and (b) in figure 84 are of same order in a_s, they even correspond to the same feynman diagram (but at different kinematical regions). Nevertheless they are treated differently in Isajet. Hence these two categories cannot directly be compared with the "2 → 2" and "2 → 3" processes of Eurojet.

Apart from such "theoretical" difficulties, Monte Carlo calculations also have more trivial uncertainties, coming from the choice of input parameters. In table 25 the variation of the dimuon rate depending upon structure functions and fragmentation parameters is listed. Such uncertainties are included in our error on the $b\bar{b}$ cross−section.

	Eichten	Duke and Qwens
ε = .03 (soft)	0.90	0.79
ε = .02 (standard)	1.00	0.83
ε = .01 (hard)	1.20	0.91

Structure functions (standard is Eichten et al.) and fragmentation parameter ε.

Table 25: Relative dimuon rate for different M − C parameters:

process	σ/nb	relative contribution
heavy flavour production		
unlike − sign events		
$b\bar{b}$ (lowest order)	2.022	55 %
$c\bar{c}$ (lowest order)	0.266	7 %
$b\bar{b}$ (higher order)	0.500	14 %
$c\bar{c}$ (higher order)	0.124	3 %
like − sign events (no mixing)		
$b\bar{b}$ (lowest order)	0.578	16 %
$c\bar{c}$ (lowest order)	0.0	0 %
$b\bar{b}$ (higher order)	0.183	5 %
$c\bar{c}$ (higher order)	0.003	
Z^0 decays		
$b\bar{b}$ (unlike − sign)	2.2×10^{-3}	
$b\bar{b}$ (like − sign)	2.2×10^{-3}	
$c\bar{c}$	0.9×10^{-3}	
$\tau^+\tau^-$	1.8×10^{-3}	

Cross − sections for dimuon production after applying standard physics cuts:

$$p_t > 3\ GeV/c,\ m^{\mu\mu} > 6\ GeV/c^2,\ \eta < 2.4$$

(no detector acceptance).

Table 26: Dimuon cross − sections for Isajet subprocesses.

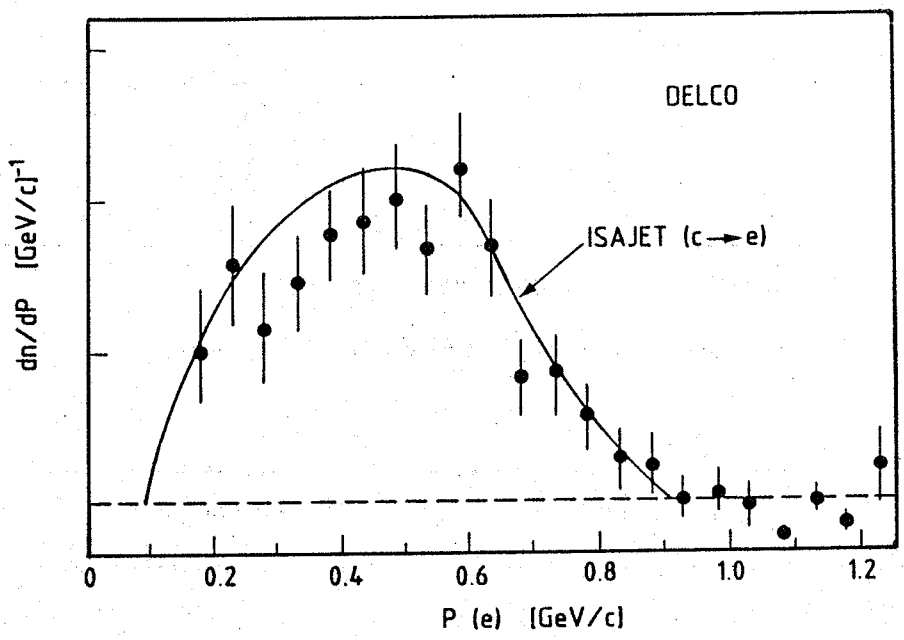

Figure 85: Measured charm fragmentation and Isajet simulation [97].

A.2.2 Eurojet

The Eurojet Monte Carlo event generator was written by A. Ali, B. Van Eijk and E. Pietarinen [98] [99]. The main difference of this program compared with Isajet is the explicit use of higher order matrix elements. Together with the lowest order $2 \to 2$ processes Eurojet uses the $O(\alpha_s^3)$ $2 \to 3$ matrix elements. Such processes are:

$$q + \bar{q} \to g + Q + \bar{Q}$$

$$g + g \to g + Q + \bar{Q}$$

$$g + q \to q + Q + \bar{Q}$$

This includes processes like gluon splitting in heavy quark pairs and the so-called flavour excitation[41]. Unfortunately these higher order diagrams have singularities, which have to be regulated by cut-off parameters. Eurojet uses a cut-off of 5 GeV p_t for the outgoing partons. Thus the Eurojet

[41] In Isajet this flavour excitation is accounted for by the heavy quark content of the structure functions. In Eurojet a heavy quark content is not admitted.

cross – sections depend slightly on this more or less arbitrary cut – off parameter. The remaing features of Eurojet are quite similar to those of Isajet:

- Use of Eichten structure functions (other choices are possible).
- Independent jet fragmentation according to Peterson. The values for the peterson ε used in Eurojet are:

$$\varepsilon(\text{charm}) = 0.05$$

$$\varepsilon(\text{beauty}) = 0.015$$

$$\varepsilon(\text{top}) = 0.0002$$

These values differ from those used in Isajet. The main reason for this is that Eurojet does not use radiative corrections in the evolution of final state quarks. Thus different ε values have to be used to obtain the correct overall fragmentation distribution. Nevertheless the charm fragmentation in Eurojet is harder than that used in Isajet. This results in a larger charm contribution to the dimuons. Eurojet predicts a charm content of 23% whereas Isajet calculates 10%. The value actually measured using the p_t^{rel} technique is 11 ± 8 % (without corrections for the different efficiency for $b\bar{b}$ and $c\bar{c}$, see chapter 8.2) which is compatible with the Isajet value, but 1.5 σ away from the Eurojet prediction.

The flavour ratio used in the Eurojet fragmentation is:

$$u : d : s = 0.41 : 0.41 : 0.18$$

thus assuming a slightly higher strangeness contribution than Isajet. The ratio of vector over pseudovector mesons is 2 : 1 for heavy mesons.

- The weak decays of heavy quarks are made using the measured branching ratios for all known decay modes. Estimates based on phase space and isospin were made for the remaining decay modes. The lepton and hadron momentum distributions from B and D decays were compared with data and showed a satisfactory agreement.

Because of technical reasons it was not possible to use the events generated by Eurojet with the complete detector simulation. This is especially important for quantities measured by calorimetry, where effects of the resolution are large. Muon properties are less affected, especially if the muons have rather low p_t .

meson	rate	BR	meson	rate	BR
B^+	36.9 %	12 %	D^+	36.9 %	18.0 %
B^0	36.9 %	12 %	D^0	36.9 %	7.5 %
B^0_s	16.2 %	12 %	F	16.2 %	8.5 %
B − baryon	10.0 %	12 %	C − Baryon	10.0 %	8.5 %

Table 27: Beauty and charm hadrons in Eurojet.

Production rate and muonic branching ratios

process	σ/nb	relative contribution
heavy flavour production		
unlike − sign events		
$b\bar{b}$ $(2 \rightarrow 2)$	2.4	42 %
$c\bar{c}$ $(2 \rightarrow 2)$	0.75	13 %
$b\bar{b}$ $(2 \rightarrow 3)$	1.2	21 %
$c\bar{c}$ $(2 \rightarrow 3)$	0.51	9 %
like − sign events (no mixing)		
$b\bar{b}$ $(2 \rightarrow 2)$	0.57	10 %
$c\bar{c}$ $(2 \rightarrow 2)$	0.0	0 %
$b\bar{b}$ $(2 \rightarrow 3)$	0.28	5 %
$c\bar{c}$ $(2 \rightarrow 3)$	0.0	0 %
Z^0 decays		
$b\bar{b}$ (unlike − sign)	4.4×10^{-3}	
$b\bar{b}$ (like − sign)	3.1×10^{-3}	
$c\bar{c}$	1.5×10^{-3}	

Cross − sections for dimuon production after applying standard physics cuts:

$$p_t > 3\ GeV/c,\ m^{\mu\mu} > 6\ GeV/c^2, |\eta| < 2.4$$

(no detector acceptance).

Table 28: Dimuon cross − sections for Eurojet subprocesses.

APPENDIX B

LIKELIHOOD FIT OF χ

The value for the mixing parameter χ (defined in formula {32}) was obtained by a maximum likelihood fit. This fit takes into account the absolute predictions for the number of like and unlike−sign events, and the differences in the two dimensional p_t distributions of muons from first and second generation decays and from background.

The distribution of the p_t of both muons, p_{t1}, p_{t2}, for like−sign events is:

$$\begin{aligned} d^2N_l/dp_{t1}dp_{t2} &= d^2N_f/dp_{t1}dp_{t2} \times [2\chi(1-\chi)] \\ &+ d^2N_s/dp_{t1}dp_{t2} \times [(1-\chi)^2+\chi^2] \\ &+ d^2N_B/dp_{t1}dp_{t2} \end{aligned} \qquad \{49\}$$

For unlike−sign events one obtains:

$$\begin{aligned} d^2N_u/dp_{t1}dp_{t2} &= d^2N_s/dp_{t1}dp_{t2} \times [2\chi(1-\chi)] \\ &+ d^2N_f/dp_{t1}dp_{t2} \times [(1-\chi)^2+\chi^2] \\ &+ d^2N_B/dp_{t1}dp_{t2} \\ &+ d^2N_c/dp_{t1}dp_{t2} \end{aligned} \qquad \{50\}$$

N_f are the events from first generation $b\bar{b}$, N_s from second generation $b\bar{b}$, N_B from decay background and N_c from $c\bar{c}$. The distributions for $b\bar{b}$ and $c\bar{c}$ were taken from Isajet. An overall normalization factor was applied in order to reproduce the observed number of events. Because of uncertainties of the measured branching ratios and fragmentation functions, the individual contributions from first and second generation $b\bar{b}$ and from $c\bar{c}$ were allowed to vary assuming gaussian errors. The semileptonic branching ratio for B−mesons, B_b, could vary by ± 0.058, for charmed mesons ("B_c") by ± 0.10 and the fraction of charm events ("f_c") by ± 50 %. The distribution for background events was obtained from the simulated background events, its normalization ("f_{bg}") could vary within 18% .

The complete likelihood function is:

$$\mathcal{L} = 1/(N_u!) < N_u >^{Nu} \exp(- < N_u >) \prod_{i(unlike)} [d^2N_u(p_{t1i},p_{t2i})/dp_{t1}dp_{t2}]/ < N_u > \times$$
$$1/(N_l!) < N_l >^{Nl} \exp(- < N_l >) \prod_{i(like)} [d^2N_l(p_{t1i},p_{t2i})/dp_{t1}dp_{t2}]/ < N_l > \times$$
$$G(f_{bg},f_{bg0},\Delta f_{bg}) \times G(B_b,B_{b0},\Delta B_b) \times G(B_c,B_{c0},\Delta B_c) \times G(f_c,f_{c0},\Delta f_c) \quad \{51\}$$

The products $\prod_{(unlike)}$ and $\prod_{(like)}$ include all non isolated unlike and like−sign events respectively. N_i is the number of actually observed events, $< N_i >$ the expectations from formulae {49} and {50} and:

$$G(x,x_0,\Delta x) = 1/\sqrt{(2\pi\Delta x)} \times \exp[-(x-x_0)^2 / 2(\Delta x)^2] \quad \{52\}$$

The negative logarithm of this likelihood function was minimized using the program package MINUIT [100] [66]. As usual in log−likelihood fits the ± 1 standard deviation error is defined by a difference of 0.5 of $\log(\mathcal{L})$, the single sided 90% confidence level by a difference of 0.82.

APPENDIX C

EFFICIENCY AND ACCEPTANCE

The efficiency of the apparatus and the acceptance of the cuts for different processes was studied with Isajet calculations including full detector simulation. In most cases the acceptance can be factorized in a process dependent part from the physics cuts, and an approximately process independent part from geometrical acceptance and technical cuts. This provides useful information for estimating rates and cross−sections avoiding the painstaking procedure of detector simulation. The overall acceptance should factorize like:

$$\eta = \eta_{cuts}\, \eta_{geo}\, \eta_{rcnstr}\, \eta_{trigger} \qquad \{53\}$$

η_{cuts} Acceptance of physics cuts: p_t, $m^{\mu\mu}$ etc. This factor is process dependent and has to be studied by Monte Carlo

η_{geo} Geometrical acceptance of the detector. In principle this is process dependent as the muon acceptance is higher in the forward region than in the central region (fig. 21). So the overall acceptance depends on the rapidity distribution of the muons. For many processes this rapidity distribution is quite uniform and an overall factor of $\simeq 0.75^2 = 0.56$ for dimuons can be used.

η_{rcnstr} Reconstruction efficiency: Fraction of muons which are reconstructed by the software and pass the technical selection cuts. As for example the CD reconstruction efficiency is non-uniform in different regions of the CD, the same arguments as above apply. Nevertheless a factor of 0.42 for both muons is a good approximation.

$\eta_{trigger}$ Trigger efficiency: Fraction of events which fire the trigger after hitting the muon chambers. As the trigger conditions varied from run to run and even within a run, this has to be calculated by averageing over the different conditions weighted by their respective lu-

minosity. It is also process dependent, as the trigger region covered only a part of the forward region. For dimuon events this is less important as the dimuon trigger covered almost the whole acceptance of the muon chambers. In addition there is a large redundancy as in most of the time only one muon must have triggered. A study of the $\varepsilon_{trigger}$ for dimuons gave an average value of 0.82 for all runs (for 1985 it was even 0.98).

Examples of cross−section calculations using these efficiencies can be found in table 29 .

process:	Dell Yan M > 11 GeV/c²	Upsilon
cuts isolation geometry reconstruction trigger	0.54 0.82 0.53 0.42 0.82	0.39 0.82 0.53 0.42 0.82
	0.086 ± 0.013	0.058 ± 0.007
Events *) Luminosity/nb^{-1} cross−section	14.8 ± 4.8 ± 2.0 659 0.26 ± 0.08 ± 0.06 nb	40 ± 7 ± 5 659 1.0 ± 0.2 ± 0.2

*) the second error is from uncertainties in the parametrizations of the mass spectra.

Table 29: Efficiencys of apparatus and cuts for Drell−Yan, and ϒ.

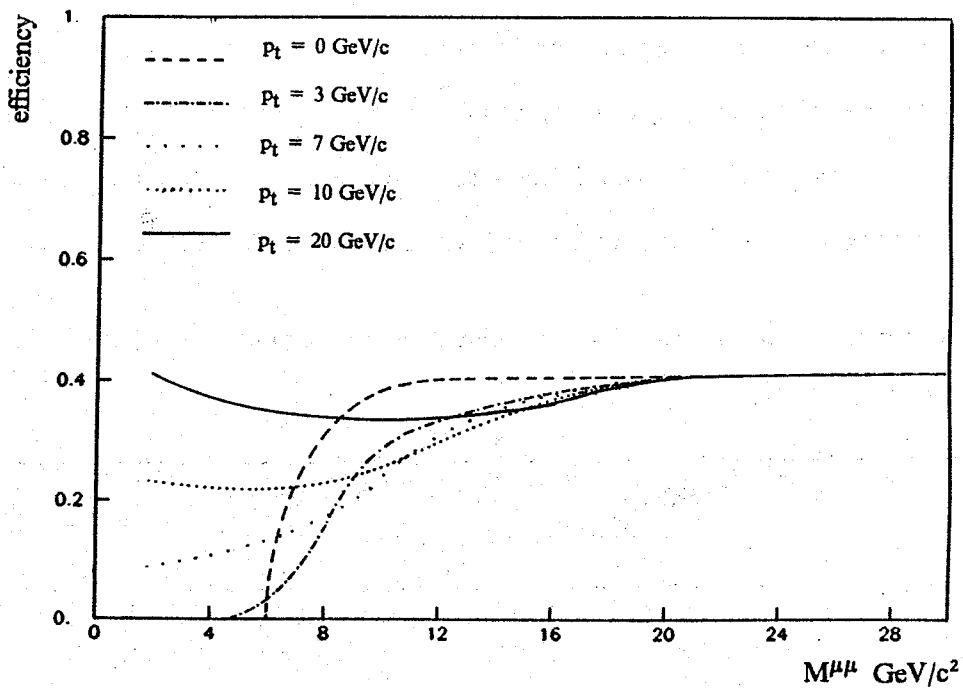

Figure 86: Acceptance of detector geometry and p_t cut. The acceptance is calculated as function of the dimuon mass for fixed p_t of the dimuon system. The rapidity distribution was chosen flat between -2 and 2. Efficiency of the trigger and of technical cuts is not included. This gives a global reduction factor of $0.42 \times 0.82 = 0.34$.

APPENDIX D

BACKGROUND OF SINGLE MUON EVENTS.

Calculating the dimuon background we started from a sample of single muons events. Thus the decay probability of each hadron besides the muon could be calculated. A similar approach for the calculation of the single muon background was not possible, as an unbiased sample of no muon events did not exist. This is not necessary if one is only interested in the inclusive background and not in a special topology of the event[42]. The inclusive muon p_t distribution can simply be calculated by convoluting the measured p_t distribution of hadrons with the probability of the hadrons to fake a muon:

$$d\sigma/dp_t(\text{faked } \mu) = \int F(p_t^h, p_t^\mu)\, d\sigma/dp_t^h\, dp_t^h \qquad \{54\}$$

The hadron p_t spectrum was measured by UA1 [55] in minimum bias data. It can be parametrized by:

$$d^2\sigma/dp_t dy = 2\pi\, A\, p_t\, p_{t0}^n / (p_t + p_0)^n \qquad \{55\}$$

$$A = 373 \pm 15$$

$$p_{t0} = 1.3 \pm 0.04$$

$$n = 9.34 \pm 0.14$$

The probability density $F(p_t^h, p_t^\mu)$ of a hadron with p_t^h to fake a muon of p_t^μ was calculated with a single track Monte Carlo which simulates a pion or kaon decay and the complete detector response. This was done in exactly the same way as for the dimuon background. The cuts applied on the faked muons were of course different, depending upon the selection criteria (e.g. tight selection). For the pion and kaon content the same assumptions as for the dimuon background were made: 21% K and 58% π . The resulting $d\sigma/dp_t$ distributions for faked muons are shown in figure 87 for the so-called loose selection, which used the same cuts on the muons as the dimuon selection, and the tight selection using more restrictive technical cuts. These background spectra are compared with the measured inclusive muon p_t distributions. The background of the loose selection is right on top of the data, it even ex-

[42] This is different for the dimuon background: As we demand a mass cut on the muon the background depends on the correlations of the muons with other particles. This can only be studied using real events.

ceeds the data at p_t between 3 and 4 GeV/c. This verifies the assumption made in the dimuon background calculation, that the low p_t single muons are dominated by background. In the case of the tight selection, which is used in the single muon analysis, the background for high p_t muons is well below the data giving room to a signal.

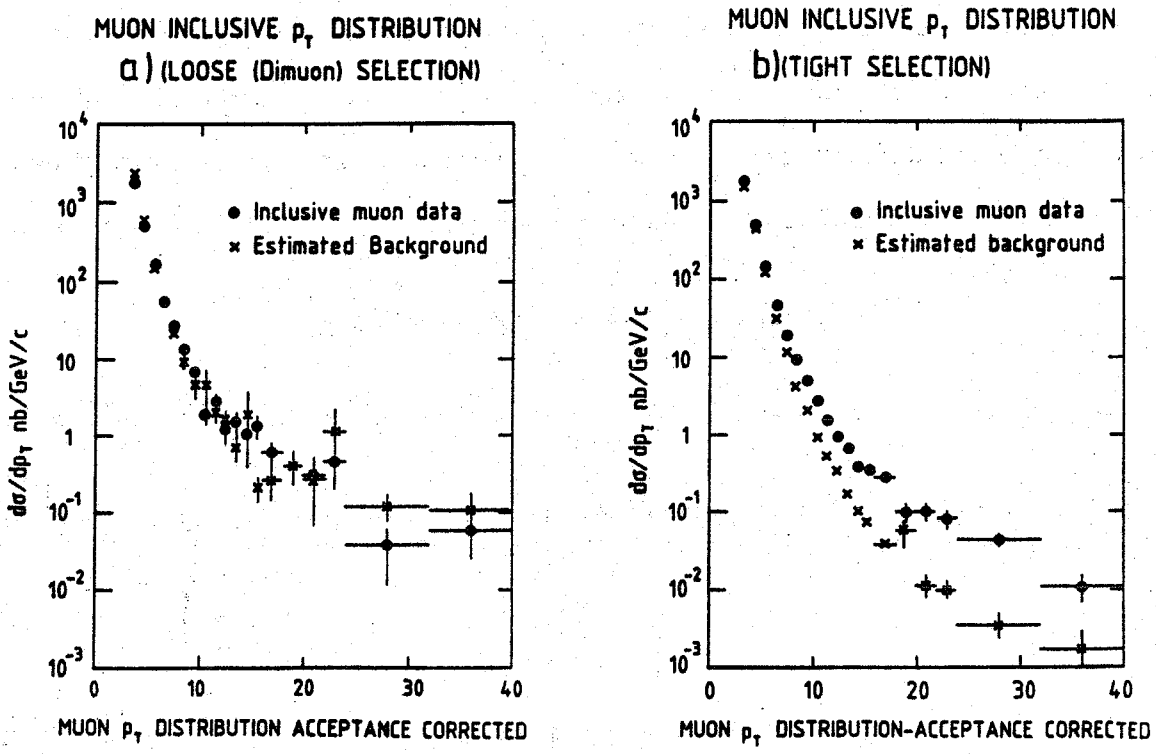

Figure 87: Inclusive $d\sigma/dp_t$ for data and calculated background
a) loose selection cuts as used for dimuons.
b) tight selection cuts as used for single muon analysis.

APPENDIX E

UA1 COORDINATE SYSTEM

We use the following conventions for the coordinates:

- The positive x−axis is along the direction of the $\bar{p}$ beam.
- The positive y−direction is vertically upwards.
- The positive z−direction is horizontally, pointing outwards the SPS cycle.
- The θ angle is defined towards the positive x−axis.
- The ϕ angle is defined in the y−z−plane perpendicular to the beam. 0^0 is along the positive z axis, 90^0 along the positive y axis.

p_t and E_t always means the vector component perpendicular to the x or beam axis.

The pseudorapidity is always calculated using: $\eta = -\ln(\tan(\theta/2))$

Acknowledgments

There is no doubt that UA1 is one of the most exciting and interesting experiments of this time. Being member of this collaboration is a great experience, and I am indebted to all the people who made it possible for me to work there.

I wish to thank Prof. Dr. H. Faissner, who gave me the opportunity to work at his institute and especially at UA1. I also want to thank my adviser, Prof. Dr. K. Eggert, for his steady interest in my work and his encourageing support.

Many people were involved in the analysis of the UA1 data and contributed with help, advice and interesting discussions to the success of this work. For that thanks to: Garry Bauer, Michel Della Negra, Nick Ellis, Achim Gaiser, Martin Jimack, Alan Norton, Thomas Redelberger, Jim Rohlf, Matthias Schröder, Bob van Eick and Klaus Wacker (and I apologize to all I have forgotten).

Special thanks go to Hans Graβmann, whose quick and critical mind spotted weak points first.

Working at UA1 is not only the pleasure of doing physics analysis, but also means hard work in order to keep the hardware running. I want to thank Dr. Hans Reithler for the many hours he spent teaching me how to operate his trigger processor.

And last but not least I have to thank all the people of the UA1 collaboration. They made all this hardware and software running and therefore made this work possible. This includes of course Carlo Rubbia, whose energetic leadership made this collaboration to what it is.

Ihnen allen ein herzliches Dankeschön !

REFERENCES

[1] S.L. Glashow, Nucl. Phys. 22 (1961) 579

S. Weinberg, Phys. Rev. Lett. 19 (1967) 1264

A. Salam, Elementary Particle Theory, (Almquist and Wiksell, Stockholm, 1968) 367

[2] G. Arnison et al., Phys. Lett. B155 (1985) 442

[3] C. Albajar et al., "Beauty production at the CERN proton−antiproton collider", Phys. Lett. B186 (1987) 237

[4] C. Albajar et al., "Search for $B^0 - \overline{B}^0$ oscillations at the CERN proton−antiproton Collider", Phys. Lett. B186 (1987) 247

[5] The evolution of the dimuon picture of UA1 can be followed by the following conference contributions:

K. Eggert "Strange Dimuon Events at the $p\bar{p}$ Collider", International Symposium on Cosmic Ray and Particle Physics, Tokyo, Japan, available as Aachen report PITHA 84/82 (RWTH Aachen) 1984

N. Ellis, "Dimuon Events at the CERN $p\bar{p}$ Collider", Proc. of the 5th topical Workshop on Proton−Antiproton Collider Physics, St.−Vincent, Italy, 1985, ed. by M. Greco (World Scientific,Singapore, 1985) 176

H.−G. Moser, Proc. of "The Quark Structure of Matter", Strasbourg− Karlsruhe (France, Germany) 1985, edited by M. Jacob and K. Winter, (World Scientific, Singapore, 1986) 317

K. Eggert, "Dimuon Events at the $p\bar{p}$ Collider", Proc. of "New Particles 85", Wisconsin (USA), edited by V. Barger, D. Cline, F. Halzen (World Scientific, Singapore, 1986) 207

K. Eggert, "B−Production and the evidence for $B^0-\overline{B}^0$ Mixing", Proc. of the 21th Recontre de Moriond, Les Arcs, France, 1986, "Progress in Electroweak Interaction", ed. by Tran Thanh Van (Edition Frontieres, 1986) 369

H.−G. Moser, "Tagging of Heavy Flavours with Dimuons at the CERN $p\bar{p}$ Collider", Proc. of the 21th Recontre de Moriond, Les Arcs, France, 1986, "Strong Interactions and Gauge Theories", ed. by Tran Thanh Van (Edition Frontieres, 1986) 331

M. Della Negra, Proc. of the 6th topical Workshop on Proton−Antiproton Collider Physics, Aachen, Germany, 1986, ed. by K. Eggert, H. Faissner, E. Radermacher (World Scientific, Singapore, 1987)

[6] The Standard Model has already become subject of textbooks. A general introduction and further references can be found e.g. in:

I.J.R. Aitchison, A.J.G. Hey, Gauge Theories in Particle Physics, (Adam Hilger, Bristol, 1982)

D.H. Perkins, Introduction in High Energy Physics, 2. edition, (Addison−Wesley, Reading, Massachusetts, 1982)

[7] M. Kobayashi, T. Maskawa, Prog. Theor. Phys. 49 (1973) 1489

[8] S.D. Drell, T.−M. Yan, Phys. Rev. Lett. 25 (1970) 316

[9] H. Graßmann, Doktorarbeit, RWTH Aachen, Germany, in preparation.

[10] S. Komamiya, Proc. of the 1985 International Symposium on Lepton and Photon Interactions at High Energies, Kyoto, ed. by M. Komuma and K. Takahashi, Japan (1985)

[11] P. Haas, et al. (CLEO), Phys. Rev. Lett. 55 (1985) 1248

H. Albrecht, et al. (ARGUS), Phys. Lett. B162 (1985) 395

[12] F. Halzen et al., Phys. Rev. D 30 (1984) 700

[13] A. D. Martin: Detecting Toponium, Conf. Proc. "New Particles 85" ed. by V. Barger, D. Cline, F. Halzen (World Scientific, Singapore 1985)

[14] G. Arnison et al., Phys. Lett. B172 (1986) 461

[15] Thorndike E.H., Ann. Rev. Nucl. Part. Sci. 35 (1985) 195

M. Gilchriese, Proc. of XXII Intern. Conference on High Energy Physics, Berkeley, USA, 1986, to be published

[16] S.W. Herb et al., Phys. Rev. Lett. 39 (1977) 252

W.R. Innes et al., Phys. Rev. Lett. 39 (1977) 1240

K. Uemo et al. Phys. Rev. Lett. 42 (1979) 486

[17] D.M.J. Lovelock et al., Phys. Rev. Lett. 54 (1985) 377

[18] A.G. Giles et al., Phys. Rev. D30 (1984) 1084

[19] C. Peterson, D. Schlatter, I. Schmitt and P.M. Zerwas, Phys. Rev. D27 (1983) 105

[20] J.P. Leville, Proc. CLEO Collab. Workshop on B Meson Decay, available as CLEO Preprint 81/05, Univ. Rochester (1981) 37

[21] I. Bigi, Phys. Lett. B169 (1986) 101

[22] S.E. Csorna et al. (CLEO), Phys. Rev. 54 (1986) 1894

[23] L.M. Sehgal, M. Wanninger, Aachen report PITHA 86/10 (1986)

[24] S. Behrends et al. (CLEO), Phys. Rev. Lett. 50 (1983) 881

[25] L. Wolfenstein, Phys. Rev. Lett. 51 (1983) 1945

[26] T.D. Lee and C.S. Wu, Ann. Rev. Nucl. Sci. 16 (1966) 511

L. Wolfenstein, CMU−HTEP−86−3, Carnegie Mellon Univ., Pittsburgh, USA

[27] A. Bean et al. (CLEO), Phys. Rev. Lett 58 (1987) 183

[28] A. Bartel et al. (JADE), Phys. Lett. B161 (1985) 197

[29] The earliest discussions on $B^0-\bar{B}^0$ oscillations can be found in:

A. Pais, S.B. Treiman, Phys. Rev. D12 (1975) 2744

L.B. Okun, V.I. Zakharov, B.M. Pontecorvo, Nuovo Cim. Lett. (1975) 218

J. Ellis, M.K. Gaillard, D.V. Nanopoulos, Nucl. Phys. B 109 (1976) 213

A. Ali, Z. Aydin, Nucl. Phys. B148 (1978) 165

[30] W.C. Louis et al, Phys. Rev. Lett., 56 (1986) 1027

[31] T. Schaad et al. (Mark II), Phys. Lett. B160 (1985) 188

[32] R. Barlow, Proc. of the 20th Recontre de Moriond, "Heavy Quarks, Flavour Mixing and CP−Violation", ed. by Tran Thanh Van (Edition Frontiers, 1985) 187

[33] L.L. Chau, Phys. Rep. 95 (1983) 1

A.J. Buras et al., MPI−PAE−PTH 7−84 (1984) and Nucl. Phys. B 245 (1984) 369

A. Ali, C. Jarlskog, ITP Univ. of Stockholm 1.4.84 and TH.3890 − CERN (1984)

J.S. Hagelin, Nucl. Phys. B193 (1981) 123

[34] M.A. Shifman and M.V. Voloshin, ITEP Reports 86,54 (1986)

[35] P. Zerwas, private communication

[36] A.J. Buras, W. Stominski and H. Steger, Nucl. Phys. B238 (1984) 529

[37] K. Kleinknecht and B. Renk, Z. Physik C34 (1987) 209

[38] D. Saxon, Proc. ot the European Physical Society Meeting, Bari, Itali, 1985, ed. by L. Nitti, G. Preparata and references therein

[39] F. Halzen, A. Martin, Proc. 4th Topical Workshop on Proton− Antiproton Collider Physics, Bern, 1984, ed. by H. Hanni and J. Schacher (CERN, Geneva, 84−09) 260

[40] V. Barger, R.N.J. Phillips, MAD−PH−155, 239, 266, Univ. of Wisconsin, Madison, USA

[41] C. Rubbia, P. McIntyre, D. Cline, Proc. of the Int. Neutrino Conference, edited by H. Faissner, H. Reithler and P. Zerwas (Vieweg, Braunschweig 1977) 683

[42] S. Van der Meer, CERN ISR−PO/72−31 (1972)

[43] G. Arnison et al. (UA1 collaboration), Phys. Lett. B122 (1983) 103
G. Banner et al. (UA2 collaboration), Phys. Lett. B122 (1983) 476

[44] G. Arnison et al. (UA1 Collaboration), Phys. Lett. B134 (1983) 398
Bagnaia et al. (UA2 Collaboration), Phys. Lett. B129 (1983) 130

[45] The history of the CERN $p\bar{p}$ project from the early proposals up to the discoveries of $W^{\pm}$ and Z^0 is nicely described in:
P. Watkins, The Story of the W and Z (Cambridge University Press, Cambridge 1986)

[46] A. Astbury et al., UA1 Proposal CERN/SPSC 78−06 (1978)
M. Barranco Luque et al., Nucl. Instrum. and Methods 176 (1980) 175
M. Calvetti et al., Nucl. Instrum. and Methods A 243 (1986) 45
M.J. Corden et al., Nucl. Instrum. and Methods A238 (1985) 273
K. Eggert et al., Nucl. Instrum. and Methods 176 (1980) 217
G. Bauer et al., Nucl. Instrum. and Methods A253 (1987) 179

[47] S.P. Denisor et al., Nucl. Phys. B61 (1973) 62

[48] A. Astbury et al., Nucl. Inst. and Methods, A238 (1985) 288

[49] G. Hilgers, H. Lehman, G. Pierschel and H. Reithler, UA1−TN−81−21, unpublished

[50] E. Pietarinen et al., IEE Trans. Nucl. Sci 32 (1985) 1463

[51] M. Pimiä, Thesis University of Helsinki, HU−P−D45 Helsinki (1985)

[52] I. ten Have, UA1−TN−85−70, unpublished

[53] K. Lacava, "Study of low E_t jets in Proton−Antiproton Collisions at $\sqrt{s}$ = 200 − 900 GeV", Proc. of the 6th Topical Workshop on Proton−Antiproton Collider Physics, Aachen, Germany, 1986, ed. by K. Eggert, H. Faissner, E. Radermacher (World Scientific, Singapore, 1987)

[54] R. Leuchs, Diplomarbeit, RWTH Aachen, Germany (1982), unpublished

[55] M. Banner et al., Phys. Lett. B122 (1983) 322

G.J. Alner et al., Nucl. Phys. B258 (1985) 505

G. Arnison et al., Phys. Lett. B118 (1982) 167

[56] N. Ellis, M. Jimack, UA1−TN−86−79 (1986), unpublished

N. Ellis, M. Jimack, UA1−TN−86−124 (1986), unpublished

[57] T. Redelberger, private communication

[58] A.L.S. Angelis et al., Phys. Lett. B87 (1979) 398;

C. Kourkoumelis et al., Phys. Lett. B91 (1980) 481;

D. Antreasyan et al., Proc. EPS Int. Conf. on High Energy Physics, Geneva (1979) 779;

J.S. Yoh et al., Phys. Rev. Lett. 41 (1978) 684

[59] G. Altarelli et al., CERN−TH 4015/84 and Fermilab−Pub−84/107 (1984)

[60] A.G. Clark et al., Nucl. Phys B142 (1978) 29;

C. Kourkumelis et al., Phys. Lett. B91 (1980) 475;

D. Antreasyan et al., Phys. Rev. Lett. 48 (1982) 302;

J. Badier et al., Z. Phys C26 (1985) 481;

A.S. Ito et al., Phys. Rev. D23 (1981) 604

[61] V. Barger and A.D. Martin, Phys. Rev. D31 (1985) 1051

[62] G. Arnison et al., Nucl. Phys. B276 (1986) 253−271

[63] E.L. Berger, J.C. Collins, D.E. Soper, Phys. Rev. D35 (1987) 2272

[64] Early measurements at UA1 indicated a rather large D^* content: $\rho \approx 0.65$: G. Arnison et al., Phys. Lett. B147 (1984) 222

However this measurement was revised and a lower value was found. The difference can be understood in terms of a trigger bias of the earlier data. For recent results: R. Frey, Proc of the APS Meeting of Division of Particles and Fields, Eugene, USA, 1985, ed. by R. H. Hwa (World Scientific, Singapore, 1986)

[65] A. H. Mueller and P. Nason, Phys. Lett. B157 (1985) 226

[66] K. Wacker, UA1−TN−87−27, unpublished

[67] A. Breakstone et al., Phys. Lett. B135 (1984) 510

[68] B. Anderson, private communication

W. Geist, private communication

[69] H. Schröder (ARGUS), Talk given at DESY−seminar, Hamburg, Germany, 24. Feb. 1987, unpublished

[70] M. Frank and P.J. O'Donnell, Phys. Lett. B159 (1985) 174

[71] J. Ellis, J.S. Hagelin, S. Rudaz, CERN−TH 4679/87 (1987)

[72] R. Leuchs, Doktorarbeit, Universität Kiel, Germany, in preparation

[73] R. Edgecock, PhD Thesis, Univ. of Birmingham, England, 1986

[74] A. Geiser, Diplomarbeit, RWTH Aachen, Germany, 1987, unpublished

[75] Particle Data Group, "Rev. of Particle Properties", Phys. Lett. 170B, 1986

[76] F. Halzen, et al., Phys. Rev. D30 (1984) 700

[77] K. Wacker, UA1−TN−86−26, unpublished

[78] J. D. Dowell, "The UA1 Experiment with ACOL", Proc. of the 6th Topical Workshop on Proton−Antiproton Collider Physics, Aachen, Germany, 1986, ed. by K. Eggert, H. Faissner, E. Radermacher (World Scientific, Singapore, 1987)

UA1 collaboration, UA1−TN−86−112, unpublished

[79] M. Suzuki, Phys. Rev. D31 (1985) 1158

[80] A.I. Sanda, Phys. Rev. Lett. 55 (1985) 2653

[81] A. J. Buras et al., MPI−PAE−PTH 7−84 (1984) and Nucl. Phys. B245 (1984) 369

[82] J.H. Christenson, J.W. Cronin, V.L. Fitch and R. Turlay, Phys. Rev. Lett. 13 (1964) 138

[83] C. Bernabeau, C. Jarlskog, Z. Phys. C8 (1981) 233−238

[84] E. Eichten, I. Hinchliff, K. Lane and C. Quigg, Rev. Mod. Phys. 56 (1984) 579

[85] D. Duke and J. Owens, Phys. Rev. D30, (1984) 49

[86] M. Glück, E. Hoffmann and E. Reya, Z. Physik C13 (1982) 119

[87] B. Combridge et al., Phys. Lett. B70 (1977) 234

[88] Z. Kunszt, E. Pietarinen, Nucl. Phys. B164 (1980) 45

[89] G.C. Fox, S. Wolfram, Nucl. Phys. B126 (1977) 298

[90] Flügge, G. Proc. of "The Quark Structure of Matter", Strasbourg – Karlsruhe (France, Germany) 26. Sept.–1. Oct. 1985, edited by M. Jacob and K. Winter (World Scientific, Singapore, 1986) 79

D. H. Saxon, Proc. of the European Physical Society Meeting on High Energy Physics, Bari, Italy by L. Nitti, G. Preparata (1985) 889

[91] R.D. Field, R.P. Feynman, Nucl. Phys. B136, (1978) 1

[92] B. Anderson, et al., Phys. Reports 97, 31 (1983)

[93] B.R. Webber, Nucl. Phys. B238 (1984) 492

[94] F.E. Paige, S.D. Protopopescu, BNL – 38034 (1986), Brookhaven National Laboratory, Upton, USA

For the generation of $b\bar{b}$, $c\bar{c}$ and Drell–Yan events the Isajet version 5.21 was used. $t\bar{t}$ and $W \rightarrow t\bar{b}$ was generated using version 5.23. Except of minor corrections both versions are equivalent.

[95] T.D. Gottschalk, CALT–68–1241 (1985)

T. Sjostrand. Phys. Lett. B157 (1983) 1945

[96] V.A. Abramorskii, O.V. Kanchelli, V.N. Gribov, Proc. of XVI Int. Conf. on High Energy Physics (Batavia Il. 1973) Vol 1, 389

[97] D.E. Koop et al. (DELCO), Phys. Rev. Lett 52 (1983) 970

M. Derrik et al. (HRS), ANL–HEP–PR–85–02

M. Althoff et al. (TASSO), Z. Phys. C22 (1984) 219

M.E. Nelson et al. (Mark II), Phys. Rev. Lett 50 (1983) 2054

[98] B. van Eijk, Proc. 5th Topical Workshop on Proton Antiproton Collider Physics, St. Vincent, 1985, ed. by M. Greco (World Scientific, Singapore, 1985), 165

A. Ali, B. van Eijk, I. ten Have, CERN−TH 4523/86

[99] B. van Eijk, Academisch Proefschrift, Amsterdam 1987

[100] F. James, M. Roos, Computer Physics Communication 10 (1975) 343

"UA1−TN" are internal technical notes of the UA1 collaboration

1. LEBENSLAUF: HANS – GÜNTHER MOSER

Am 18 Januar 1958 wurde ich als erster Sohn des Industriekaufmanns Klaus Moser und dessen Ehefrau Elisabeth Moser, geb. Mohr, in Mannheim geboren.

Von 1964 an besuchte ich die Grundschule in Feucht bei Nürnberg. 1968 wechselte ich an das Leibniz Gymnasium in Altdorf, wo ich 1978 das Abitur erhielt.

Juli 1978 bis September 1979 leistete ich Wehrdienst in Roth bei Nürnberg und Landsberg/Lech.

Im Wintersemester 1979 begann ich das Physikstudium an der Universität Erlangen – Nürnberg. Die Vordiplomprüfung bestand ich im November 1981. Im Frühjahr 1983 begann ich bei Prof. Dr. H. Wegener meine Diplomarbeit zum Thema: "Untersuchungen von Materialien kurzer Strahlungslänge für Kalorimeter mit optischer Auslese". Während meiner Diplomarbeit verbrachte ich zwei Monate als Sommerstudent am Crystal Ball Experiment bei DESY, Hamburg. Die Diplomprüfung bestand ich im Mai 1984.

Im August 1984 erhielt ich eine Stelle als wissenschaftlicher Mitarbeiter im III Physikalischen Institut der RWTH Aachen, unter Leitung von Prof. Dr. H. Faissner. Meine Arbeit erfolgte am UA1 Experiment im CERN bei Genf. Dort begann ich auch, betreut von Prof. Dr. K. Eggert, an meiner Dissertation arbeiten.